NUREG/CR-6584, Vol. 2

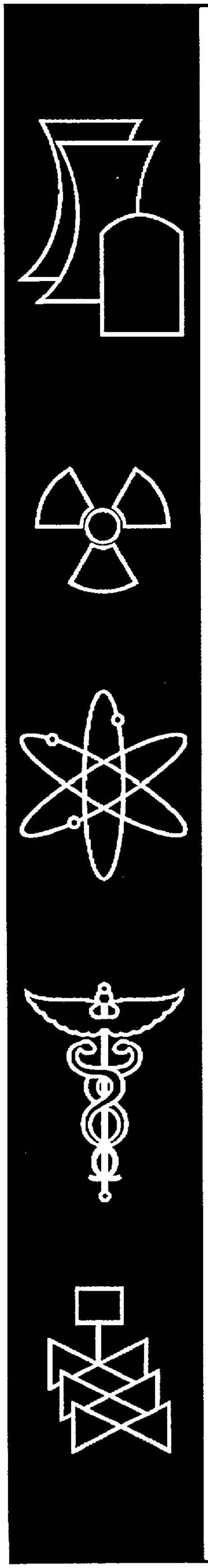

Evaluation of the Hualien Quarter Scale Model Seismic Experiment

Geotechnical Site Characterization Review

City College of New York

U.S. Nuclear Regulatory Commission
Office of Nuclear Regulatory Research
Washington, DC 20555-0001

AVAILABILITY OF REFERENCE MATERIALS IN NRC PUBLICATIONS

NRC Reference Material

As of November 1999, you may electronically access NUREG-series publications and other NRC records at NRC's Public Electronic Reading Room at www.nrc.gov/NRC/ADAMS/index.html.
Publicly released records include, to name a few, NUREG-series publications; *Federal Register* notices; applicant, licensee, and vendor documents and correspondence; NRC correspondence and internal memoranda; bulletins and information notices; inspection and investigative reports; licensee event reports; and Commission papers and their attachments.

NRC publications in the NUREG series, NRC regulations, and *Title 10, Energy*, in the Code of *Federal Regulations* may also be purchased from one of these two sources.

1. The Superintendent of Documents
   U.S. Government Printing Office
   Mail Stop SSOP
   Washington, DC 20402–0001
   Internet: bookstore.gpo.gov
   Telephone: 202-512-1800
   Fax: 202-512-2250
2. The National Technical Information Service
   Springfield, VA 22161–0002
   www.ntis.gov
   1–800–553–6847 or, locally, 703–605–6000

A single copy of each NRC draft report for comment is available free, to the extent of supply, upon written request as follows:

Address: Office of the Chief Information Officer,
Reproduction and Distribution
Services Section
U.S. Nuclear Regulatory Commission
Washington, DC 20555-0001
E-mail: DISTRIBUTION@nrc.gov
Facsimile: 301–415–2289

Some publications in the NUREG series that are posted at NRC's Web site address www.nrc.gov/NRC/NUREGS/indexnum.html are updated periodically and may differ from the last printed version. Although references to material found on a Web site bear the date the material was accessed, the material available on the date cited may subsequently be removed from the site.

Non-NRC Reference Material

Documents available from public and special technical libraries include all open literature items, such as books, journal articles, and transactions, *Federal Register* notices, Federal and State legislation, and congressional reports. Such documents as theses, dissertations, foreign reports and translations, and non-NRC conference proceedings may be purchased from their sponsoring organization.

Copies of industry codes and standards used in a substantive manner in the NRC regulatory process are maintained at—

The NRC Technical Library
Two White Flint North
11545 Rockville Pike
Rockville, MD 20852–2738

These standards are available in the library for reference use by the public. Codes and standards are usually copyrighted and may be purchased from the originating organization or, if they are American National Standards, from—

American National Standards Institute
11 West 42nd Street
New York, NY 10036–8002
www.ansi.org
212–642–4900

Legally binding regulatory requirements are stated only in laws; NRC regulations; licenses, including technical specifications; or orders, not in NUREG-series publications. The views expressed in contractor-prepared publications in this series are not necessarily those of the NRC.

The NUREG series comprises (1) technical and administrative reports and books prepared by the staff (NUREG–XXXX) or agency contractors (NUREG/CR–XXXX), (2) proceedings of conferences (NUREG/CP–XXXX), (3) reports resulting from international agreements (NUREG/IA–XXXX), (4) brochures (NUREG/BR–XXXX), and (5) compilations of legal decisions and orders of the Commission and Atomic and Safety Licensing Boards and of Directors' decisions under Section 2.206 of NRC's regulations (NUREG–0750).

NUREG/CR-6584, Vol. 2

Evaluation of the Hualien Quarter Scale Model Seismic Experiment

Geotechnical Site Characterization Review

Manuscript Completed: October 2000
Date Published: March 2001

Prepared by
C. A. Miller, C. J. Costantino[a]
J. A. Pires, C. J. Higgins[b]

[a]City College of New York, Principal Contractor
Earthquake Research Center
Department of Civil Engineering
New York, NY 10031

[b]Applied Research Associates, Inc., Subcontractor
4300 San Mateo Boulevard, N.E.
Albuquerque, NM 87110

H. L. Graves, NRC Project Manager

Prepared for
Division of Engineering Technology
Office of Nuclear Regulatory Research
U.S. Nuclear Regulatory Commission
Washington, DC 20555-0001
NRC Job Code W6769

ABSTRACT

The primary objective of the Hualien Soil-Structure Interaction Experiment, also known as the Hualien Large Scale Seismic Test (LSST), is to obtain seismic soil-structure interaction (SSI) data for stiff soil site conditions that might resemble those encountered at prototypical nuclear power plant sites. An international consortium was established to carry out the Hualien LSST project. The consortium consisted of: the Electric Power Research Institute (EPRI), the Taiwan Power Company (Taipower), the U.S. Nuclear Regulatory Commission (NRC), the Tokyo Electric Power Company (TEPCO), the Central Research Institute of the Electric Power Industry (CRIEPI) of Japan, the French Commissariat A L'Energie Atomique (CEA), the Electricite de France (EdF) and Framatome.

ARA acted as a subcontractor to the City College of New York (CCNY) and CCNY was the primary technical contractor for the NRC for the Hualien SSI Experiment. The scope of work done by ARA for the Hualien SSI experiment was, primarily, to assist CCNY and the NRC with: site characterization issues, the development of site models and the review of the instrumentation plan for the project. In this report, a review and assessment of the geotechnical site characterization is presented. The report consists of a detailed description of the methods used and of the results obtained as well as an assessment of those results and of the recommended soil parameters. This review is followed by analysis of the forced vibration test data and selected recorded earthquake loading data for further interpretation and evaluation of site conditions and soil parameters to be used in analytical calculations. The report concludes with a summary of the major findings and uncertainties encountered in the site characterization and their implications on the interpretation of the results of the experiment and on soil-structure interaction analysis procedures, as well as recommendations for further studies related to the Hualien SSI experiment.

Of special significance is the identification of anisotropic in-situ conditions for the stiff gravelly soils beneath the foundation of the model. For this soil, the propagation speed of the shear waves varies with the horizontal direction considered. This condition was not expected during the site characterization efforts and only was identified after analysis and interpretation of the forced vibration tests of the model performed prior to and following the placement and compaction of the backfill.

TABLE OF CONTENTS

LIST OF FIGURES

LIST OF TABLES

EXECUTIVE SUMMARY

The primary objective of the Hualien Soil-Structure Interaction Experiment, also known as the Hualien Large Scale Seismic Test (LSST), is to obtain seismic soil-structure interaction (SSI)data for stiff soil site conditions that might resemble those encountered at prototypical nuclear power plant sites. An international consortium was established to carry out the Hualien LSST project. The consortium consisted of: the Electric Power Research Institute (EPRI), the Taiwan Power Company (Taipower), the U.S. Nuclear Regulatory Commission (NRC), the Tokyo Electric Power Company (TEPCO), the Central Research Institute of the Electric Power Industry (CRIEPI) of Japan, the French Commissariat A L'Energie Atomique (CEA), the Electricite de France (EdF) and Framatome.

ARA acted as a subcontractor to the City College of New York (CCNY) and CCNY was the primary technical contractor for the NRC for the Hualien SSI Experiment. The scope of work done by ARA for the Hualien SSI experiment was, primarily, to assist CCNY and the NRC with: site characterization issues, the development of site models and the review of the instrumentation plan for the project. In this report, a review and assessment of the geotechnical site characterization is presented. The report presents a detailed description of the methods used and of the results obtained as well as an assessment of those results and of the recommended soil parameters. This review is followed by analysis of the forced vibration test data and selected recorded earthquake loading data for further interpretation and evaluation of site conditions and soil parameters to be used in analytical calculations. The report concludes with a summary of the major findings and uncertainties encountered in the site characterization and their implications on the interpretation of the results of the experiment and on soil-structure interaction analysis procedures, as well as recommendations for further studies related to the Hualien SSI experiment.

A comprehensive site characterization program was conducted by CRIEPI between 1990 and 1994. This site characterization program paid particular attention to the soil conditions to a depth of about 12 m below the ground surface (GL-12m). In this regard, the site characterization was at least as thorough as those commonly used for actual, prototypical, sites. In particular, a detailed characterization was made for the surface layer of sand from GL0 to GL-5m, for the gravel beneath the foundation and in the free-field from GL-5m to GL-12m, and for the as-built backfill soil. A somewhat less detailed characterization was provided for the gravel between GL-12m and GL-20m. The site characterization for depths below about GL-20m appears to have been beyond the scope of the effort by CRIEPI and, at present, it seems to rely almost exclusively on the scoping geophysical study performed in the early stages of the Hualien SSI program by the Institute of Earth Sciences (IES) of the Academia Sinica. This characterization may be limited for the purposes of detailed correlation analysis studies with the ground accelerations recorded in the down-hole arrays, which extended to a depth of about GL-52.5m. Examples of such correlation studies are: site amplification studies and deconvolution analysis.

An important feature of the site characterization was that it paid particular attention to the effect of the various construction operations on the in-situ shear wave speed and soil stiffness. This was shown by CRIEPI to be important for the cohesionless soils encountered whose stiffness and strength depend on the effective stress conditions at the site.

The procedures and results of the site characterization program conducted by CRIEPI, which took place over a span of about 4 years from 1990 to 1994, were periodically reported to the other members of the Hualien SSI consortium and their contractors. They and CRIEPI evaluated these procedures and results and recommended new tests as deemed necessary. As a consequence, the results obtained by CRIEPI and given in this report have been thoroughly reviewed and provide an adequate representation of the site conditions. However, additional comments need to be made pertaining to some aspects of the data obtained by CRIEPI and reproduced in this report. These comments are as follows.

Shear wave speeds measured with down-hole, cross-hole and suspension logging, are consistently greater than those inferred from laboratory tests on samples collected by ground freezing techniques from the gravelly soil layer at and below the depth of the model foundation (5 m below the ground surface). The reasons for such discrepancies are not known at present. These discrepancies have been attributed to possible samples disturbance resulting from high fine contents of the order of 15 to 25%. They may be the result of numerous pebbles or cobbles as large as 10 to 20 cm in diameter that would require testing specimens greater than those used, or a result of the difficulty to obtain in-situ shear wave speed measurements for a gravel with numerous pebbles or cobbles as large as 10 to 20 cm in diameter. They may also be the result of soil anisotropy as discussed below.

In-situ saturated densities recommended by CRIEPI for the as-built backfill soil and the gravelly soil to a depth of about 20 m below the ground surface (GL 0m) are about 2,390 kg/m3 (a dry density of 2,200 kg/m3) and 2,420 kg/m2, respectively. These are unusually high densities, which are similar to those of concrete. The gravelly soil is a well-graded soil for which coefficients of uniformity of the order of 150 to 400 were computed. Such a gradation may lead to a very low void ratio, which would explain the high bulk density of this soil. The backfill soil is not well graded, and its reported dry density of about 2,200 kg/m2, which is based on the quality control tests conducted for the backfill compaction, is unusually high for a compacted soil. It is also noted that the dry densities for the reconstituted backfill material used to establish the variation of the secant shear modulus and damping ratio with shear strain (see Figure 33 in the report) are about 10% less than that recommended for the in-situ conditions for FVT-2 analysis.

A Poisson's ratio of 0.48 is recommended for the backfill soil between GL-2m to GL-4m (backfill 2 in Figure 6) for the FVT-2 analysis. The Poisson's ratio for this soil computed from measured S and P wave speeds is 0.24. Full saturation must be assumed for a Poisson's ratio of 0.48. It is improbable that the backfill soil from GL-2m to GL-4m would have been fully-saturated at the time of the FVT-2 test. Full saturation is more likely in early 1994 when significant earthquake loads were recorded at the site. Nevertheless, full saturation will depend on whether the depth of the groundwater table at the site remains approximately equal or changes significantly from year to year and/or throughout the year.

Cross-hole logging results reveal S wave speeds from GL-5m to about GL-12m that appear to be significantly different in two approximately orthogonal directions both before excavation and after construction of the model. The data, however, show considerable scatter and the difference between the wave speeds in the two orthogonal directions is apparent only in terms of the averages of the measurements in each direction. Prior to the forced vibration tests, the possibility of anisotropic site conditions with two principal directions of shear wave propagation in the horizontal direction was not expected. The forced vibration test data and the recorded earthquake ground motion data, however, reveal that this anisotropy appears to be the actual site condition.

Soil anisotropy may also be responsible, in part, for the smaller shear wave speeds inferred from the laboratory testing as compared to those from in-situ shear wave speed measurements. Assuming that the soil anisotropy is preserved through the sampling process, the shear deformation of the soil under torsional and triaxial loading conditions is not likely to be representative of the soil stiffness in the strong direction. Indirect evidence of this is that the shear wave speeds in the sands measured in the laboratory are not less than those measured in the field, and the sands encountered in the upper 5 meters appear to be isotropic. It is also possible that the soil anisotropy is not preserved during sampling and that a simple consolidation of the specimen under isotropic stress conditions will not properly reconstitute the in-situ conditions. Shear strength parameters for the gravelly obtained from triaxial testing are also likely to be affected by anisotropy and the triaxial test results are more likely to be representative of the soil strength in the weak direction rather than that in the strong direction, if the soil strength is anisotropic as the shear stiffness appears to be.

Forced vibration test (FVT) data were analyzed to assess the suitability of the soil models proposed by CRIEPI for the analysis of those forced vibration tests. Analysis of the forced vibration test data permits the identification of two sets of soil properties that provide the best correlation between the measured and computed FVT-1 (without embedment) and FVT-2 (with embedment) responses, and are designated the best-estimated soil properties for FVT-1 and FVT-2, respectively. Of greater interest for the interpretation of the SSI response under earthquake loading are the best-estimated soil properties for the embedded foundation. These best-estimated soil properties account for the site anisotropy, are average values over the volume of the gravel soil beneath the foundation and over the backfill height, and are suitable for SSI analysis under low-level earthquake loading, i.e., such that the response remains in the linear, low-strain, range. For stronger earthquake loads, they should be coupled with the nonlinear stress-strain parameters obtained by CRIEPI and described in this report, in order to obtain constitutive models with various degrees of sophistication for the soils at the site.

The following observations and conclusions can be made on the basis of the review and analysis described in this report:

1. Analysis of the forced vibration test data indicated that the soil model proposed by CRIEPI could not reproduce well the observed results. Specifically, analysis of the forced vibration test data prior to the construction of the backfill (FVT-1) revealed anisotropic in-situ conditions for the gravel beneath the foundation, with different shear wave propagation speeds in different horizontal directions. The causes of the gravel anisotropy, however, still remain to be explained. Analysis of the forced vibration test data for the embedded case (FVT-2) permitted identification of average soil properties for the backfill and foundation soil.

2. On the basis of the FVT-2 data analysis a set of soil parameters denoted the best-estimated soil properties for FVT-2 are recommended for the soil-structure interaction analysis of the model under low-level lateral dynamic loading, including earthquake loading, i.e., lateral loading such that the response remains in the linear, low-strains, range. The values recommended are spatial averages. Namely the value for the foundation soil is an average over the volume of the soil beneath the foundation to a depth of 12 m below ground level, and the value for the backfill soil is an average over the height of the backfill. The values recommended here differ somewhat

from those proposed by CRIEPI, with the major difference being the identification of anisotropy in the foundation soil.

3. For strong lateral dynamic loading, including earthquake loading, such that non-linear soil behavior is anticipated, the best-estimated soil properties for FVT-2 should be used together with the values obtained by CRIEPI for the properties that describe the non-linear soil behavior. These properties include, at a minimum, the variation of the secant shear modulus and damping ratio with shear strain. For more sophisticated constitutive modeling, appropriate for nonlinear time-history analysis, additional soil properties such as shear strength parameters, soil response under cyclic hydrostatic loading, and the secant shear modulus for triaxial compression tests, were obtained by CRIEPI and are reported here. However, all properties needed for nonlinear soil modeling have been determined on the basis of laboratory testing and may not account for the in-situ soil anisotropy.

4. The site investigations conducted by CRIEPI focused primarily on the soils encountered to a depth of about 20 m below ground level. The site characterization for depths greater than about 20 m relies on scoping geophysical studies conducted by the IES either on the planning or preliminary stages of the Hualien SSI Experiment and large penetration test data at one location. A more detailed characterization of the free-field soils at depths greater than 20 m below ground level may be desirable for site amplification and deconvolution analysis studies for correlation analysis with the ground motions recorded in the down-hole arrays, which extend to a depth of about 52.5 m below ground level.

5. A very comprehensive and rigorous site characterization program was conducted by CRIEPI between 1990 and 1994, which was at least as thorough as those commonly used for actual power plant sites. Nevertheless, considerable scatter can be observed on the data collected, particularly, for the in-situ shear wave speed measurements. Some of the scatter is the result of the soil anisotropy and some may be the result of random spatial variability of the shear wave speed. However, large uncertainties can still be observed even when the soil anisotropy is taken into consideration. Even greater scatter was encountered in the identification of the shear wave speed in the backfill.

6. Average values, averaged over a given soil volume, of the shear wave speeds were recommended by CRIEPI and in this study. Such spatial averages are useful for SSI analysis with the so-called spring method of analysis but may create difficulties with the more detailed and comprehensive finite element procedures whose results may be sensitive to local variations of the soil properties.

7. After the FVT-2 test, the shear wave speeds initially proposed for the as-built backfill (Phase IV-A) were found to be much too large and not representative of the backfill conditions near the containment walls. New in-situ tests were conducted (Phase IV-B) which lead to shear wave speeds in the backfill near the containment wall about 30 percent less that those initially estimated.

8. Cross-correlation analysis of earthquake ground accelerations recorded with the down-hole array indicates that the vertical shear wave propagation speed in the gravel differs significantly for particle motions in the NS and EW directions, with the larger wavespeeds in the NS direction. Those results were confirmed by cross-spectral density analysis of recorded down-hole ground accelerations conducted by CRIEPI.

9. The fundamental soil-structure interaction frequencies under some of the recorded earthquake loads computed using the best-estimated soil properties for FVT-2 are 15 to 20 percent greater than those identified on the basis of the recorded responses. This, implies that non-linear effects may have influenced the soil-structure interaction under the recorded loads. It is noted that the earthquake loads recorded are considered to be weak to moderate as compared to the seismic design loads (SSE) for most nuclear power plant seismic category I structures.

10. A limited sensitivity analysis of the SSI response under two recorded earthquake loads was conducted using a cross-anisotropic spring model for SSI analysis. Equivalent linear parameters were found which provided a fair agreement between the observed and computed responses. Floor response spectra were predicted well with the equivalent linear system for frequencies greater than about 4.5 Hz, which includes the apparent fundamental SSI frequencies. However, the floor response spectra ordinates computed with the equivalent linear system were smaller than those observed for frequencies between about 1.5 and 4.5 Hz.

11. Transfer functions from the free-field motion to the roof response under recorded earthquake loading show evidence of site anisotropy beneath the foundation. Since the effects of the site cross-anisotropy were not significant for the embedded foundation under the forced vibration testing (FVT-2) as a consequence of the lateral constraint of the isotropic backfill, this also appears to be evidence of reduction of the backfill contribution to the stiffness and damping of the SSI system.

Uncertainties in the in-situ values of the soil properties were clearly illustrated with the results of the forced vibration tests, which revealed the unexpected effects of site anisotropy in the soil-structure interaction. Site anisotropy is not normally considered in most soil-structure interaction studies. This experiment indicates that, however, that the cross-anisotropy might occur.

Apart from the site anisotropy, the site characterization results show that considerable scatter in the in-situ values of the soil properties is still present even when thorough and sophisticated site characterization procedures are used. While spatial averages of the measured values may be adequate for SSI analysis with the simple spring method, the spatial variability of the soil properties creates difficulties for detailed finite element models whose results may be sensitive to localized variations in the soil properties.

Modeling uncertainties are, however, more evident in the analysis of the response under earthquake loads. The results of the experiment indicate that non-linear soil behavior seems to be have occurred under weak earthquake loads. The behavior of the model under a more severe earthquake loading remains to be observed. In face of the already observed non-linear effects under weak earthquake loading and the unexpected effect of soil anisotropy, it appears worthwhile to extend for some time monitoring of the instrumentation already installed for the Hualien SSI experiment.

Furthermore, more detailed analysis of the recorded earthquake data at the site should also be continued. This analysis should address the following: (1) site amplification and deconvolution analysis studies, including the effect of soil anisotropy; (2) the adequacy of nonlinear time-history analysis procedures used in conjunction with simplified SSI methods such as the spring method, and of equivalent linearization procedures used with complex finite element methods, to represent the localized non-linear effects observed under earthquake loads; (3) the effects of kinematic interaction and wave scattering in the response; and (3) the sensitivity of the response under earthquake loading to modeling and parametric uncertainties, including site cross-anisotropy and non-linear effects.

ACKNOWLEDGEMENTS

The authors wish to acknowledge the contributions to this study of Professors C. A. Miller and C. J. Costantino of the City College of New York (CCNY). A special acknowledgement is given to Mr. Herman Graves, the Project Manager of the Hualien SSI Experiment for the Nuclear Regulatory Commission. Recognition is also due to Dr. H. T. Tang of the Electric Power Research Institute who directed the consortium of researchers conducting the Hualien SSI project.

The authors also gratefully acknowledge the permission given by CRIEPI to publish (adapt or reprint) figures and tables from several of its publications and handouts to the consortium members that are directly related to their site characterization work for the Hualien SSI experiment.

1. INTRODUCTION

The primary objective of the Hualien Soil-Structure Interaction Experiment, also known as the Hualien Large Scale Seismic Test (LSST), is to obtain seismic soil-structure interaction (SSI) data for stiff soil site conditions that might resemble those encountered at prototypical nuclear power plant sites. Specifically, the objectives of the Hualien LSST project can be summarized as follows (Tang *et al.,* 1991):

1. To obtain SSI data under earthquake loads at a stiff soil site having soil conditions similar to those encountered at prototypical nuclear power plant sites;
2. To verify the applicability for prototypical plant sites of the SSI methodologies and findings qualified against the Lotung LSST;
3. To quantify issues such as structural deformation, torsional response, spatial in-coherency effects and others, that could not be investigated or lacked resolution during the Lotung study;
4. To further promote and develop the technical approaches for realistic SSI analysis;
5. To support the resolution of USI A-40 - Seismic Design Criteria - (Shaukat, Chokshi and Anderson, 1989).

A international consortium was established to carry out the Hualien LSST project. The consortium consisted of: the Electric Power Research Institute (EPRI), the Taiwan Power Company (Taipower), the U.S. Nuclear Regulatory Commission (NRC), the Tokyo Electric Power Company (TEPCO), the Central Research Institute of the Electric Power Industry (CRIEPI) of Japan, the French Commissariat A L'Energie Atomique (CEA), the Electricite de France (EdF) and Framatome. To accomplish the program objectives, the following tasks were initially planned by the consortium:

1. Site characterization
2. Model design and construction
3. Instrumentation layout and implementation
4. Forced vibration testing
5. Analytical evaluation
6. Synthesis of results and findings
7. Development of technical guidelines for realistic SSI analysis approaches

ARA acted as a subcontractor to the City College of New York (CCNY) and they were the primary technical contractor for the NRC for the Hualien SSI Experiment. The scope of work done by ARA was, primarily, to assist CCNY and the NRC with: (1) site characterization issues and the development of site models, and (2) the review of the instrumentation plan for the project. Specifically, during the course of the project ARA reviewed and analyzed geologic and soil data obtained by others, recommended in-situ measurements to improve the reliability of soil data, recommended soil parameters for use in analytical calculations, and reviewed the suitability of the instrumentation plan and instruments developed and/or installed by others.

In this report, a review and assessment of the geotechnical site characterization is presented. The summary and review of the instrumentation plan are included as part of the CCNY report on the Hualien SSI experiment. Since the geotechnical investigations for the Hualien SSI experiment were divided into several phases that took place over a number of years, a chronological review of those investigations has been selected in order to facilitate the interpretation of the results obtained. The report presents a detailed description of the methods used and of the results obtained as well as an assessment of those results and of the recommended soil parameters. This review is followed by analysis of the forced vibration test data and selected recorded earthquake loading data, for further interpretation and evaluation of site conditions and soil parameters to be used in analytical calculations. The report concludes with a summary of the major findings and uncertainties encountered in the site characterization and their implications on the interpretation of the results of the experiment and on soil-structure interaction analysis procedures, as well as recommendations for further studies related to the Hualien SSI experiment.

2. SOURCES[1]

The site characterization program for the Hualien SSI experiment was, primarily, developed and conducted by CRIEPI. The program which included soil sampling by ground freezing techniques, large penetration tests (LPT), seismic refraction surveys, PS-logging, laboratory soil testing and analytical soil modeling, was divided into several phases executed between 1990 and 1994. At the planning phases of the project, scoping geologic and soil data were obtained by the Institute of Earth Sciences (IES) of the Academia Sinica and by United Geotech, Inc. on behalf of Taipower. The major sources for this review are, therefore, the results of studies conducted or sponsored by members of the consortium such Taipower and CRIEPI. Under the consortium agreement, data generated for the Hualien SSI project by a member of the consortium are available to all members[1]. The primary sources used for this review consist of:

1. Institute of Earth Sciences (IES), "Briefing on Hualien Stiff Site," (slides summarizing results of a preliminary study by IES of the Hualien site).
2. United Geotech, Inc., *(1990),* "Final Report of Geophysical Survey at Hualien Stiff Site for Lotung Large Scale Seismic Test Program," prepared for Taiwan Power Company, February.
3. CRIEPI, (1991), "Interim Report on the Geotechnical Investigation (Oct. to Dec. 1990) of Hualien Site," *CRIEPI*, August.
4. CRIEPI, (1992), "Interim Report on the Geotechnical Investigation Results of Hualien Site (Part 2)," *CRIEPI,* April.
5. CRIEPI, (1993a), "Status Report on Geotechnical Investigation at Hualien Site," *CRIEPI*, January.
6. CRIEPI, (1993b), "The Unified Model of the Ground for FVT-1 Analysis," *CRIEPI*, January 15, 1993, (addendum: fax to H. L. Graves, US NRC from T. Kokusho, CRIEPI, March 13).
7. CRIEPI, (1993c), "On the Unified Model for Analysis," *CRIEPI*, April.
8. CRIEPI, (1993d), "The Unified Model of the Ground for FVT-2 Analysis," *CRIEPI*, July 23.
9. CRIEPI, (1993e), "Main Results of March'93 CRIEPI Investigation," *CRIEPI,* November 1.
10. CRIEPI, (1993f), "Raw Data of Laboratory Test Results of Backfill Material," *CRIEPI,* November.
11. CRIEPI, (1994a), "Status Report on Geotechnical Investigation at Hualien Site," *CRIEPI*, January, 1993, rev. June 7-8, 1994.
12. CRIEPI, (1994b), "Digital Data of $G/G_0 \sim \gamma/\gamma_r$ and $h \sim G/G_0$ Relations of the Backfill Material for Numerical Analysis," *CRIEPI*, June 7~8.
13. CRIEPI, (1994c), "Additional Geophysical Survey on the Gravel Ground and the Backfill in 1994," *CRIEPI,* June.
14. CRIEPI, (1995a), "Non-Linearity of Ground Materials," *CRIEPI*, April, 18.
15. CRIEPI, (1995b), "Result of the Additional Geotechnical Site Soil Investigation: Focusing on the Survey of the Heterogeneity of Backfill and Foundation Gravel Zones Around the Part Just Underneath the Contact Plane Carried out Partly in April'94 and Mainly in October'94 by CRIEPI," *CRIEPI,* July.

---

[1] The authors have the owners permission to publish (adapt or reprint) figures and tables provided in the sources listed.

Other sources, which are listed only in the REFERENCES section of this report, include:

1. Technical articles presented at the 11th, 12th and 13th SMiRT Conferences held in 1991, 1993 and 1995, respectively, and at the 11th World Conference on Earthquake Engineering held in 1996;
2. Reports describing the instrumentation, forced vibration tests and earthquake data collected as part of the Hualien SSI experiment; and
3. Prediction and correlation analyses conducted by members of the Hualien SSI experiment consortium or their contractors for the forced vibration tests and recorded earthquake events.

All sources are referred to as needed[1]

---

[1] The authors have the owners permission to publish (adapt or reprint) figures and tables provided in the sources listed.

3. GENERAL SITE DESCRIPTION

The site for the Hualien SSI experiment is located in an area of high seismicity along the east coast of Taiwan, as shown in Figure 1, which was subjected in the past to about as many destructive earthquakes as the site for the Lotung SSI experiment (Tang *et al.*, 1991). According to a study performed by Taipower and the Institute of Earth Sciences (IES) of the Academia Sinica, the geology of the Hualien site is part of the Milun formation which, in general, consists of unconsolidated, massive and poorly-bedded conglomerative composed of pebbles with diameters varying from 10 to 20 cm (4 to 9 in.). The gravel at the site is made up of the by-products of metamorphic rocks such as quartzite, chlorite schist, graphite schist and crystalline limestone. Geologic logging identified the following soils at the site: a backfill material from 0 to 0.85 m depth; a silty sand with little gravel from 0.85 m to about 5.40 m depth; and a gravel with medium to coarse-grained sand from about 5.40 to about 50.0 m.

The location of the groundwater table at the site appears to have significant fluctuations. Accordingly, it was measured to be at 2.0 m to 4.4 m below grade in September of 1989, whereas a measurement in April of 1990 reported a measurement of 0.66 m below grade. There appears to be some uncertainty as to the depth of the groundwater table at the site.

Geophysical and boring tests conducted in 1989 by United Geotech, Inc. (United Geotech, Inc., 1990) for Taipower, indicated the presence of a gravel formation extending to a depth of about 125 to 140 m, underlain by a mudstone formation with a thickness of about 130 m, which is likely to be underlain by metamorphic rocks. The P and S wave velocities identified by United Geotech, Inc. (1990) are as given in Table 1.

Table 1. P and S wave speeds at the site from a preliminary geophysical survey

Depth	**Lithology**	**P-wave Speed (m/sec)**	**S-wave Speed (m/sec)**	**Comment**
1.4 - 5 m	Overburden sand and gravel	400	133	V_P : refraction data V_S: down-hole data
5 - 50 m	Gravel formation	1800 – 2000	333 - 556	V_P: refraction and reflection data V_S: down-hole data
50 - 140 m			–	
140 - 270 m	Mudstone material	~2700	–	V_P: reflection data
> 270 m	Underlying rock	~3200	–	V_P: reflection data

The wave speeds shown in Table 1 are to be used for qualitative assessments only.

Shear wave speeds from 18.5 to 200 m depth were measured with a PS-logging survey conducted by the Institute of Earth Sciences (IES). The values obtained have been reported by CRIEPI (1993d) and are shown in Table 2.

Table 2. Shear wave speeds from 18.5 m to 200 m from a IES survey

Depth (m)	18.5 - 47.0	47.0 - 70.0	70.0 - 116.5	116.5 - 160.0	160.0 - 176.0	176.0 - 200.0
V_S (m/sec)	478	545	502	624	667	885

Initial soil borings and LPT tests conducted by CRIEPI (CRIEPI, 1991) revealed that the top 5 m below ground level consist of loose to medium silty sand and the layer below consists of dense to very dense gravelly soils with gravel size particles ranging from 3 cm to 7 cm.

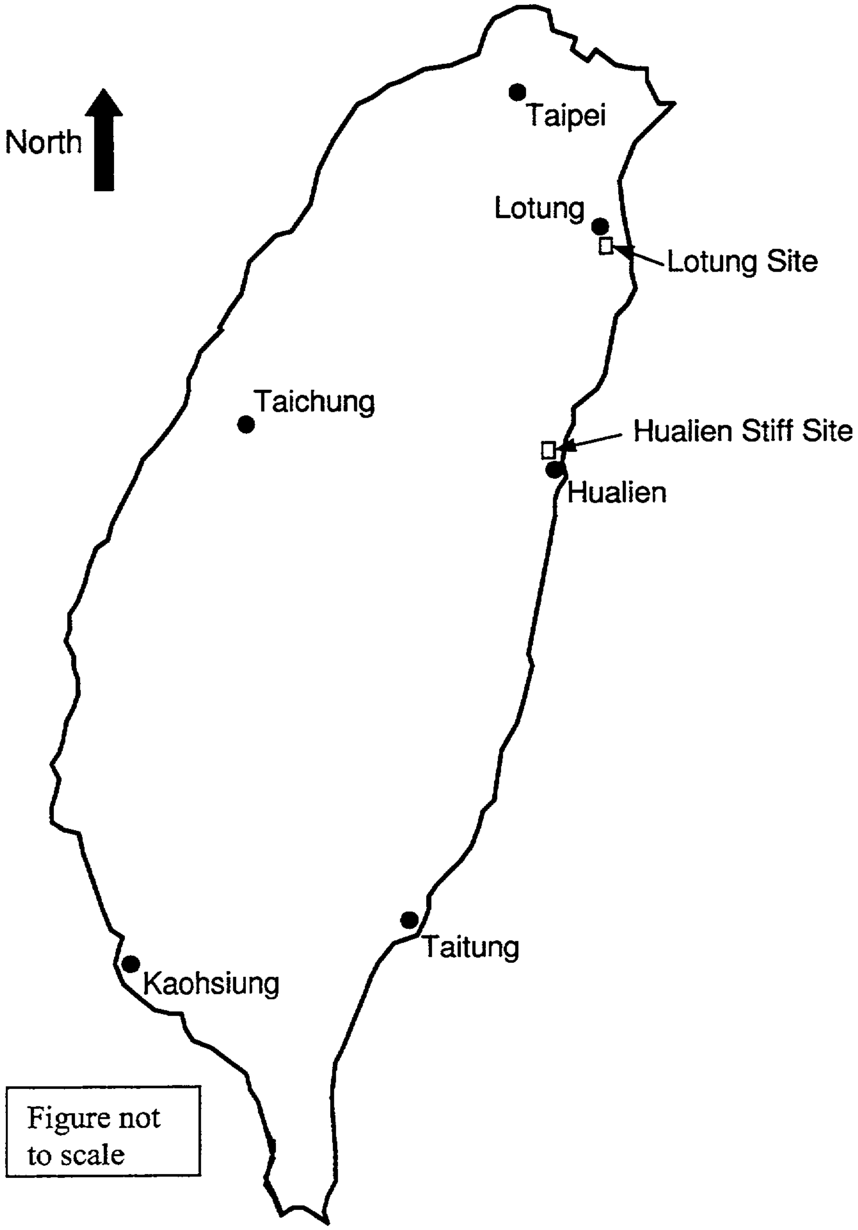

Figure 1 Location of Hualien and Lotung large scale seismic testing sites [from Tang *et al.*, 1991]

4. SPECIMEN STRUCTURE

A brief description of the test model is presented here. This description is needed to identify critical dimensions, the shape of the model and some of its material properties, as well as the various soil zones, including the backfill, for which detailed geotechnical characterizations are required. It is also needed for the interpretation of the forced vibration and earthquake loading data.

The test specimen is, approximately, a ¼-scale model of typical commercial reinforced concrete cylindrical containment buildings in the USA, France, Taiwan and Japan. A cross-section of the model before construction of the backfill together with some of its relevant dimensions are shown in Figure 2. The diameter of the cylindrical shell portion of the model is about 10 m and its wall thickness is 0.30 m. The total height of the model is 16 m, which includes a 3.0 m thick foundation slab and a 1.5 m thick roof slab. The total weight of the model is about 14,000 kN, which is more than ¼ of the prototype weight in order to achieve the desired soil-structure interaction frequency requirements and soil bearing conditions. The foundation plate of the model was placed on the top of the dense to very dense gravelly soil layer at a depth of 5 m below the ground surface (GL -5m), which is the approximate location of the horizontal boundary between the uppermost loose to medium sand layer and the dense to very dense gravelly soil layer.

Material properties of the concrete shell are, approximately: Young's modulus, E_c = 28,200,000 kN/m^2 (4,093 ksi); unit weight, $\gamma_c = 24.5$ kN/m^3 (156 pcf); and Poisson's ratio $\nu = 0.2$.

A plant north has been defined for the Hualien LSST (TECPO, 1993a). As indicated in Figure 2, the plant north is obtained by rotating 41.25^0 from the magnetic north to the west. This direction coincides with the alignment of the entrance to the marble plant facility where the SSI experiment is located as discussed below (see Figure 5), which is a direction of significance for the site characterization as discussed in the next chapter. The assumed plant north direction was defined and used as a reference direction for the forced vibration tests. In fact, lateral loading directions for the forced vibration tests were in the assumed plant NS and plant EW directions and, accordingly, horizontal displacement responses for those tests were also recorded in those two assumed directions. This convention was not used for any other purpose during the HLSST experiment.

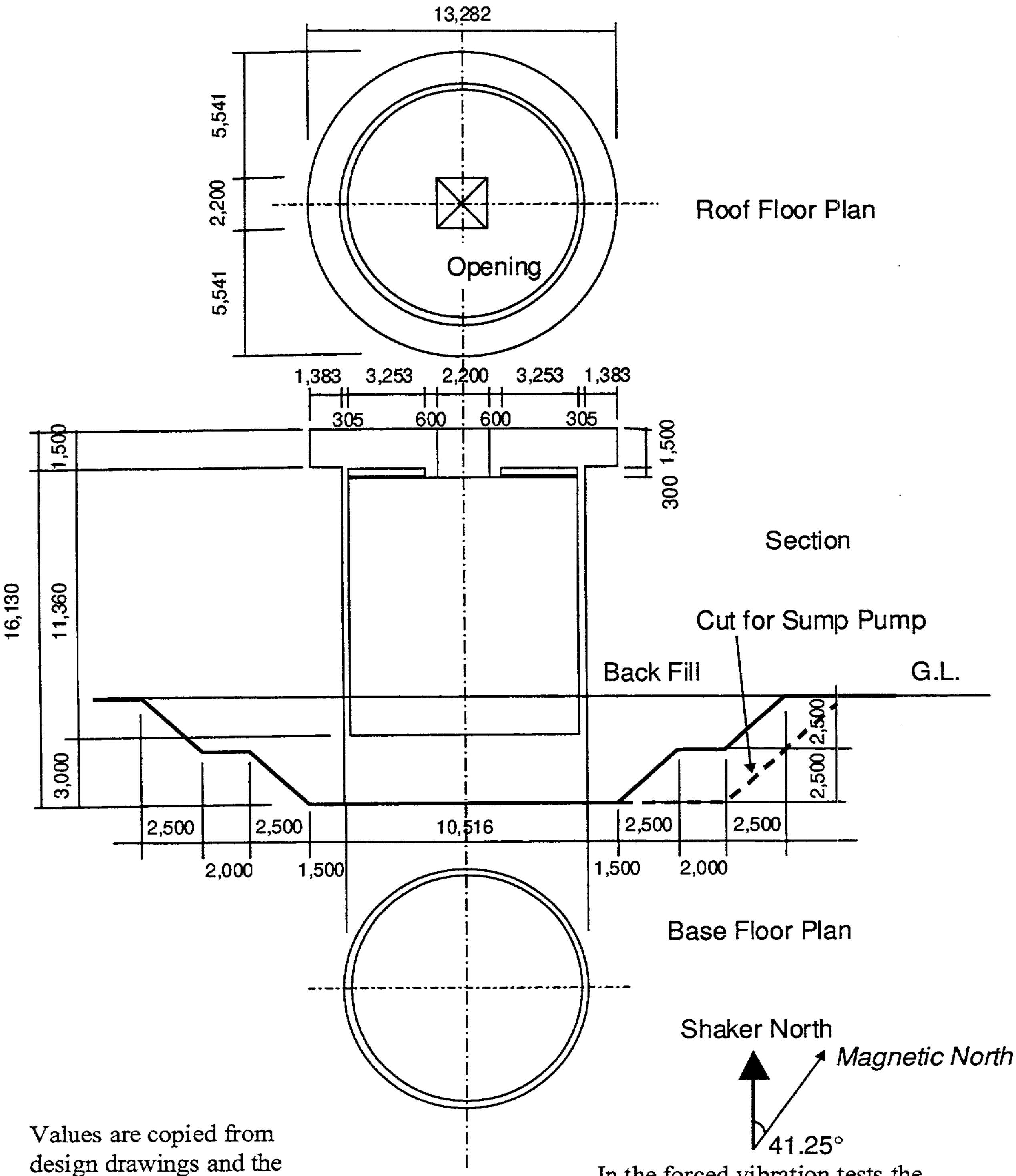

Values are copied from design drawings and the figure is not to scale.

In the forced vibration tests the shaker north is obtained by rotating 41.25° west from the *magnetic north.*

Figure 2. Structure and foundation of containment model (all dimensions are in mm) [Morishita et al., 1993, TEPCO, 1993a]

5. GEOTECHNICAL INVESTIGATION

In-situ testing, soil sampling and laboratory testing were extensively conducted to quantify the properties of the natural soils and backfill deemed relevant for the interpretation and prediction of the test results. In particular the following aspects were given special attention: (1) location of layer boundaries; (2) in-situ soil density, shear wave speed and material damping at small-strains; (3) nonlinear stress-strain properties, i.e., variation of damping and secant shear modulus with strain; (4) water saturation; (5) spatial variation of soil properties; and (6) testing and characterization of the as-built backfill material.

The site characterization program was designed to address the need for accurate soil properties at the various phases of the Hualien SSI experiment. The Hualien LSST requires that the model structure be subjected to forced vibration tests before and after construction of the backfill in order to investigate the effect of embedment in the soil-structure interaction. Since the shear wave speeds of the cohesionless soils encountered at the site depend on the effective confining pressure, the soil properties beneath the model foundation and its proximity are expected to change during the various phases of the experiment as a result of excavation, model construction and backfill placement and compaction. To address those needs, the site characterization program by CRIEPI consisted of a initial site characterization using soil borings and large penetration tests (LPT) and the following 4 phases:

I. The collection of undisturbed soil samples and the performance of a series of geophysical tests prior to the excavation operations required for the model foundation.

II. Geophysical tests and the collection of undisturbed soil samples following the excavation operations.

III. Geophysical tests conducted after construction of the model and before the backfill placement, which are needed to interpret the results of forced vibration tests without embedment.

IV. Large penetration tests and geophysical tests conducted after placement of the backfill, which are needed to establish the soil properties required to interpret the forced vibration tests with embedment and the model response to earthquake loading.

Laboratory tests were, of course, conducted on the soil samples collected in the various phases indicated above. Analyses were also conducted to simulate the effect of excavation, de-watering, containment bearing pressure and backfill placement on the effective stresses.

For further reference, a general view of the Hualien site, which is located inside a marble plant facility in Hualien, as well as views of the LPT boring locations and refraction survey lines for the initial subsurface exploration are shown in Figures 3, 4 and 5, respectively. Also for further reference, the soil layers and soil types for which detailed geotechnical characterization was conducted are shown in Figure 6.

5.1 *Initial Site Characterization Using the Large Penetration Test (LPT)*

The large penetration test (LPT) is a penetration test similar in concept to the standard penetration test (SPT) and was especially developed to investigate gravelly soils in Japan. Like the SPT, the LPT allows for the collection of disturbed soil samples and the measurement of the penetration resistance of the soil in terms of the numbers of blows required to achieve a standardized penetration of the probe. Specifically, the LPT penetration resistance, N_{LPT}, is measured by the number of blows by a free-falling mass of 100 kg dropping from a height of 150 cm required for a 30 cm penetration of the probe. Detailed LPT description and comparisons between the LPT and SPT can be found in Yoshida *et al.* (1988). In particular, an empirical relation used by CRIEPI (CRIEPI, 1993a) is as follows: $N_{SPT} = 1.5 \times N_{LPT}$ for sand and $N_{SPT} = 2.0 \times N_{LPT}$ for gravel.

LPT locations are shown in Figures 4 and 5 (locations B1, B2, B3, B4 and B4′). Disturbed soil samples were also collected at those locations for further laboratory testing for soil classification purposes. For further reference, it is noted that boreholes B3, B2 and B1 are not aligned in either the actual NS direction or the so-called plant (or shaker) NS direction as shown in Figure 5.

Table 3. LPT results (reproduced from CRIEPI, 1993a)

Depth (m)	**B-1**	**B-2**	**B-3**	**B-4**	**B-4′**
1.15 - 1.45	5	5	6	6	--
2.15 - 2.45	7	5	5	6	--
3.15 - 3.45	9	5	7	8	10
4.15 - 4.45	8	7	7	15	--
5.15 - 5.45	28	22	28	36	--
6.15 - 6.45	25	33	29	33	25
7.15 - 7.45	33	25	30	28	--
8.15 - 8.45	38	21	28	21	--
9.15 - 9.45	33	22	25	19	27
10.15 - 10.45	38	25	30	29	--
11.15 - 11.45	24	36	28	24	--
12.15 - 12.45	23	46	23	36	30
13.15 - 13.45	29	23	35	44	--
14.15 - 14.45	25	41	25	30	--
15.15 - 15.45	33	39	25	49	39
16.15 - 16.45	35	56	26	49	--
17.15 - 17.45	40	30	26	52	--
18.15 - 18.45	30	44	33	59	41
19.15 - 19.45	32	--	27	60	--
20.15 - 20.45	31	--		66	--

Large penetration tests were conducted to about GL-20m at boreholes B1, B3, B4 and B4′ and to about GL-40m at borehole B2 which is located under the center of the model foundation. N_{LPT} values ranged from 5 to 10 for the sandy soils encountered in the upper 5 m and from 20 to 40 for the gravelly soils encountered from GL-5m to GL-20m (CRIEPI, 1991, 1992 and 1993a). Correlations between LPT measurements and soil index properties indicate a loose to medium sandy soil down to GL-5m and a dense to very dense gravelly soil from about GL-5m to GL-20m. This pattern was consistently observed at all locations where large penetration tests were conducted, which indicates an approximately horizontal boundary between the two soil layers at about GL-5m. The results reported by CRIEPI are shown in Table 3 above.

5.2 *Seismic Refraction and PS-Logging*

A summary of the geophysical surveys initially planned for the site characterization is presented below. Those surveys took place between November of 1990 and June of 1993. However, it was determined late in 1993 that a new series of in-situ tests including geophysical surveys were needed to better characterize the in-situ soil properties of the as-built backfill in the vicinity of the model. Those new tests were conducted in April and October of 1994 and are addressed in Section 5.2.4 below.

Refraction Surveys. – Refraction surveys were conducted early in the site investigation, before excavation, along two 115-m lines that passed through the center of the model and are denoted line-A and line-B. As shown in Figure 5, Line-A runs in the direction of boreholes B3 and B5 and line-B is inclined 45^0 counterclockwise with respect to line-A. Elastic waves generated at a point in each of the seismic lines were picked up by geophones spaced at 5-m intervals along line-A and line-B. Pulses for the P and S waves were generated by the vertical and horizontal strike of a sledge-hammer on the top and side of plank placed on the surface of the ground. For the S wave generation the plank was stabilized by the weight of the front wheel of a van. After excavation, refraction surveys were also conducted along those same directions but on two 10-m long seismic refraction lines.

To measure the shear wave velocities in the backfill, refraction surveys were conducted following its construction along three 10-m long lines denoted A-line, B-line and C-line and one 5-m long line denoted D-line, all located in the proximity of the model as shown in Figure 7.

Down-Hole Logging. -- A schematic representation of the down-hole logging procedure utilized is shown in Figure 8. P waves were generated by a vertical blows of a sledge-hammer to the top of a plank placed on the ground surface, whereas S waves were generated by horizontal strikes to the side of the plank which was stabilized by a vertical weight. Down-hole loggings were conducted at borings A1, B2, B2′, B5, and B6 whose locations are shown in Figures 4 and 9.

P and S wave velocities were measured at A1, B2, B2′, B5 and B6 before the excavation, at A1 and B3 after the excavation and before the backfill construction, and at A1 and B2′ after backfill construction.

Cross-Hole Logging. – A schematic representation of the cross-hole procedure utilized is shown in Figure 10. S wave motions were created within the source borehole using a S-wave generator. Wave propagation paths for the cross-hole loggings are shown in Figure 9. S wave velocities were measured on three different paths identified as follows:

1. Method A, for shear waves generated at B2′ and received at B5, A3 and B6;
2. Method B, for shear waves generated at A2 and received at B2′, A3 and B6; and
3. Method C, for shear waves generated at A4 and received at B2′ and A1.

Except for the A-method from B2′ to A3, S wave velocities were measured by those 3 methods before excavation, after excavation and after the model construction. After the backfill construction shear wave velocities were measured only the A-method from B2′ to A3.

Following the backfill construction cross-hole logging was conducted between two new boreholes denoted C1 and C2 (see Figure 7) to measure the shear wave speed in the backfill.

Seismic Tomography. – This method is similar to the cross-hole logging and utilized boreholes B2′ and A1. Elastic S waves generated within B2′ were picked up by the geophone set within A1 and 6 velocity gages located between the boreholes and under the containment foundation plate as shown in Figure 11. This model was used after the excavation (phase II) and after the model construction (phase III).

5.2.1 Phase I - Before Excavation

The results of the refraction surveys, down-hole and cross-hole P and S waves speed measurements obtained by CRIEPI (CRIEPI, 1993a) are shown in Figures 12 to 14.

Sand Layer. -- Down-hole measurements indicate a layer down to GL-2m with shear wave speeds V_S = 90 to 130 m/sec, over a layer with V_S = 190 to 230 m/sec that extends to about GL-5m (see Figure 12).

The cross-hole measurements indicate a gradual increase of the shear wave speed from about 150 m/sec to about 230 m/sec from the ground surface to GL-5m (see Figure 12).

The refraction survey results shown in Figure 13 indicate shear wave speeds ranging from 194 m/sec to 158 m/sec along line-A and from 192 m/sec to 182 m/sec along line B. It also identified a nearly horizontal layer boundary at a depth ranging from 5 to 6 m.

Down-hole measurements indicate a P wave speed V_p = 330 to 390 m/sec from the ground surface to GL-2m, and V_p = 880 to about 1200 m/sec from GL-2m to GL-5m (see Figure 14).

From the ground surface to a depth of about 2 m the refraction survey identified P wave speeds ranging from 310 m/sec to 550 m/sec along line-A and from 280 m/sec to 640 m/sec along line-B (see Figure 13). From GL-2m to a depth of about 5 to 6-m the P wave velocities measured by the refraction method ranged from 950 m/sec to 1,150 along line-A and from 850 m/sec to 1,110 along line-B (see Figure 13).

Gravel Layer. -- Down-hole measurements identify a layer with V_S = 310 to 390 m/sec from GL-5m to GL -12m, and a lower layer below GL-12m with $V_S \cong 480$ m/sec (see Figure 12).

Cross-hole measurements indicate shear wave speeds between GL-5m and GL-12m that range from about 270 m/sec to about 400 m/sec (see Figure 12).

S wave speeds from 320 m/sec to 363 m/sec along line-A and from 330 m/sec to 377 m/sec along line-B were measured by the refraction survey to a depth of about 20 m (see Figure 13).

Down-hole measurements shown in Figure 14 indicate P wave speeds ranging from 1250 to about 1500 m/sec from GL-5m to GL-12m, and a P wave speed of about 2270 m/sec below GL-12m.

P wave speeds measured with the refraction method (see Figure 13) range from 1,730 m/sec to 2,050 m/sec for line-A and from 1,660 to 1,800 m/sec along line-B.

A summary of the Phase-I results is shown in Table 4.

Table 4. P and S wave speeds measured before excavation (data from CRIEPI, 1993a)

Depth (m)	**Layer Description**	**Down-Hole**		**Cross-Hole**	**Refraction Survey**	
		V_S (m/sec)	**V_P (m/sec)**	**V_S (m/sec)**	**V_S (m/sec)**	**V_P (m/sec)**
0 - 2 m	Loose to medium sand	90 - 130	330 - 390	Gradual increase from 150 to 230	160 - 190	280 - 640
2 - 5 m	Lose to medium sand	190 - 230	880-1200			850-1150
5 - 12 m	Dense to very dense gravel	310 - 390	1250-1500	270 - 400	320 - 390	1660-2050
> 12 m	Dense to very dense gravel	480	2270	--		

5.2.2 Phase II - After Excavation

As a result of the dependency of the soil shear modulus and, consequently, the shear wave speed on the effective confining stress, it was deemed necessary to determine the shear wave speed in the soil layers following excavation. Comparisons of the S and P wave velocities obtained by CRIEPI before and after excavation are shown in Figures 15 and 16. The general trend is for the shear wave speeds after excavation (labeled 92 in Figures 15 and 16) to be significantly smaller than those before excavation at about GL-5m and to approach the S wave speeds prior to excavation as the depth increases. At about GL-12m the differences in S wave speeds before and after excavation are small.

To establish an empirical relation between the effective confining stress and the S wave speed, laboratory cyclic triaxial tests were conducted on 300 mm diameter undisturbed soil samples recovered from below GL-5m using a ground freezing sampling technique. This procedure lead to an empirical relationship of the form $V_S \propto (\sigma'_{3m})^{0.3}$, where σ'_{3m} is the mean effective confining stress.

This empirical relationship together with the change in mean effective ground stress resulting from the excavation (computed using the solution for a uniformly loaded area on a elastic homogeneous half-space) was used to predict the S wave speed after excavation. Good results were obtained by CRIEPI using this procedure (CRIEPI, 1993a, Kokusho *et al.*, 1993). On this basis, it was concluded that the reduction of the S wave speed following excavation was a result, primarily, of the reduction in confining stress and not the result of soil disturbance from the excavation operations.

The results of the seismic refraction surveys conducted along 10-m long lines oriented as those used in Phase I, indicated P wave speeds from 1820 to 1830 m/sec from GL-5m to GL-8m and S wave speeds from 120 to 150 m/sec from GL-5m to GL-6.5m, and from 240 to 260 m/sec from GL-6.5m to GL-8 m.

5.2.3 Phase III - After Model Construction

S wave speed measurements under the containment were made following construction of the model in November of 1992 using the cross-hole and tomography procedures described above.

The results obtained by CRIEPI are shown in Figure 17 (CRIEPI, 1993c). The measured shear wave speeds show a large scatter with an average value of about 317 m/sec. Furthermore, the values obtained for the S wave velocities were, generally, significantly less than those predicted on the basis of the computed change in effective confining stress, with the exception of those obtained between B2′ and A1.

The results indicate the highest shear wave speeds between B2′ and A1, and the lowest speeds also in the B2′-A1 direction but between A4 and B2′, i.e., the shear wave velocities are higher near the center of the containment and lower near the periphery. It is noted that the velocities near the center of the containment were actually similar to those predict by the change in effective confining stress from construction of the model. Additionally, the velocities measured from A2 to B2′, are less than those obtained along the B2′-B6 and B2′-B5 paths. This, could also be because the A2-B2′ path is affected more by the conditions in the containment periphery than the other two paths.

It is also noted that, the S wave speeds measured in the A4-A1 direction are generally higher than those measured in the directions transverse to it. Also, as shown in Figure 17, average shear wave speeds at a given depth in the A4-A1 direction are considerable greater than average shear wave speeds at the same depth but on the transverse direction. In general, it appears that the average S wave velocities in the A4-A1 direction are greater than those in the direction perpendicular to it. It also seems that the S wave velocities are greater near the center of the containment and smaller near its periphery. This latter observation could be a result of smaller confining stresses near the periphery of the foundation as a result of zero lateral surcharge prior to the construction of the backfill, as well as of more severe soil disturbance near the foundation periphery from excavation and construction operations.

5.2.4 Phase IV - After Backfill Construction

The objectives of the subsurface investigation conducted in this phase were: (I) to determine the dynamic properties of the soils under the foundation following construction of the backfill; and (II) to determine the dynamic properties of the as-built backfill soil.

Early geophysical and laboratory tests for this phase were conducted in March and June of 1993. However, it was later determined that most of the in-situ tests for the backfill soil had been conducted a too great a distance from the model (about 3.0 m) and that additional tests would be needed to characterize the backfill properties closer to the containment walls. Therefore, another series of in-situ tests was carried out in April and October of 1994. Accordingly, this phase is divided into phases IV-A and IV-B for the purposes of this review.

Phase IV-A: March and June of 1993. – CRIEPI performed the following tests:

1. For soils just beneath the foundation:
    1.1. down-hole method at B2′ and
    1.2. cross-hole method between B2′ and A3.
2. For the backfill:
    2.1. soil sampling and laboratory testing,
    2.2. down-hole method at C2,
    2.3. cross-hole method between C1 and C2 and
    2.4. refraction survey along the lines A-D located around the model.

The locations of the new boreholes and seismic refraction lines are shown in Figure 7.

S wave speeds obtained by the down-hole and cross-hole methods for the soil under the model are shown in Figure 18. The down hole data were obtained at two sensors placed 1-m apart. Data from the lower sensor is denoted series-1 whereas data from the upper sensor are denoted series-2. The measured speeds are highest near the base of the model and gradually decrease to about GL-7m. Below about GL-7m the S wave speeds again increase as the depth below the foundation increases. The observed behavior seems to be in agreement with the increase in confining stresses from the containment bearing pressure. From the data shown in Figure 18 an average value of 383 m/sec for the S wave speed was determined by CRIEPI (CRIEPI, 1993f) for the soil beneath the foundation from GL-5m to GL-12m.

The S wave speeds computed from the geophysical tests on the backfill are shown in Figure 19. The cross-hole results which indicate S wave speeds less than those measured by the down-hole method, were deemed to be unreliable because of the difficulty in picking the arrival times of the waves. Therefore, CRIEPI recommended the average shear wave speed from the down-hole method for the as-built backfill soil, V_S = 400 m/sec. These results were later found to be insufficient to characterize the backfill properties in the vicinity of the model.

Phase IV-B: April and October of 1994.

A series of in-situ tests were conducted to better establish the in-situ properties of the as-built backfill soils in the vicinity of the containment. The following tests were performed by CRIEPI (CRIEPI, 1995b) for that purpose:

1. Five LPT tests at locations D1, D4, D5, D6 and D10 to a depth of 15.3 m below grade level (borehole locations are shown in Figures 20 and 21); three LPT tests at locations D3, D8 and D11 to a depth of 5.3 m below grade level; and a SPT at location D9 to 15.3 m below grade.
2. Eight suspension logging tests at boreholes D3, D4, D5, D6, D8, D9, D10 and B6, for direct in-situ measurement of S wave velocities.
3. Three down-hole logging tests at boreholes C1, D5, D6 and D9.

The LPT data are shown in Table 5. The following observations can be made on the basis of the data shown in Table 5 and their comparison with the LPT data from 1990 shown in Table 3:

1. LPT blowcounts around the containment from about GL-5m to about GL-7m are consistently less than those obtained during the initial phase of the subsurface investigation at boreholes B1, B2, B3 and B4; and
2. LPT blowcounts in the backfill range from 10 to 18 but consistently decrease to small values at a depth of about 4.3 m below grade, indicating that the backfill may not be well compacted at that depth (about 4.3 m below grade).

Table 5. LPT and SPT data (reproduced from CRIEPI, 1995b)

Depth (m)	D1	D4	D5	D6	D10	D9 (SPT)	D3	D8	D11
1.3	10	17	17	8	29	23	11	15	12
2.3	14	13	16	14	12	20	10	15	8
3.3	18	7	19	18	14	29	18	24	15
4.3	5	0.42	5	9	10	17	10	5	14
5.3	14	12	31	15	12	16	24	23	
6.3	21	42	33	15	19	31			
7.3	33	26	29	17	26	33			
8.3	22	24	24	70	22	35			
9.3	23	22	37	30	25	53			
10.3	38	20	50	38	24	44			
11.3	47	85	42	39	17	41			
12.3	43	46	33	35	21	87			
13.3	26	43	32	33	20	121			
14.3	30	25	33	41	25	46			
15.3	32	43	57	60	31	87			

With the data collected CRIEPI proposed empirical correlations between the large penetration test blowcount and the S wave speed at the site, as well as a correlation between the SPT and LPT blowcounts. Shear wave speeds measured with the geophysical tests and computed from the correlations with the LPT are shown in Figures 22 to 25 for the backfill and the gravel below the area adjacent to the boundary of the foundation (gravel 2′ in Figure 6), respectively. The data show considerable scatter. The S wave speeds computed from the LPT data appear to show less scatter than those from direct geophysical measurements. However, it must be noted that scatter in the S wave speed correlations with the LPT have not been accounted for in Figures 23 and 25.

On the basis of the results shown in Figures 22 to 25, CRIEPI (CRIEPI, 1995b) suggested average values for the S wave velocities for the backfill in the vicinity of the containment and for the gravel soil in the outer periphery of the foundation from GL-5m to GL-8m, which is labeled gravel 2′ in Figure 6. The suggested average values are shown in Table 6.

Table 6. S wave speeds for soils in the vicinity of the model (reproduced from CRIEPI, 1995b)[1]

Soil Type	Backfill 1 and 2 (GL0 - GL-4m)	Backfill 3 (GL-4m - GL-5m)	Gravel 2′ (GL-5m - GL-8m)
Shear Wave Speed (m/sec)	300	250	280

[1] Soil layers and types are identified in Figure 6.

5.2.5 Poisson's Ratio

Poisson's ratio for the soils were determined based on the P and S wave velocities measured for the various soil layers and zones and taking the average values (CRIEPI, 1993d; CRIEPI, 1995b). The values obtained are shown in Table 7.

Table 7. Poisson's ratios computed from measured P and S wave speeds (reproduced from CRIEPI, 1995b)

Soil Type	Before Backfill (FVT-1)	After Backfill (FVT-2 and Earthquake)
Sand 1 (0 - 2.0 m)	0.38	0.38
Sand 2 (2.0 - 5.0 m)	0.48	0.48
Gravel 1 (5.0 - 12.0 m) (under the foundation)	0.47	0.48
Gravel 2 (5.0 - 12.0 m)	0.47	0.47
Gravel 2' (5.0 - 12.0 m)	0.47	0.47
Gravel 3 (12.0 -20.0 m)	0.47	0.47
Backfill 1 (1 - 2.0 m)	--	0.38
Backfill 2 (2.0 - 4.0 m)	--	0.48[1]
Backfill 3 (4.0 - 5.0 m)	--	0.48

[1] The Poisson ratio for this layer computed from the measured P and S wave velocities is 0.24; a value of 0.48 was suggested by CRIEPI assuming full saturation and a groundwater table at about GL-2m.

5.3 *Soil Sampling*

In addition to the disturbed samples collected with the LPT probe, the sampling methods used by CRIEPI included the collection of undisturbed samples using both non-freezing and freezing sampling techniques as summarized in Table 8 below (CRIEPI, 1993a).

Table 8. Undisturbed sampling methods used (reproduced from CRIEPI, 1993a)

Sample size (for triaxial testing)	Sampling method	Sampling Depth (m)	Date
Silty sand $\phi = 50$ mm, H = 100 mm	Non-freezing sampling	1.0 - 5.0 m	December 1990
Sand and gravelly soil $\phi = 100$ mm, H = 200 mm	Freezing sampling	5.0 - 20.0 m	December 1990
Gravelly soil $\phi = 300$ mm, H = 600 mm	Freezing sampling	5.0 - 6.0 m	March 1992

Non-freezing sampling was performed using a sampler with triple tubes with a inner-diameter of approximately 120-mm especially developed to obtain high-quality samples of sands. The non-freezing sampling locations are indicated in Figure 26. To minimize sample disturbance the samples taken from the ground were frozen while still in the PVC inner tube of the sampler. After freezing the samples, the PVC tube was removed, the samples were cut with a portable saw into parallelepipeds 120-mm long with a 80×80 mm^2 cross-section, and then wrapped and kept in cooling boxes with dry ice for shipping to the laboratory. A detailed description of the samples collected can be found in CRIEPI (1993a). Fine sand, medium sand with boulders and silt were encountered above a depth of about 4 m whereas sand and gravel were encountered below that depth. The samples collected in this manner were later used for testing in a triaxial apparatus for 50 mm diameter samples.

The location of freezing sampling with 100 mm diameter samples are also shown in Figure 26. A detailed description of the freezing sampling method is given in CRIEPI (1993a). With this method the ground was frozen by injecting liquid nitrogen in boreholes located on the sides of the locations from were the samples would be extracted. The sampler used had a inner diameter of 101 mm and a diamond bit at the lower end for coring the samples. A detailed description of the samples is also given in CRIEPI (1993a). Large boulders or cobbles with diameters ranging from 6 cm to more than 20 cm were encountered in the sampled cores particularly between GL-5m and GL-8m. The samples collected were tested in a triaxial apparatus for 100 mm diameter samples.

Frozen samples with 300 mm diameter samples were extracted from the locations shown in Figure 27 using another ground freezing sampling technique. The samples were used for a more detailed investigation of the gravelly soils with boulders and cobbles encountered between GL-5m and GL-6m, in particular to study the effect of sample size (diameter) on the shearing stress-strain relation. With this ground freezing sampling technique, a soil block with an approximate diameter of 1,500 mm and a depth of about 1,250 mm was frozen in-situ by the circulation of liquid nitrogen through the ground and subsequently removed from the ground. This soil block was then placed in a cooling box and bored to remove cylindrical specimens 300 mm in diameter and about 600 mm long. Those samples were tested in a triaxial testing apparatus for 300 mm diameter samples. A detailed description of the sampling process and the cored samples can be found in CRIEPI (January, 1993a).

5.4 *Laboratory Testing*

The Specific gravity and grain-size distribution tests.

1. Soil density testing.
2. Monotonic triaxial extension and compression testing.
3. Cyclic compression tests (triaxial consolidation tests).
4. Strain-controlled and stress-controlled cyclic triaxial tests.

The specific gravity and grain-size distribution tests were performed using disturbed samples and all other

Monotonic static triaxial compression and extension tests were performed to obtain the strength properties of the soils, i.e., effective stress internal friction angle and apparent cohesion, as well as the E_{50} secant shear moduli for the soils, which is the secant shear modulus measured in the triaxial compression tests at a deviatoric stress equal to one-half the deviatoric stress at failure.

The cyclic compression tests were performed to establish the soil behavior for loading and unloading under hydrostatic stresses as needed for constitutive modeling. These tests were conducted using the triaxial apparatuses for 50 and 100 mm diameter samples and especially designed instrumentation as described in CRIEPI (January, 1993a).

Strain-controlled triaxial tests were conducted to determine the nonlinear shearing stress-strain properties for the soils which were given in terms of strain-compatible modulus and damping (*i.e.,* the so-called $G/G_0 \sim \gamma/\gamma_r$ and $h \sim G/G_0$ relations); whereas stress-controlled triaxial tests were performed to determine the undrained cyclic strength of the soils.

5.4.1 Specific Gravity and Grain-Size Distribution

Gravel. -- The specific gravity of the soil particles tested ranges from 2.646 for grain-sizes between 38.1 and 50.8 mm, to 2.798 for grain-sizes between 0.074 and 0.105 mm. In general, the specific gravity was found to be greater for the smaller size particles.

The grain-size distributions for the gravelly soils tested indicate fines content from 15% to 25%, maximum grain-sizes from 25.4 mm to 100 mm and mean grain-sizes from 0.4 mm to 3.5 mm. The gravelly soils encountered were found to be well-graded soils with coefficients of uniformity, C_u, ranging from about 68 to about 437 with most values of the order of 200.

Backfill. – The specific gravity for the backfill soils ranges from 2.651 for grains-sizes between 4.76 and 9.52 mm to 2.753 for grain-sizes less than 0.25 mm. Generally, the specific gravity of the backfill soil particles was found to increase as the grain-size diminished.

Grain-sizes for the backfill soils ranges from 38.1 mm to less than 0.25 mm, with about 8.8% by weight less than 0.25 mm. With a coefficient of uniformity of about 28 and a coefficient of curvature of about 5.5, this is a gap-graded soil according to the USCS standards.

5.4.2 Dry Density

The dry densities for the loose to medium sand and the dense to very dense gravel were calculated from the size, weight and water content of the undisturbed samples obtained by the ground freezing sampling method, and were found to be almost constant through the depth of each layer. The dry densities of the sands and gravels are about 1.5 (g/cm^3) and 2.2 (g/cm^3), respectively. Saturated densities for the sands and gravels were found to be 1.93 (g/cm^3) and 2.42 (g/cm^3), respectively.

The saturated and dry densities of the gravelly soil appear to be extremely high, with the saturated density approximately equal to that of concrete. This appears to be, in part, the result of a well-graded grain size distributions with coefficients of uniformity of the order of a few hundred. It is noted that dry densities of the order of 2.2 (g/cm^3) have been reported for some well-graded silty gravels with similar coefficients of uniformity (Hough, 1969; Holtz and Kovaks, 1982). The densities reported by CRIEPI (CRIEPI, 1993a) may, therefore, be credible for the gravelly soils encountered at the site.

The dry density of the backfill soil was determined by in-situ quality control tests for the backfill compaction performed by Taipower Corporation (TPC), and was found to be almost uniform with depth and approximately equal to 2.22 (g/cm^3) (CRIEPI, 1993f). Dry densities as high as these have been reported for compacted gravelly soils (U.S. Army Engineer Waterways Experiment Station, 1960). The dry densities were used by CRIEPI to compute bulk densities for the backfill assuming the degree of saturation for each layer. On this basis, the total densities of the backfill soil were reported to be: 2.33 (g/cm^3) from the ground surface to GL-2m; and 2.39 (g/cm^3) from GL-2m to GL-5m. Those densities were not altered upon revision of the shear wave velocities of the backfill soils in the vicinity of the model (CRIEPI, 1995b), a revision that resulted in a considerable reduction of the shear wave speed.

5.4.3 Monotonic Triaxial Compression and Extension Tests

Triaxial compression and extension tests were conducted to determine the shear strength parameters of the sand and gravel under monotonic loading to failure. Sand samples were cut to a 5 cm diameter and a 10 cm length, whereas all gravel samples were cut to a 10 cm diameter and a 20 cm length. The specimens were consolidated isotropically and then the axial load was either increased or decreased to failure under drained conditions at a strain rate of 0.5%/min. A detailed description of all samples used and of the results obtained can be found in CRIEPI (January, 1993a). A summary of the principal results thus obtained is given in Table 9.

Table 9. Shear strength parameters under monotonic loading (reproduced from CRIEPI, 1993a)

Soil Type	Triaxial Compression		Triaxial Extension	
	Internal friction angle (degrees)	Apparent cohesion (kN/m^2)	Internal friction angle (degrees)	Apparent cohesion (kN/m^2)
Sandy soil GL-3.56m - GL-4.04m)	27.6	17.2	–	–
Gravelly soil (GL-8.1m - GL-8.9m)	39.7	32.3	35.8 (GL-8.92m – GL-9.54 m)	–
Gravelly soil (GL-17.7m - GL-18.3m)	40.2	94.1	–	–

The relation between the E_{50} secant modulus, *i.e.*, the secant modulus for a deviatoric stress equal to $(1/2)\times(\sigma_1 - \sigma_3)_{\text{failure}}$, and the effective confining pressure, was also obtained from the triaxial compression tests. These relations, which are important for constitutive modeling of the soil, are shown in Table 10.

Table 10. E_{50} Secant modulus vs. effective confining stress (reproduced from CRIEPI, 1993a)

Soil Type	E_{50} Secant modulus vs. Effective confining stress, σ_c' (kN/m^2)
Sandy soil (GL-3.56 – GL-4.04m)	$E_{50} = 838.9\ \sigma_c'^{\,0.70}$
Gravelly soil (GL-8.1m - GL-8.9m)	$E_{50} = 21{,}315\ \sigma_c'^{\,0.40}$
Gravelly soil (GL-17.7m - GL-18.3m)	$E_{50} = 11{,}858\ \sigma_c'^{\,0.55}$

5.4.4 Consolidation Tests

Cyclic hydrostatic (consolidation) tests were also conducted by CRIEPI (CRIEPI, 1992, 1993a) using the triaxial apparatus to obtain parameters required for constitutive modeling of the soils. Non-contact lateral displacement sensors were used to avoid membrane penetration effects. Each consolidation test consisted of a initial isotropic consolidation phase followed by the application of loading-unloading cycles of increasing hydrostatic pressure. Specimen volume changes were, of course, measured at each loading step. Idealized consolidation properties for the sand and gravel obtained on the basis of those tests are given in Table 11 below.

Table 11. Idealized consolidation properties (reproduced from CRIEPI, 1993a)

Soil Type	Mean Effective Stress in (kN/m^2)	Compression Index, C_c	Swelling Index, C_S
Sandy soil	29.4 - 98	0.0226	0.0128
	98 - 294	0.0300	0.0212
	294 - 588	0.0737	0.0226
Gravelly soil	49 - 98	0.00546	0.00446
	98 - 294	0.0152	0.00503
	294 - 588	0.0169	0.00373

5.4.5 Nonlinear Shearing Stress-Strain Relation

Strain-controlled cyclic triaxial tests were carried out to determine the strain-dependency of the secant shear modulus and damping ratio with shear strain (CRIEPI, 1994a) for strains ranging from about 10^{-5} to about 10^{-3}. To establish the secant shear modulus and damping ratios CRIEPI used triaxial tests and the following specimen sizes:

1. 100 mm and 300 mm diameter samples, with lengths of 200 and 600 mm, respectively, for gravel; and,
2. 50 mm and 100 mm diameter samples for sands.

Special instrumentation procedures were used to obtain reliable results. Those procedures included: installation of the load transducers in the pressure cells to avoid friction between the axial rod and the pressure chamber; use of non-contact type displacement transducers without hysteretic damping installed in the pressure chamber; and targets for the displacement transducers attached to the lateral surface of the samples to avoid bedding errors at the sample ends. Accelerometers were also attached to the lateral surface of the gravel samples to measure the shear wave speed in a sample under a given confining pressure subjected to torsional shear waves generated by the blow of hammer on a steel plate projecting from a rod aligned with the axis of the sample.

Conventional triaxial testing procedures used in Japan were used for the soils sampled by non-freezing methods. For the samples obtained by the freezing method special procedures were used as described next. The samples were allowed to thaw completely under drained conditions under a isotropic pressure less than the effective confining stress for cyclic loading. After thawing, the specimens were saturated through a procedure that included the use of back pressure until the B-coefficient became equal to or greater than 0.90. For the cyclic loading the effective confining pressure was, in principle, made equal to the effective overburden pressure. Then, cyclic shear strains at 1 Hz frequency were applied under undrained conditions. After cycling at a given loading level, the specimens were drained to remove any excess pore pressure that might have been generated, and then subjected to undrained cyclic loading at a higher strain level.

Laboratory determination of shear wave speed

Gravel -- The samples depth, effective confining pressure of the test, σ_c', small-strains shear modulus (G_m at $\gamma \approx 5\times10^{-6}$), bulk density and the computed shear wave speed under the test effective confining pressure are shown in Table 12 [Tajimi Engineering Services, Ltd., 1996].

Table 12. Small-strain shear modulus and shear wave speeds for gravel from triaxial tests (from Tajimi Engineering Services, Ltd., 1996)

Sample No.	Depth (m)	σ_c' (kN/m^2)	G_m at $\gamma\approx5\times10^{-6}$ (kN/m^2)	ρ_t (ton/m^3)	V_S (m/sec)	σ_c' (kN/m^2)	V_S[1] (m/sec)
2	5.06-5.62	78.4	140,140	2.47	238	64.7	224
3	5.14-5.78	78.4	176,400	2.47	267	66.6	254
5	5.18-5.78	78.4	140,140	2.46	239	67.6	229
6	5.14-5.78	78.4	175,420	2.48	266	66.6	253
8	5.18-5.78	78.4	156,800	2.46	253	67.6	242
9	5.08-5.68	78.4	142,100	2.46	241	65.7	229
S1-2c	5.38-5.58	88.2	227,360	2.55	285	67.6	262
S1-3a	6.06-6.26	88.2	222,460	2.49	299	76.4	287
S1-3c	7.09-7.29	98.0	161,700	2.39	268	91.1	262
S1-4c	7.81-8.01	118	145,040	2.34	249	101	229
S1-4d	8.02-8.22	118	147,000	2.37	249	104	229
S1-4e	8.23-8.43	118	160,720	2.40	259	107	251
S1-4f	8.44-8.64	118	200,900	2.41	289	110	283
S2-5a	9.90-10.10	137	243,040	2.42	317	130	311
S2-5b	10.41-10.61	147	203,840	2.45	289	137	283
S2-7a	11.88-12.08	167	308,700	2.44	356	144	342

[1] Corrected for actual effective confining pressure which was less than that used in the test.

The shear wave speeds computed from the triaxial test data are less than those obtained from the in-situ geophysical tests, namely, down-hole and cross-hole logging. It has been pointed out in (Tajimi Engineering Services, Ltd., 1996) that the estimated effective overburden pressure for the free-field are 10 to 20% less than the effective confining pressure in the free-field. Taking into account that the shear speed measured in the laboratory for 300-mm diameter specimens is approximately proportional to $(\sigma_c')^{0.3}$ the shear velocities shown in Table 12 can be corrected to the estimated overburden effective stress in the free-field. The corrected values obtained by Tajimi Engineering Services, Ltd., are shown in Table 12.

The shear wave speeds for the gravel computed on the basis of the triaxial tests (and shown in Table 12) are about 20 to 25% less than those obtained using PS-logging. The reasons for these discrepancies have not been explained. Results reported by CRIEPI (CRIEPI, 1993a) indicate that shear wave speeds for the gravel measured using triaxial testing data and torsional shear wave tests are generally less than those from the in-situ shear wave measurements with down-hole and cross-hole logging, whereas the shear wave speeds for the sands measured in the laboratory are similar to those measured in the field. The reasons for the shear wave speeds in the gravel measured in the laboratory to be smaller than those measured in the field has not been explained. It is, however, of interest to notice that to a depth of about 15 m below ground level shear wave speeds measured in the laboratory are approximately equal to the lower bound of the shear wave speeds measured with the cross-hole logging method.

Backfill. -- Shear wave speeds for the backfill soils determined on the basis of cyclic triaxial data are shown in Table 13. The average shear wave speed from the laboratory data compares well with the 300 m/sec average suggested by CRIEPI on the basis of the phase IV-B PS-logging and LPT data.

Table 13. Small-strain shear modulus and shear wave speeds for backfill from triaxial tests (from Tajimi Engineering Services, Ltd., 1996)

Sample No.	σ_c' (kN/m^2)	G_m at $\gamma=5\times10^{-6}$ (kN/m^2)	ρ_t (ton/m^3)	V_S (m/sec)
1	98.0	222,460	2.39	305
2	49.0	147,000	2.39	248
3	49.0	94,080	2.39	198
5	49.0	231,280	2.39	311
6	29.4	156,760	2.39	258
	49.0	201,880	2.39	291
	68.6	237,160	2.39	315
	98.0	292,040	2.39	350

Strain-Dependent Secant Shear Modulus and Damping Ratio

The strain-dependency data for the secant shear modulus and damping ratio of sands and gravels (CRIEPI, 1993a, 1994a) are shown in Figures 28 to 32 for various confining pressures. The data are from specimens obtained using freezing sampling methods and for 100mm- and 300mm-diameter specimens. The specimens identified by the S symbols are 100mm-diameter specimens while specimens No. 5 and No. 6 are 300mm-diameter specimens. The data indicate the following damping ratio (h) at small strains:

1. 2-percent for the sandy soils (100mm-diameter specimens), and for the 300mm-diameter specimens of gravelly soil (No. 5 and No. 6) sampled between GL-4.5m and GL-6.5m and tested at confining pressures of 78.4 kN/m^2 (representing soil between GL-4.5m and GL-6.5 m) and 588.0 kN/m^2 representing soil below GL-20m.
2. Between about 5- and 7-percent for the 100 mm specimens of gravelly soils.

It was noticed by CRIEPI (CRIEPI, 1993a), that the damping ratio of gravelly soils is smaller for the 300mm-diameter specimens than for the 100mm-diameter specimens, especially at the low strain levels (γ less than about 2×10^{-5}), whereas the secant shear moduli are approximately equal for both sample sizes. That is, there appears to be a scaling effect as far as the small-strains hysteretic damping of the gravelly soil is concerned.

Cyclic triaxial tests were also conducted to establish the secant shear moduli and damping ratios for the as-built backfill soils. The specimens tested were reconstituted by vibration compaction (CRIEPI, 1993f, 1994b). The results obtained are shown in Figure 33.

On the basis of the data shown in Figures 28 to 33, and on the basis of the apparent scaling effect on the equivalent damping ratio, CRIEPI (CRIEPI, 1995a) recommended strain-dependent secant shear moduli and damping ratios for use in the FVT-2 and earthquake response analysis. Their recommended values are shown in Tables 14 and 15 for the soil types shown in Figure 6. Nonlinear stress-strain relations were not recommended for the gravelly soil below GL-20 m.

The shear modulus ratio and damping ratio for sand and backfill soils are based on the test data shown in Figures 28 and 33, respectively. The shear modulus ratio vs. shear strain relationships ($G/G_m \sim \gamma$) for gravel 1 and gravel 2 are based on the test results for the 100mm-diameter specimens taken from depths between GL-6.5m and GL-13.0m, *i.e.*, those shown in Figure 30. This relationship for gravel 3 is based on the data shown in Figure 31.

The damping ratio vs. strain ($h \sim \gamma$) relationship for gravel 1 and gravel 2 is derived from the ($G/G_m \sim \gamma$) relation adopted for this soil as indicated above and the ($G/G_m \sim h$) relation obtained with the 300mm-diameter specimens taken from depths between GL-4.5m and GL-6.5m (see Figure 29). Similarly, the ($h \sim \gamma$) relation for gravel 3 is derived from the ($G/G_m \sim \gamma$) relation adopted for this soil as indicated above and the ($G/G_m \sim h$) relation obtained with the 300mm-diameter specimens taken from depths between GL-4.5m and GL-6.5m (see Figure 29). This is done to account for the effect of sample size on the damping ratio that was detected by comparing the results of tests with 100mm- and 300mm-diameter specimens.

It is noted that the shear strains in Figures 28 to 33 are scaled with respect to the confining pressure and that the cyclic triaxial tests were performed under isotropic confining pressures. It is, however, recommended in CRIEPI (1995a) that the vertical effective stress be used in lieu of the confining pressure to assess the effect of confinement on the nonlinear shearing stress-strain relation. This approach was used by CRIEPI to obtain the relationships recommended in Table 14 and Table 15. For the sand, backfill, and gravel 2, the vertical effective stress was taken to be the overburden stress, while for gravel 1 and gravel 3, the vertical effective stress was calculated taking into account the effect of the sequence of construction operations (including excavation) on the vertical effective stresses.

Table 14. G/G_m- γ and h - γ for FVT-2 and earthquake response analysis for sands and backfill soils (reproduced from CRIEPI, 1995a)

Sand 1 and 2			**Backfill 1 and 2**		
γ	G/G_m	**h (%)**	γ	G/G_m	**h (%)**
≤4.4E-06	1.00	2.0	≤ 2.5E-06	1.00	2.0
5.3E-06	0.99	2.0	3.4E-06	0.99	2.0
7.0E-06	0.98	2.1	4.2E-06	0.98	2.0
8.8E-06	0.96	2.2	5.1E-06	0.97	2.0
1.3E-05	0.94	2.3	6.7E-06	0.94	2.0
1.8E-05	0.91	2.5	8.4E-06	0.92	2.0
2.6E-05	0.87	2.8	1.3E-05	0.87	2.1
3.5E-05	0.83	3.2	1.7E-05	0.83	2.3
4.5E-05	0.81	3.5	2.5E-05	0.76	3.0
5.3E-05	0.78	3.9	3.4E-05	0.70	3.7
7.0E-05	0.74	4.5	4.2E-05	0.66	4.3
8.8E-05	0.70	5.1	5.1E-05	0.62	4.8
1.3E-04	0.63	6.4	6.7E-05	0.55	5.9
1.8E-04	0.57	7.5	8.4E-05	0.50	6.7
2.6E-04	0.47	9.5	1.3E-04	0.40	8.4
3.5E-04	0.39	11.4	1.7E-04	0.33	9.7
4.4E-04	0.33	13.0	2.5E-04	0.25	11.2
5.3E-04	0.29	14.3	≥3.4E-04	0.21	12.3
≥7.0E-04	0.24	16.0	--	--	--

Table 15. G/G_m- γ and h - γ relations for FVT-2 and earthquake response analysis for gravel soils (reproduced from CRIEPI, 1995a)

Gravel 1 (5 -12 m) (under foundation)			**Gravel 2 (5 - 12 m) (free-field)**			**Gravel 3 (12 - 20 m)**		
γ	G/G_m	h (%)		G/G_m	h (%)	γ	G/G_m	h (%)
≤5.1E-06	1.00	2.0	≤4.7E-06	1.00	2.0	≤4.9E-06	1.00	2.0
6.1E-06	0.99	2.1	5.7E-06	0.99	2.1	5.9E-06	1.00	2.0
8.1E-06	0.96	2.2	7.5E-06	0.96	2.2	7.8E-06	0.98	2.1
1.0E-05	0.94	2.4	9.4E-06	0.94	2.4	9.8E-06	0.96	2.2
1.5E-05	0.89	2.9	1.4E-05	0.89	2.9	1.5E-05	0.92	2.6
2.0E-05	0.85	3.4	1.9E-05	0.85	3.4	2.0E-05	0.89	2.9
3.1E-05	0.78	4.2	2.8E-05	0.78	4.2	2.9E-05	0.83	3.5
4.1E-05	0.73	4.9	3.8E-05	0.73	4.9	3.9E-05	0.79	4.1
5.1E-05	0.69	5.4	4.7E-05	0.69	5.4	4.9E-05	0.75	4.6
6.1E-05	0.65	6.0	5.7E-05	0.65	6.0	5.9E-05	0.72	5.0
8.1E-05	0.59	6.9	7.5E-05	0.59	6.9	7.8E-05	0.67	5.6
1.0E-04	0.54	7.6	9.4E-05	0.54	7.6	9.8E-05	0.63	6.3
1.5E-04	0.47	8.8	1.4E-04	0.47	8.8	1.5E-04	0.56	7.4
2.0E-04	0.41	9.8	1.9E-04	0.41	9.8	2.0E-04	0.50	8.3
3.1E-04	0.34	11.0	2.8E-04	0.34	11.0	2.9E-04	0.42	9.6
4.1E-04	0.29	11.9	3.8E-04	0.29	11.9	3.9E-04	0.37	10.6
5.1E-04	0.26	12.4	4.7E-04	0.26	12.4	4.9E-04	0.33	11.1
6.1E-04	0.24	12.8	5.7E-04	0.24	12.8	5.9E-04	0.29	11.8
≥8.1E-04	0.20	13.4	≥7.5E-04	0.20	13.4	≥7.8E-04	0.24	12.7

For each soil, the shear modulus ratio (G/G_m) is taken to be 1.0 for strains less than those shown in Tables 14 and 15, and it is kept equal to the minimum value shown in Tables 14 and 15 for strains greater than those shown in these tables. Similarly, the damping ratios (h) are kept equal to the maximum values in Tables 14 and 15 for strains greater than those shown in these tables, and it kept equal to 0.02 for strains less than those shown in the tables.

5.4.6 Undrained Cyclic Shearing Strength

Undrained stress-controlled triaxial cyclic loading tests were conducted by CRIEPI to investigate the soil potential for liquefaction. The tests conducted measured the cyclic stress ratio $\sigma_d/(2\sigma_c^{'})$, where σ_d is the deviatoric stress and $\sigma_c^{'}$ is the effective confining stress, required to reach a double-amplitude (DA) strain of 2% and 5% (sands) and 2% (gravelly soil). The effective confining stress for each sample was representative of that at the depth from which the sample was taken. For the sand (GL-3.19m – GL-3.81m) the cyclic stress ratios to reach a DA of 5% and 2 % in 20 cycles were 0.35 and 0.26, respectively. For the dense gravelly soils and 100mm-diameter specimens, the cyclic stress ratios required to reach a DA of 2% were: 0.44 (GL-5.06m – GL-6.26m), 0.24 (GL-7.81m – GL-8.64m) and 0.35 (GL-14.92 – GL-16.27m). For a 300mm-diameter sample of the dense gravelly soil taken between GL-5.06m – GL-6.26m, the cyclic stress ratio was 0.26. More Details description of these tests can be found in CRIEPI (1993a).

The undrained cyclic shear strengths of the gravelly soil are generally higher than those of the sandy soils encountered at the site. However, the undrained cyclic resistance of the gravel determined on the basis of the stress-controlled triaxial tests on samples taken by a ground freezing technique, is not that much higher than those for the sand. This does not appear to be consistent with the fact that the undrained cyclic strengths of the gravel predicted on the basis of the LPT blowcount are much greater than those of the sand. Given that the fine contents of the gravel samples ranges from 9.4% to 25.8%, CRIEPI suggested that the samples obtained by the freezing method may still be disturbed for the purpose of determining the undrained strength of the soil, which is a credible explanation considering the very high in-situ density estimated for this soil. For that reason, CRIEPI proposes that the undrained cyclic shear strength of the gravel be determined from correlations with LPT results. This, leads to much higher undrained shear strengths for the gravel than those predicted on the basis of the laboratory data. On this basis, CRIEPI (1993a) proposed the undrained cyclic strengths summarized in Table 15 for the granular soils encountered at the site.

Table 16. Undrained cyclic shearing strength for 2% double amplitude (DA) strain in 20 cycles (reproduced from CRIEPI, 1993a)

Soil Type	**Depth (m)**	**Undrained Cyclic Shearing Resistance ($\sigma_d/2\sigma_c'$)**
Loose to medium sand	0 - 4.5 m	0.32 (for DA=5%)
Dense to very dense gravel	4.5 - 6.5 m	0.99
Dense to very dense gravel	6.5 - 13 m	0.49
Dense to very dense gravel	13 - 20 m	0.38

5.5 *Commentary*

A comprehensive site characterization program was conducted by CRIEPI between 1990 and 1994. Their site characterization program paid particular attention to the soil conditions to a depth of about 12 m below the ground surface (GL-12m). In this regard, their site characterization program was at least as thorough as those commonly used for actual, prototypical, sites. In particular, a detailed characterization was made for the surface layer of sand from GL0 to GL-5m, for the gravel beneath the foundation and in the free-field from GL-5m to GL-12m, and for the as-built backfill soil. A somewhat less detailed characterization was provided for the gravel between GL-12m and GL-20m. The site characterization for depths below about GL-20m appears to have been beyond the scope of the effort by CRIEPI and, at present, it seems to rely almost exclusively on the scoping geophysical study performed in the early stages of the Hualien SSI program by the Institute of Earth Sciences (IES) of the Academia Sinica. This characterization may be limited for the purposes of detailed correlation analysis studies with the ground accelerations recorded in the down-hole arrays, which extended to a depth of about GL-52.5m. Examples of such correlation studies are: site amplification studies and deconvolution analysis.

The procedures and results of the site characterization program conducted by CRIEPI, which took place over a span of about 4 years from 1990 to 1994, were periodically reported to the members of the Hualien SSI consortium and their contractors. They and CRIEPI evaluated those procedures and results and recommended new tests as deemed necessary. As a consequence, the results obtained by CRIEPI and summarized above have been thoroughly reviewed and should provide an adequate representation of the site conditions. However, additional comments need to be made pertaining to some aspects of the data obtained by CRIEPI and presented above. These comments are as follows:

Shear wave speeds measured with down-hole, cross-hole and suspension logging are consistently greater than those inferred from laboratory tests on samples collected by ground freezing techniques. The reasons for such discrepancies are not known at present. These discrepancies have been attributed to possible samples disturbance resulting from high fine contents of the order of 15 to 25%. They may be the result of numerous pebbles or cobbles as large as 10 to 20 cm in diameter that would require testing specimens greater than those used, or a result of the difficulty to obtain in-situ shear wave speed measurements for a gravel with numerous pebbles or cobbles as large as 10 to 20 cm in diameter. They may also be the result of soil anisotropy as discussed below.

In-situ saturated densities recommended by CRIEPI for the as-built backfill soil and the gravel to a depth of about 20 m below ground level are about 2,390 kg/m^3 (a dry density of 2,200 kg/m^3) and 2,420 kg/m^2, respectively. These are unusually high densities which are similar to those of concrete. The gravel is a well-graded soil for which coefficients of uniformity of the order of 150 to 400 were computed. Such a gradation may lead to a very low void ratio which would explain the high bulk density of this soil. The backfill soil is not well-graded, and its reported dry density of about 2,200 kg/m^2, which is based on the quality control tests conducted for the backfill compaction, is unusually high for a compacted soil. It is also noted that the dry densities for the reconstituted backfill material used to establish the variation of the secant shear modulus and damping ratio with shear strain (see Figure 33) are about 10% less than that recommended for the in-situ conditions for FVT-2 analysis.

A Poisson's ratio of 0.48 is recommended for the backfill soil between GL-2m to GL-4m (backfill 2 in Figure 6) for the FVT-2 analysis. The Poisson's ratio for this soil computed from measured S and P wave speeds is 0.24. Full saturation must be assumed for a Poisson's ratio of 0.48. It is improbable that the backfill soil from GL-2m to GL-4m would have been fully-saturated at the time of the FVT-2 test. Full saturation is more likely in early 1994 when significant earthquake loads were recorded at the site. Nevertheless, full saturation will depend on whether the depth of the groundwater table at the site remains approximately equal or changes significantly from year to year and/or throughout the year.

Cross-hole logging results reveal S wave speeds from GL-5m to about GL-12m that appear to be significantly different in two approximately orthogonal directions both before excavation and after construction of the model. The data, however, show considerable scatter and the difference between the wave speeds in the two orthogonal directions is more apparent in terms of the averages of the measurements in each direction. Prior to the forced vibration tests, the possibility of anisotropic site conditions with two principal directions of shear wave propagation in the horizontal direction was not expected. The forced vibration test data and the recorded earthquake ground motion data, however, reveal that this anisotropy appears to be the actual site condition.

Soil anisotropy may also be responsible, in part, for the smaller shear wave speeds inferred from the laboratory testing as compared to those from in-situ shear wave speed measurements. Assuming that the soil anisotropy is preserved through the sampling process, the shear deformation of the soil under torsional and triaxial loading conditions is not likely to be representative of the soil stiffness in the strong direction. Indirect evidence of this is that the shear wave speeds in the sands measured in the laboratory are not less than those measured in the field, and the sands encountered in the upper 5 meters appear to be isotropic. It is also possible that the soil anisotropy is not preserved during sampling and that a simple consolidation of the specimen under isotropic stress conditions will not properly reconstitute the in-situ conditions. Shear strength parameters for the gravel obtained from triaxial testing are also likely to be affected by anisotropy and the triaxial test results are more likely to be representative of the soil strength in the weak direction rather than that in the strong direction, if the soil strength is anisotropic as the shear stiffness appears to be.

In the following, the forced vibration test data is analyzed to assess the suitability of the soil models proposed by CRIEPI for their analysis. Analysis of the forced vibration test data permits the identification of two sets of soil properties that provide the best correlation between the measured and computed FVT-1 and FVT-2 responses, and are designated the best-estimated soil properties for FVT-1 and FVT-2, respectively. Of greater interest for the interpretation of the SSI response under earthquake loading are the best-estimated soil properties for FVT-2, *i.e.*, for the embedded foundation. Those best-estimated soil properties account for the site anisotropy, are average values over the volume of the gravel 1 soil and the backfill height, and are suitable for SSI analysis under low-level earthquake loading, *i.e.*, such that the response remains in the linear, low-strain, range. For stronger earthquake loads, they should be coupled with the nonlinear stress-strain parameters obtained by CRIEPI and described above, in order to obtain constitutive models with various degrees of sophistication for the soils at the site.

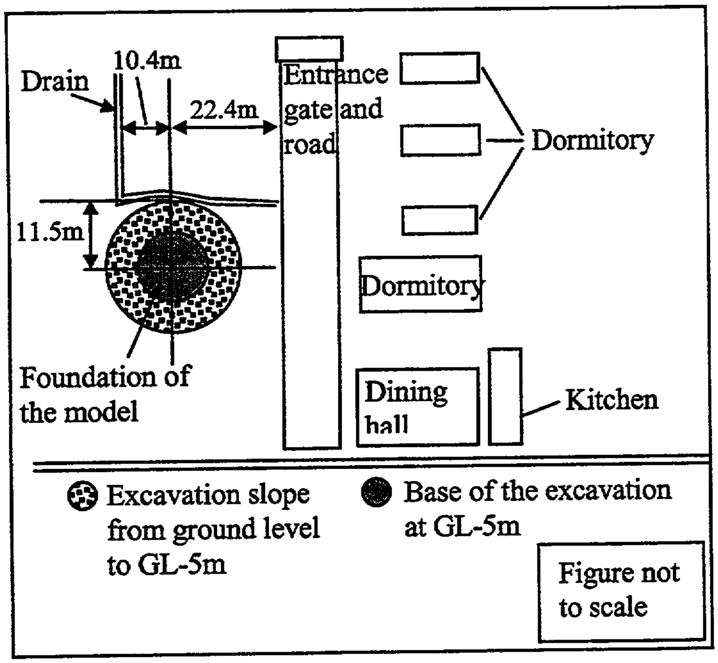

Figure 3 Site plan [from Kokusho *et al.*, 1993]

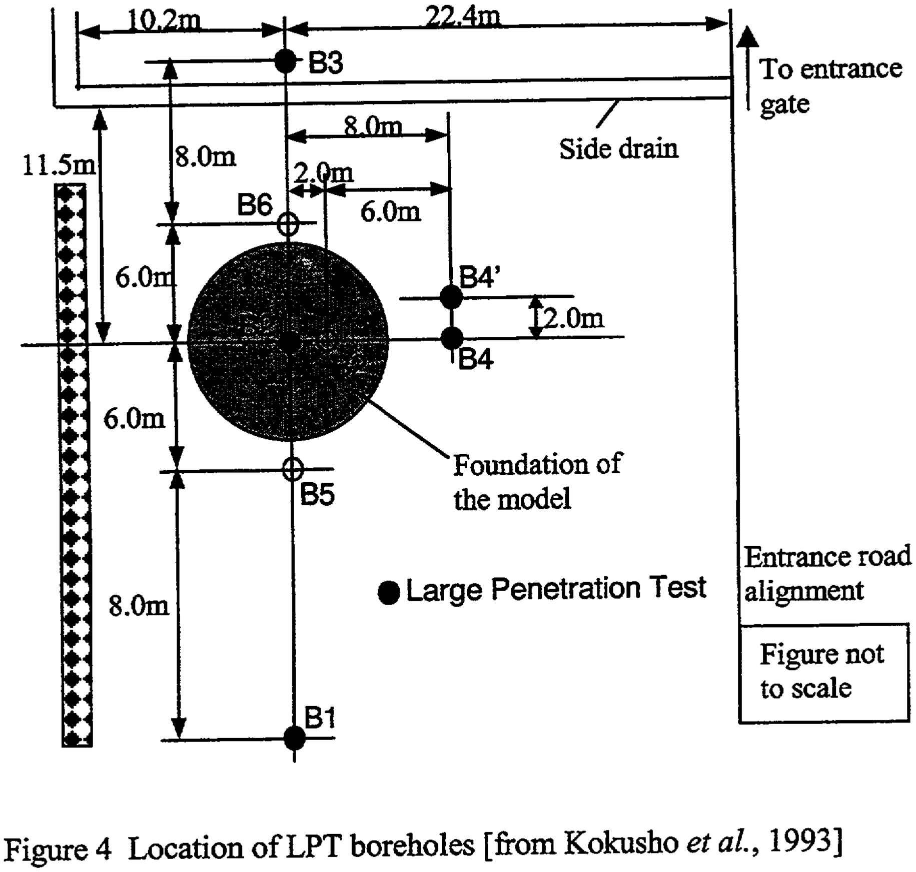

Figure 4 Location of LPT boreholes [from Kokusho *et al.*, 1993]

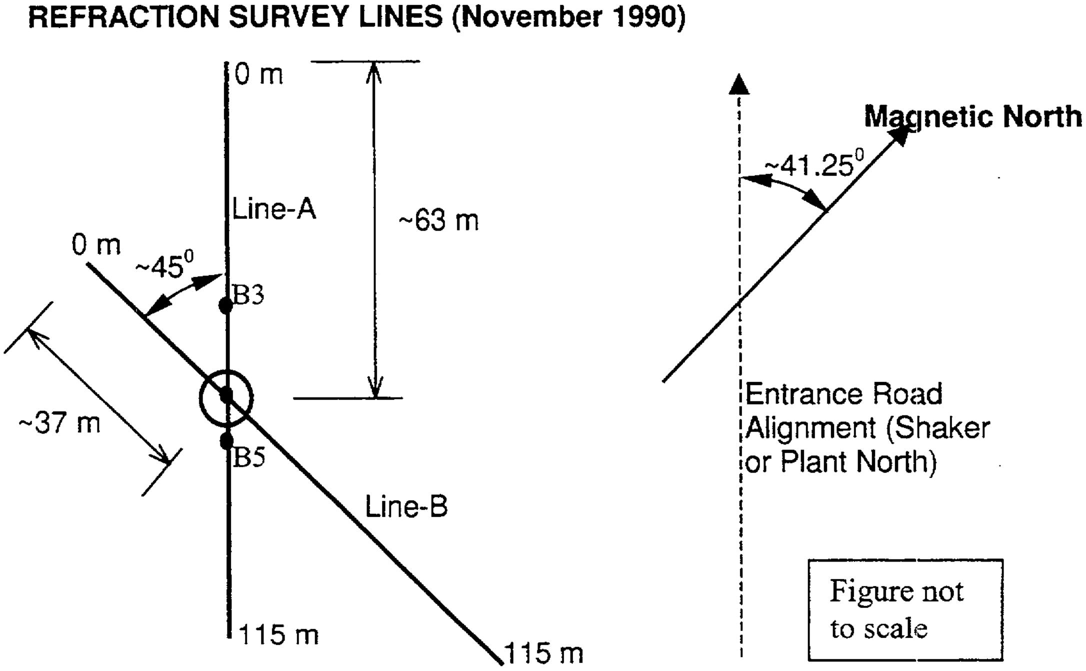

Figure 5 Alignement of November 1990 refraction survey lines

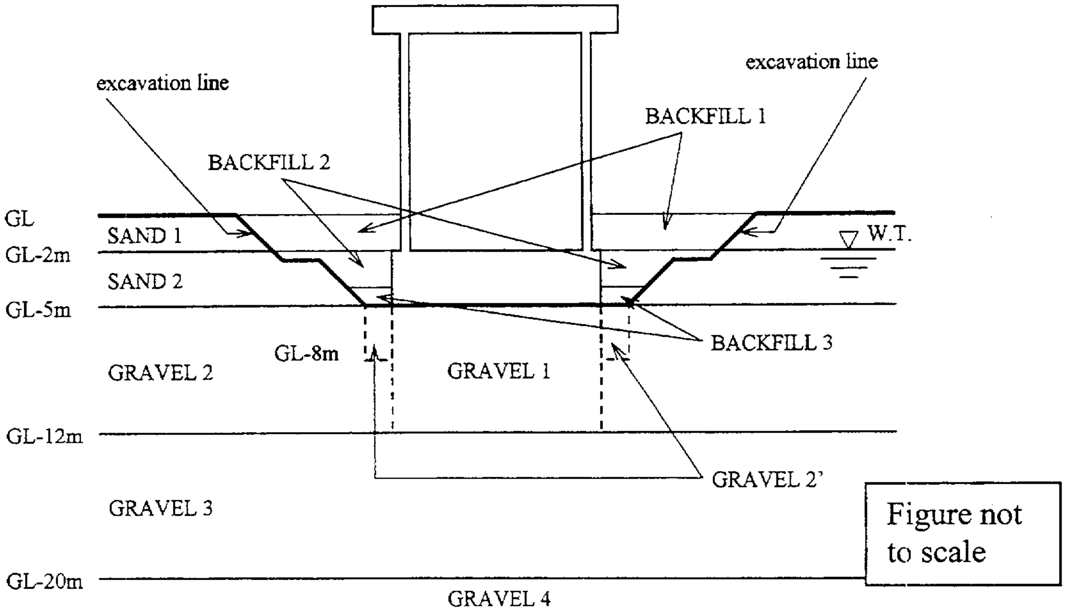

Figure 6 Soil layers and soil types identified in the site characterization [reproduced from CRIEPI, 1995b]

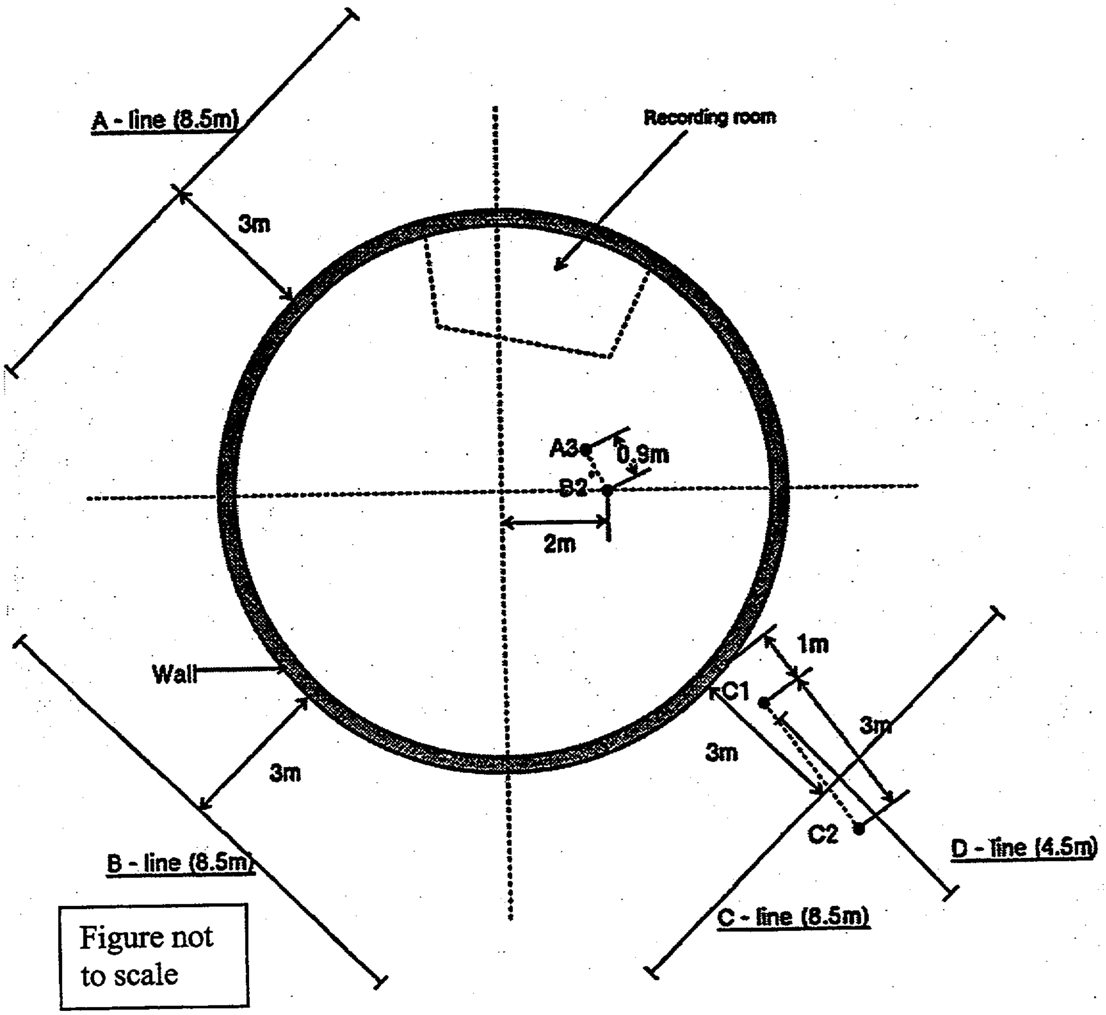

Figure 7 Refraction survey lines and PS-logging borings for Phase IV-A [reproduced from CRIEPI, 1993d]

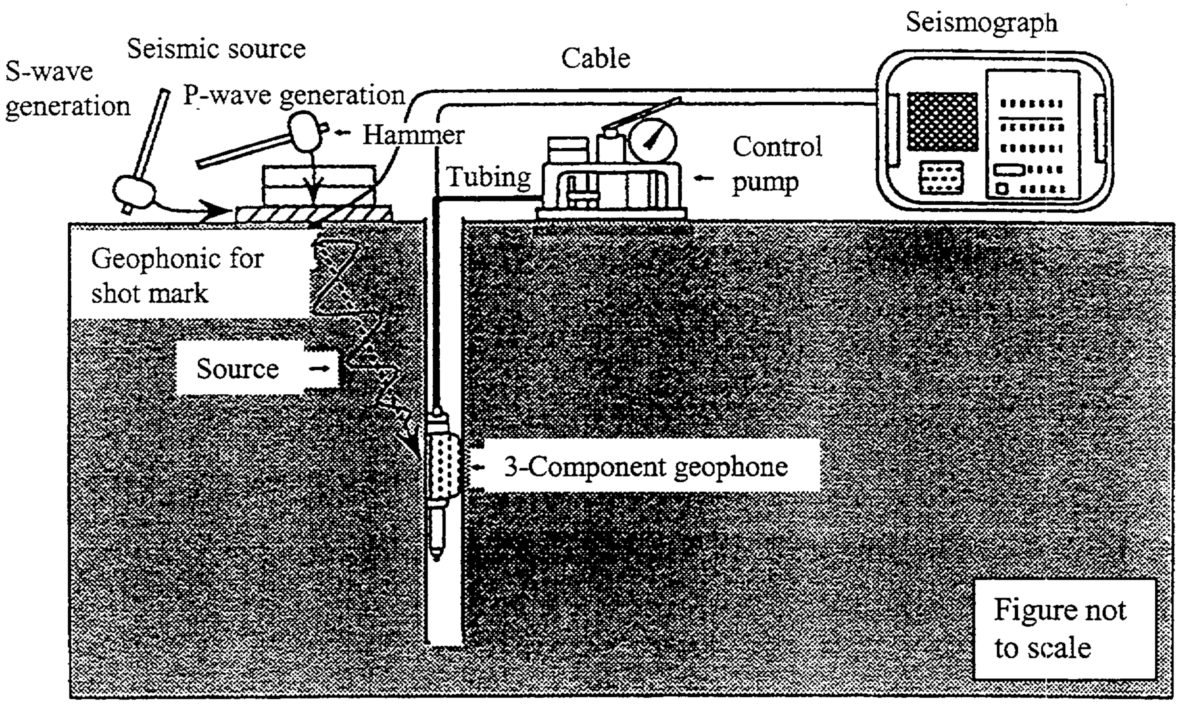

Figure 8 Setup for down-hole logging [reproduced from CRIEPI, 1991]

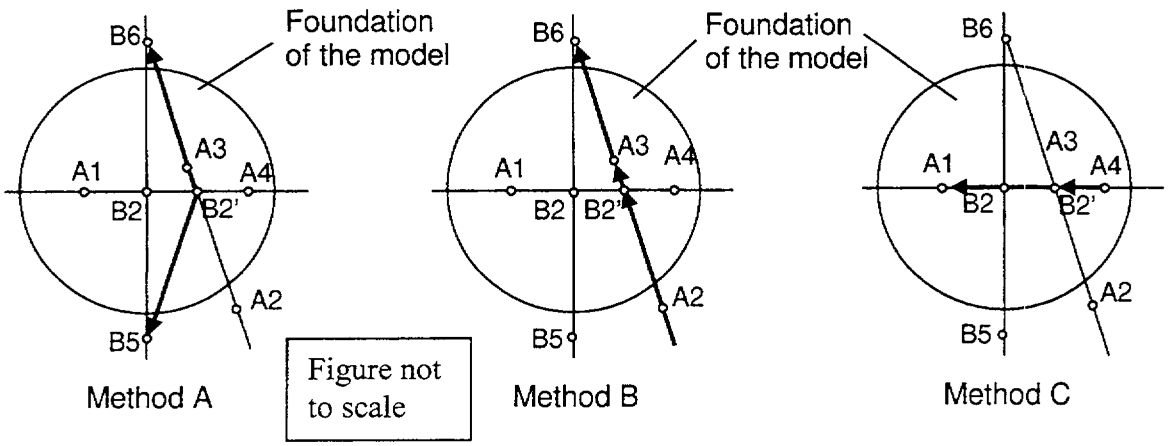

Figure 9 Down-hole logging locations and wave paths for cross-hole logging [reproduced from CRIEPI, 1993c]

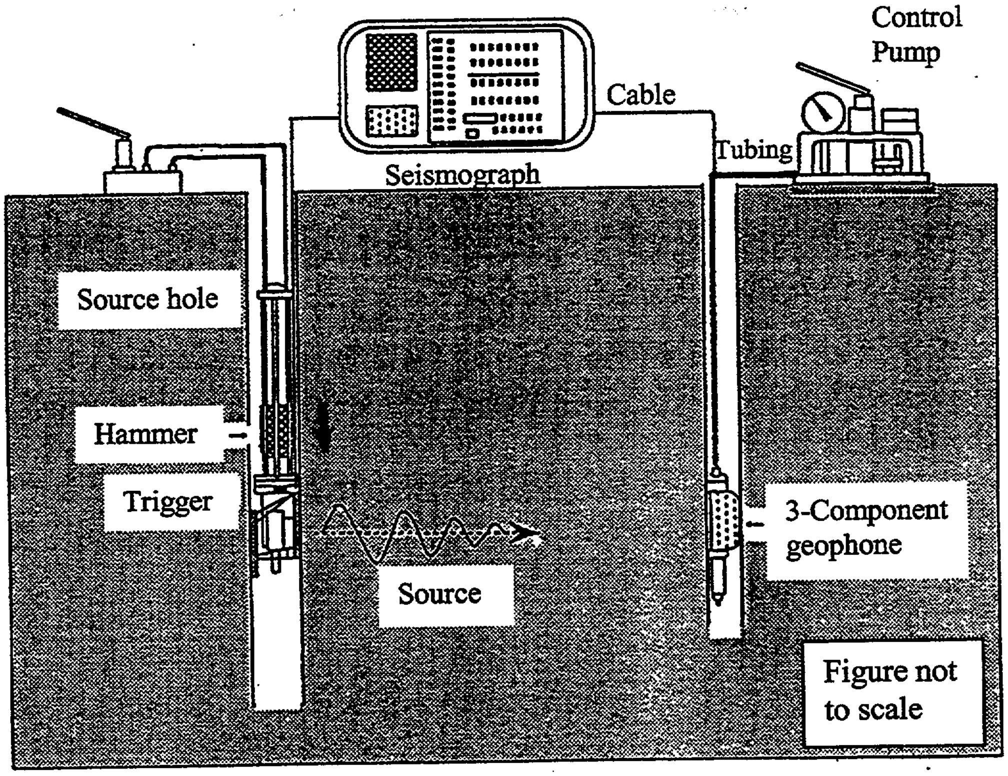

Figure 10 Setup for cross-hole logging [reproduced from CRIEPI, 1991]

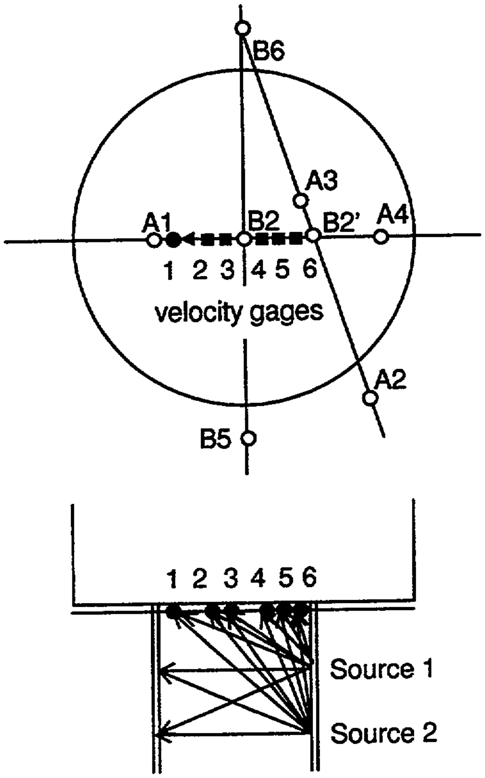

Figure not to scale

Figure 11 Seismic tomography location [reproduced from CRIEPI, 1993a]

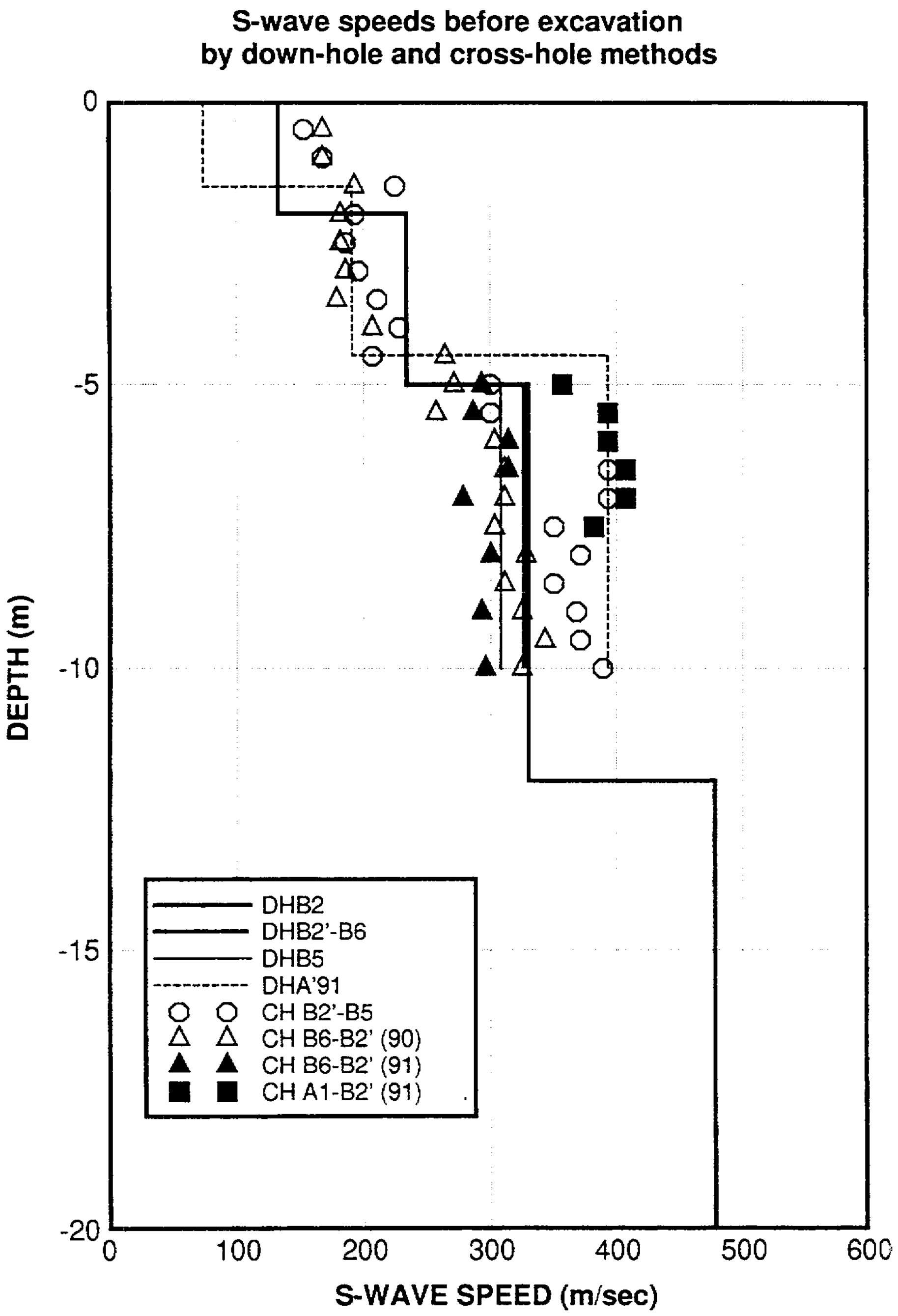

Figure 12 S-wave velocities before excavation by down-hole (DH) and cross-hole (CH) logging [reproduced from CRIEPI, 1993a]

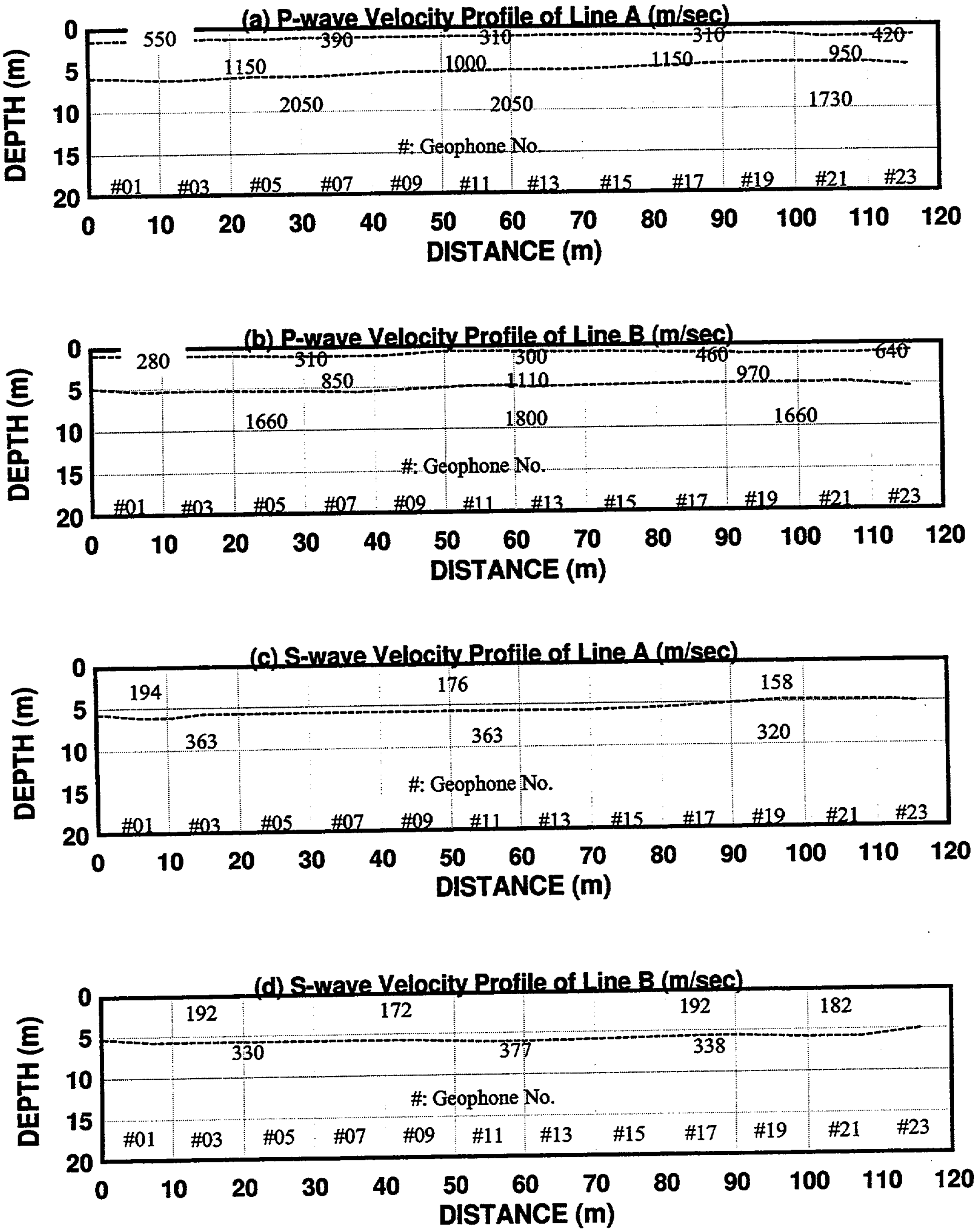

Figure 13 Results of seismic refraction survey before excavation [reproduced from CRIEPI, 1993a]

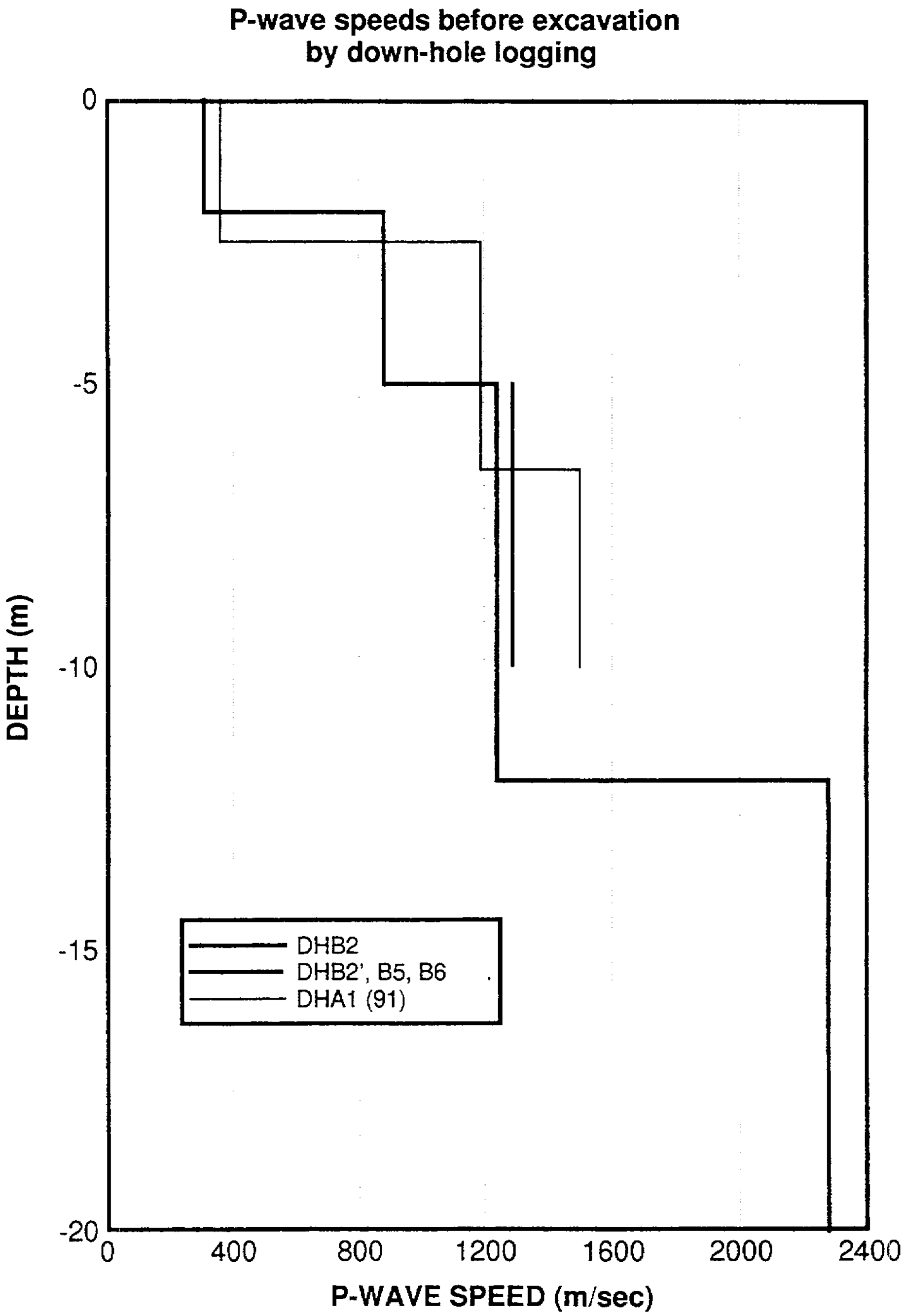

Figure 14 P wave velocities before excavation by down-hole (DH) logging [reproduced from CRIEPI, 1993a]

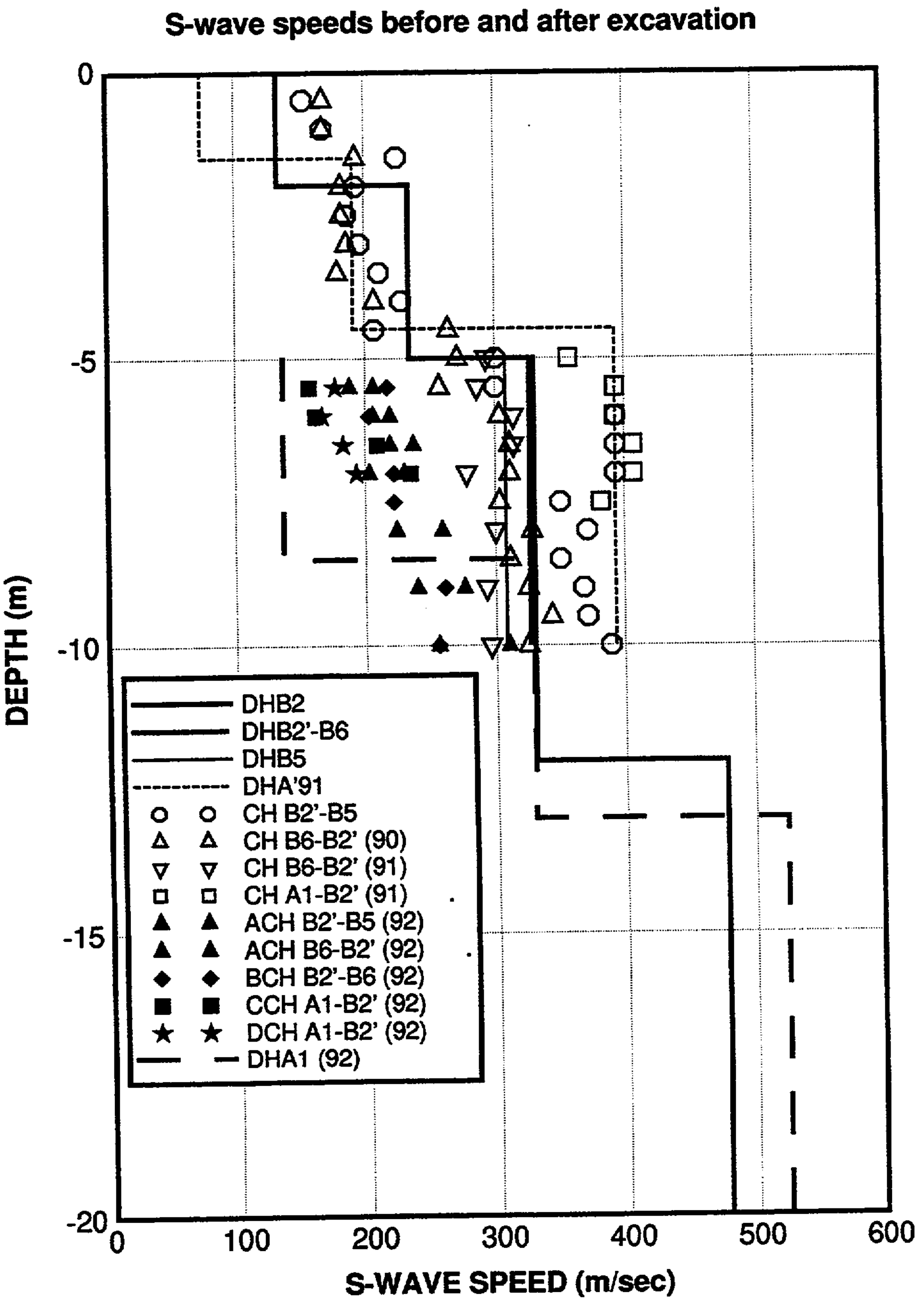

Figure 15 S-wave velocities measured before and after excavation [reproduced from CRIEPI, 1993a]

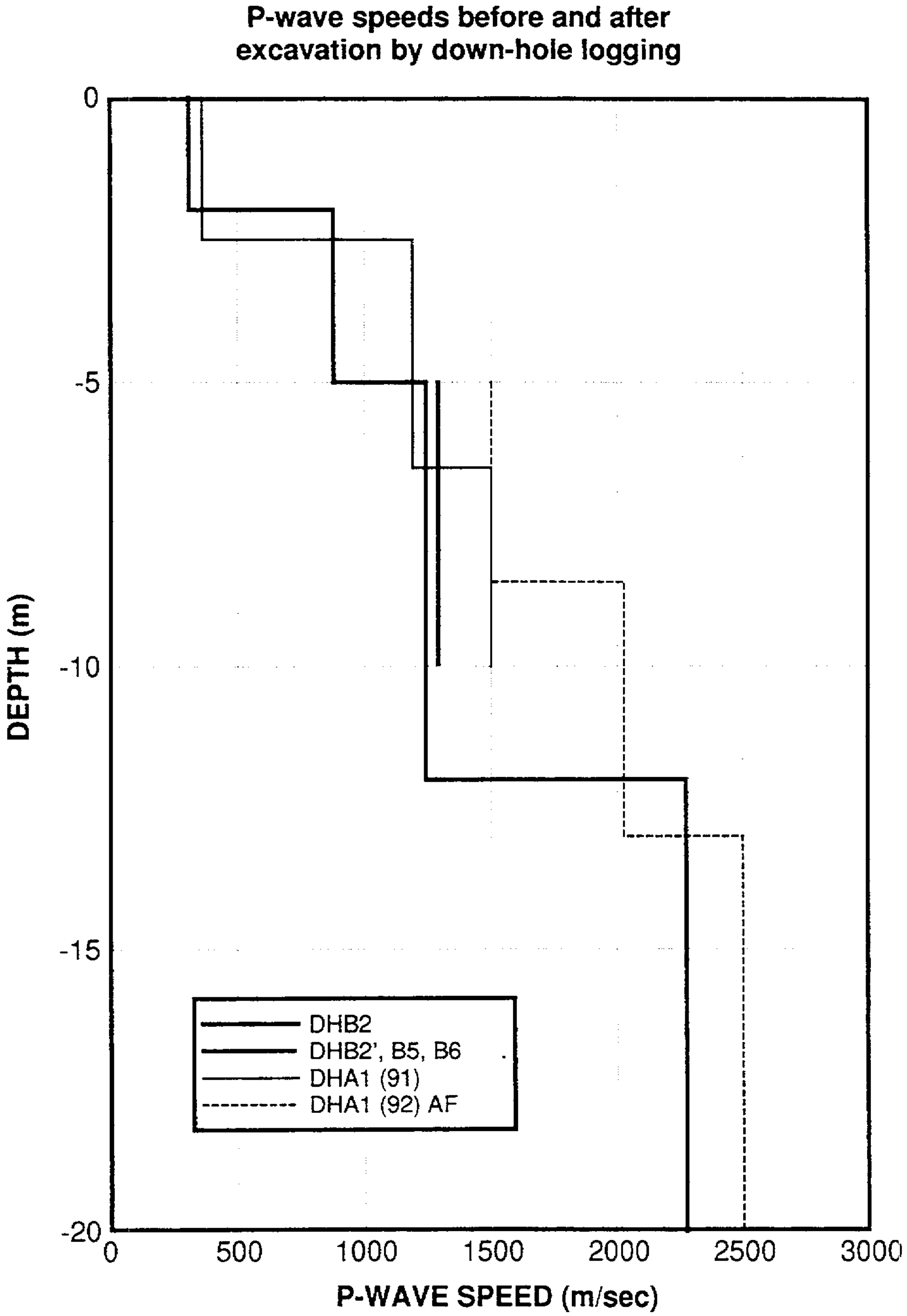

Figure 16 P wave velocities measured before and after excavation [reproduced from CRIEPI, 1993a]

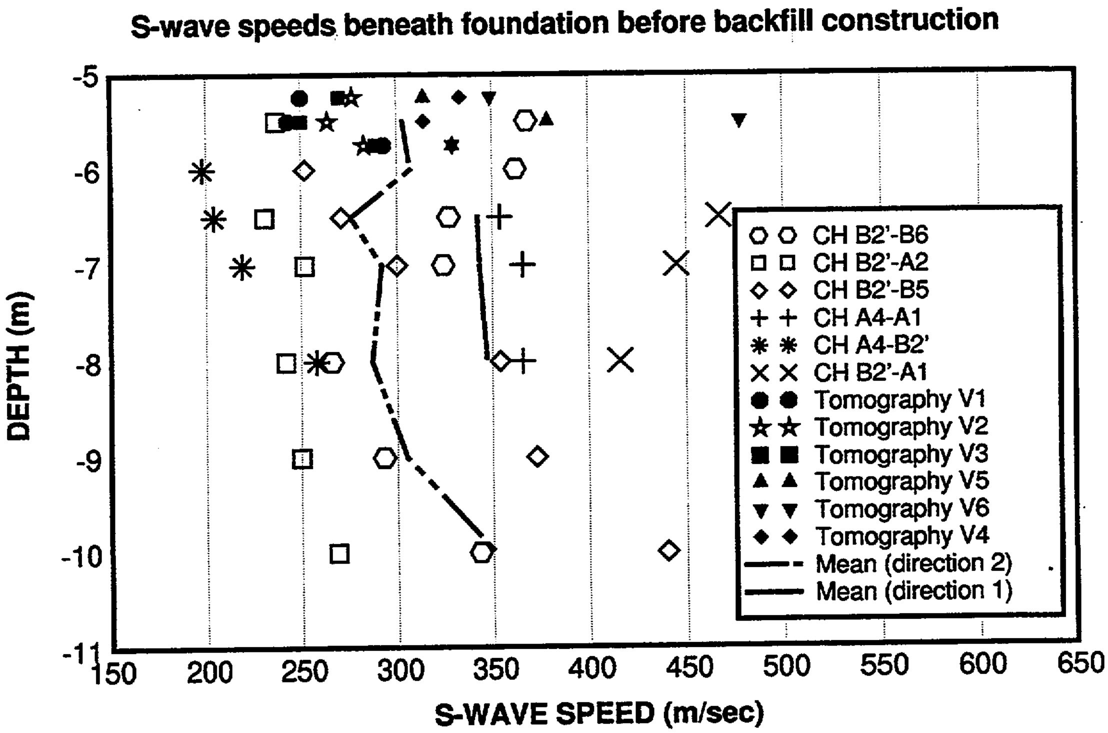

Figure 17 S wave velocities beneath the model foundation after model construction and before backfill placement [reproduced from CRIEPI, 1993c]

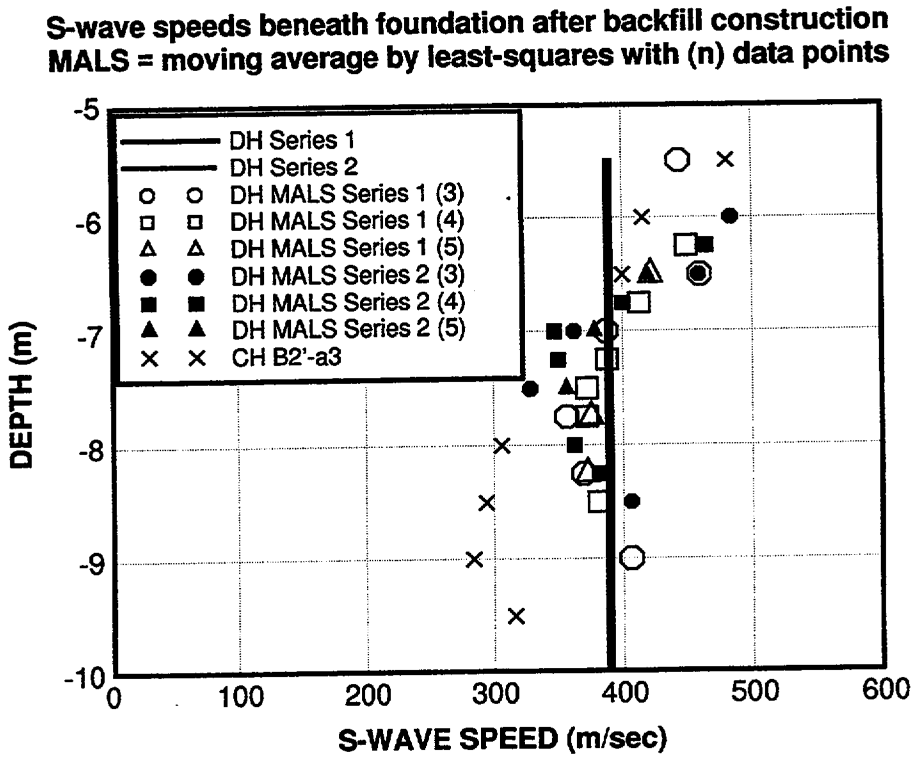

Figure 18 S wave velocities beneath the model foundation after backfill construction [reproduced from CRIEPI 1993d]

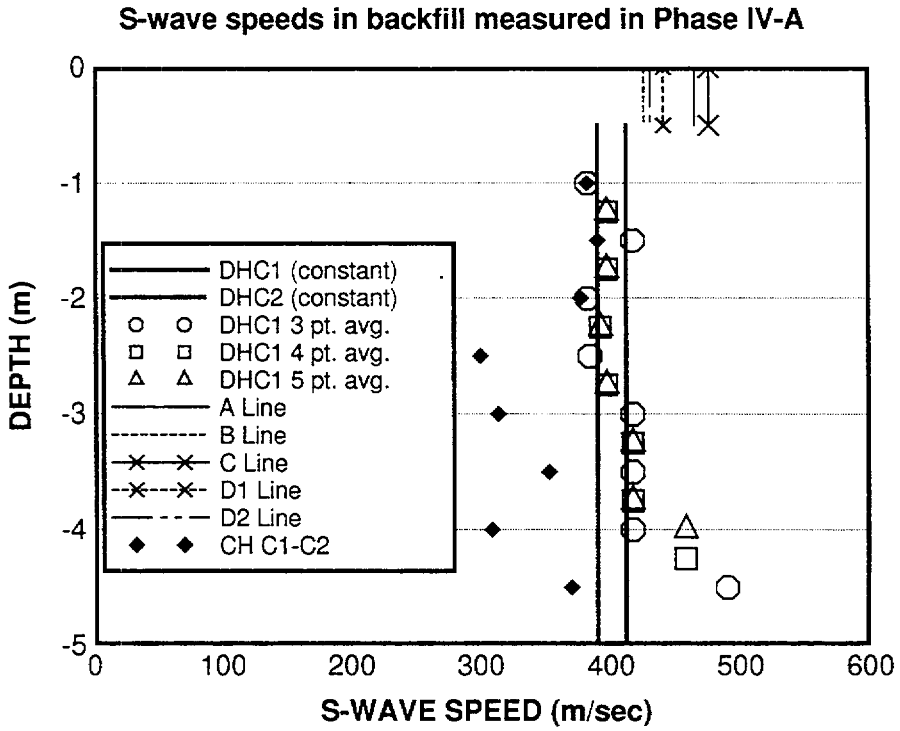

Figure 19 S wave velocities in the backfill measured in 1993 (Phase IV-A) [reproduced from CRIEPI 1993d]

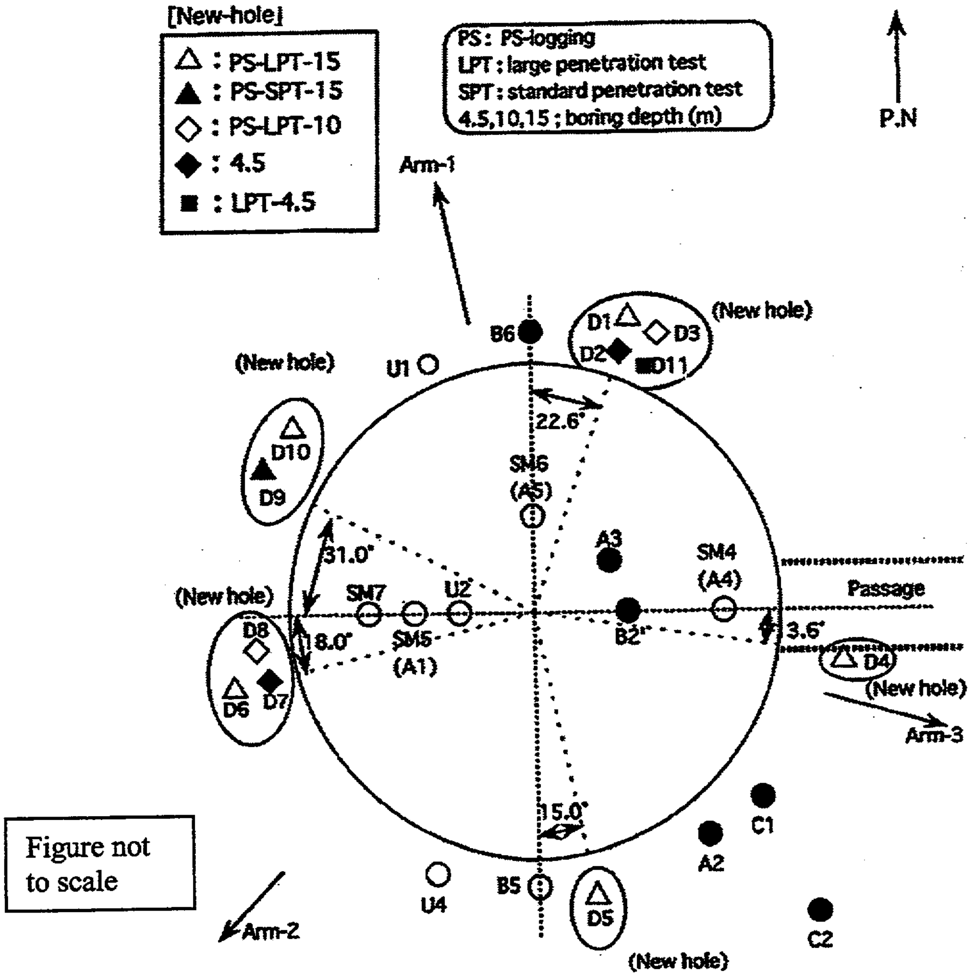

Figure 20 Location of 1994 LPT borings (Phase IV-B) [reproduced from CRIEPI, 1994c]

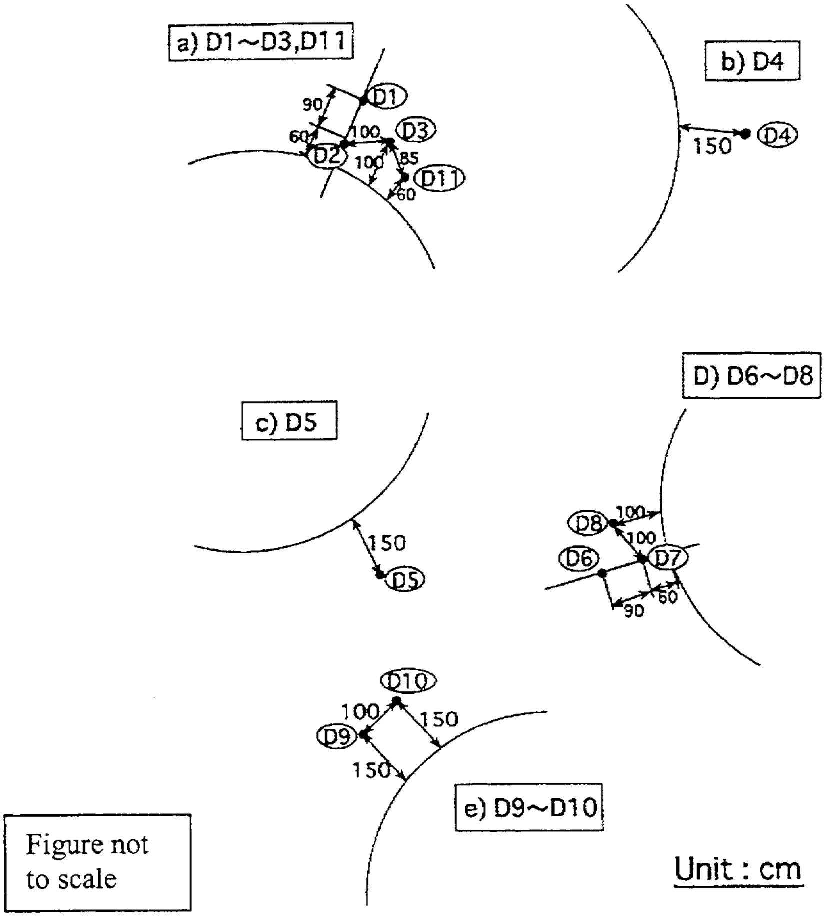

Figure 21 Details of 1994 LPT locations (Phase IV-B) [reproduced from CRIEPI, 1994c]

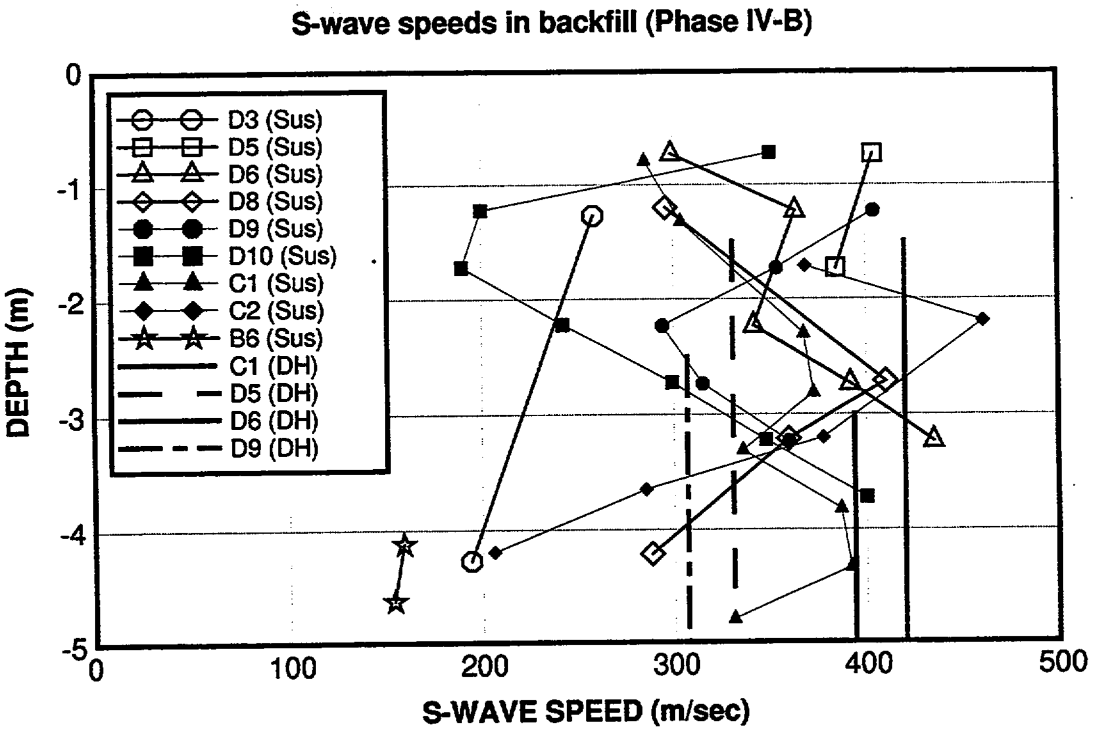

Figure 22 S wave velocities in the backfill by PS-logging (Phase IV-B) [reproduced from CRIEPI, 1995b]

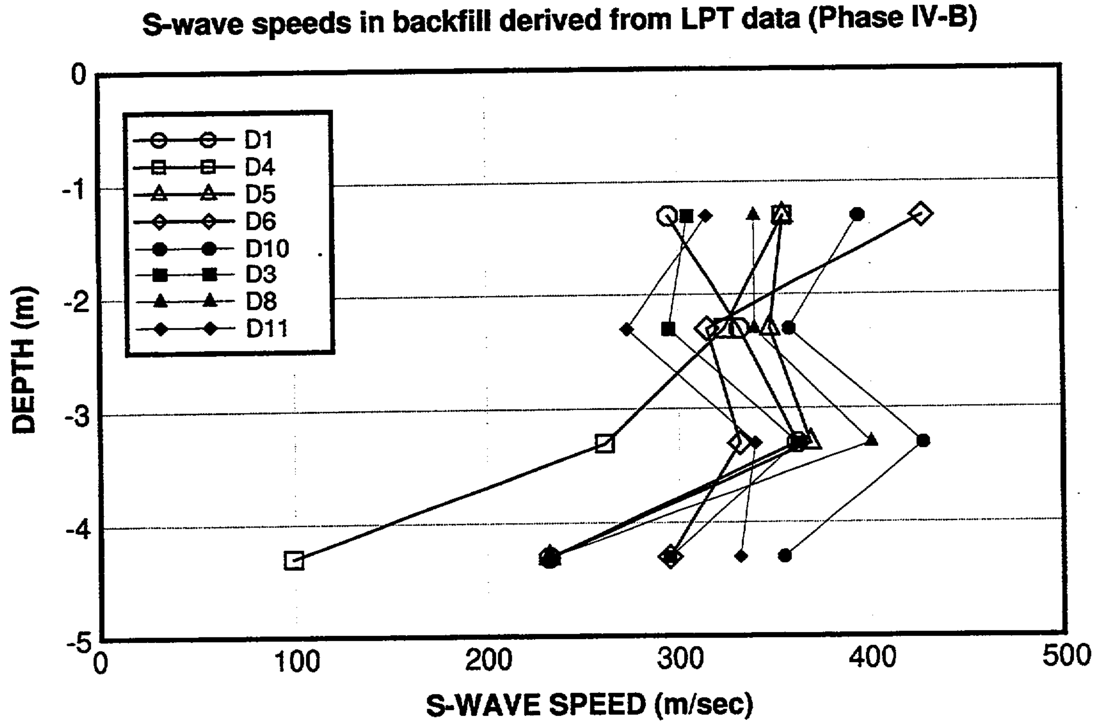

Figure 23 S wave velocities in the backfill from LPT data (Phase IV-B) [reproduced from CRIEPI, 1995b]

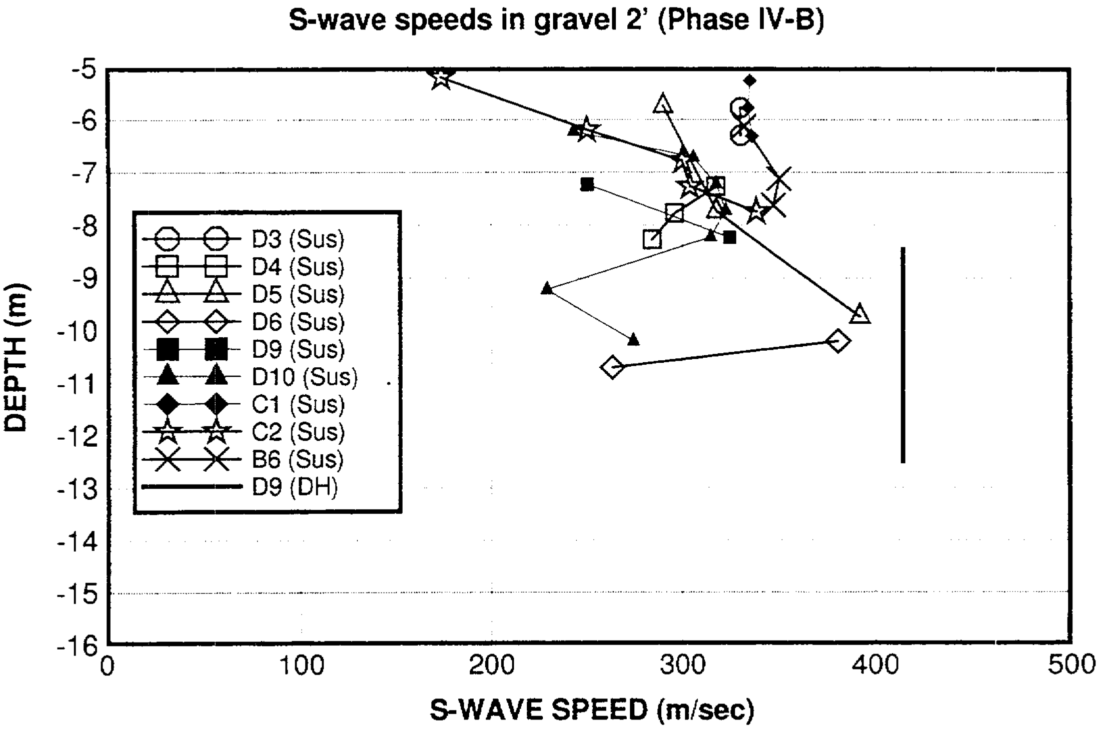

Figure 24 S wave velocities in gravel 2′ by PS-logging (Phase IV-B) [reproduced from CRIEPI, 1995b]

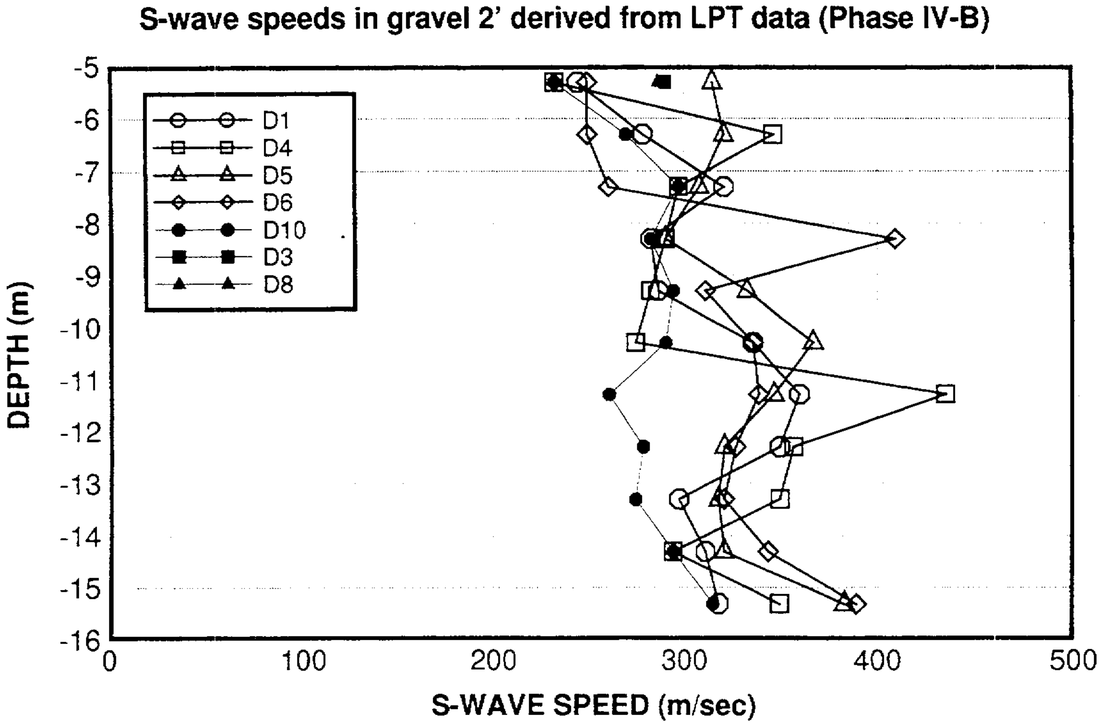

Figure 25 S wave velocities in gravel 2′ from LPT data (Phase IV-B) [reproduced from CRIEPI, 1995b]

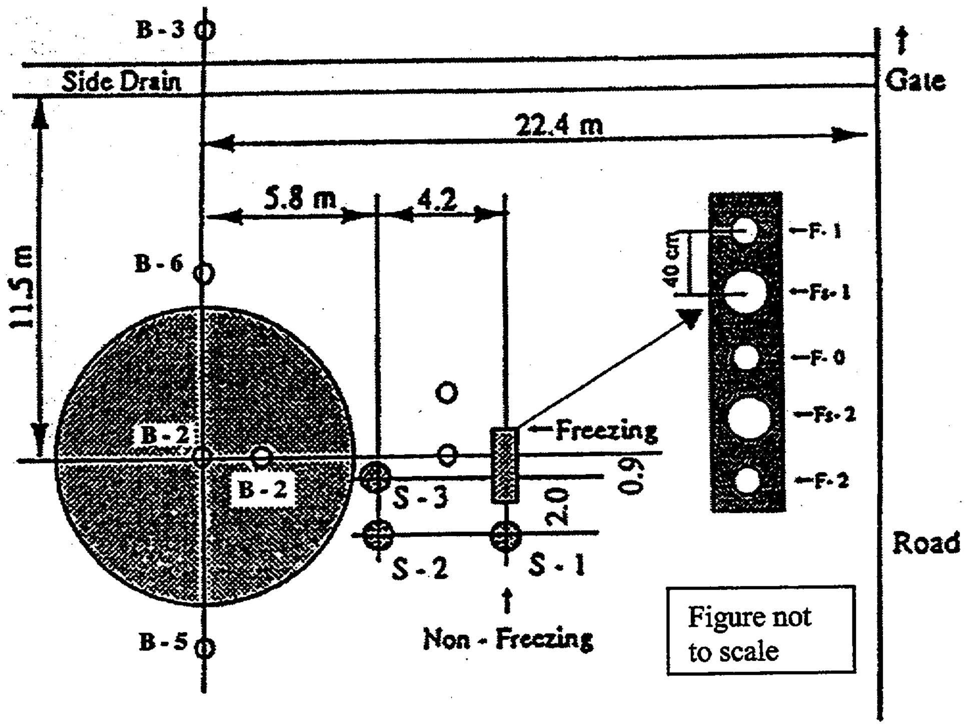

Figure 26 Sampling locations before excavation [reproduced from CRIEPI, 1993a]

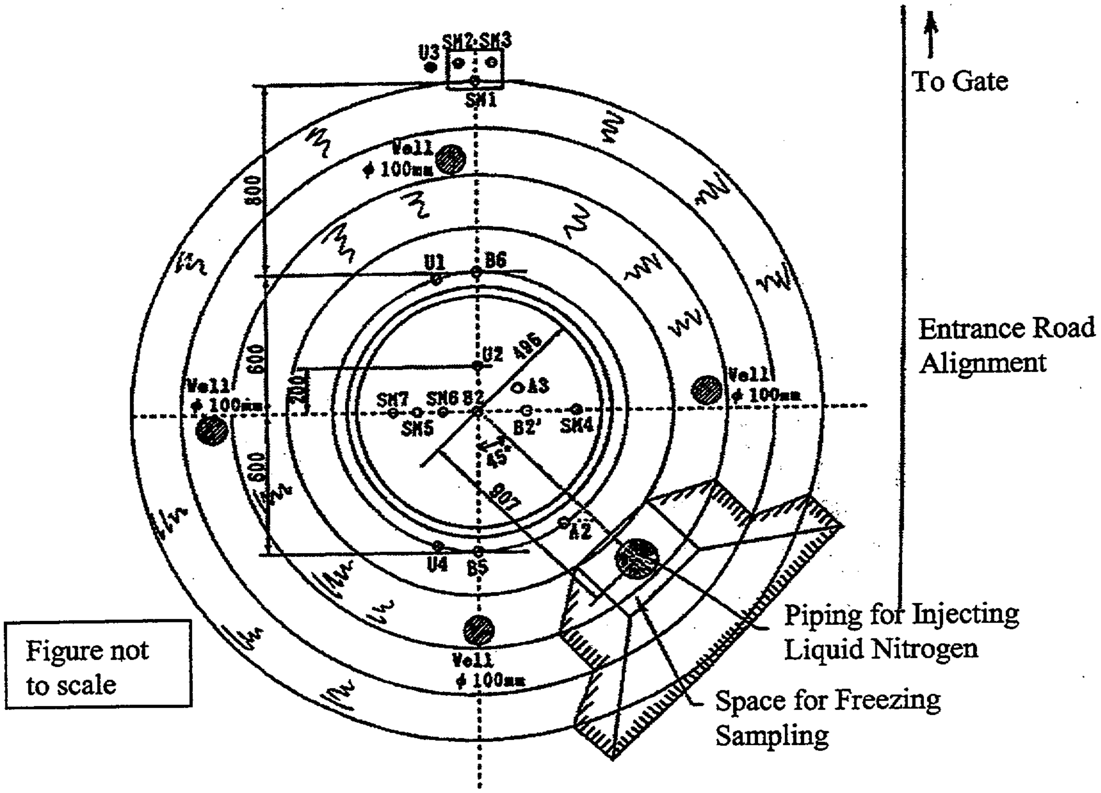

Figure 27 Location of ground freezing sampling after excavation at GL-5m [reproduced from CRIEPI, 1993a]

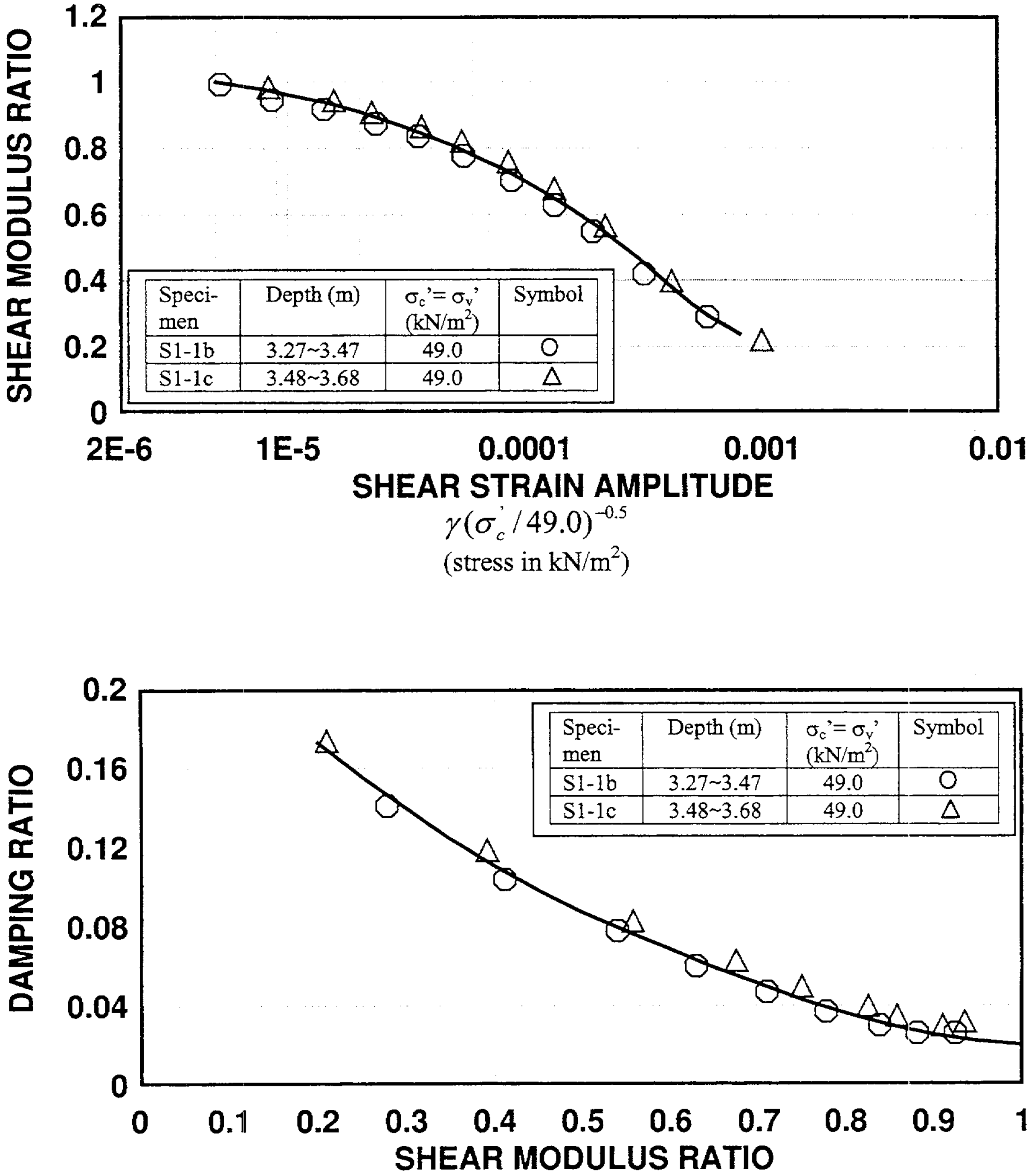

Figure 28 Secant shear modulus ratio (G/G_m) and damping ratio (h) for sand [reproduced CRIEPI, 1994a]

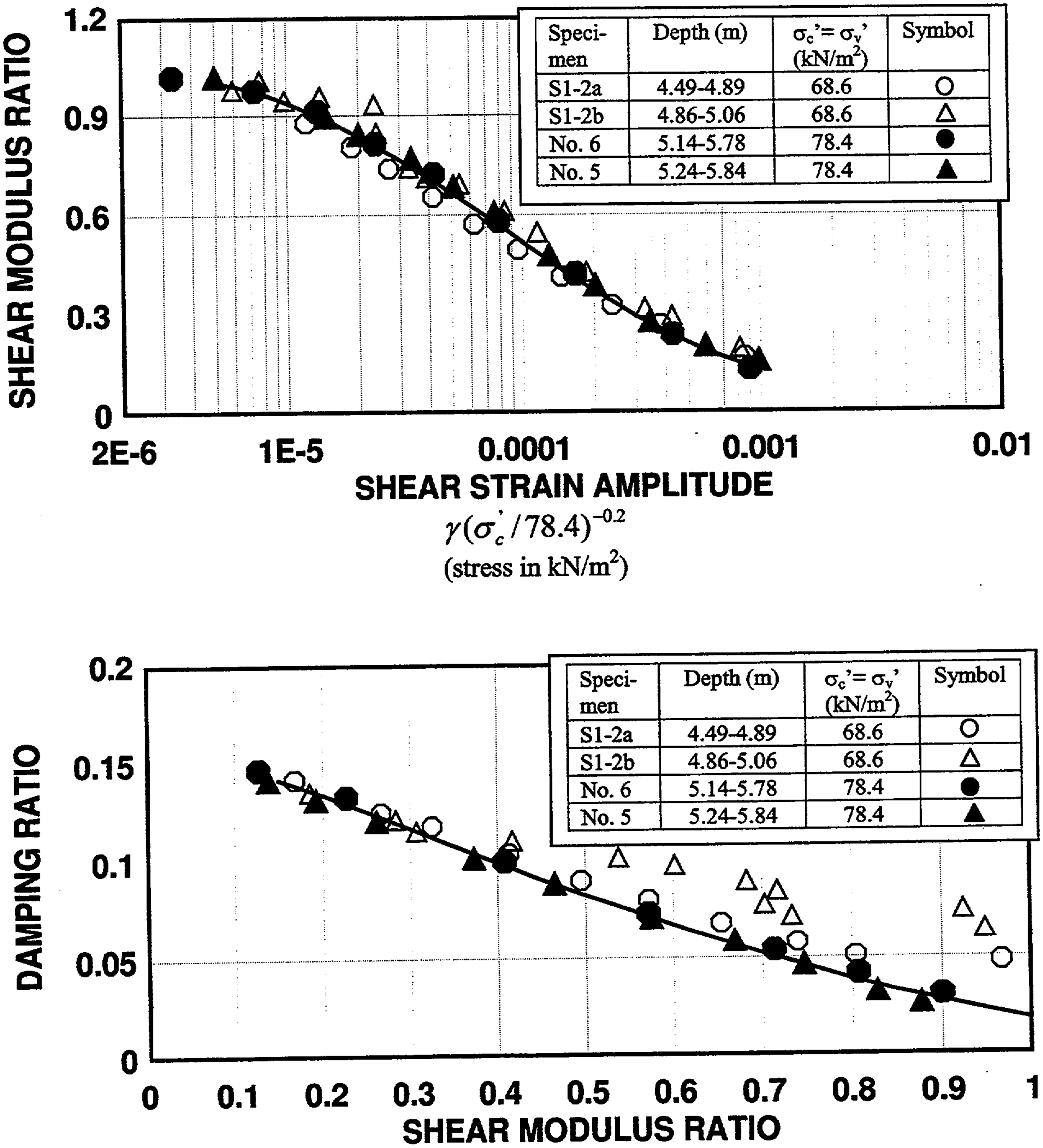

Figure 29 Secant shear modulus ratio (G/G_m) and damping ratio (h) (GL-4.5m to GL-6.5m) [reproduced from CRIEPI, 1993a and 1994a]

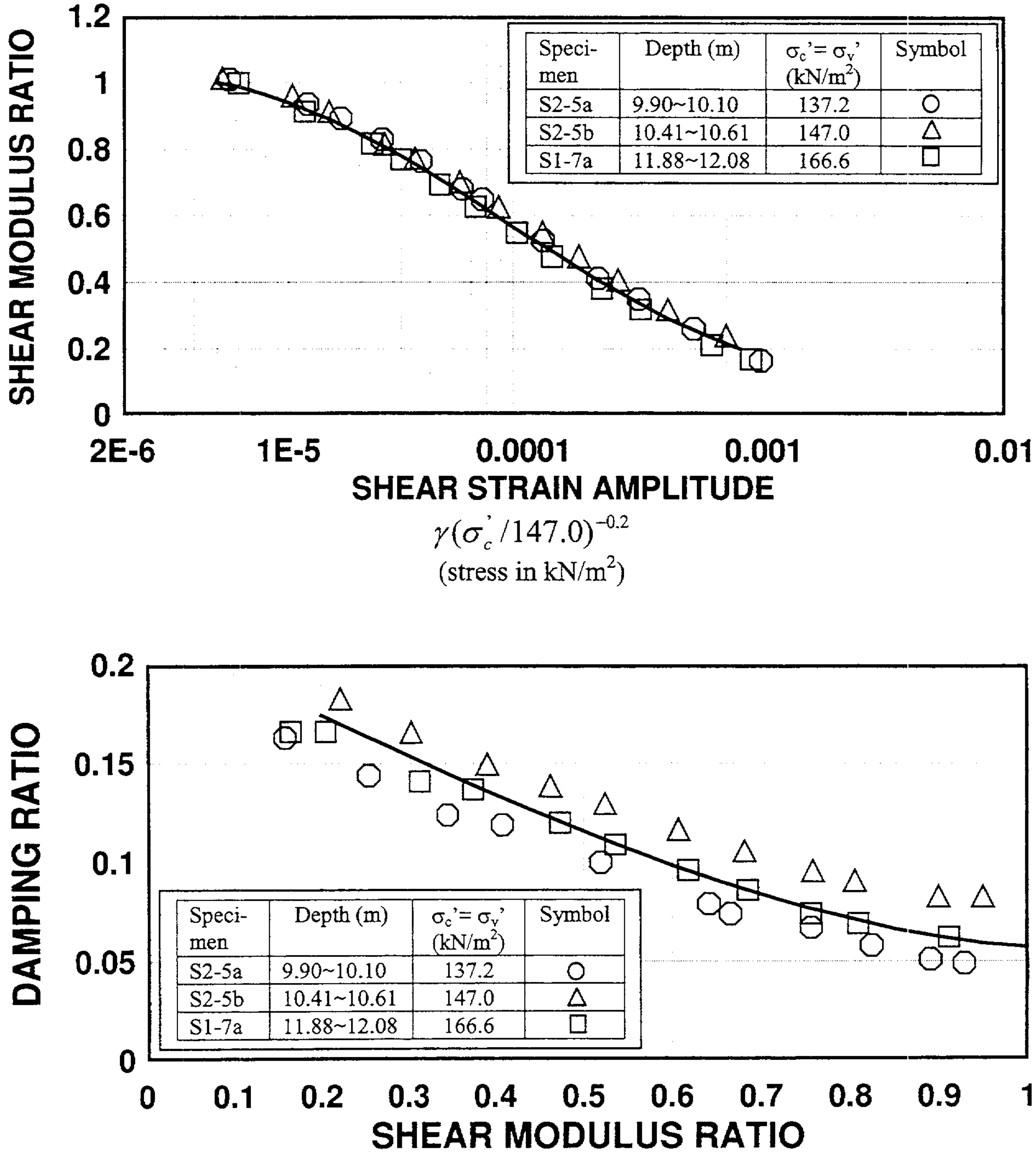

Figure 30 Secant shear modulus ratio (G/G_m) and damping ratio (h) (GL-6.5m to GL-13m) [reproduced from CRIEPI, 1994a]

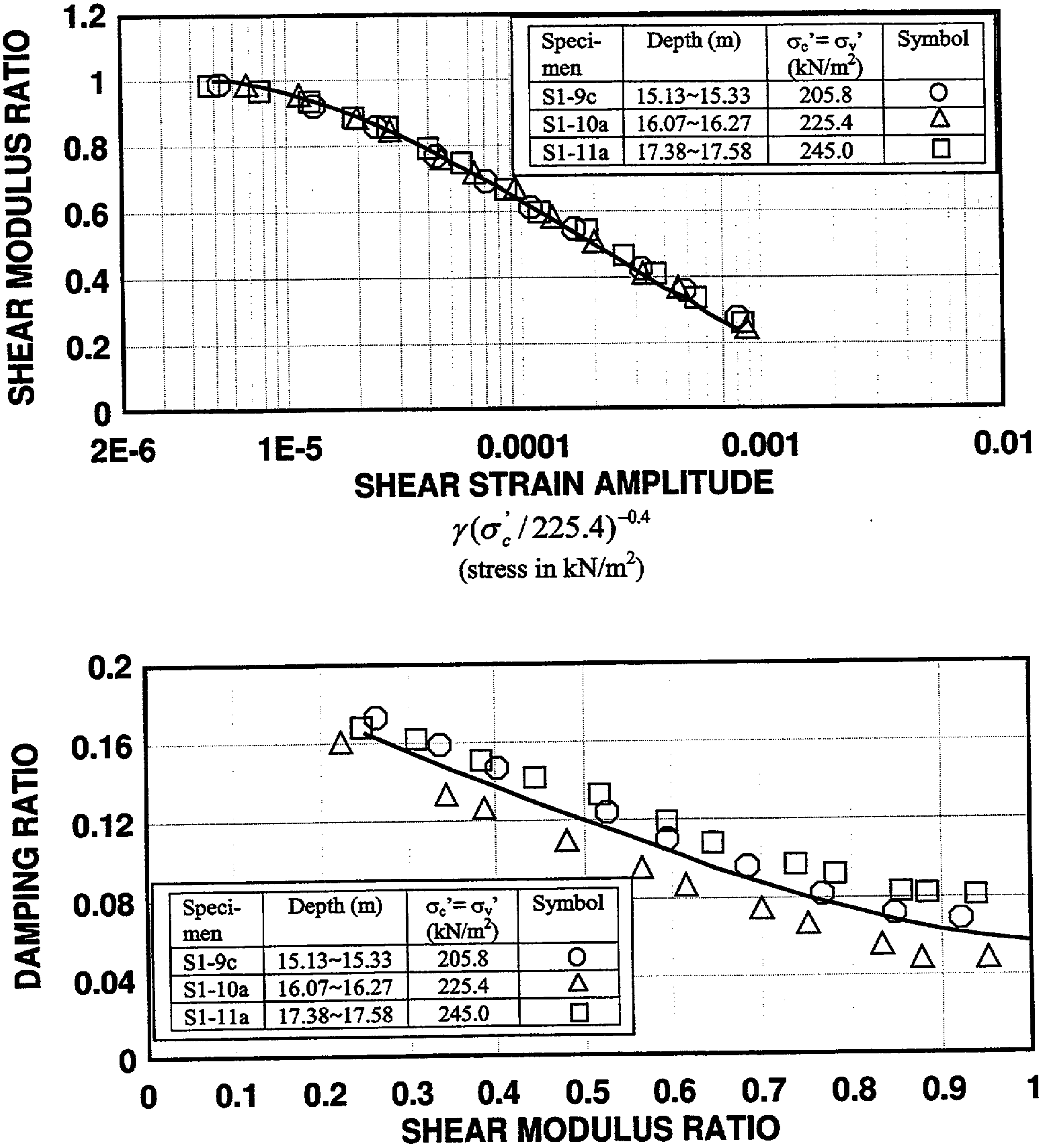

Figure 31 Secant shear modulus ratio (G/G_m) and damping ratio (h) (GL-13m to GL-20m) [reproduced from CRIEPI, 1994a]

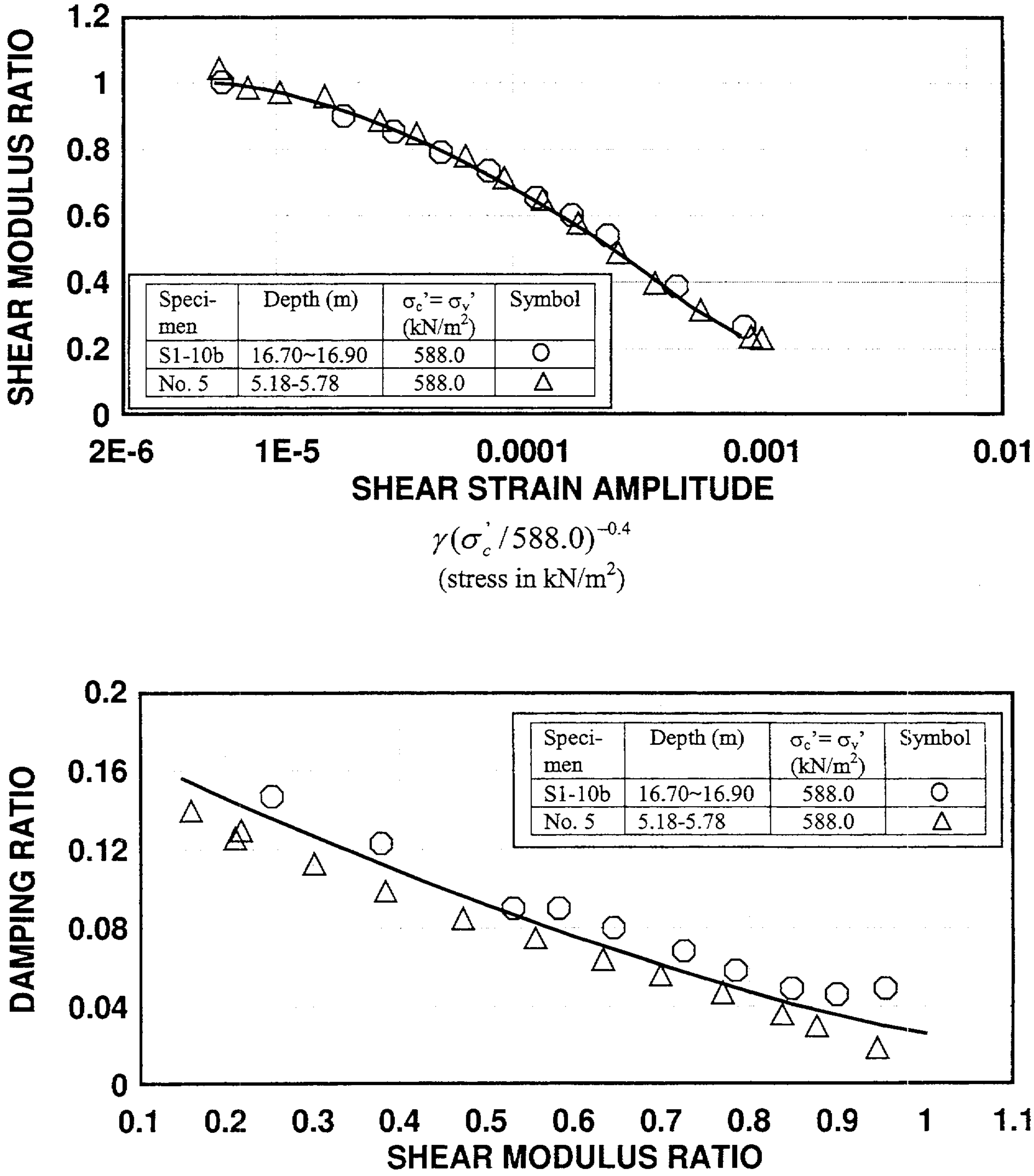

Figure 32 Secant shear modulus ratio (G/G_m) and damping ratio (h) for gravel below GL-20m [reproduced from CRIEPI, 1994a]

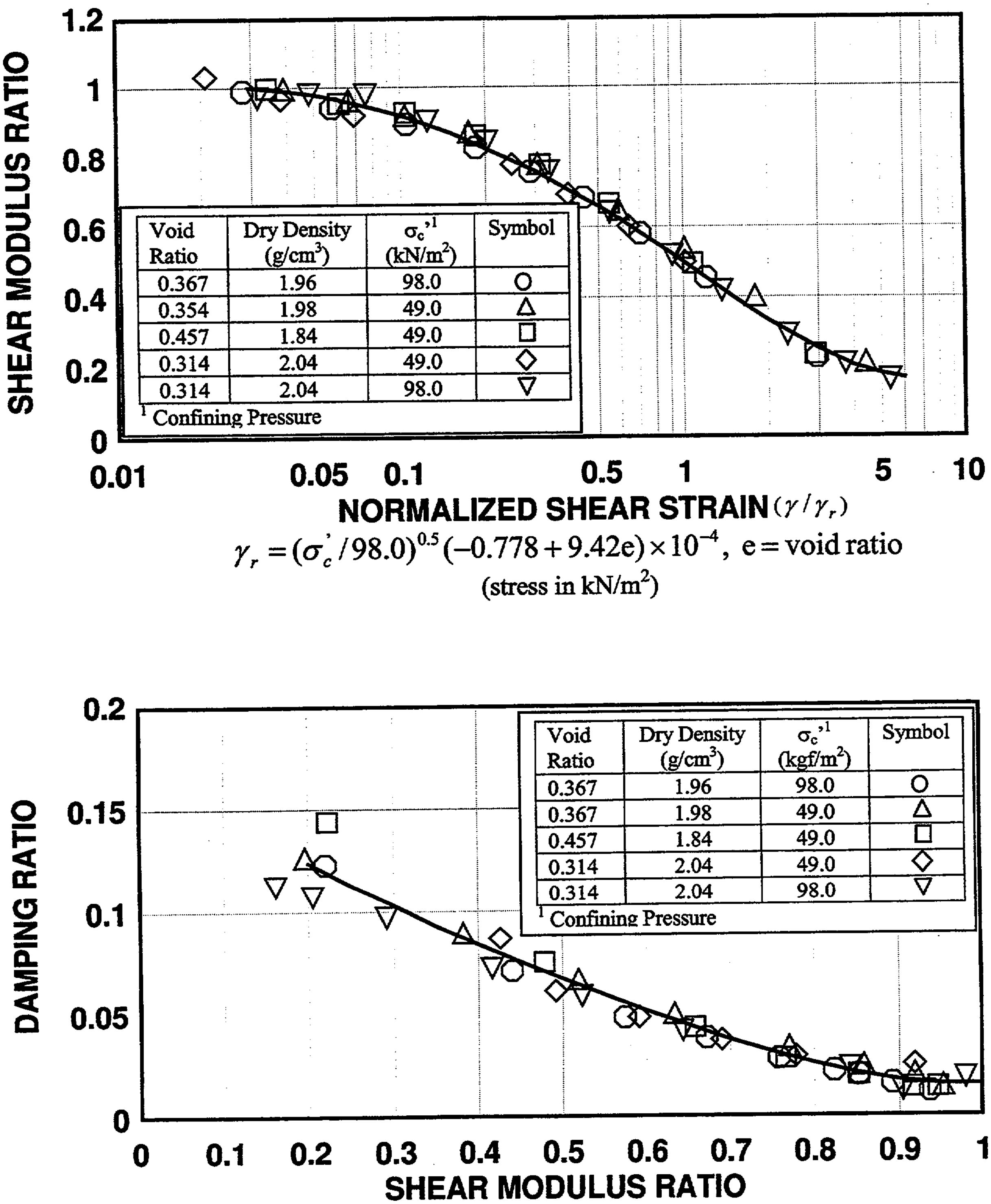

Figure 33 Secant shear modulus ratio (G/G_m) and damping ratio (h) for as-built backfill [reproduced from CRIEPI, 1994b]

6. FORCED VIBRATION TESTS

Forced vibration tests designated Forced Vibration Test 1 (FVT-1) and Forced Vibration Test 2 (FVT-2) were conducted in October and November of 1992 (FVT-1) and in February of 1993 (FVT-2), with the purpose of determining the dynamic behavior and properties of the soil-structure system at low-level vibrations, *i.e,* in the linear elastic range. To assess the effect of embedment, the FVT-1 was conducted before construction of the backfill and the FVT-2 after construction of the backfill. For both tests horizontal steady-state excitations in two orthogonal directions (plant NS and EW directions as shown in Figures 2 and 5) were applied to the roof floor (RF) and first floor (FF), which is the top of foundation slab, whereas vertical excitations were applied to the first floor level only. Both tests were conducted by TEPCO and Kajima (TEPCO, 1993a; TEPCO and KTRI, 1993a; TEPCO, 1993b; Morishita *et al.*, 1993, Kobayashi *et al.*, 1996).

External steady-state harmonic forces were generated by the exciter described in Morishita *et al.* (1993) mounted either on the roof floor (RF) or on the first floor (FF) of the model. Horizontal loads were applied in both the NS and EW direction at both the roof floor and first floor and vertical loads were applied only at the first floor. The response of the test model and surrounding soil at each sensor is given in terms of the displacement amplitude and phase lag to the exciting force, measured using displacement-meters with the layout shown in Morishita *et al.* (1993). To reduce noise, special recording and measuring procedures based on cross-correlation analysis between the loading and response records were used.

At least two approaches can be used to interpret in-situ soil properties from the measured FVT data. One approach is to compare measured responses to those predicted by analytical models incorporating the soil properties. This is an indirect approach because the analysis results integrate the effects of all model parameters (V_P, V_S, ρ, ν, etc.) and do not easily permit discrimination of the effects of individual parameters. A second approach involves direct interpretation of soil wave-speeds from measured soil responses at various ranges from the rocking structure. This approach permits direct estimates of soil wave-speeds. Both approaches are considered here.

6.1 *Forced Vibration Test 1 (FVT1)*

Observed Response

The more significant aspects of the observed response under lateral loading can be identified from the results shown in Figures 34 to 39. Shown in those figures are: (1) NS and EW roof responses for NS roof loading (Figures 34 and 35); (2) EW and NS roof responses for EW roof loading (Figures 36 and 37); and (3) vertical roof response under vertical first floor loading (Figures 38 to 40). The relevant aspects of the data shown are as follows:

1. The fundamental frequency of the soil-structure system under the horizontal loads appears to be between 4.1 and 4.6 Hertz;
2. The system response under horizontal loads is non-classical in the sense that its transfer function shows two closely spaced peaks at 4.1 and 4.6 Hertz;
3. The response under the NS horizontal loading differs from that under the EW horizontal loading;

4. For horizontal loading in one direction there is significant response on the transverse direction (cross-axis response) which indicates that <u>anisotropic</u> soil conditions or non-homogeneous soil properties exist at the site;
5. The EW direction appears to be stiffer than the NS direction; and
6. The results from the vertical excitation indicate a vertical system frequency of about 11 Hertz and a highly damped vertical vibration mode. The vertical frequency response function differs from the classical response of rigid foundations in that it exhibits two peaks: one at a frequency slightly less than 10 Hz and the other at a frequency slightly above 10 Hz. This non-classical behavior appears to be related either to the deformation of the foundation plate or to the soil anisotropy. A comparison of the roof and basement responses indicates that the axial deformation of the containment shell contributes to about 12% of the total roof response.

Although not shown in Figures 34 to 38, it is noted that analysis of the data collected reveals little or negligible torsional response of the model under all loading conditions and insignificant rocking response under the vertical loading. The absence of significant torsional response under lateral loading, implies that the cross-axis response observed cannot be explained as a result of torsion. It also implies that, for a given direction, the horizontal responses under lateral loading recorded at each floor do not differ much from sensor to sensor and can be well represented by the motion of any of the floor sensors in the direction of interest.

A summary of the peak roof responses that includes the contributions of rigid body sliding, rigid body rocking and structural deformation to the total response is given in Table 16. The results shown are averages of displacements recorded or computed directly from the data.

Table 17. Summary of observed lateral peak roof responses for FVT-1 roof loading

Response in (μm/ton)	**NS Loading**			**EW Loading**		
	NS-Response		EW Response	EW-Response		NS Response
	1st Peak	2nd Peak		1st Peak	2nd Peak	
Total Response	216.1 (4.1 Hz)	120.8 (4.6 Hz)	133.6 (4.2 Hz)	132.1 (4.1 Hz)	180.3 (4.6 Hz)	128.6 (4.2 Hz)
Rigid Body Sliding	23.6 (10.9 %)	15.4 (12.8 %)	15.7 (11.8 %)	16.8 (12.7 %)	20.1 (11.2 %)	15.5 (12.1 %)
Rigid Body Rocking	145.8 (67.5 %)	80.3 (66.5 %)	97.2 (72.8 %)	85.1 (64.4 %)	123.6 (68.6 %)	96.5 (75.0 %)
Structural Deformation	46.7 (21.6 %)	25.1 (20.8 %)	20.7 (15.5 %)	30.2 (22.9 %)	36.6 (20.3 %)	16.6 (12.9 %)

The observed results indicate significant structural deformation contribution to the total response. This is to be expected and it is indeed a welcome result, since the experiment has been designed, in part, to analyze the effect of the structural response on the soil-structure interaction, an effect that could not be properly investigated with the Lotung LSST. When the structural deformation contributes significantly to the total response, it must be accounted for in the SSI analysis (Wolf, 1985) and rigid body models cannot be used. Accordingly, the flexibility of the structure is accounted for in all SSI analysis conducted for this study.

Computed Response Under Lateral Loading

The unified soil model for the FVT-1 analysis was suggested by CRIEPI (CRIEPI, January 15, 1993) based upon the site characterization effort reviewed above. Soil properties relevant for the FVT-1 are shown in Table 17. The model assumes homogeneous and isotropic soil conditions at the site.

Table 18. Unified model properties for base soil before backfill (FVT-1)

Material	**Depth (m)**	**Mass Density (kg/m^3)**	**Shear Wave Speed (m/sec)**	**Poisson's ratio**	**Damping Ratio (%)**
Foundation	5 - 12	2420	317	0.47	2
Base	> 12	2420	476	0.47	2

Classical foundation vibration models, the so-called spring-method models for soil-structure interaction (SSI) analysis, are used in this study to verify the ability of the unified soil model to produce the measured FVT1 results. Since the FVT1 results show strong evidence of either a non-isotropic soil condition or non-homogeneous soil properties under the foundation, an extension of the spring-method that can account for non-isotropic horizontal soil conditions is proposed and used here for the soil-structure interaction analysis.

The major assumptions of the SSI model used are:

1. There are two orthogonal horizontal directions, denoted here as principal directions, such that loading in each one of these directions produces no cross-axis response;
2. For loading in a principal direction the soil-structure system can be analyzed using the classical stick model approach and their respective impedance functions developed for isotropic soil conditions on the basis of the S wave speed for this principal direction;
3. The impedance functions for isotropic soil conditions determined for each principal direction can be combined in the same manner as the stiffnesses of a beam with a non-symmetric cross-section under pure biaxial bending; and
4. The structural stiffness and the inertia of the structure and its foundation are considered isotropic.

Besides the customary parameters used for SSI analysis the following two parameters are introduced: the ratio, ***n***, of the impedance in the major principal direction to the impedance in the minor principal direction (greater than one) and the angle, α, measured counterclockwise from the major principal direction (*i.e.*, the direction with the greatest S wave speed) to the direction of loading.

The method and equations proposed by Beredugo and Novak (1967) are used to determine the soil impedance functions for the principal directions. Although that method does account for coupling between the rocking and sliding modes of vibration in the case of a surface foundation, the results obtained with it are generally similar to those obtained with other procedures that account for this coupling effect, *e.g.*, Kausel *et al.* (1978). However, for the case of embedded foundations, the approach by Beredugo and Novak has definite advantages over most other spring-methods for soil-structure interaction. Most notably, its advantages include (Lin, 1982):

1. different elastic properties can be used for the backfill and underlying foundation soil, which is the most commonly encountered situation and the case for the Hualien LSST;

2. the frequency dependence of the side layer impedance functions is independent of that for the underlying foundation material; and
3. different functions have been developed for the impedance functions of the side layer for sliding, rocking and torsional modes of vibration.

Given its advantages for the SSI analysis of embedded structures the approach by Beredugo and Novak is chosen for the SSI analysis. Details of the SSI model used for this study are given in **Appendix A.**

The fixed base structure is represented by a massless cantilever with cross-section properties equal to those of the containment shell, and with the roof mass concentrated at the free end. Both bending and shear deformations are accounted for in the calculation of the lateral stiffness of the containment shell. The fundamental frequency of the fixed-base structure computed in this manner with $E_c = 28{,}200{,}000$ kN/m^2 (as given in Ch. 4) and $\nu = 0.2$, is 11.1 Hz, which is similar to the fundamental frequency of 10.7 Hz computed with more refined structural models (Miller and Costantino, 1994).

The SSI response obtained using the unified soil model for FVT-1 and the fixed-base structural stiffness indicated above matches well the recorded responses. However, analysis of the contribution from each mode of deformation to the total response lead to the conclusion that the fixed-base structure was too stiff and that the rocking response of the soil was excessive. Accordingly, the stiffness of the fixed-base structure was reduced and the soil properties varied until a good fit to the contribution of each mode of deformation to the total response was obtained. The best-estimated soil properties obtained in this manner are shown in Table 18. To obtain a good fit to the structural deformation response, the fixed-base structural stiffness was reduced to about 71% of its original value, *i.e.*, $E_c = 20{,}000{,}000$ kN/m^2 was used. This stiffness reduction is needed because the concrete shell stiffness is less than its linear elastic stiffness; and, as discussed in Appendix A, only the mass of the roof is included in the fixed-base structural model whereas the mass of the concrete shell is considered as part of the rigid foundation.

Table 19. Best-estimated soil properties from SSI analysis of FVT-1

Material	**Depth (m)**	**Density (kg/m^3)**	**S-Wave Speed Principal Direction (m/sec)**	***n***	**α**	**Poisson's ratio**	**Damping Ratio (%)**
Foundation	5 - 12	2420	319	1.25	-35°	0.48	2.5

It is noted that the shear wave speed shown in Table 18 is for the major principal direction, which, for ***n*** = 1.25, implies a S wave speed of 285 m/sec for the minor principal direction and S-wavespeeds of about 296 m/sec for the plant NS direction and 308 m/sec in plant EW direction. The major principal direction, *i.e.*, the one with the greatest S wave speed, is found by rotating 35^0 counterclockwise from the plant (shaker) EW direction. Using a different approach Morishita *et al.* (1993) determined that the major principal direction as defined here could be found by rotating 34^0 counterclockwise from the plant EW direction.

Since this is a layered site with a softer layer underlain by a stiffer layer at a depth H, the rocking stiffness was multiplied by the following factor suggested by Gazetas (1982)

$$k_L = (1.+\frac{1}{6}\frac{R}{H}) / (1+\frac{1}{6}\frac{R}{H}\frac{G_1}{G_2})$$

where R = foundation radius, H = depth to the underlying stiffer layer, G_1 = soil shear modulus for the upper (foundation) layer and G_2 = soil shear modulus for the lower (base) layer. Here, the shear modulus for the foundation soil was computed with the data in Table 18 and that for the base layer with the data in Table 17.

Table 20. Summary of computed lateral peak roof response for FVT-1 roof loading

Response (μm/10kN)	**NS Loading**		**EW Loading**	
	NS-Response	**EW-Response**	**EW-Response**	**NS-Response**
Total Response	219.4 (at 4.2 Hz)	133.4 (4.3 Hz)	181.7 (4.6 Hz)	133.4 (4.3 Hz)
Rigid Body Sliding	16.7 (7.46%)	--	13.3 (7.3 %)	--
Rigid Body Rocking	158.5 (72.2 %)	--	126.8 (69.8 %)	--
Structural Deformation	44.2 (20.1 %)	--	41.7 (22.9 %)	--

The results obtained with the best-estimated properties are shown in Figures 41 to 46 for the lateral loading and a summary of the peak results obtained is shown in Table 19. The total response results shown in Figures 41 to 46 compare well with the measured ones. The computed contributions of each mode of deformation to the total response also compare well with the measured ones but not as well as for the total response.

On the basis of the observed test results and of the analytical modeling the following conclusions can be made:

1. Site conditions averaged under the model foundation and its periphery are anisotropic as a result of possible non-homogeneous soil conditions.
2. The plant EW direction appears to be stiffer than the NS direction, a conclusion, which is somewhat evident in the S wave speed data shown in Figure 17.
3. The major principal direction (*i.e.,* that with the greatest stiffness) can be obtained by rotating 35^0 counterclockwise from the plant (or shaker) EW direction.
4. Average S wave velocities in the major and minor principal direction for the soil under the foundation from GL-5m to GL-12m are found to be, approximately, 319 m/sec and 285 m/sec, whereas the average S wave velocities in the EW and NS directions are about 308 and 296 m/sec, respectively.
5. Rigid body sliding appears to be underestimated by the analytical model.
6. A hysteretic damping ratio $h \approx 2.5\%$ leads to analytical results that more closely match the observed response than the 2% value recommended by CRIEPI.

Computed Response Under Vertical Loading

The vertical response was analyzed using the so-called spring method for soil-structure interaction analysis to verify the ability of the unified soil model to produce the observed results. Since the observed data show significant axial deformation of the containment shell and some deformation of the foundation plate, an attempt was made to include such modes of deformation in the SSI analysis. Accordingly, the model used in the analysis considered the following three degrees-of-freedom: the rigid body vertical deformation of the foundation; the axial deformation of the containment shell; and the relative deformation between the rigid body deformation of the foundation and the total deformation of the center of foundation plate. In the model, the containment shell is supported on the rigid foundation whereas the foundation plate is partly supported in the rigid foundation and partly supported on the ground.

The foundation plate is on top of a 7-m thick layer of gravel with an estimated shear wave speed of about 317 m/sec according to the unified model for FVT-1 (see Table 17) which is underlain by a stiffer layer of gravel with an estimated shear wave speed of 476 m/sec. Given that the foundation radius is 5.41 m, this implies that layered site conditions must be accounted for in the analysis. As an approximation, the impedance functions for a rigid square foundation on a layer with shear wave speed increasing from V_{ST} at the top to V_{SB} at the bottom, over a half-space with shear wave speed V_{SR}, are used in this study, with the static stiffness for a circular foundation used in place of that for the square foundation. These impedance functions are taken from Wolf (1988) and are based on the results obtained by Wong and Luco (1985). The impedance functions reported are for a Poisson's ratio, $\nu = 1/3$. However, the soil below the foundation is believed to be saturated, which means that its Poisson's ratio is, approximately, equal to 0.5. Generally, the frequency term of the impedance function for $\nu = 0.5$ is much smaller than that for $\nu = 1/3$ for frequencies greater than about $1.5V_S/R$, where R is the foundation radius and V_S is the shear wave speed. Accordingly, the stiffness term of the impedance function at a given frequency is multiplied by a correction factor. This correction factor is equal to the ratio of the stiffness for $\nu = 0.5$ to that for $\nu = 0.4$ reported in Gazetas (1991) for the vertical vibration of a rigid circular footing on a homogeneous half-space. The damping term is not corrected because it is, generally, not significantly affected by this change in Poisson's ratio.

As referred to above, a 3 degrees-of-freedom model is used in the analysis. One of the degrees-of-freedom is used to account for the flexibility of the base plate. This degree-of-freedom is supported by the rigid foundation degree-of-freedom and by the soil. Concentrated springs and dampers are used to represent those supports. The stiffness and damper of the ground support are taken to be those for a rigid circular plate with half the radius of the foundation plate, and they are assumed to be frequency independent, *i.e.*, the zero-frequency values are used. The stiffness of the attachment to the rigid foundation should, in principle, be derived from the first mode of vibration of a clamped thick circular plate. Here, for simplicity, that stiffness is computed such that the total deformation of the plate under static loading is, approximately, that observed under low-frequency loading. The mass of this degree-of-freedom is taken to be that of a plate with a radius equal to one-half the radius of the foundation plate. A sensitivity analysis revealed that the response of the roof plate is relatively insensitive to the stiffness, damping and mass used for the supports of this degree-of-freedom.

The results obtained with this SSI model and the soil properties shown in Table 20 and a Young's modulus of 20×10^6 kN/m^2 for the concrete shell are shown in Figures 47 and 48. A relatively good agreement between the calculated and measured responses is observed. The analytical model cannot represent the double peak in the observed response and the rapid amplitude decay for frequencies greater than those for the peak values. Such discrepancies may be either the result of using frequency dependent stiffness and damping derived for a rigid foundation when this is a flexible foundation, or the result of soil anisotropy.

Table 21. Best estimate soil properties from SSI analysis of FVT-1 vertical loading

Material	**Depth (m)**	**Mass Density (kg/m^3)**	**Shear Wave Speed (m/sec)**	**Poisson's ratio**	**Damping Ratio (%)**
Foundation	5 - 12	2420	305	0.48	2
Base	> 12	2420	467[1]	0.48	2

[1] A value of 410 m/sec was used in the calculations to account for the fact that the impedance functions considered were derived for a underlying half-space with a mass density equal to 1.3 times the density of the surface layer, whereas the densities of the surface layer and half-space are identical for this site.

Soil Wave-Speeds from Measured Soil Responses

During the FVT-1 tests, soil response was measured at three ranges from the structure. Measurements were made along a North Radial and along a East Radial. The measurements were made at the foundation level (designated BS) at a range of 1.5 m, at the mid-depth in the excavation (designated MS) at a range of 6.0 m and at the ground surface (designated TS) at a range of 9.5 m. Figure 49 shows the location of the measurements in both FVT-1 and FVT-2.

The soil response can be used to estimate the wavespeeds in the soil. The analysis is based upon the fact that a traveling wave emanating from a steady state source will show a continuously increasing phase shift with respect to the wave source as the distance from the source increases. In uniform, elastic material the increase will be linear. The wavespeed can be computed from:

$$C_R = \frac{2\pi f \Delta R}{\Delta \phi}$$

where C_R = wavespeed, f = frequency, ΔR = distance between measurements and $\Delta\phi$ = phase shift difference between two measurements. For a vertically vibrating foundation, most of the energy propagating away is in the Rayleigh (surface) wave. The vertical vibrating foundation condition is a convenient experiment for estimating the Rayleigh wave speed. Since the Rayleigh wave speed is 90 to 95% of the shear wave speed (93% for $\nu = 0.25$, 96% for $\nu = 0.50$) an estimate of the shear wavespeed can be derived. Richart, Hall and Woods (1970) described the analysis method. They suggest that, since the bulk of the surface wave travels in a zone about one wave length deep, at a layered site the inferred wavespeed can be estimated as representative of the speed at a depth of one-half the wave length. More recently, it has been suggested (*e.g.,* Gazetas, 1991) that for inhomogeneous soil deposits the Rayleigh wave speed from the above equation corresponds to a depth of about 1/3 of the wavelength, the depth of the center of the surface wave displacement profile.

In the following, the north and east sides and directions refer to the plant north and corresponding east identified in Figure 2. Under the FVT-1 vertical loading test (FF-UD), vertical responses were measured as follows:

1. East side at the BS and MS levels; and
2. North side at the MS level.

The data set has limitations for several reasons, namely:

1. measurements were made at different elevations (BS, MS, TS);
2. measurements were relatively close to the source (surface waves not fully developed);
3. measurements were only made on the east and north sides; and
4. only a few measurements were made.

Nevertheless, the data are used here to gain further insight into the implied wavespeeds. The slant range between measurement locations was used in the analysis rather than the radial distance. Amplitude and phase measurements at the foundation and at the BS and MS locations are shown in Figures 50 and 51. The amplitude data clearly shows the attenuation of amplitude with distance. However, there is strong similarity in the spectral shape in the neighborhood of the peak responses. The phase relations contain both foundation response information and traveling wave information. Traveling wave information is obtained by computing the phase differences between different locations.

The phase differences BS-FF, MS-FF, and MS-BS are shown in Figure 52 and the phase differences MS-FF(east) are shown in Figure 53. These should show linear relations for a half-space. The results are approximately linear to about 14 Hz. The results below 14 Hz can be used to estimate the surface wavespeeds at depths corresponding to one-third of the wavelength for frequencies below 14 Hz. The data above 14 Hz are irregular. Since the higher frequencies sample the shallower depths, these results may indicate layering and/or be tainted by stepped measurement locations and/or result from the lack of a fully developed surface wave at these frequencies.

Wavespeeds estimated from the linear fits to the phase difference measurements on the East side of the structure are shown as a function of depth in Figure 54. The wavespeeds computed between FF and BS are the lowest, between BS and MS the highest and between FF and MS in between. The average of the cross-hole logging results beneath the foundation for two approximately orthogonal directions are also shown in Figure 54. The cross-hole speeds shown are averages for measurements in the A1-A4 direction (see Figure 9) labeled EW in Figure 54, and for measurements in the B2′-B6 direction (see also Figure 9) labeled NS in Figure 54. It is noticed that the S wavespeeds inferred from the forced vibration tests are lower than those recommended by CRIEPI for the unified soil model for FVT-1 (CRIEPI, 1993c).

S-wave speeds computed from the phase differences for the north locations are also shown in Figure 54. The estimates suggest that the north wavespeeds are about 90% of the east wavespeeds. The averages of the cross-hole measurements under the foundation show a similar trend.

6.2 *Forced Vibration Test 2*

Observed Response

The more relevant aspects of the observed response can be identified from the results shown in Figures 55 to 60. Shown in those figures are: (1) NS and EW roof responses for NS roof loading (Figures 55 and 56); (2) EW and NS roof responses for EW roof loading (Figures 57 and 58); and (3) vertical roof response under vertical first floor loading (Figures 59 and 60). The relevant aspects of the data shown are as follows:

1. The fundamental frequency of the soil-structure system under the horizontal loads appears to be about 6.1 Hertz for both directions.
2. The system response under horizontal loads shows only one peak for each loading direction.
3. NS and EW along-axis and cross-axis responses are similar for both loading cases.
4. Cross-axis responses although significant are a much smaller percentage of the along-axis as compared to the FVT-1 response.
5. Vertical excitation results indicate a vertical system frequency of about 12 Hertz (based on the frequency for a phase angle of 90^0) and a highly damped vertical vibration mode. The maximum displacement is about 60% of that for the FVT-1, whereas the fundamental frequency was approximately equal to that measured in the FVT-1, indicating that the backfill effect is an increase in damping (Miller and Costantino, 1994). Horizontal displacements were negligible for this mode of vibration, but the containment shell axial deformation appears to contribute about 12% to the displacement of the roof plate. Additionally the response appears to differ from the classical response for rigid foundations in that it has two peaks in the vicinity of 10 Hz.

Although not shown in Figures 55 to 60, analysis of the data collected reveals little or negligible torsional response of the model under all loading conditions. This implies that the cross-axis response observed cannot be explained as the results of torsion. It also implies that, for a given direction, the horizontal responses under lateral loading recorded at each floor do not differ much from sensor to sensor and can be well represented by the motion of any of the floor sensors in the direction of interest.

A summary of the more significant peak responses under the lateral loading including the contributions of rigid body sliding, rigid body rocking and structural deformation to the total response is given in Table 21. The results shown are averages of the displacements recorded or directly computed from the data.

Table 22. Summary of observed lateral peak roof response for FVT-2 roof loading

Response in (μm/ton)	**NS Loading**		**EW Loading**	
	NS-Response	**EW-Response**	**EW-Response**	**NS-Response**
Total Response	63.9 (6.1 Hz)	13.1 (6.2 Hz)	59.5 (6.2 Hz)	13.2 (6.2 Hz)
Rigid Body Sliding	2.5 (3.9 %)	0.82 (6.3 %)	2.8 (4.7 %)	0.84 (6.4 %)
Rigid Body Rocking	34.7 (54.3 %)	8.49 (64.8 %)	34.1 (57.3 %)	7.55 (57.2 %)
Structural Deformation	26.7 (41.8 %)	3.79 (28.9 %)	22.6 (38.0 %)	4.81 (36.4 %)

Computed Response Under Lateral Loading

The unified soil model for the FVT-2 analysis was suggested by CRIEPI (CRIEPI, 1995b) on the basis of the site characterization work reviewed above. Soil properties relevant for the FVT-2 analysis are shown in Table 22. As for the FVT-1 case, the unified soil model assumes homogeneous and isotropic soil conditions at the site.

SSI analyses for the FVT-2 case were conducted using the lumped-mass SSI model for anisotropic site conditions described above. All the assumptions made in the development of the model for the FVT-1 analysis are retained and, in addition, a isotropic as-built backfill soil is assumed. For the gravel-1, it is assumed that the ratios of the S wave speeds in the major and minor principal directions and the orientation of the principal directions are those determined on the basis of the FVT-1 data.

Table 23. Unified model properties for base soil after backfill[1]

Material	Depth Increment (m)	Mass Density (kg/m^3)	Shear Wave Speed (m/sec)	Poisson's ratio	Damping Ratio (%)
Sand 1	0 - 2 m	1690	133	0.38	2
Sand 2	2 - 5 m	1930	231	0.48	2
Backfill-1 above W.T.	0 - 2 m	2330	300	0.38	2
Backfill-2 below W.T.	2 - 4 m	2390	300	0.48	2
Backfill-3 below W.T.	4 - 5 m	2390	250	0.48	2
Gravel-1 (foundation)	5 - 12 m	2420	383	0.48	2
Gravel-2′	5 - 8 m	2420	280	0.48	2
Gravel-2	5 - 12 m	2420	333	0.47	2
Gravel-3	12 - 20 m	2420	476	0.47	2

[1] The soil types are identified in Figure 6.

The containment stiffness and the soil properties were varied to obtain a good fit to the observed response including the contributions of the various modes of deformation to the total response. The "best-estimated" soil properties obtained on this basis are shown in Table 23.

Table 24. Best-estimated soil properties for base soil and backfill from SSI[1] analysis of FVT-2

Material	Depth (m)	Density (kg/m^3)	S Wave Speed (m/sec)	n	α	Poisson's ratio	Damping Ratio (%)
Backfill	0 - 5 m	2390	309	1.0	--	0.33	2
Gravel-1 (foundation)	5 - 12 m	2420	393[2]	1.25	-35^0	0.48	2
Gravel-3	12 - 20 m	2420	476	1.25	-35^0	0.48	2

[1] The soil types are identified in Figure 6.

[2] For the major principal direction.

To obtain a good fit to the structural deformation response and still use a simple single-degree-of-freedom model for the fixed-base structure, the Young's modulus of the containment shell concrete was reduced to about 81% of its original value, *i.e.*, $E_c = 23{,}000{,}000$ kN/m^2 was used. The structural stiffness for the FVT-2 analysis is greater than that for the FVT-1 case because the lower part of the containment shell is confined by the backfill, which effectively reduces its free span.

The S wave velocities for gravel-1 for the two principal directions determined on the basis of SSI analysis of the FVT-2 data are 393 and 352 m/sec, respectively, whereas those for the loading directions, plant NS and EW, are 380 and 365 m/sec, respectively. An important parameter for the SSI analysis of embedded structures is the effective embedment length, *i.e.,* the depth of effective contact between the backfill and structural walls. Here, an effective embedment of 5.0 m is used. It should be noted, however, that other combinations of effective embedment lengths and S wave velocities for the backfill may also provide a good fit to the observed response. Embedment lengths slightly less than the actual one may be justified on the basis that the stiffness and strength of the backfill near the ground surface are likely to be small.

A summary of the response obtained using the best-estimated soil properties is given in Figures 61 and 62 and in Table 24. A good agreement can be obtained between the measured and computed responses, but the SSI model used appears to overestimate the damping of the SSI system.

Table 25. Summary of computed lateral roof responses for FVT-2 roof loading

Response in (μm/10 kN)	**NS Loading**		**EW Loading**	
	NS-Response	**EW-Response**	**EW-Response**	**NS-Response**
Total Response	56.0 (6.1 Hz)	11.5 (6.2 Hz)	55.7 (6.25 Hz)	11.2 (6.2 Hz)
Rigid Body Sliding	2.3 (4.1 %)	–	2.2 (4.0 %)	–
Rigid Body Rocking	32.8 (58.6 %)	–	32.0 (57.4 %)	–
Structural Deformation	20.9 (37.3 %)	–	21.5 (38.6 %)	–

The following observations pertinent to the site characterization can be made on the basis of the measured and computed responses and the soil properties in Tables 19 and 20:

1. Local soil anisotropy is not as evident as it is for the FTV-1 case; this, is because the SSI is dominated by the foundation embedment and the as-built backfill appears to be isotropic.
2. The best-estimate average soil properties for the soil under the foundation are similar to those proposed in the unified model for FVT-2 analysis.
3. The contributions of all deformation modes to the total response appear to be well represented by the analytical model, including the contribution from rigid body sliding which was considerably underestimated by the FVT-1 analysis. It is possible that the rigid body sliding was underestimated in the FVT-1 analysis as the result of a thin weak soil layer under the foundation that may have been significant for the FVT-1 case but not significant for the embedded case.

Computed Response Under Vertical Loading

The soil-structure interaction response under vertical loading was computed using the same analytical model as for the FVT-1 case. To account for the embedment, the static stiffness of the corresponding surface foundation is usually multiplied by a factor greater than one, which depends on the ratio of the embedment depth to the foundation radius. Those factors are, generally, available for cases in which the backfill soil and the soil above the embedment depth have the same properties as the soil below the foundation plane. Here, the backfill soil and the soil above the foundation plane are considerably less stiff than the soil beneath the foundation. For this reason, as well as for simplicity, the static stiffness for the surface case is not corrected for the embedded condition. The damping coefficient for the embedded case is taken to be 25% greater than that for the surface case for all frequencies. This is based on the fact that the damping coefficients for an embedded foundation on a homogeneous half-space are about 25% greater than those for a surface foundation on the same half-space. However, the stiffness coefficient is multiplied by the following corrective factor suggested in Gazetas (1991):

$$\chi = \left[1.0 - 0.09(D/R)^{3/4} a_0^2\right]$$

where D = depth of embedment, R = foundation radius and $a_0 = \omega R/V_S$, where ω = frequency in rad/sec and V_S = shear wave speed. The response results computed in this manner, with the soil properties shown in Table 25 and a Young's modulus of 20×10^6 kN/m^2 for the concrete shell are shown in Figures 63 and 64. The resonant frequency based on a phase lag of 90 degrees is about 12 Hz, which is similar to that observed in the test. However, the computed frequency response function does not represent well the amplitude decay for frequencies greater than those of the peak response. This could be because the stiffness and damping vary with frequency in a manner that differs from that assumed here.

Table 26. Best-estimated soil properties from SSI analysis of FVT-2 vertical loading

Material	Depth (m)	Mass Density (kg/m^3)	Shear Wave Speed (m/sec)	Poisson's ratio	Damping Ratio (%)
Foundation	5 - 12	2420	365	0.48	2
Base	> 12	2420	467	0.48	2

[1] A value of 410 m/sec was used in the calculations to account for the fact that the impedance functions considered were derived for a underlying half-space with a mass density equal to 1.3 times the density of the surface layer, whereas the densities of the surface layer and half-space are identical for this site.

Soil Wave-Speeds from Measured Soil Responses

The method described to estimate surface wave speeds in the ground from the measurements of soil response under the FVT-1, is used here in conjunction with the FVT-2 vertical loading. Measurements were made at the same locations as in the FVT-1 (see Figure 49) except that all measurements were made at the ground surface, which simplifies the geometry. In the following, the north and east sides and directions refer to the plant (or shaker) north and corresponding east referred to in Figure 2.

East side measurements at the foundation and at the BS and MS locations are shown in Figures 65 and 66. The amplitude plot clearly shows the attenuation of amplitude with range. However, the BS amplitudes are not as attenuated as in the FVT-1, apparently due to the backfill. Since the phase relations contain both foundation response information and traveling wave information, the traveling wave information is obtained by computing the phase differences between different locations.

The phase differences BS-FF, MS-FF, and MS-BS are shown in Figure 67. These show piecewise linear relations. Since the higher frequencies sample the shallower depths, these results may indicate layering and/or the lack of a fully developed surface wave at these frequencies.

The phase differences between the foundation and the MS measurements on the north and east sides are compared in Figure 68. The phase differences for the north direction are about 20-25% higher than those for the east direction. This implies that wavespeeds in the north direction are about 80-85% of those in the east direction. This is consistent with the FVT-1 results and with an estimate that the NS axis speed is about 80-90% of that in the EW direction.

Wavespeeds estimated from the piecewise linear fit to the phase differences on the east and north sides of the structure are shown in Figure 69 as a function of depth. The data show an increase in wavespeed with depth. Average shear wave speeds for the free-field from cross-hole logging before the excavation are also shown in Figure 69. These wavespeeds are averages of the measurements in A1-A4 direction (see Figure 9) labeled EW in Figure 69 and of the measurements in the B2′-B6 direction (see also Figure 9) labeled NS in Figure 69. As in the FVT-1 analysis, the shear wavespeeds in the base material are less than those recommended for the free-field in the FVT-2 unified model and the wavespeed to the north is lower than to the east, as noted earlier.

6.3 *Summary of FVT Analysis*

The following conclusions can be derived from the SSI analysis of the forced vibration tests presented above:

1. Soil conditions at the site are non-isotropic, *i.e.,* there appear to be two principal directions of shear wave propagation in the gravel beneath the foundation. The major principal direction - that with the highest S wave speed - can be obtained by rotating 35^0 counterclockwise from the plant (or shaker) EW direction.
2. The average soil properties recommended by CRIEPI for the gravel-1 soil for the FVT-1 and FVT-2 analyses are, approximately, equal to the best-estimated gravel-1 properties in the major principal direction.
3. Average soil properties recommended by CRIEPI (CRIEPI, 1995b) for the gravel 1 soil and for the as-built backfill soil for the FVT-2 analysis, are similar to the best-estimate properties determined on the basis of the SSI analysis of the FVT-2 data.
4. The effects of soil anisotropy are only slightly evident under the FVT-2 loading. This is because the SSI is strongly affected by the confining backfill which may be considered isotropic.
5. The shear wave speeds for the soil beneath the foundation required to compute vertical responses similar to those observed in the tests are about 10% less than those in the unified soil model for both the FVT-1 and FVT-2 cases.
6. The best-estimated soil properties determined on the basis of the FVT-2 data, which are shown in Table 23, are similar to those in the unified soil model for FVT-2 recommended by CRIEPI (CRIEPI, 1995b). Use of the soil properties in Table 23 should provide adequate

estimates of SSI response under low-level lateral loads, *i.e.*, lateral loads such that the soil behavior will remain in the linear range.

The SSI analyses presented do not allow for accurate statements about the in-situ S wave speeds in the gravel-3 as well as the assessment of other constitutive modeling soil properties needed for soil modeling in the nonlinear and inelastic ranges. Given the dimensions of the containment model, the depth of the gravel-3 layer and the small stresses induced by the shaker loading, this soil (gravel 3) is not expected to have been a major factor in the SSI response under the forced vibration tests. In this study, the stiffness of the gravel-3 is used only to modify the stiffness of the gravel-1, as indicated above, with the assumption that the gravel-3 is anisotropic with the same principal directions and the same ratio of the S wave speeds in the directions as the gravel-1.

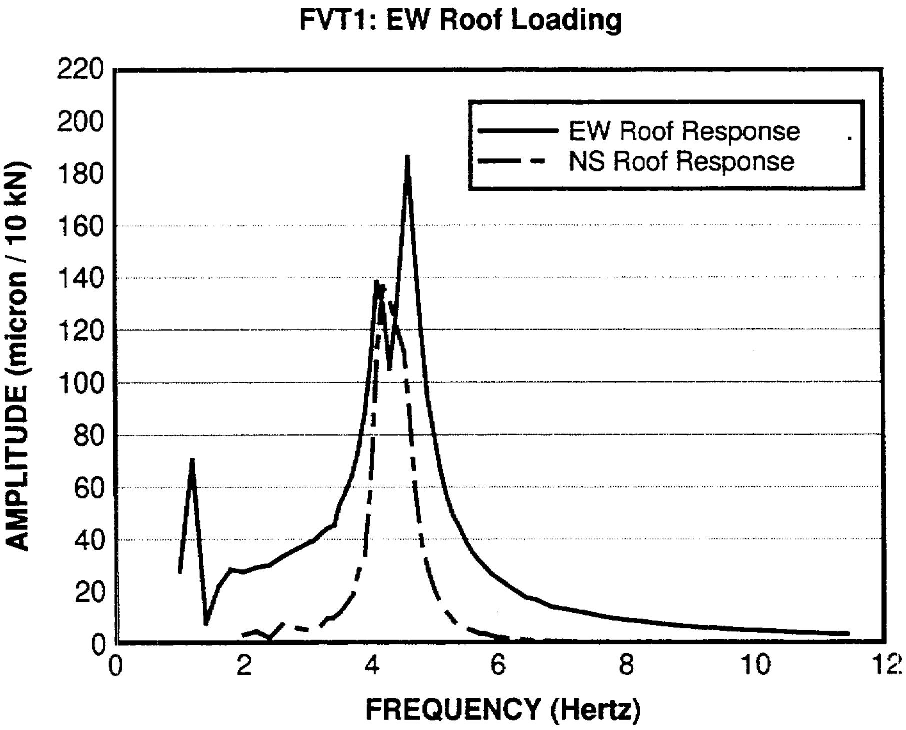

Figure 34 NS and EW roof responses under NS roof loading (FVT-1)

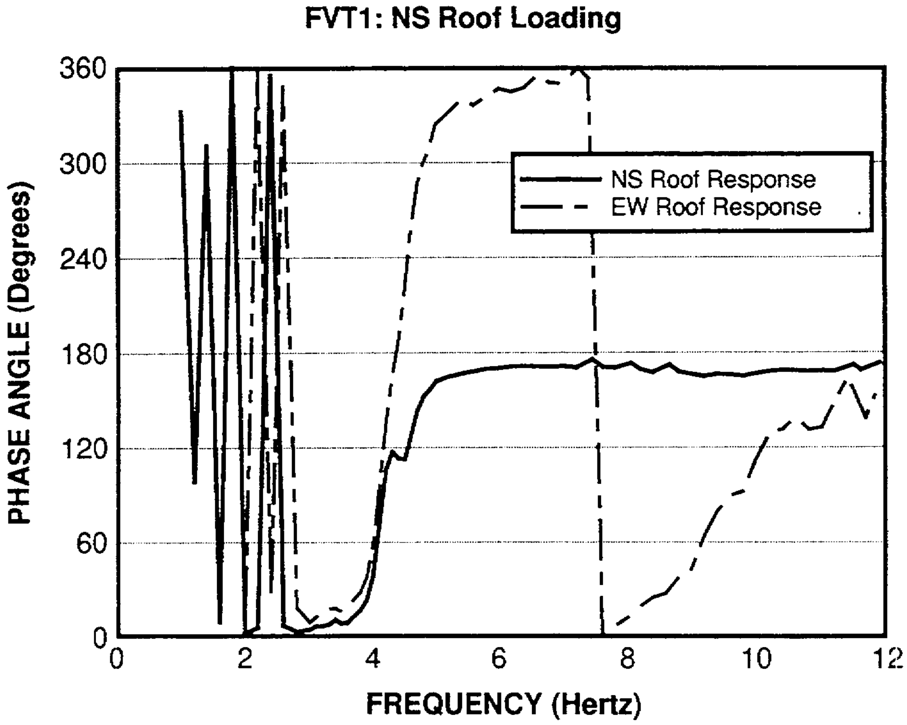

Figure 35 Phase angles for NS and EW roof responses under NS roof loading (FVT-1)

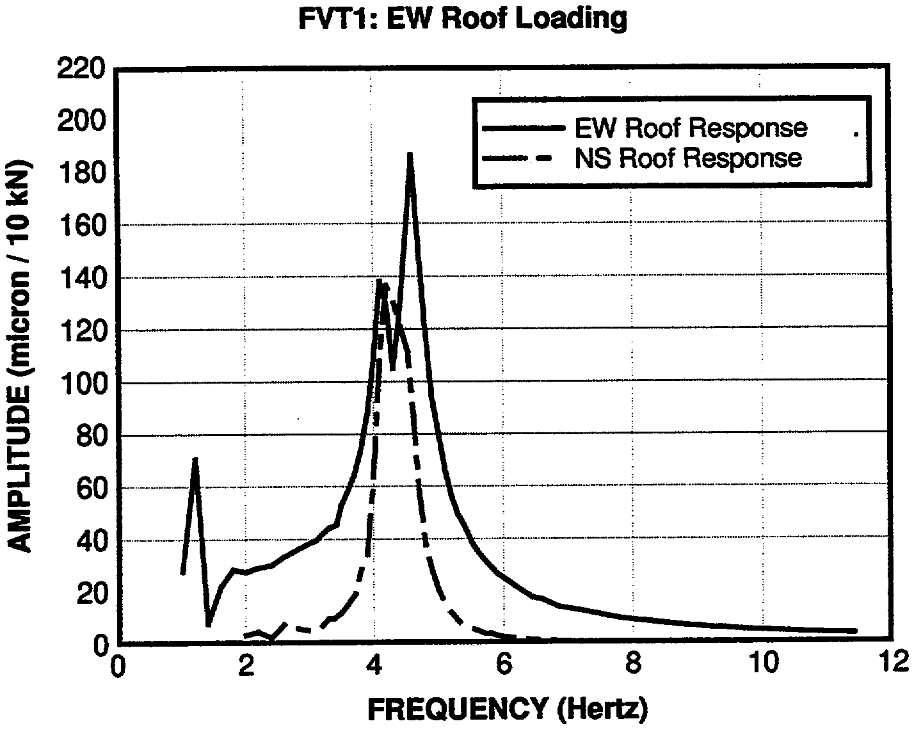

Figure 36 EW and NS roof responses under EW roof loading (FVT-1)

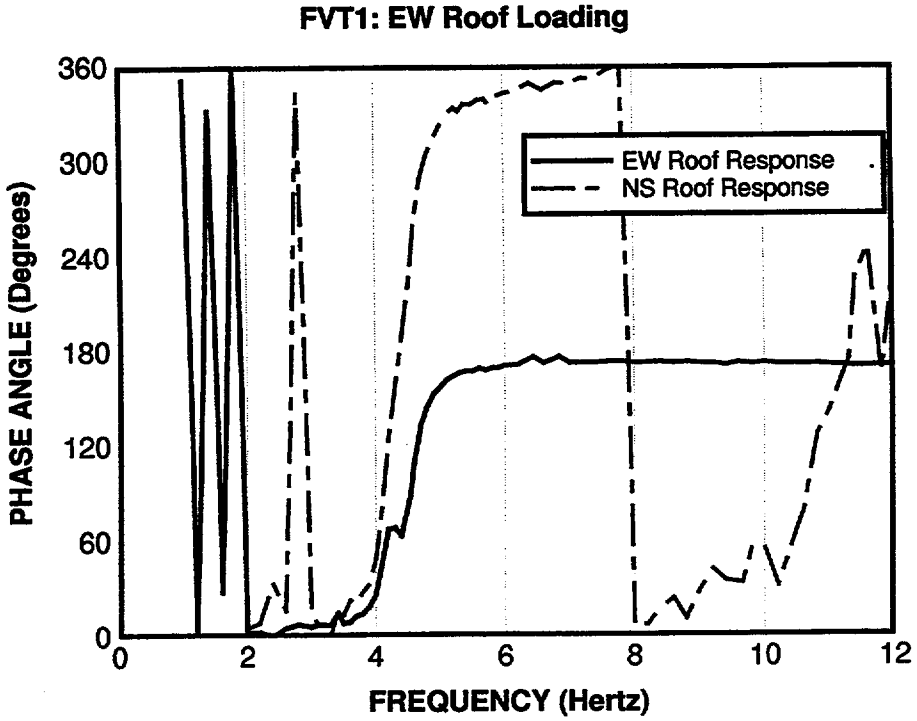

Figure 37 Phase angles for NS and EW roof responses under EW roof loading (FVT-1)

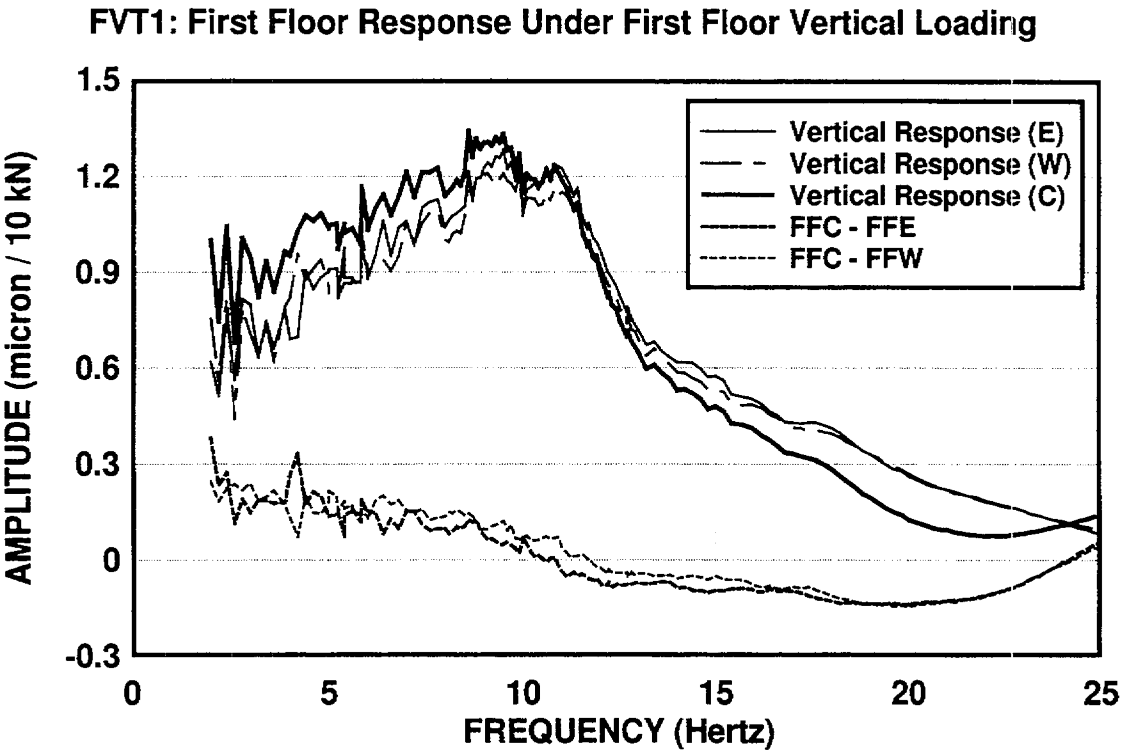

Figure 38 First floor response under first floor vertical loading (FVT-1)

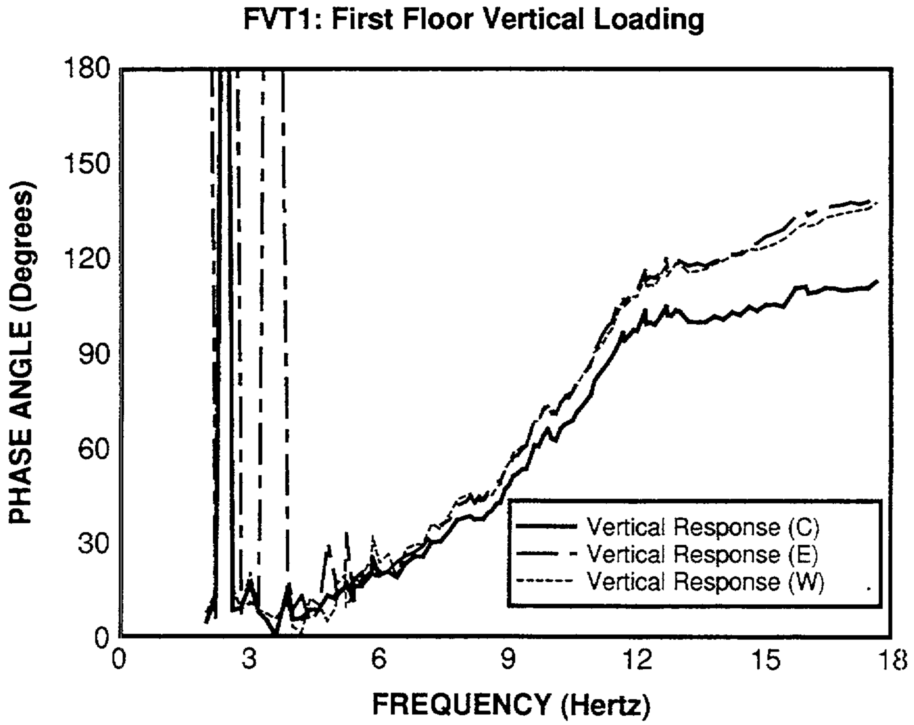

Figure 39 Phase angles of first floor response under first floor vertical loading (FVT-1)

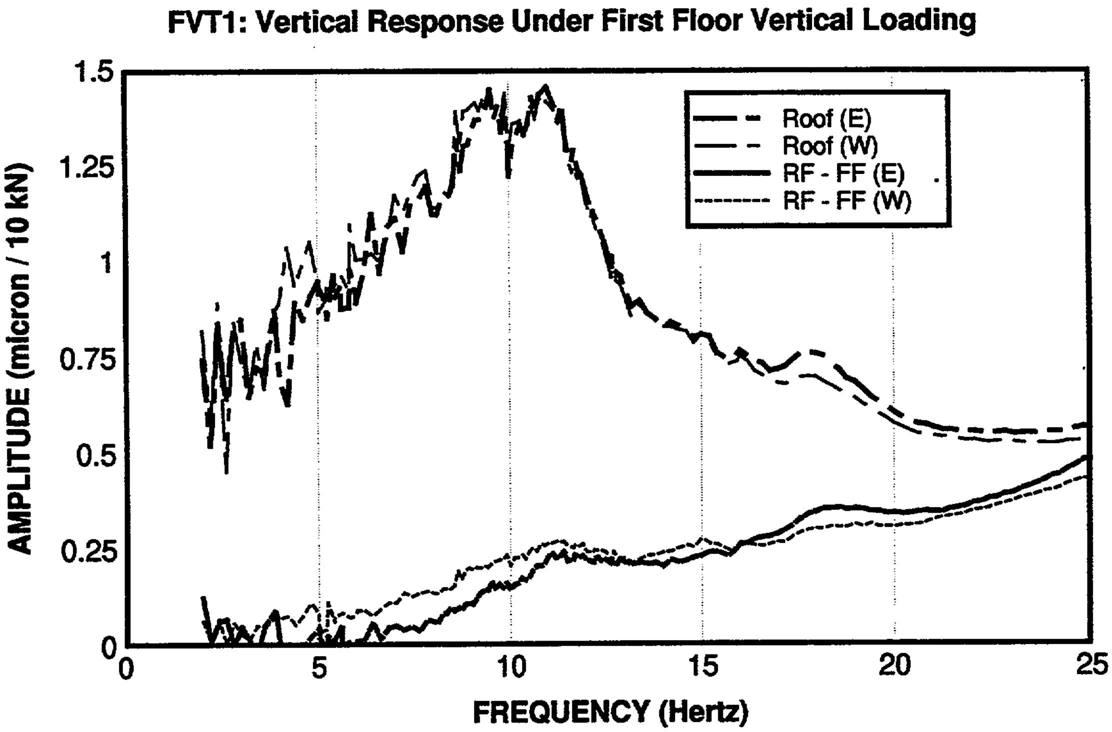

Figure 40 Vertical roof response under first floor vertical loading (FVT-1)

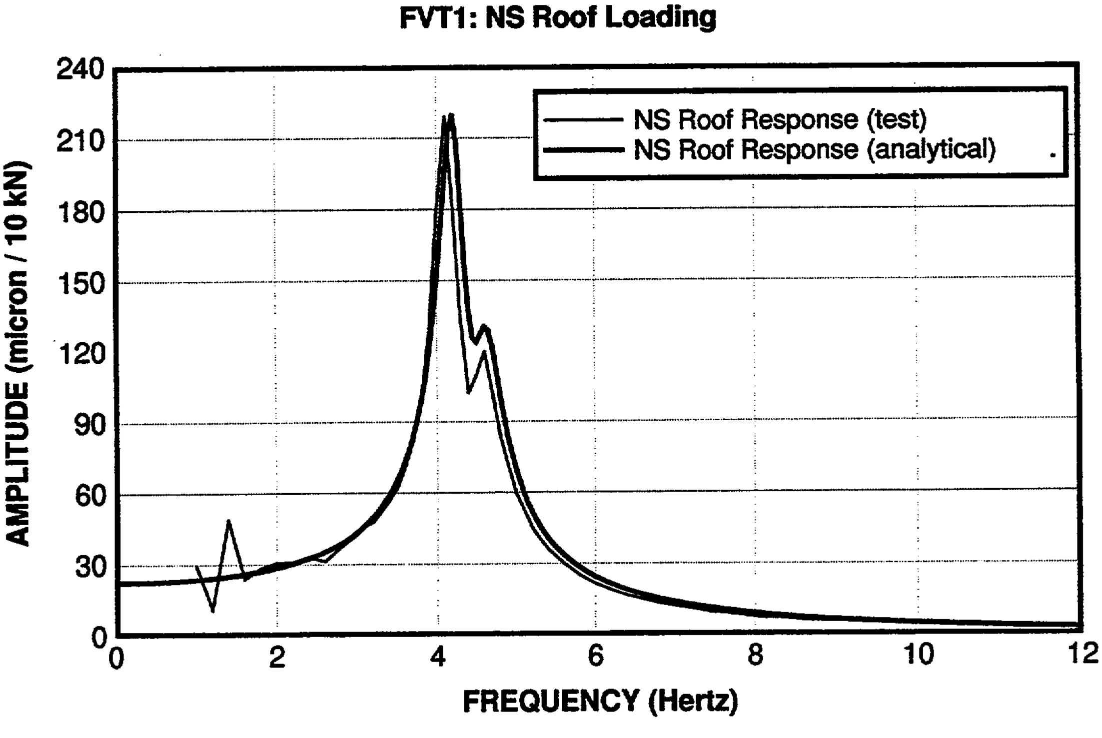

Figure 41 Computed NS roof response for NS roof loading (FVT-1)

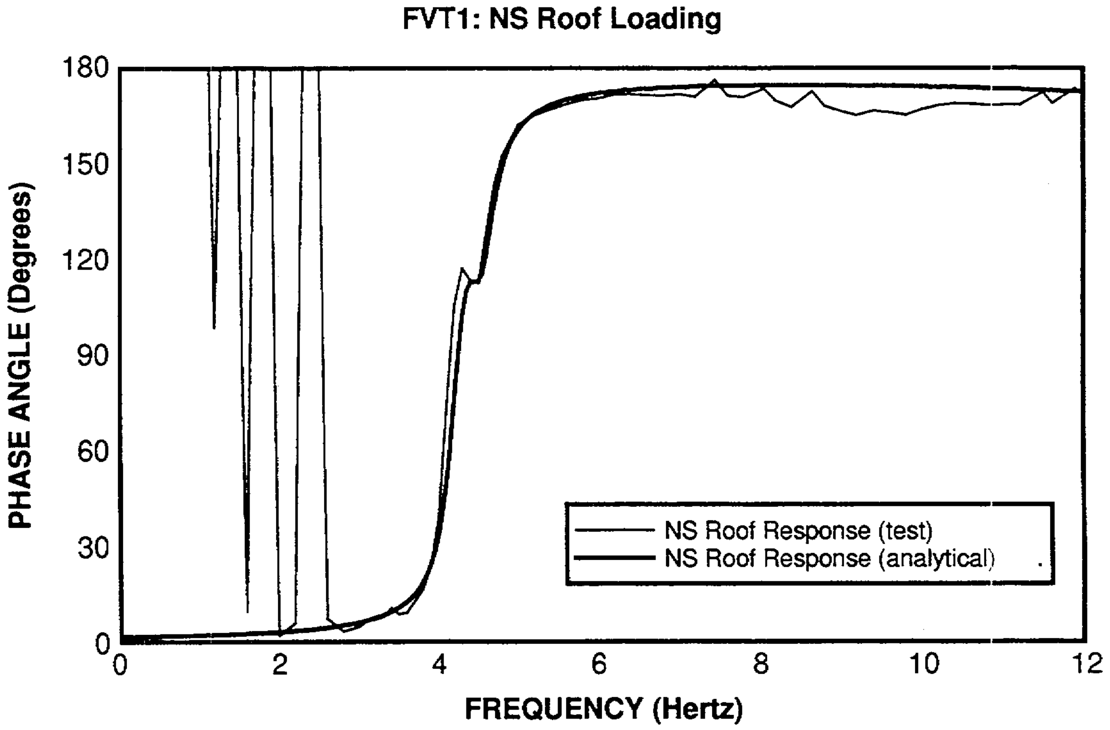

Figure 42 Computed phase angle for NS roof response under NS roof loading (FVT-1)

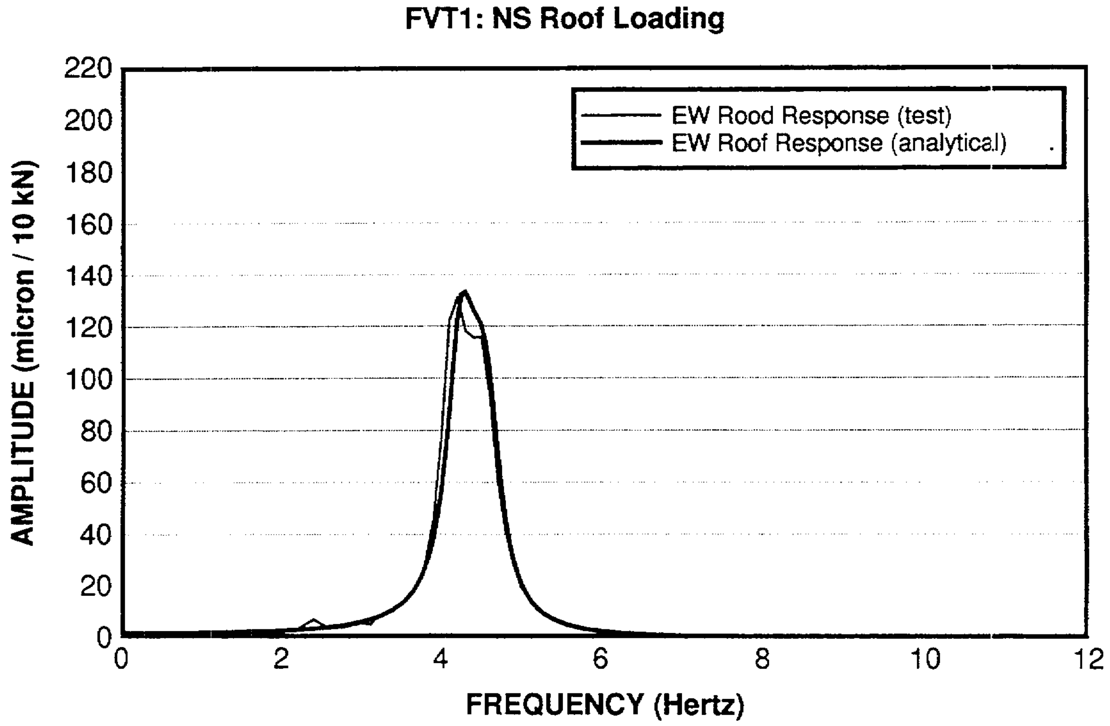

Figure 43 Computed EW roof response for NS roof loading (FVT-1)

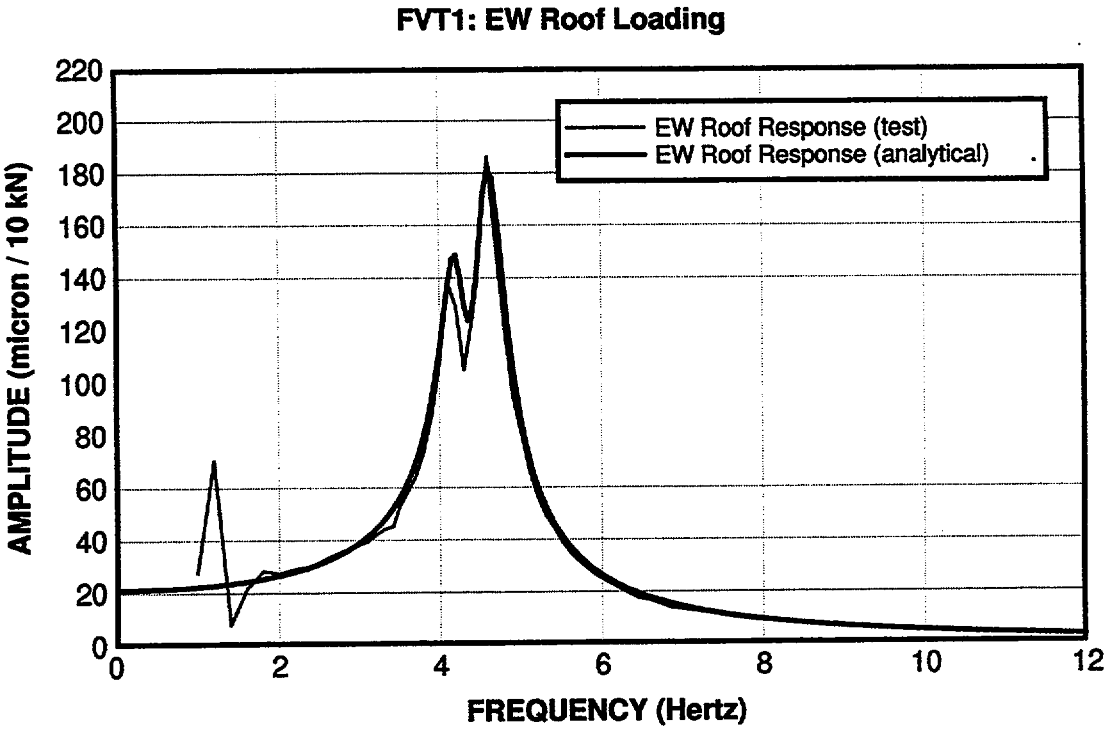

Figure 44 Computed EW roof response for EW roof loading (FVT-1)

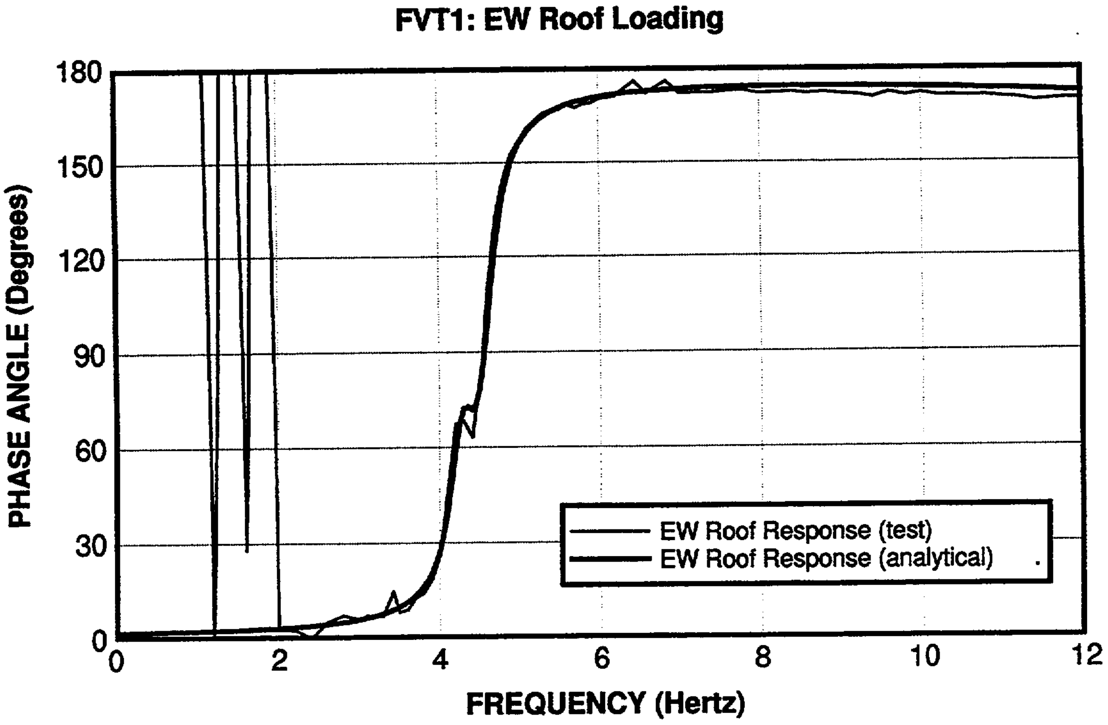

Figure 45 Computed phase angle for EW roof response for EW roof loading (FVT-1)

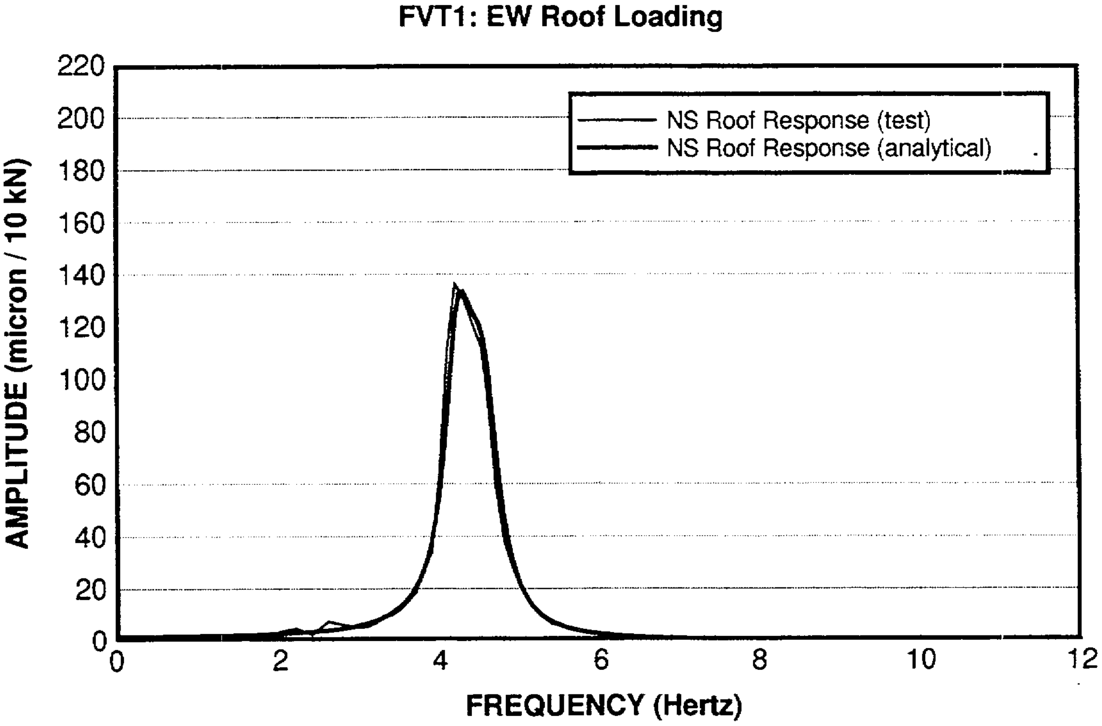

Figure 46 Computed NS roof response for EW roof loading (FVT-1)

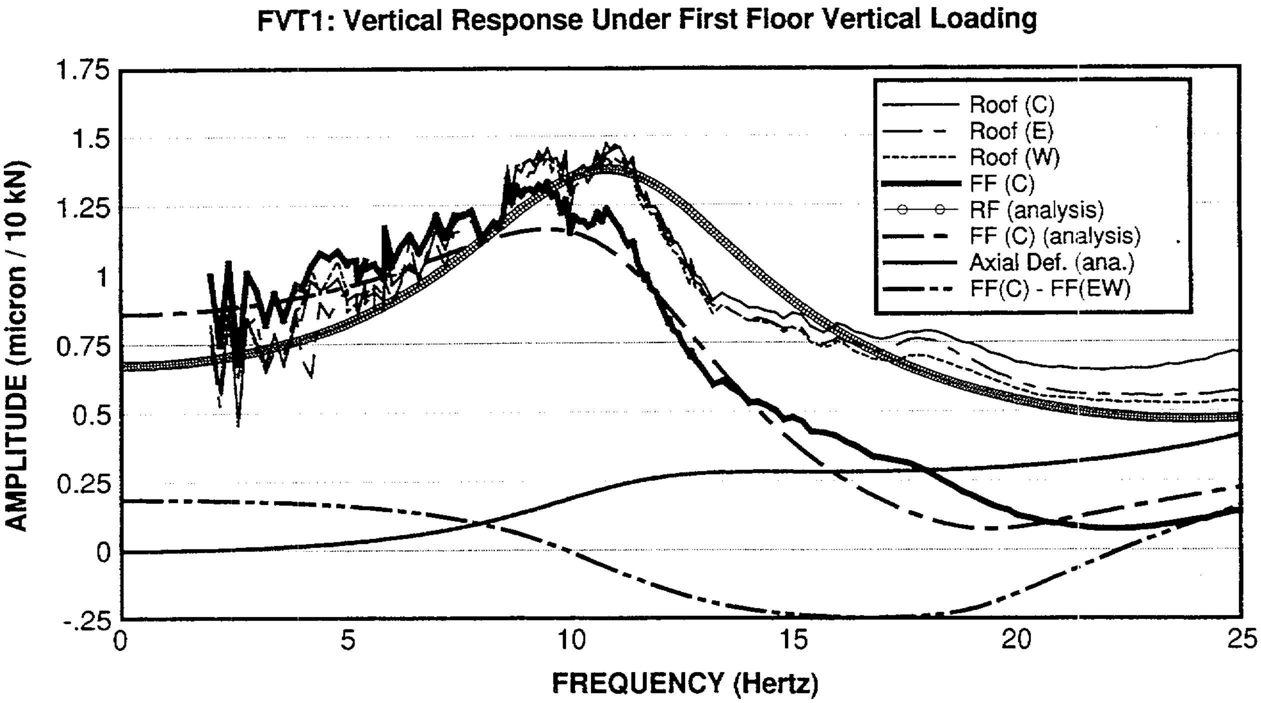

Figure 47 Computed vertical roof response under vertical loading (FVT1)

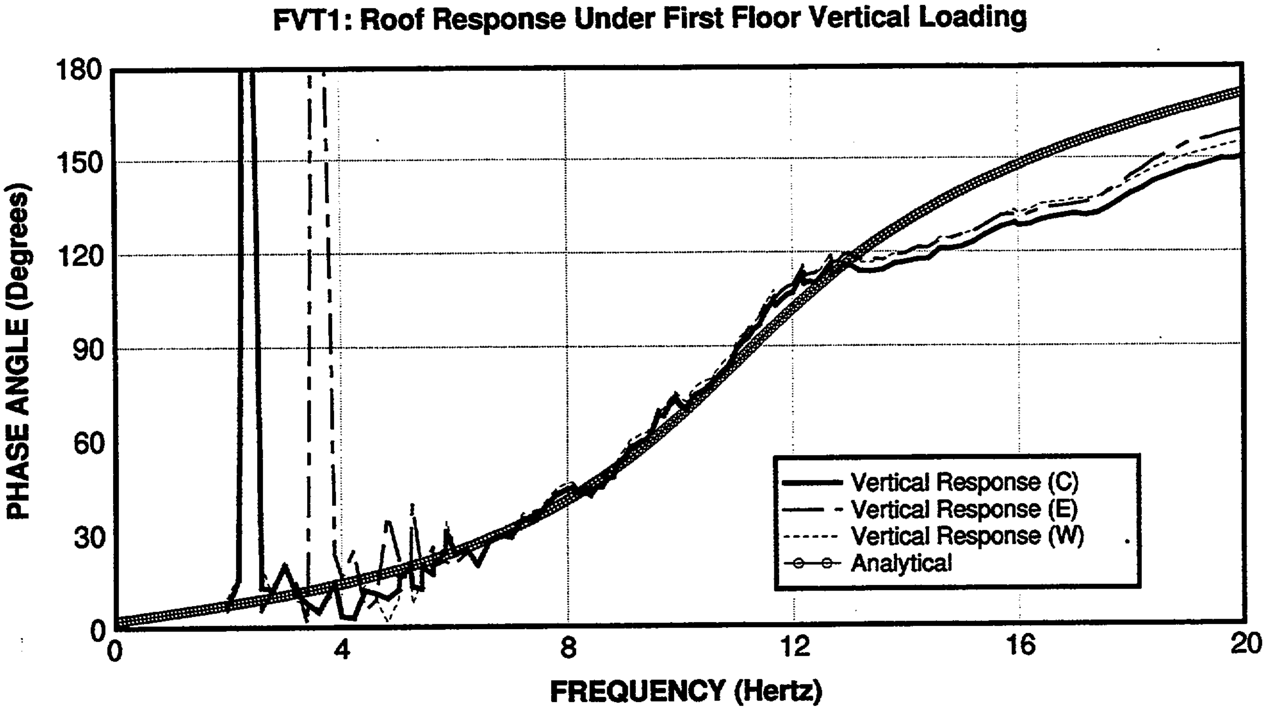

Figure 48 Computed phase angles for vertical roof response under vertical loading (FVT-1)

Measuring Points on East Radial (all dimensions in meters)

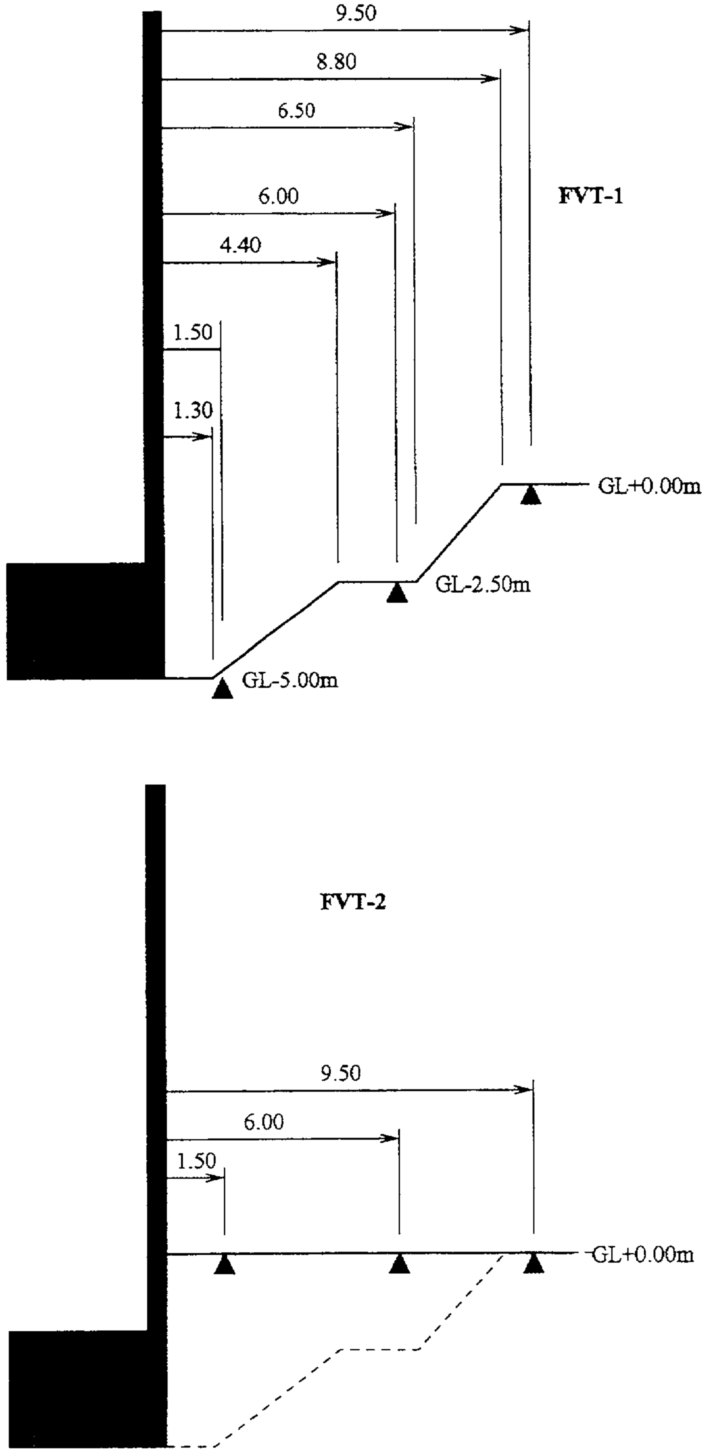

Figure 49 Locations of ground response measurements for FVT-1 and FVT-2

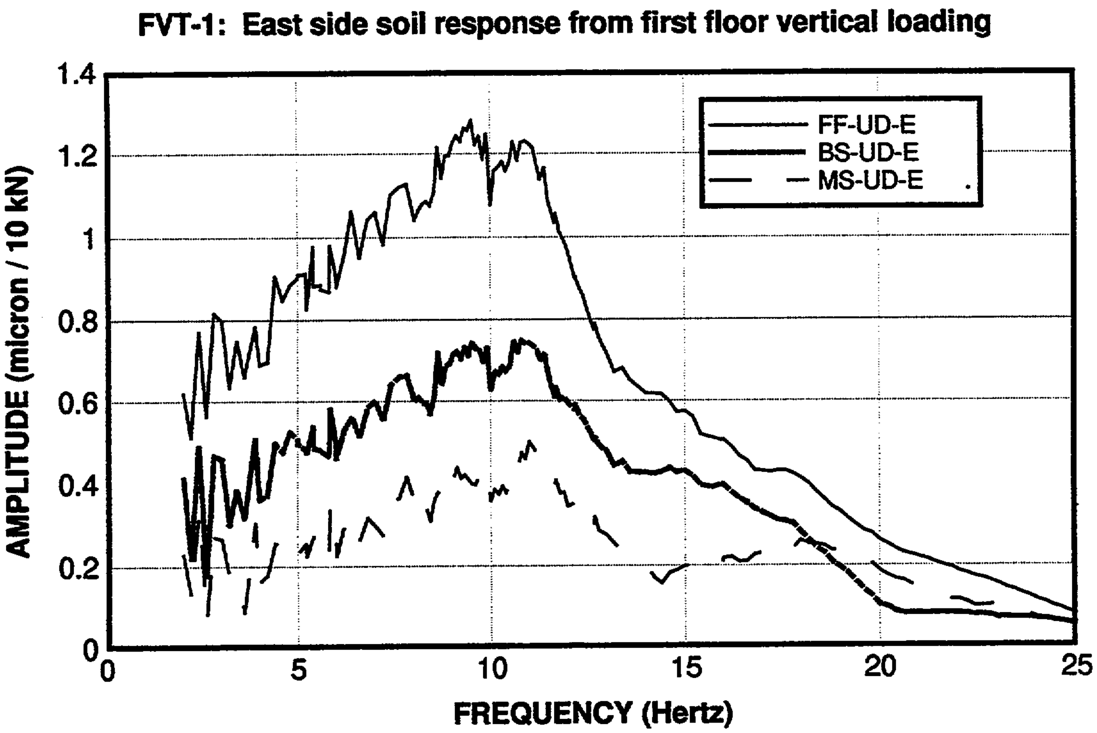

Figure 50 Vertical response amplitude on the east radial from FVT-1 vertical load

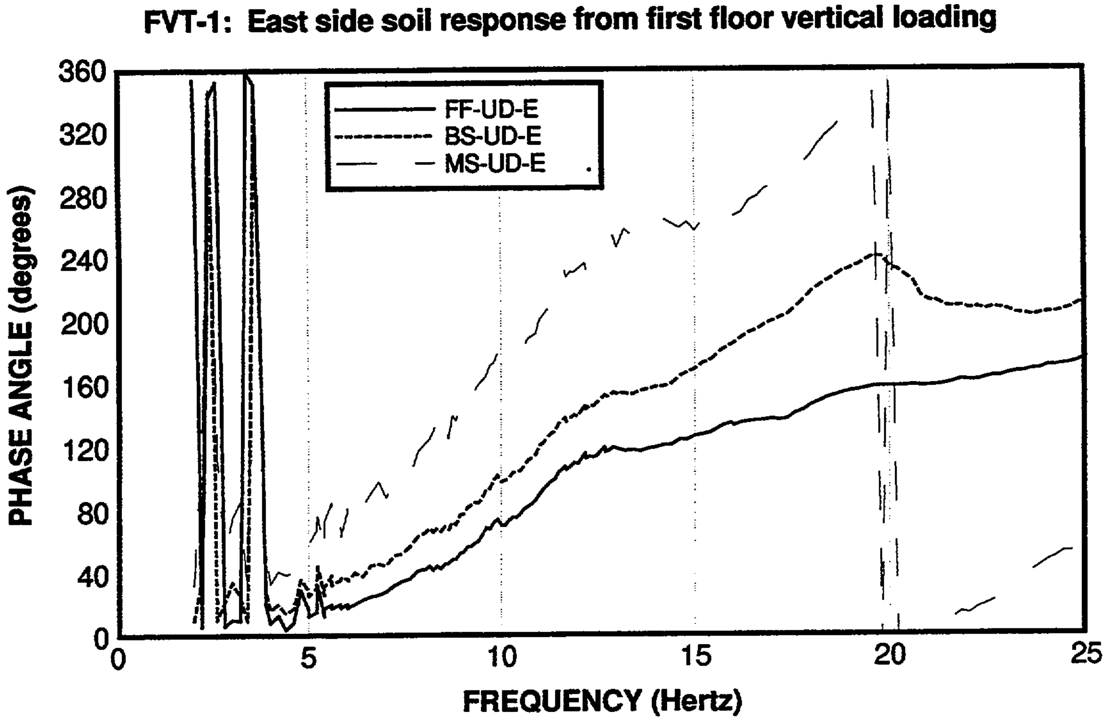

Figure 51 Vertical response phases on the east radial from FVT-1 vertical loading

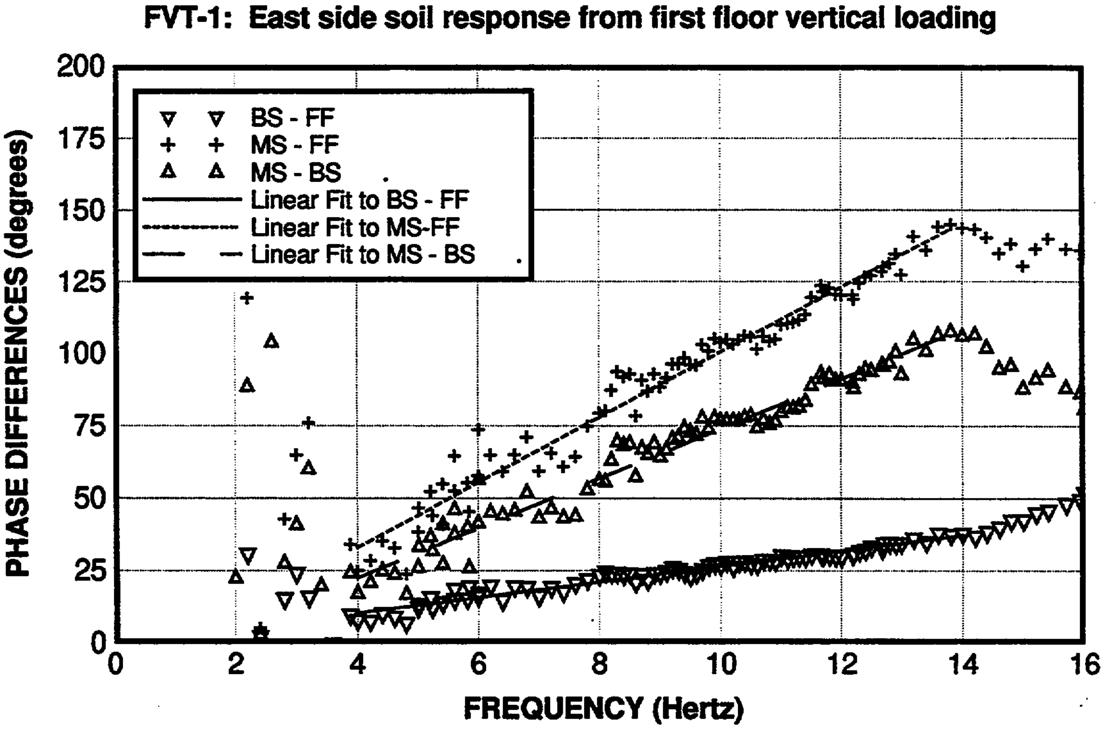

Figure 52 Phase differences for vertical measurements on east radial (FVT-1 vertical loading)

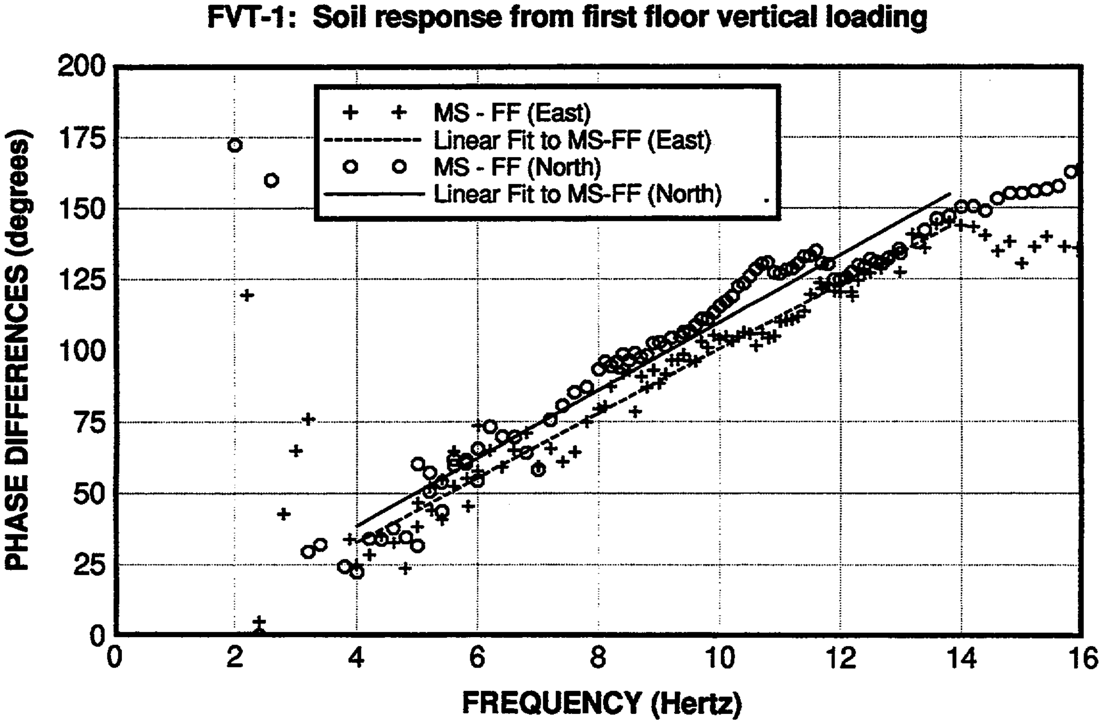

Figure 53 Phase differences along north and east radial (FVT-1 vertical loading)

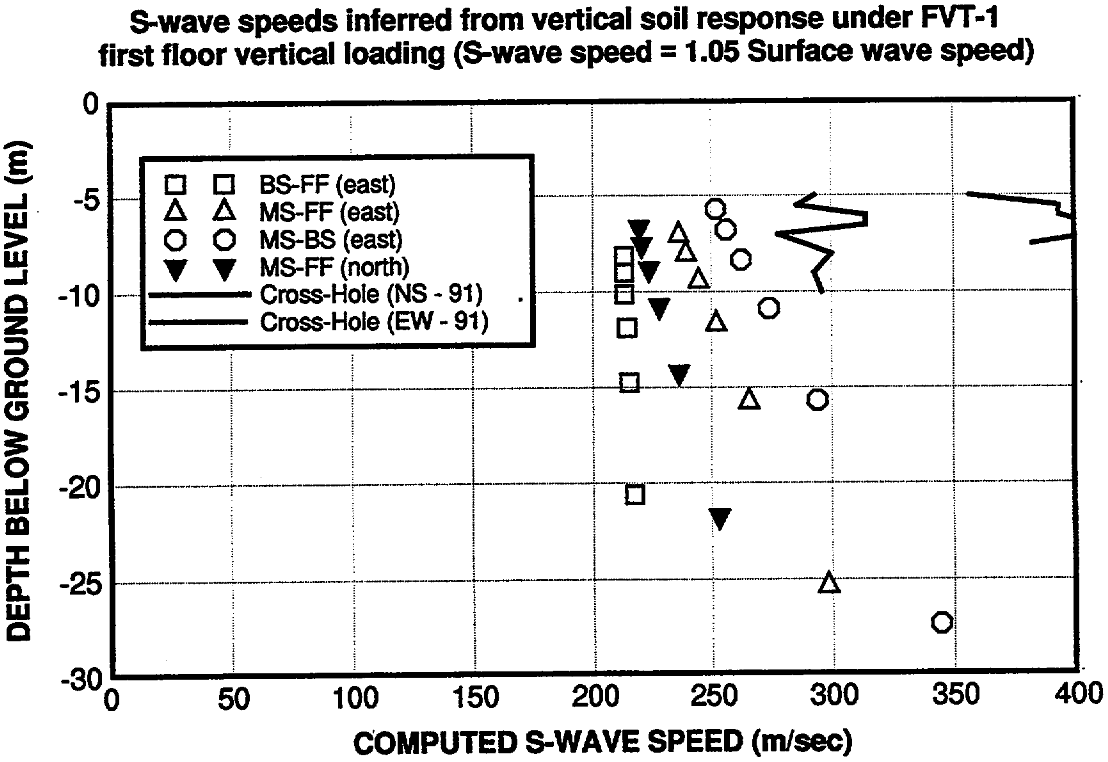

Figure 54 S-wave velocities interpreted from soil response under FVT-1 vertical loading

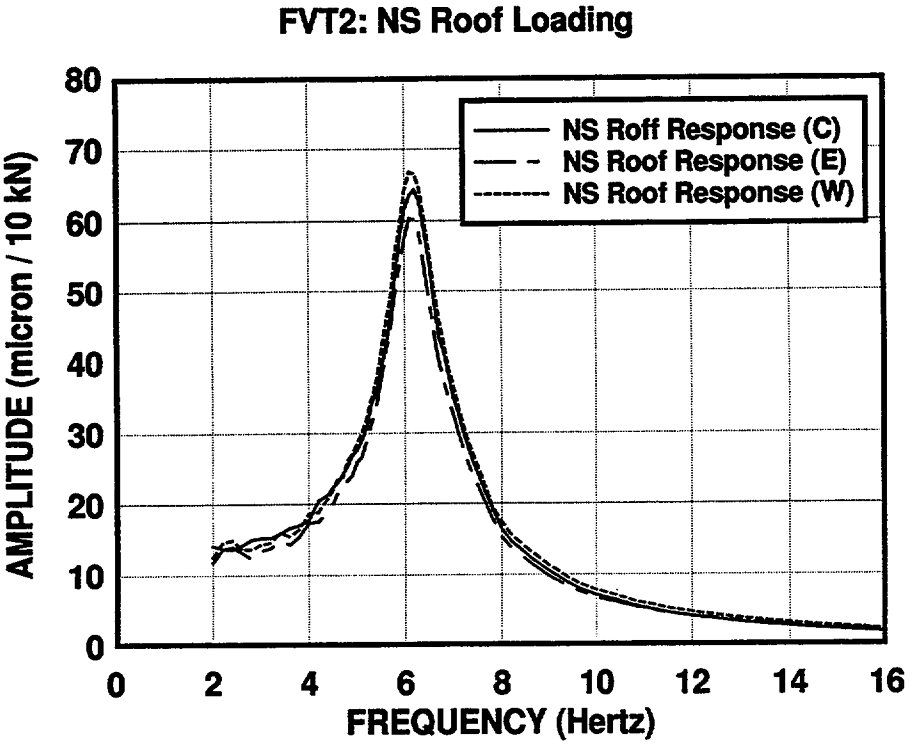

Figure 55 NS roof response for NS roof loading (FVT-2)

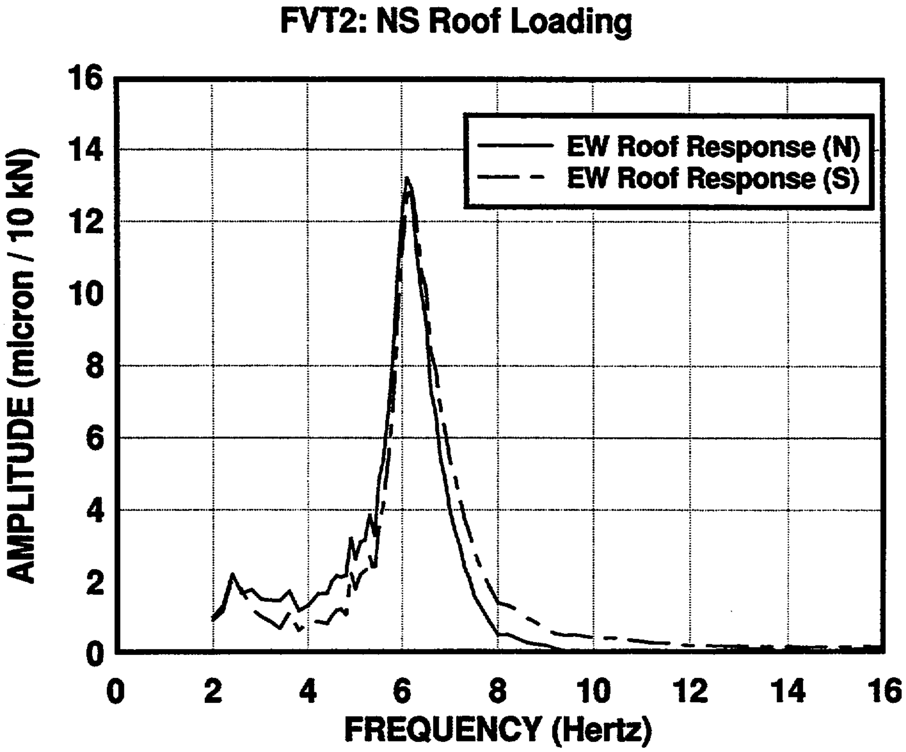

Figure 56 EW roof response for NS roof loading (FVT-2)

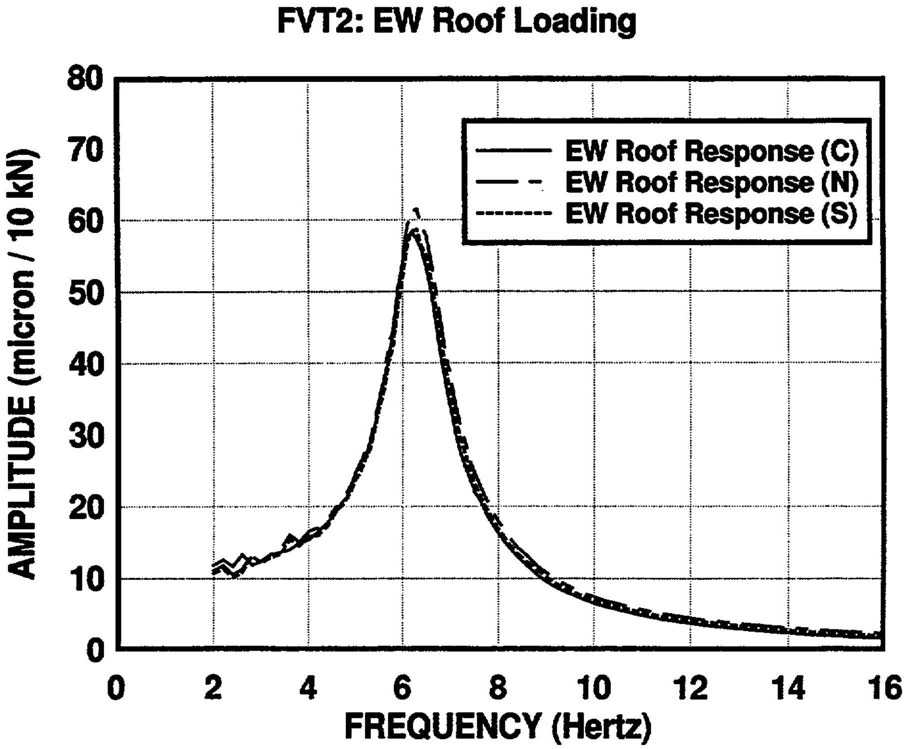

Figure 57 EW roof response for EW roof loading (FVT-2)

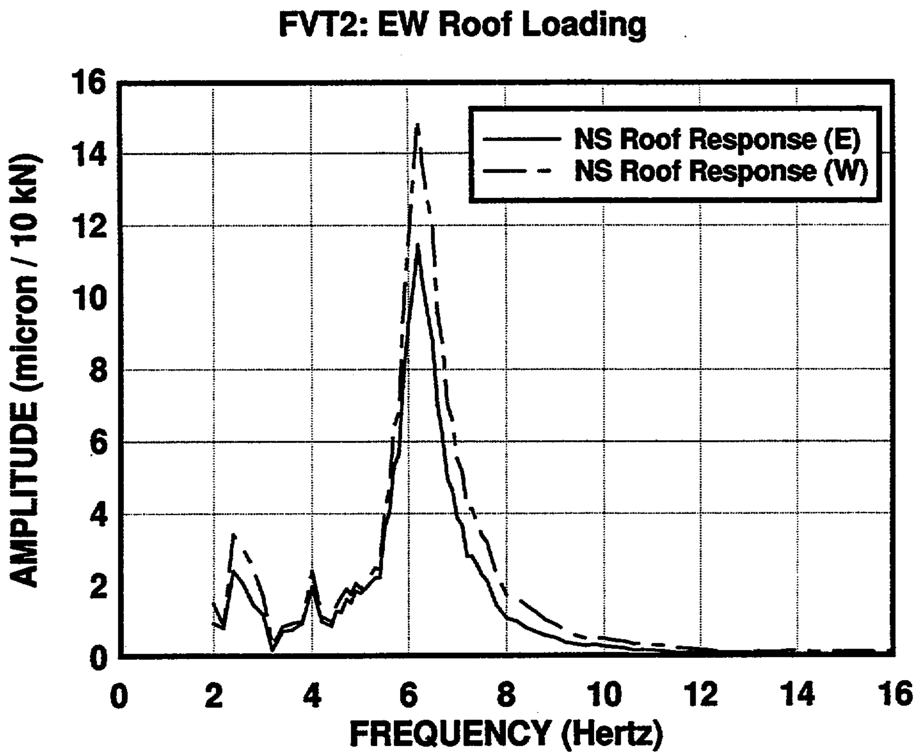

Figure 58 NS roof response for EW roof loading (FVT-2)

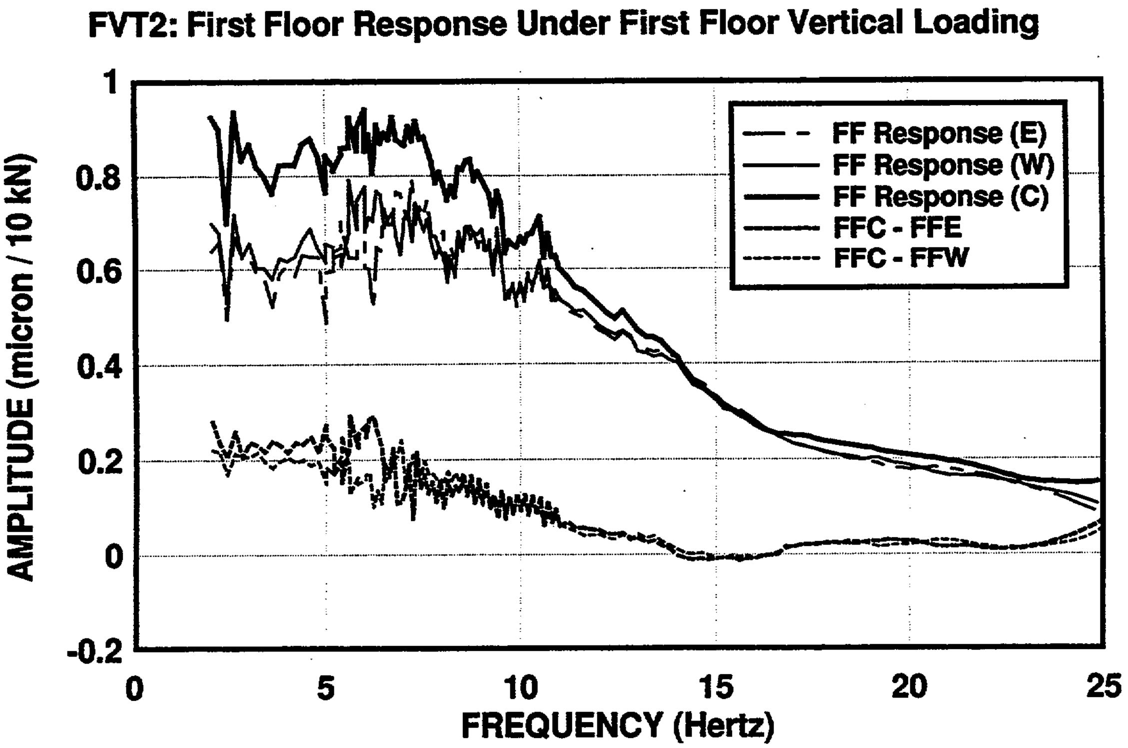

Figure 59 First floor response under first floor vertical loading (FVT-2)

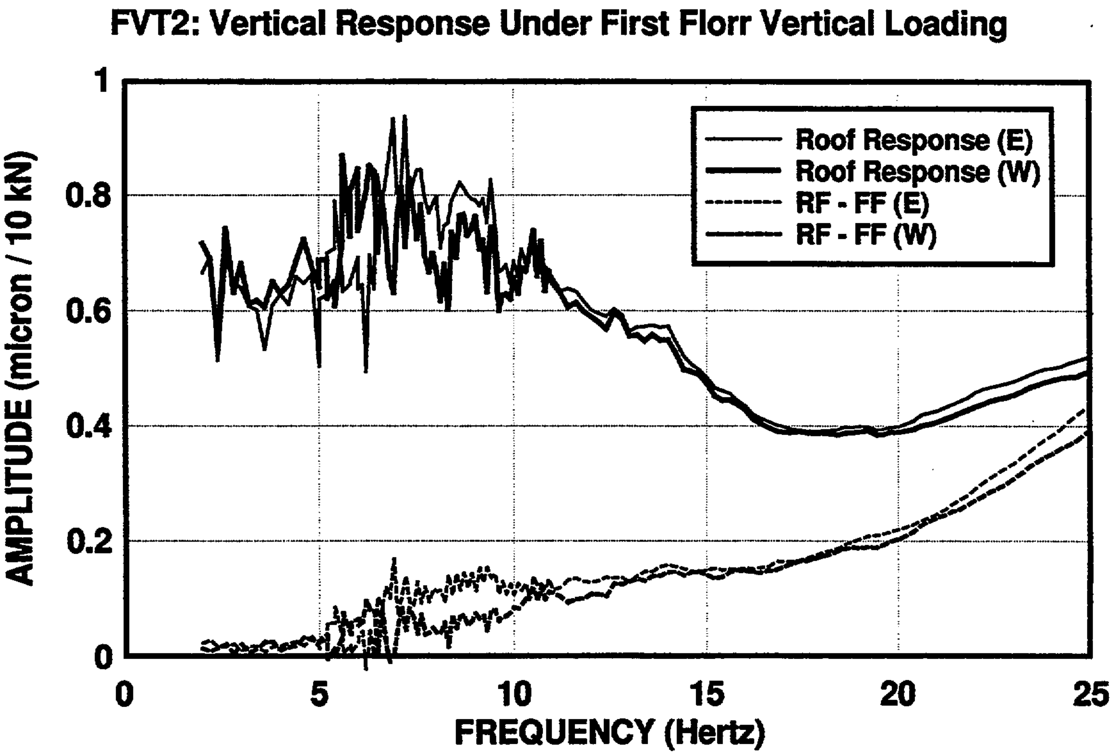

Figure 60 Roof response from first floor vertical loading (FVT2)

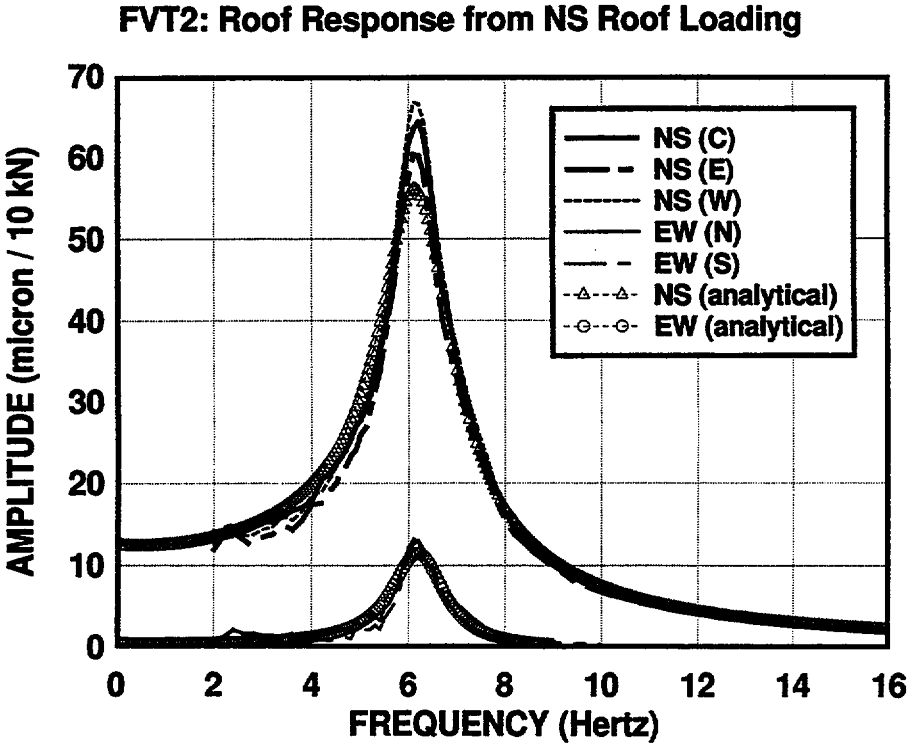

Figure 61 Computed NS and EW roof responses for NS roof loading (FVT-2)

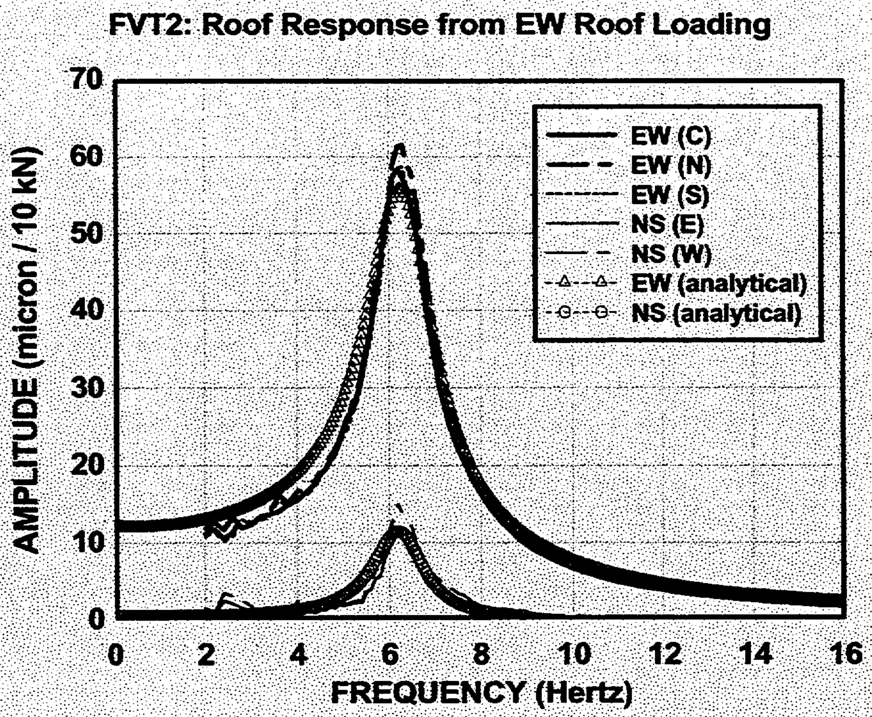

Figure 62 Computed EW and NS roof responses for EW loading (FVT-2)

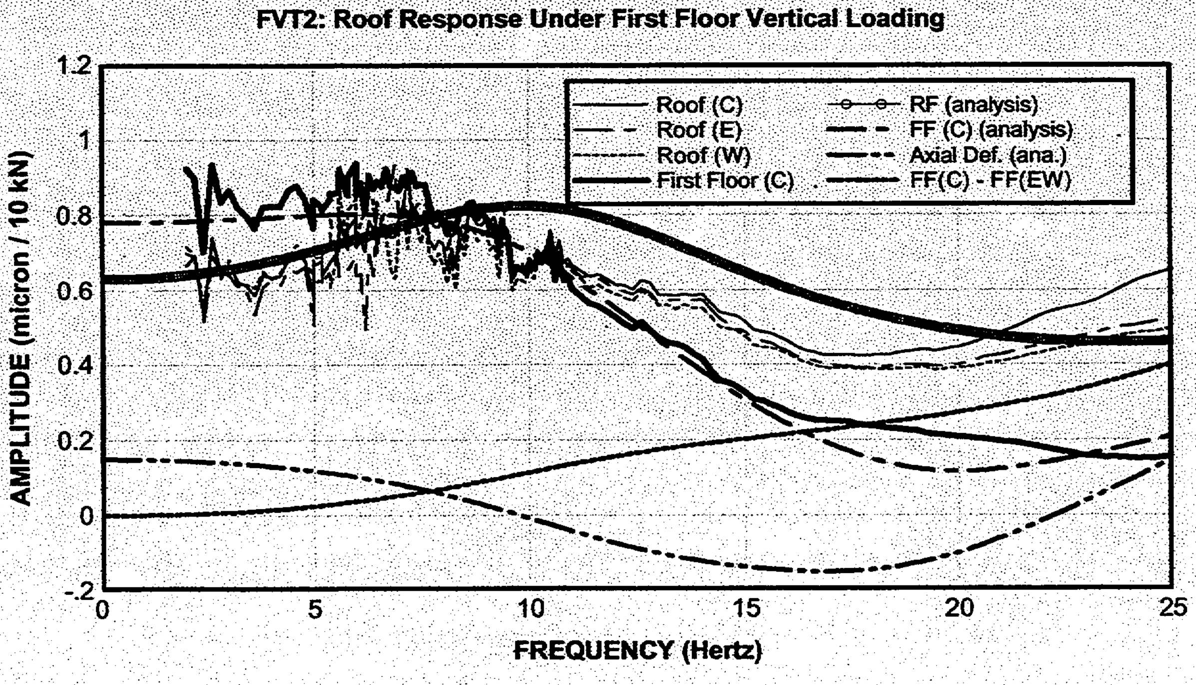

Figure 63 Computed vertical roof response under vertical loading (FVT-2)

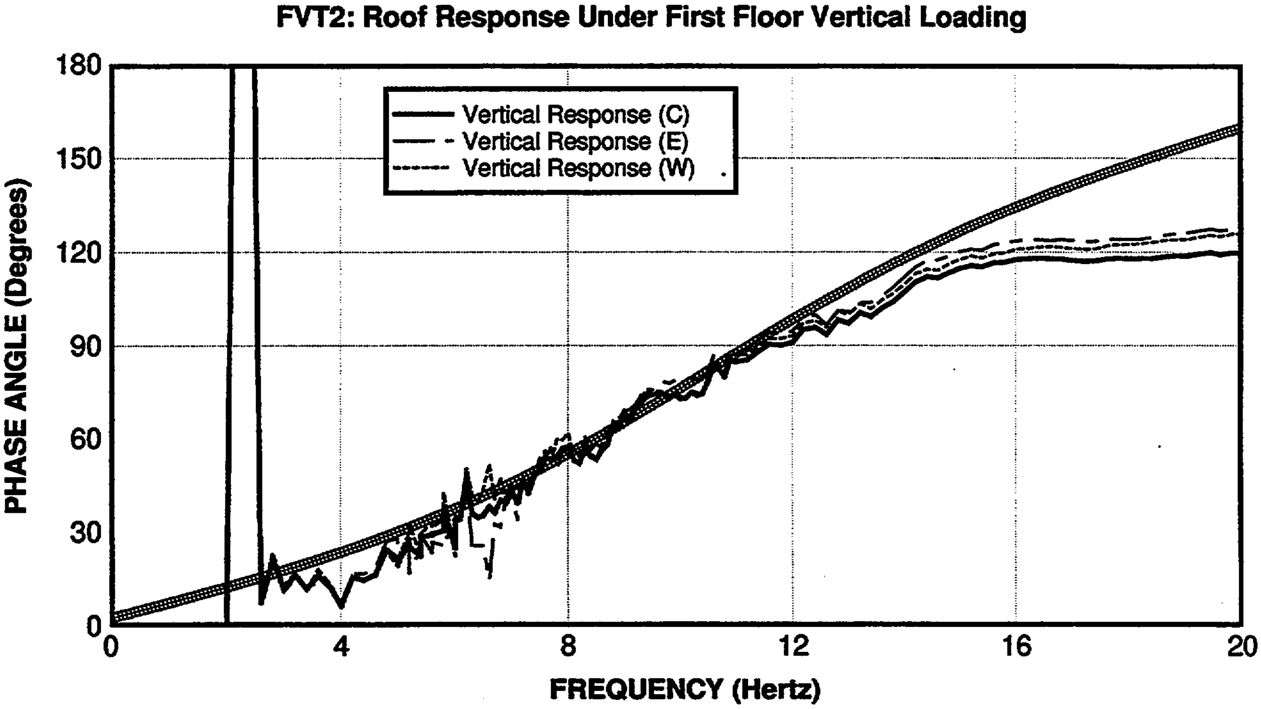

Figure 64 Computed phase angles for vertical roof response under vertical loading (FVT-2)

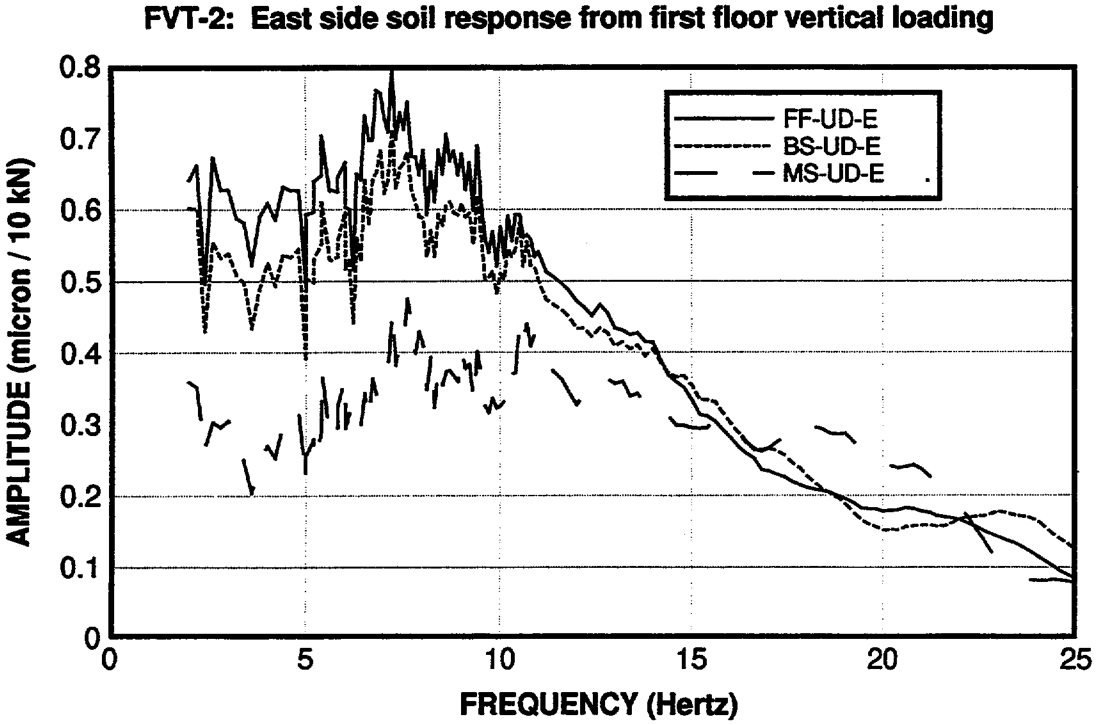

Figure 65 Vertical response amplitudes on the east radial under FVT-2 vertical loading

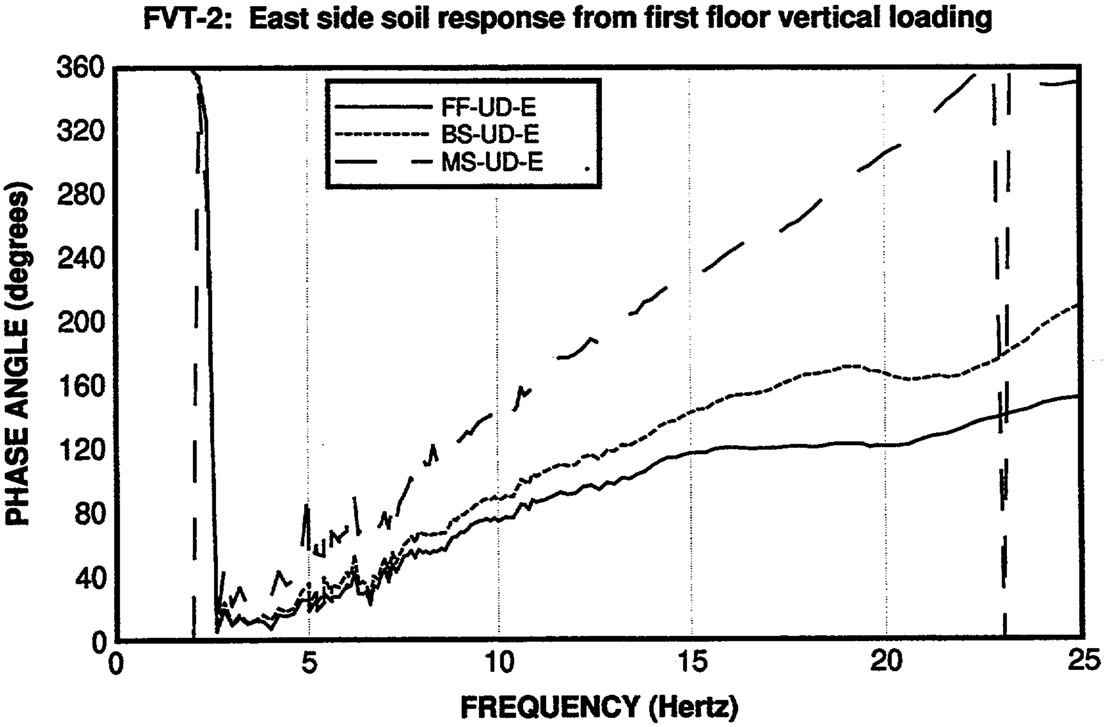

Figure 66 Vertical response phases on the east radial from FVT-2 vertical loading

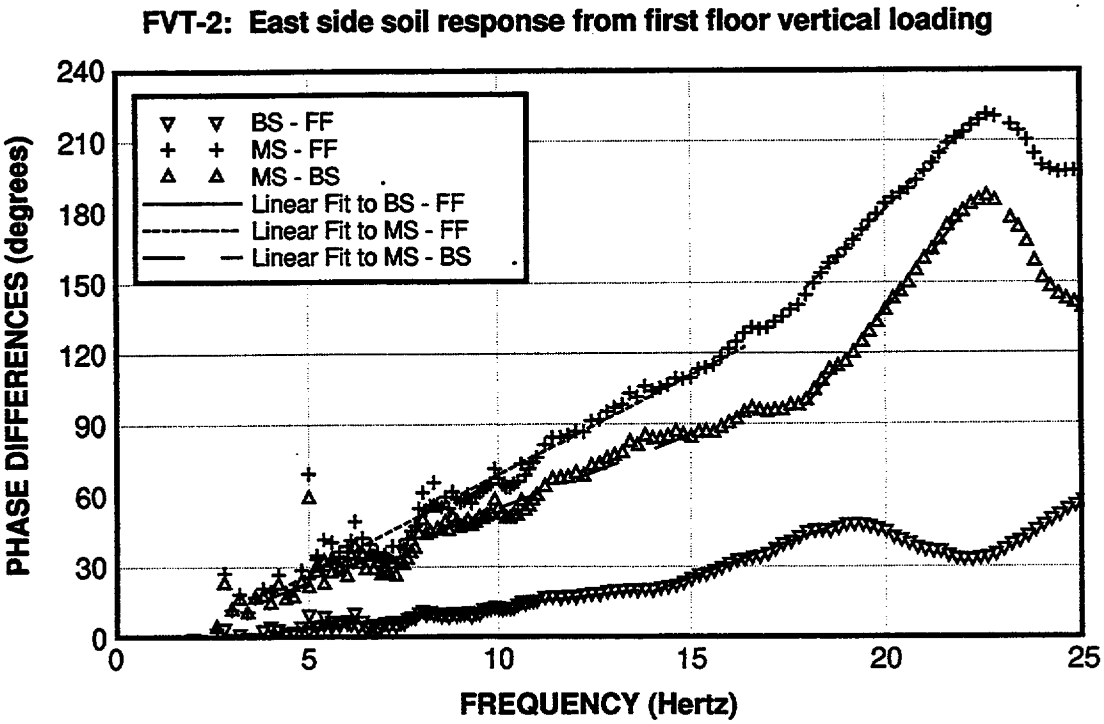

Figure 67 Phase differences on east radial (FVT-2 vertical loading)

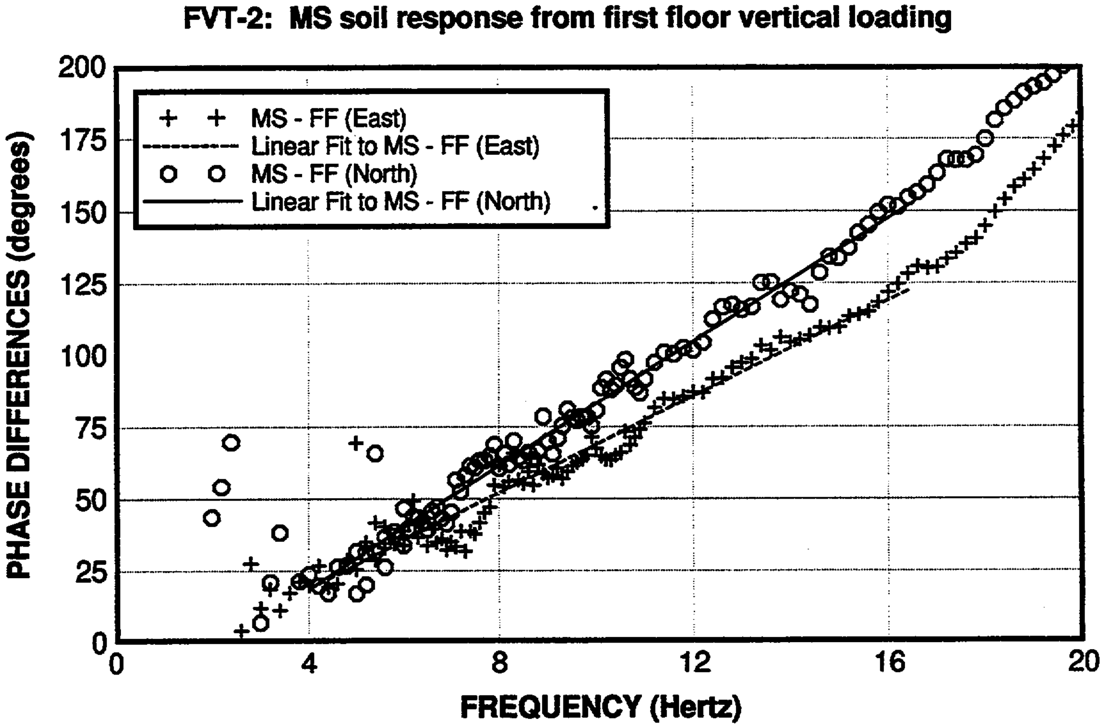

Figure 68 Phase differences along the north and east radial (FVT-2 vertical loading)

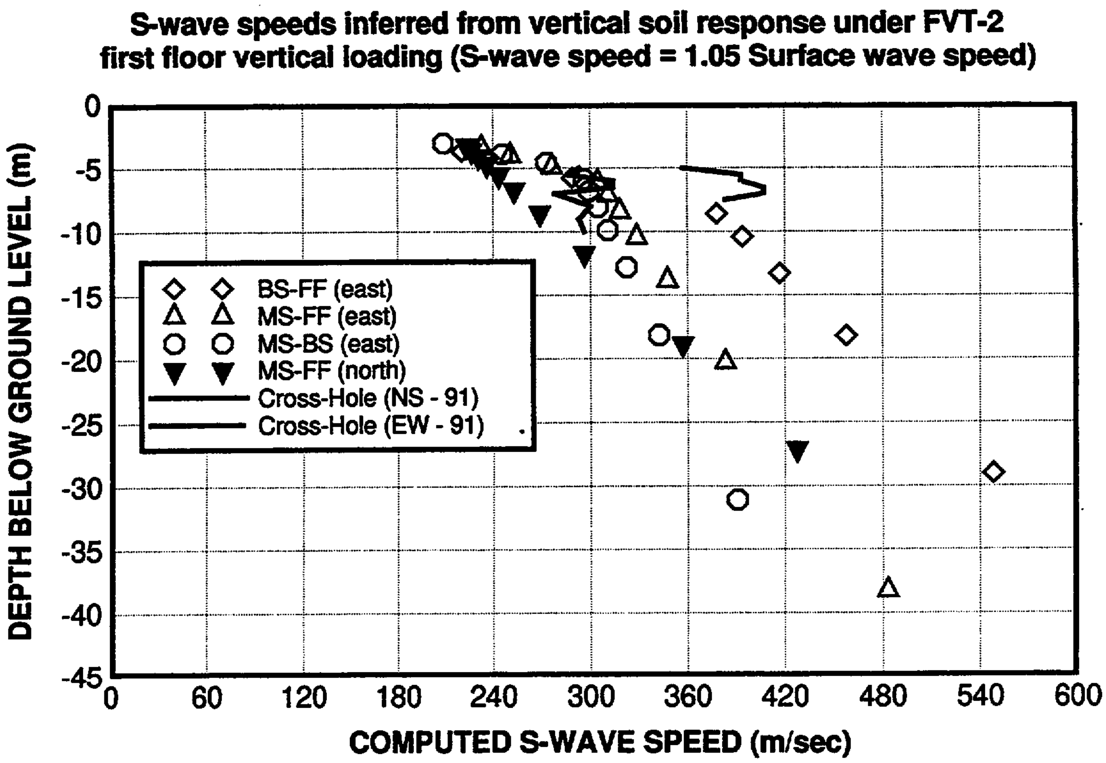

Figure 69 S-wave velocities interpreted from soil measurements under FVT-2 vertical loading

7. EARTHQUAKE LOADS

Recorded earthquake ground motions at the site are used here, primarily, to assess the results of the site characterization program reviewed above. Accordingly, the following analyses were conducted:

1. cross-correlation analysis of recorded ground motions have been conducted to investigate the predominant direction of the shear wave propagation at the site as well as the vertical propagation speed of the shear waves at the site;
2. soil-structure interaction analysis of the model under selected earthquake loading.

The analysis results, which are summarized below, indicate the following:

1. A nearly vertical propagation of the shear waves in the upper 52.5m for the earthquake ground motions considered in this study.
2. The vertical shear wave propagation in the free-field appears to be significantly different for the NS and EW ground motions, which indicates anisotropic site conditions, *i.e.,* shear waves that propagate at different speeds for particle motions in NS and EW directions. Similar results have been reported by Ueshima and Okano (1996) on the basis of cross-spectral analysis of recorded ground-motions.
3. The fundamental frequencies of vibration for the soil-structure interaction system under the earthquake loads analyzed are significantly smaller than those observed under the FVT-2, which implies either nonlinear soil deformation or containment-soil separation under the earthquake loads examined, or both. Since the recorded earthquake ground motions were not particularly strong it seems that nonlinear effects will play an even more significant role under severe earthquake loads.

Earthquake ground accelerations at the site have been recorded in the vertical direction (V) and in two orthogonal horizontal directions. The horizontal directions chosen were the magnetic north and the magnetic south directions, which are designated the L and T directions, respectively. The magnetic declination at the site is, approximately, 3^0 west and, therefore, the ground accelerations are approximately recorded in the actual NS and EW directions.

The ground motion instrumentation layout is shown in Figure 70. There are 15 surface ground motion stations (A-series) located along 3 lines denoted ARM1, ARM2 and ARM3 as shown in Figure 70. On each arm 5 ground motion stations are installed as follows: the first station is located close to the outside wall of the containment and the other 4 stations are located at, approximately, D/2, 1.5D, 2.5D and 5D from the first station, where D is the diameter of the model. Three down-hole arrays (D-series) have also been installed as follows: one at the end of ARM1 and two others located at the beginning and end of ARM2. All down-hole arrays consist of 4 accelerometers at depths of, approximately, 5.25, 15.75, 26.25 and 52.5 meters below grade.

Reference directions used in the Hualien LSST project are also shown in Figure 70. Those directions are: the NS direction which is used as a reference for the horizontal components (L) of the earthquake accelerations (ground accelerations and structural responses), as well as a reference for the placement of accelerometers in the model; the shaker or plant north direction which was used as a reference for the forced vibration tests; and the entrance road alignment which can be used as a reference for some of the seismic refraction survey lines and cross-hole logging paths. In the Hualien SSI experiment, the shaker (plant) North-South coincides with entrance road alignment.

Accelerometers were also installed in the containment model at the following elevations: at the top of the basement on the inside of the containment wall (BA-series); inside the containment wall mid-way between the ground level and the bottom of the roof plate (WH-series); at the top of the roof plate (RF-series); and inside the containment wall at about the ground level elevation (WL-series). The BA, WH and RF series consist of 4 accelerometer stations installed at the north, south, east and west ends of the model, whereas the WL series consists of only two stations located at the north and east ends of the containment. Additionally, a fifth accelerometer station is located near the center of the roof plate. All those accelerometer stations can record accelerations in the V, L and T directions.

Additional site instrumentation consisted of: pressure transducers beneath the foundation and between the embedded wall and backfill; pore pressure and settlement gauges; and inclinometers. A detailed description of the location and characteristics of that instrumentation is not given here. Instead, they will be referred to as needed.

Since the data acquisition instrumentation has been fully operational several earthquakes have been recorded at the site. A list of the earthquakes recorded and their principal characteristics is given in Tables 27 and 28 (Yang *et al.*, 1995, Ueshima and Okano, 1996).

Table 27. Characteristics of earthquakes recorded at the Hualien SSI experiment site

Event Label	**Date**	**Magnitude (M_L)**	**Focal Depth (km)**	**Epicenter**		
				Distance (km)	**Longitude (E)**	**Latitude (N)**
EQ1	Sep.09.93	4.2	21.1	7.6	121 - 40.34	23 - 58.16
EQ2	Jan.20.94	5.6	49.5	24.4	121 - 51.14	24 - 03.89
EQ3	May.30.94	4.5	18.5	9.6	121 - 34.20	24 - 05.40
EQ4	Jun.05.94	6.2	5.3	54.0	121 - 50.40	24 - 27.60
EQ5	Oct.05.94	5.8	31.3	--	121 - 43.22	24 - 09.38
EQ6	Feb.23.95	5.8	21.7	21.8	121 - 41.22	24 - 12.22
EQ7	May.01.95	4.9	8.4	4.6	121 - 39.11	24 - 02.66
EQ8	May.02.95	4.6	8.9	1.7	121 - 38.04	24 - 00.74

Table 28. Characteristics of earthquakes recorded at the Hualien SSI experiment site (cont'd)

Event Label	Date	Azimuth[1] (degree)	A, P, S,I[2]	Maximum acceleration (gal)	
				Roof (RFEL[3])	Ground (A15L[4])
EQ1	Sep.09.93	133.67	26,00,0,92	32.9	11.6
EQ2	Jan.20.94	77.48	42,42,7,92	71.3	32.2
EQ3	May.30.94	328.40	34,41,7,92	37.6	34.1
EQ4	Jun.05.94	24.50	36,41,7,92	64.7	41.8
EQ5	Oct.05.94	173.8	32,35,7,92	--	--
EQ6	Feb.23.95	18.75	42,41,7,92	53.8	48.9
EQ7	May.01.95	48.71	42,41,7,92	166.6	134.8
EQ8	May.02.95	107.65	42,41,7,92	72.8	87.9

[1] Azimuth of a line from the center of the model to the epicenter.

[2] A = number of accelerometers triggered; P = number of pressure gages triggered; S = number of settlement transducers triggered; and I = number of recording stations installed.

[3] L-direction motion measured on the roof of the model.

[4] L-direction motion measured at ground level.

7.1 *Cross-Correlation Analysis*

The cross-correlation function between two down-hole ground acceleration time-histories, $C_{ij}(\tau)$, has been used extensively to determine the travel time of random signals between two recording stations (Bendat and Piersol, 1986, Bendat and Piersol, 1980) and has been applied for the identification of shear velocities in Lotung LSST site (Elgamal *et al.*, 1995). The method relies on the fact that the major peak of the cross-correlation function between the ground acceleration time-histories recorded at two down-hole stations will be offset from the origin (time) by an amount τ_d, as opposed to the major peaks of the auto-correlation function for each of those time-histories which occurs at $\tau = 0$. For vertically propagating shear waves and two recording stations a distance *d* apart the signal propagation speed, *i.e.*, the shear wave speed in the soil for vertically propagating shear waves, is given by

$$V_S = d / \tau_d$$

Certain conditions must, however, be met to obtain reliable estimates of the shear wave velocities. In particular, the method cannot be applied to narrow-banded records (Bendat and Piersol, 1980) because the major peak of the cross-correlation function cannot be estimated with sufficient accuracy. It is also desirable that the wave propagation speed allow for a sufficient large travel time so that measurement errors are not a large percentage of the travel time itself. Additionally, it is expected that the earthquake loading does not induce significant nonlinear soil response. Also, when the objective is the measurement of vertically propagating shear waves, it is necessary that the recorded time-history is not dominated by surface waves (Elgamal *et al.*, 1995).

Earthquakes EQ2, EQ6 and EQ7 were the only ones used for this study since data for other earthquakes were not available to the authors at the time of the analysis. The auto-correlation functions of the recorded accelerograms revealed that the band-width of earthquake EQ6 may not be sufficiently large to obtain accurate results. Therefore, only earthquakes EQ2 and EQ7 were used. Prior to the determination of the shear wave speed, a sensitivity analysis was performed to determine the sensitivity of the cross-correlation and auto-correlation functions to the time-windows used for the analysis. On that basis, it was concluded that the cross-correlation functions were not too sensitive to the time-windows used and, more importantly, the sensitivity of the time delay τ_d to the time-windows selected was not significant. On the basis of that sensitivity analysis time-windows were also selected for each earthquake.

Cross-correlation functions for ground accelerations recorded at the same depth are shown in Figures 71 to 80 for earthquakes EQ2, EQ6 and EQ7. The major peaks of the cross-correlation functions are offset by negligible or very small time lags, indicating a near vertical propagation of shear waves at the site for the three earthquakes.

Examples of cross-correlation functions for ground motions recorded in the down-hole array at the end of ARM2 (see Figure 70) are shown in Figures 81 to 84. The wave propagation delays, τ_d, for the incident waves (positive time delays) can be seen in those figures. Time delays, however, become difficult to identify for the more closely-spaced stations such as, for example, stations D27 and D28. This is, in part, the result of relatively high shear wave velocities at the Hualien stiff soil site. A summary of the shear wave velocities between down-hole recording stations directly determined from the cross-correlation functions of the ground accelerations recorded at those stations is shown in Table 27.

Table 29. Shear wave velocities between down-hole recording stations

Down-Hole Stations	**EQ2**				**EQ7**			
	NS (magnetic)		**EW (magnetic)**		**NS (magnetic)**		**EW (magnetic)**	
	τ_d (sec)	**V_S (m/sec)**	**τ_d (sec)**	**V_S (m/sec)**	**τ_d (sec)**	**V_S (m/sec)**	**τ_d (sec)**	**V_S (m/sec)**
D28 - A25	0.1225	429	0.185	284	0.1425	368	0.2075	253
D28 - D25	0.105	450	0.180	263	0.115	411	0.180	263
D28 - D26	0.075	490	0.110	334	0.080	459	–	–
D28 - D27	0.05	583	0.070	375	0.050	525	0.075	350
D27 - D25	0.0575	365	0.100	210	0.0675	311	0.080	263
D26 - D25	–	–	0.0425	247	0.040	265	–	–
D14 - A15	0.115	457	0.170	308	0.1475	356	0.190	276
D14 - D11	0.100	473	0.165	286	0.120	394	0.1575	300
D14 - D12	0.070	525	0.105	350	0.085	432	0.105	350
D14 - D13	0.035	750	0.06	438	0.055	477	0.070	375
D13 - D11	0.050	420	0.0975	215	0.065	323	0.060	350
D12 - D11	–	–	0.05	210	–	–	0.045	233

The following observations can be made on the basis of the results shown in Table 27:

1. for both earthquakes the shear waves appear to propagate significantly faster for particle motions in the NS plane than for particle motions in the EW plane which may imply anisotropic site conditions;
2. SV wave velocities for the NS direction are similar to those obtained from the geophysical survey but those for the EW direction are significantly smaller; and
3. NS shear wave speeds inferred from the EQ7 data are smaller than those predicted on the basis of the EQ2 data; since the peak ground accelerations from EQ7 in the NS direction are greater than those from EQ2, this appears to be the result of nonlinear soil response under EQ7.

The results in Table 27 show some apparent discrepancies such as, for example, the decrease in the average shear wave speed from D28-A25 to D28-D25 for EQ2 in the EW direction, as well as the rapid decrease in the average wave speed from D28-D25 to D28-A25 for EQ7 in the NS direction. Additionally, the time delays for the reflected wave, negative peak values, differ significantly from those of the incident waves.

Such discrepancies may be the result of soil anisotropy and possible nonlinear soil response. For an anisotropic medium the cross-correlation analysis should take into consideration that the recorded signal for a given direction at a specified station (output) depends on the recorded signals in two orthogonal directions at a lower station (input). Such coupling between the two ground motion directions, which in the linear range exists for all but the two principal directions, is not accounted for in this study. As previously mentioned, the shear wave speeds at the site were also investigated by Ueshima and Okano (1996) using cross-spectral density analysis of the recorded accelerations. On the basis of their study, Ueshima and Okano concluded that the major principal direction (strong axis) is oriented about10^0 east from the magnetic north at the site. Since the angle of the principal directions with the L and T directions is small, the error on the uncoupled cross-correlation analysis presented here is also expected to be small. However, non-linear soil response may have occurred under the EQ6 load, which may explain, in part, some of the discrepancies in the results.

The results shown in Table 27 and wavespeeds between other down-hole stations computed from them are shown in Figures 85 and 86. Those results can be compared with the average shear wave speeds for the free-field identified by Ueshima and Okano on the basis of EQ2 and EQ4 data which are shown in Table 28.

Table 30. Average free-field shear wave speeds identified by Ueshima and Okano (1996)

LAYER	**Shear Wave Speed (m/sec)**		
	Unified Model for FVT-2	**Strong Axis**	**Weak Axis**
GL0.0 - GL-5.0m	192	209	183
GL-5.0m - GL-12.0m	333	341	201
GL-12.0m - GL-52.5m	476	469	358

One-dimensional deconvolution studies conducted by others for the prediction and correlation analyses, using methods like those in the program SHAKE (Schnabel, 1972) together with the unified soil model for FVT-2 recommended by CRIEPI (CRIEPI, 1993d and 1995b), resulted in good predictions of the observed free-field peak ground accelerations for the L-direction (NS) and poor predictions of the observed free-field peak ground accelerations for the T-direction

(EW). This may be a consequence, in part, of the anisotropic free-field site conditions with soil properties in the NS direction similar to those of the unified soil model but significantly different for the EW direction. The following two alternatives can be used in deconvolution studies for correlation with the observed soil responses: (1) a conventional deconvolution analysis using ground motions and soil properties referred to the principal directions and (2) a deconvolution analysis that accounts for soil anisotropy and coupling between ground motions in two horizontal directions together with the recorded ground motions (L and T directions). The second alternative should be used if the principal directions vary from layer to layer.

7.2 *Earthquake Response Analysis*

Soil-structure interaction analyses of the containment model under the EQ6 and EQ7 earthquake loads were conducted to interpret in-situ soil properties from the recorded data. These were the only earthquake loads analyzed, primarily because ground motion and structural response records from other earthquake events were not available to the authors when the analyses were performed. Nevertheless, those two earthquakes (EQ6 and EQ7) have significantly different ground motion intensities and frequency contents such that different soil-structure interaction responses are expected under each one of those loads.

The soil-structure interaction model used for the earthquake response analysis is identical to the one used for the interpretation of the FVT-2 test data. The method accounts for anisotropic soil conditions and earthquake loading in two orthogonal horizontal directions. It is recalled that, with the exception of the of the soil anisotropy, the small strain values of the soil properties recommended in the unified soil model for FVT-1 analysis appeared to represent well the average soil properties beneath the model's foundation for that phase of the project. It is also recalled that the unified soil model for FVT-2 analysis recommended in CRIEPI (1995) also appears to represent well the average properties at low-strain levels of the as-built backfill soil as well as the soil beneath the foundation. The best-estimated average properties for the backfill and foundation soil, *i.e.,* those that provided a better match to the observed response, are shown in Table 23. Soil-structure interaction analysis of the model under lateral loading using those soil properties should provide adequate estimates of the response under low-level earthquake loads, *i.e.*, such that the soil response remains in the linear range.

Soil-structure interaction analysis of the containment model under the selected earthquake loads revealed that the fundamental frequency of the soil-structure system computed with the soil properties shown in Table 23 is about 15 to 20% greater than those inferred from the data. Since the soil-structure interaction model together with the soil properties shown in Table 23 represents well the soil-structure interaction system in the linear range, it can be concluded that nonlinear effects have significantly affected the soil-structure interaction under these earthquake loads. It must be noticed, however, that the backfill stiffness below about GL-2m may be somewhat less than that for the FVT-2 test as a result of a higher water table in the backfill at the time of the earthquake loads.

To assess the extent of the soil stiffness and support reductions as compared to those in the FVT-2 test, a brief sensitivity analysis was conducted to estimate equivalent linear soil properties and other SSI parameters such as an effective embedment length, *d*, that result into a fair agreement between the observed and computed responses. Accordingly, the soil properties of the backfill and foundation soil were varied until the desired fair agreement to the observed structural response was obtained. In this sensitivity analysis, the angle between the principal direction of soil stiffness (higher stiffness) and the magnetic EW direction (T) was kept equal to 75-degrees, i.e., a value of $\alpha = -75^0$ was used as input for this SSI analysis. It is recalled that, on the basis of the FVT-1 and FVT-2 analyses, the major principal direction for the site anisotropy was found to be about 35-degress counterclockwise from the plant (shaker) East, which corresponds to 76.25-degrees counterclockwise from the magnetic East (T). As an approximation the value of 75-degress was used in the sensitivity analysis.

Here, the computed and observed responses are compared on the basis of the pseudo-acceleration response spectra of the roof response for a damping ratio of 0.5-percent. Further evaluation of the computed response is made by comparing the analytical transfer functions of the roof response with those obtained on the basis of cross-spectral analysis of the recorded roof and free-field accelerations.

Ground accelerations recorded at station A13 are used as the input free-field ground accelerations for all analyses. To account for kinematic interaction effects, the following approximation has been suggested to compute the input ground motions at the base of the SSI springs (Kausel *et al.*,1978):

$$\ddot{a} = \mathrm{IFT}\begin{cases} F(\Omega)\cos\left(\dfrac{\pi}{2}\dfrac{f}{f_n}\right), \text{if } f \le 0.7 f_n \\ F(\Omega) \times 0.453 \quad ,\text{if } f > 0.7 f_n \end{cases}$$

$$\ddot{\phi} = \mathrm{IFT}\begin{cases} F(\Omega) \times 0.257 \times \left[1 - \cos\left(\dfrac{\pi}{2}\dfrac{f}{f_n}\right)\right] / R, \text{if } f \le f_n \\ F(\Omega) \times 0.257 / R \qquad\qquad ,\text{if } f > f_n \end{cases}$$

Where $\ddot{a}$ = horizontal ground acceleration, $\ddot{\phi}$ = acceleration of the rigid foundation rotation, $F(\Omega)$ = Fourier spectrum of the free-field surface ground acceleration, R = foundation radius, IFT = inverse Fourier transform, f = frequency in Hz, $f_n = V_S/4H$, where H = depth from ground surface to the foundation plane and V_S = shear wave speed from the ground surface to H. Sensitivity analysis shows that, for this SSI system, the response spectra ordinates of the computed roof accelerations do not change significantly whether either the surface ground motions or the kinematic motions are used as input. For simplicity, the results presented below are for input horizontal ground accelerations equal to the recorded surface ground accelerations and input rocking accelerations equal to $\ddot{\phi}$.

7.2.1 Earthquake of February 23, 1995 (EQ6)

Pseudo-acceleration response spectra for 0.5% damping of the L and T components of the free-field ground accelerations (station A13), and of the L and T components of the roof response (station RFN) are shown in Figures 87 and 88, respectively. These figures allow for a quick identification of the frequency content of the input and output motions. Pseudo-acceleration response spectra of the recorded and computed NS and EW components of the roof response, for a damping ratio of 0.5%, are shown in Figures 89 to 92 for two sets of soil properties. The response spectra shown in Figures 89 to 90 are for the soil properties in Table 29, whereas the response shown in Figures 91 and 92 is for the properties in Table 30. In one case full embedment (*d* = 5.0 m) is considered whereas a partial embedment of 3.5 m is considered for the other case. Higher shear wave speeds are used for the partially embedded case as compared to the full embedment case, in order to obtain similar fundamental frequencies of vibration. The results obtained for *d* = 5.0 m appear to compare better with the observed response than those for *d* = 3.5 m. For both cases, the computed response does not compare well with the observed response for frequencies between about 1.5 and 5.0 Hz. This may be a consequence of approximating a nonlinear system by an equivalent linear system, and using input motions at the base of the SSI springs that do not properly account for the so-called kinematic soil-structure interaction effects.

Recorded and computed time-histories of the roof response for *d* = 5.0 m are shown in Figure 93. It can be seen that the compute response differs from the recorded one for the longer period components. Transfer functions between the free-field acceleration and the roof response are shown in Figures 94 and 95. The cross-spectral density analysis reveals fundamental frequencies of 5.4 and 5.0 Hz, for the L and T directions, respectively, whereas the fundamental frequencies from the SSI analysis are about 5.4 Hz for both the L and T directions. Although the foundation soil is considered anisotropic, it is assumed in the analysis that the soil stiffness reduction and the embedment condition are the same in all directions. This, may not be the actual case.

Table 31. Soil properties for the earthquake response analysis with *d* = 5.0 m (EQ6)

Material[1]	**Depth (m)**	**Density (kg/m^3)**	**S-Wave Speed**[2] **(m/sec)**	***n***	**α**	**Poisson's ratio**	**Damping Ratio (%)**
Backfill	0 - 5 m	2390	220	1.0	--	0.33	2
Gravel-1 (foundation)	5 - 12 m	2420	340[2]	1.25	-75^0	0.48	2
Gravel-3	12 - 20 m	2420	476	1.25	-75^0	0.48	2

[1] The soil types are identified in Figure 6.

[2] For the major principal direction.

Table 32. Soil properties for the earthquake response analysis with *d* = 3.5 m (EQ6)

Material[1]	**Depth (m)**	**Density (kg/m^3)**	**S-Wave Speed**[2] **(m/sec)**	***n***	**α**	**Poisson's ratio**	**Damping Ratio (%)**
Backfill	0 - 5 m	2390	250	1.0	--	0.33	2
Gravel-1 (foundation)	5 - 12 m	2420	360[2]	1.25	-75^0	0.48	2
Gravel-3	12 - 20 m	2420	476	1.25	-75^0	0.48	2

[1] The soil types are identified in Figure 6.

[2] For the major principal direction.

Less soil stiffness reduction would be required if the shear wave speeds for the gravel determined on the basis of laboratory testing (see Tables 12 and 13) were used in the analysis. There appears to be however, no strong reason to prefer the laboratory based shear wave speeds over those from direct shear wave measurements. In fact, the best-estimated soil properties determined on the basis of the FVT-2 analysis are closer to the in-situ measurements than to the wavespeeds determined on the basis of the laboratory tests.

7.2.2 Earthquake of May 1, 1995 (EQ7)

Pseudo-acceleration and pseudo-speed response spectra for 5% damping of the L and T components of the free-field ground accelerations (station A13) and of the L and T component of the roof response (station RFN) are shown in Figures 96 and 97. As before, these response spectra allow for an approximate identification of the frequency content of the input and output motions as well as of the dominant SSI frequencies. Pseudo-acceleration response spectra for recorded and computed NS and EW components of the roof response and for a damping ratio of 0.5% are shown in Figures 98 and 99 for two sets of soil properties. The computed response spectra shown in Figure 98 is for d = 5.0 m and the soil properties in Table 31, whereas that in Figure 99 is for d = 3.0 m and the soil properties in Table 32. As before, the fundamental frequencies of vibration are the same for both sets of soil properties and embedment depths. With the exception of the frequencies between 1.5 and 4.5 Hz, the computed response compares well with the measured response for both the L and T directions.

Recorded and computed roof response time-histories d = 3.0 m are shown in Figure 100. The peak accelerations of the roof response are underestimated by the model, particularly for the T direction. Transfer functions between the free-field ground acceleration and the roof response are shown in Figures 101 and 102. The fundamental frequency in the L direction from the cross-spectral analysis is about 5.1 Hz, whereas those from the SSI analysis are about 5.15 Hz for both directions. The cross spectral density analysis does not reveal a clear resonant frequency for the T direction which, however, appears to be between 5.0 and 5.5 Hz. The transfer functions computed with the SSI model and the cross-spectral analysis show evidence of anisotropic site conditions.

Table 33. Soil properties for the earthquake response analysis with d = 5.0 m (EQ7)

Material[1]	**Depth (m)**	**Density (kg/m^3)**	**S-Wave Speed[2] (m/sec)**	n	α	**Poisson's ratio**	**Damping Ratio (%)**
Backfill	0 - 5 m	2390	210	1.0	--	0.33	2
Gravel-1 (foundation)	5 - 12 m	2420	330[2]	1.25	-75^0	0.48	2
Gravel-3	12 - 20 m	2420	476	1.25	-75^0	0.48	2

[1] The soil types are identified in Figure 6.

[2] For the major principal direction.

Table 34. Soil properties for the earthquake response analysis with $d = 3.0$ m (EQ7)[1]

Material[2]	Depth (m)	Density (kg/m^3)	S-Wave Speed[3] (m/sec)	n	α	Poisson's ratio	Damping Ratio (%)
Backfill	0 - 5 m	2390	250	1.0	--	0.33	2
Gravel-1 (foundation)	5 - 12 m	2420	355[2]	1.25	-75^0	0.48	2
Gravel-3	12 - 20 m	2420	476	1.25	-75^0	0.48	2

[1] $d = 3.0$ m for the L direction and $d = 4.0$ m for the T direction.

[2] The soil types are identified in Figure 6.

[3] For the major principal direction.

It is noteworthy that nonlinear effects are significant under earthquake loads that can be considered weak to moderate as compared to those used in the design of most nuclear plant seismic category I structures. This may be a result, in part, of the stiff foundation soils and as-built backfill soils considered in the experiment. For those soils, the secant shear stiffness decreases very rapidly with shear strain. This can be observed, for example, with the data in Table 14a, which indicate that the secant shear modulus of the backfill is reduced to about 62% and 40% of the elastic modulus for shear strains of the order of 5.1×10^{-5} and 1.3×10^{-4}, respectively. Under the EQ7 load, peak rigid body rocking rotations equal to about 5.2×10^{-5} were computed in the SSI analysis. Assuming that the rigid body rocking rotation of the model with respect to the baseline of the SSI springs is an approximation to the shear strains in the backfill in the vicinity of the model, the computed rocking rotation is an indication of nonlinear response of the backfill soil at the interface with the containment walls. This implies that, for this case, the decrease of the fundamental frequency of vibration can be attributed to the non-linear deformations imposed by structure on the backfill and, possibly, the foundation soil.

7.3 *Summary of Earthquake Data and Response Analysis*

Cross-correlation analysis of the earthquake ground motion data recorded indicates that the earthquake induced shear waves at the site propagate in a nearly vertical direction for the three earthquake events analyzed, and that there appear to a strong free-field anisotropy such that the speed of vertical shear wave propagation in the gravel is 20 to 40% greater for particle motions in the NS direction than for particle motions in the EW direction. Site anisotropy had also been determined on the basis of the analysis of the forced vibration test data. The cross-hole logging data obtained prior to the excavation and after excavation and construction of the model show evidence of this site anisotropy to about GL-12m.

The site anisotropy identified above, *i.e.*, vertical shear wave propagation speeds that differ for particle motions in the NS and EW directions, should be taken into consideration for site amplification and deconvolution analysis studies for correlation analysis with the recorded ground motions at the site. It should also be taken into consideration for the study of kinematic soil-structure interaction effects and the evaluation of scattering motions.

The earthquake response analyses presented indicate that the soil-structure interaction response under the earthquake loads investigated has been affected by nonlinear effects. Namely, transfer functions from the free-field ground motions to the roof response indicate dominant soil-structure interaction frequencies that are about 15 to 20% less than those observed in the FVT-2 test. Those transfer functions also indicate the evidence of soil anisotropy in the foundation soil. Since the effects of soil anisotropy are not so readily apparent in the FVT-2 test (embedded case) as they are in the FVT-1 test (surface foundation), this seems to imply that either the backfill stiffness was reduced under the earthquake loading or the effective embedment length decreases in such a manner that the anisotropy of the foundation soil becomes apparent.

It is noteworthy that nonlinear effects have shown to be significant under earthquake loads that may be considered weak to moderate as compared to those used in the design of most nuclear power plant seismic category I structures.

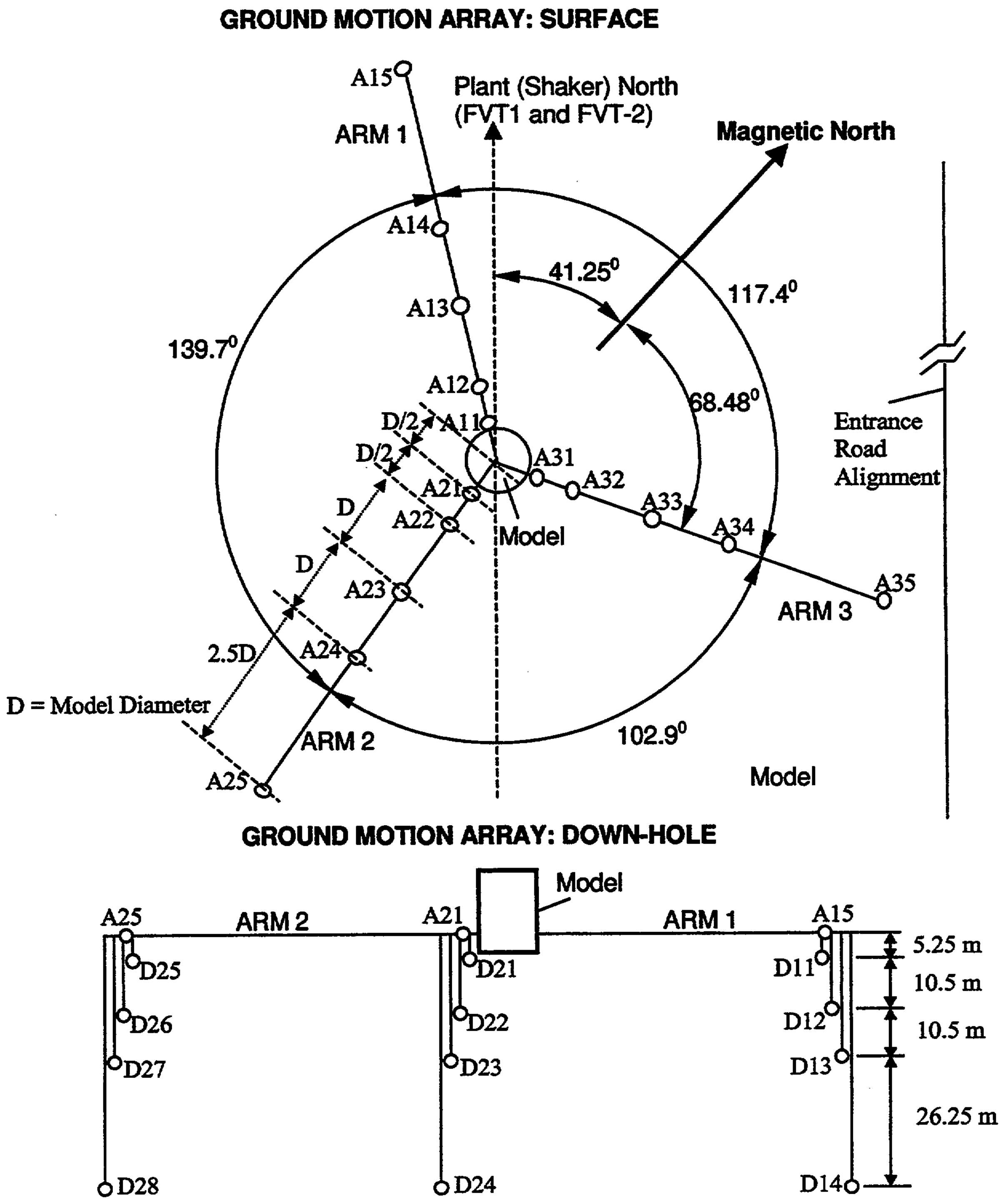

GROUND MOTION ARRAY: SURFACE

GROUND MOTION ARRAY: DOWN-HOLE

Figure 70 Ground motion array for the Hualien LSST

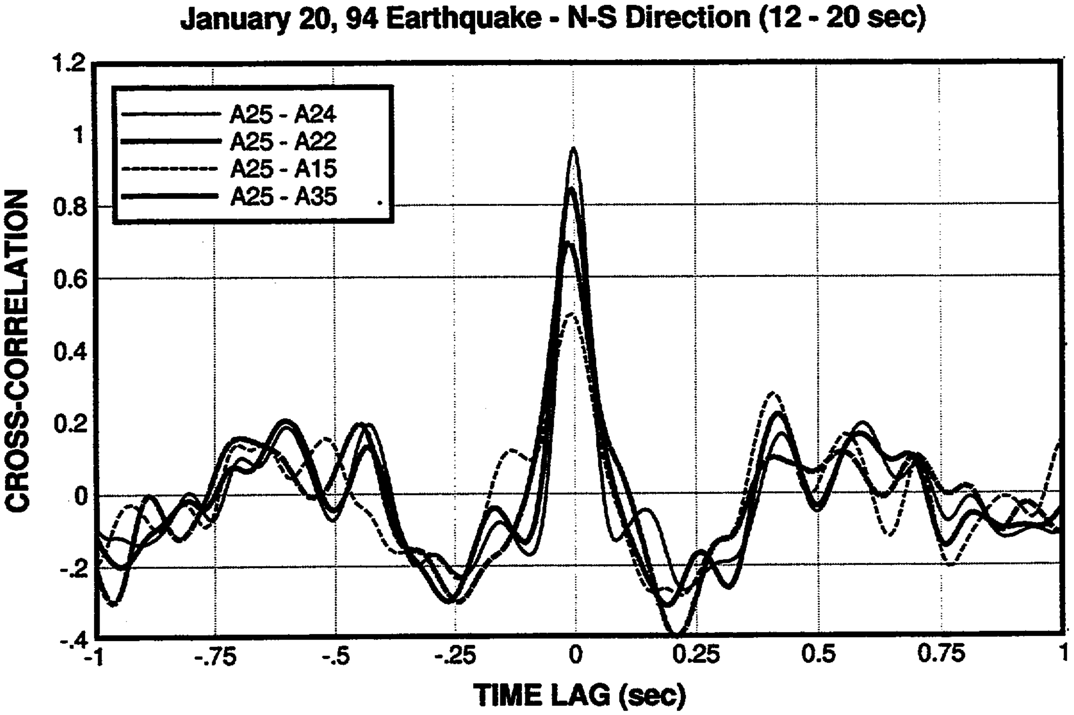

Figure 71 Cross-correlation function for surface NS accelerations (EQ2)

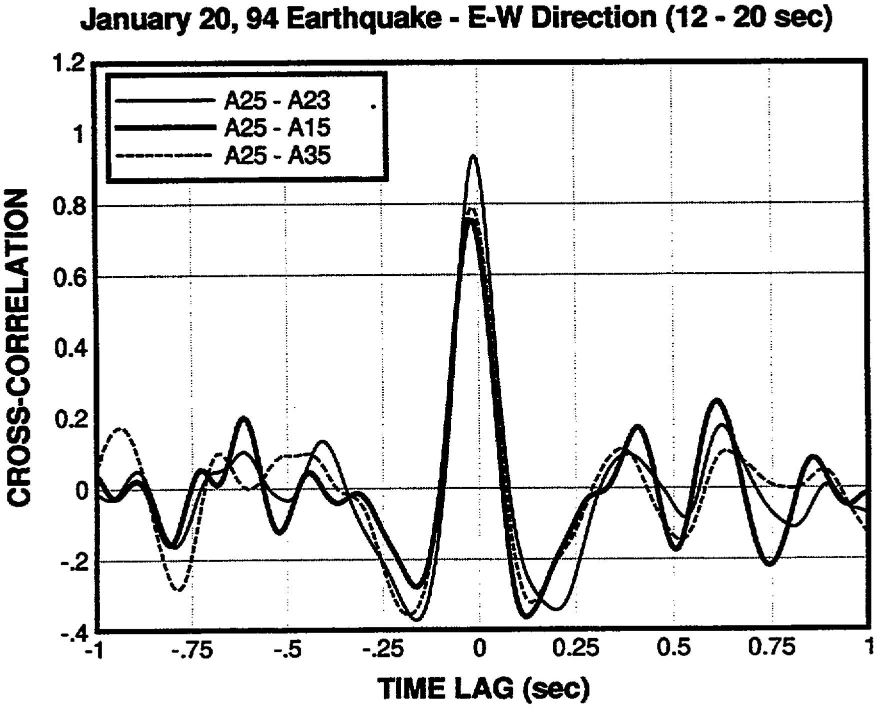

Figure 72 Cross-correlation function for surface EW accelerations (EQ2)

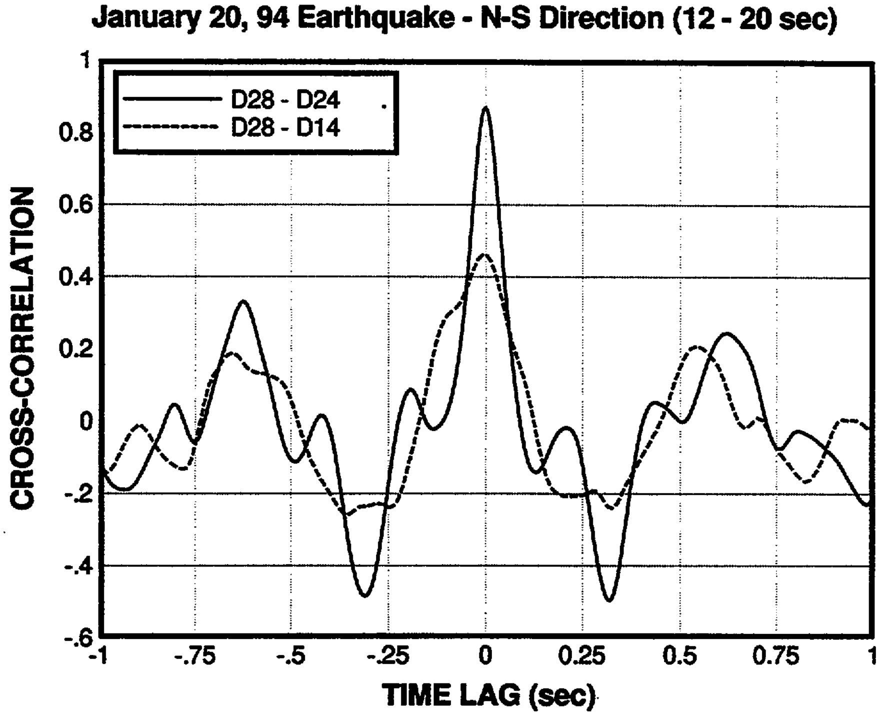

Figure 73 Cross-correlation function for NS accelerations at -52.5 m (EQ2)

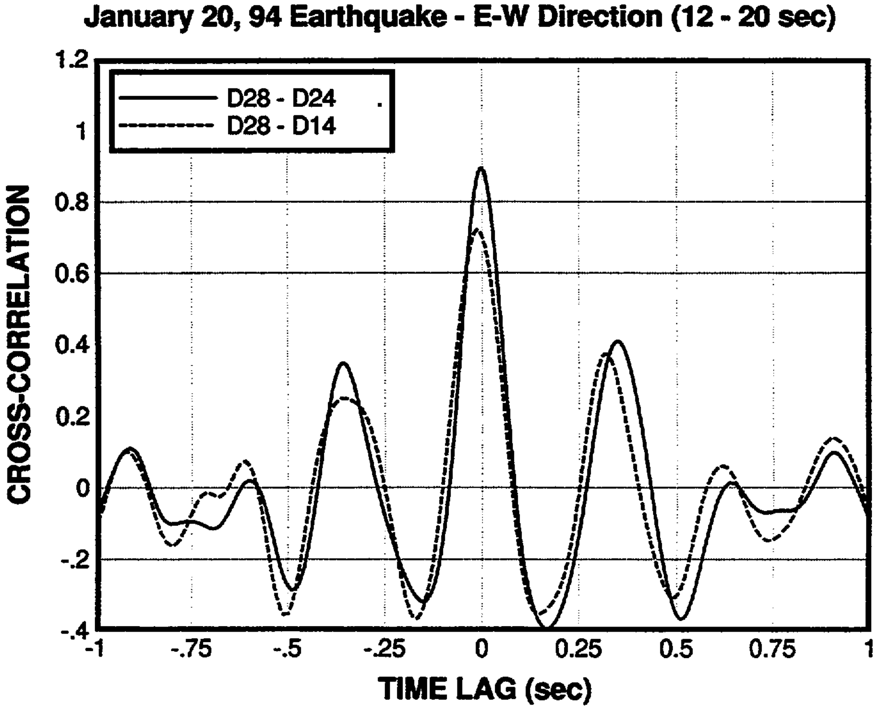

Figure 74 Cross correlation function for EW accelerations at -52.5 m (EQ2)

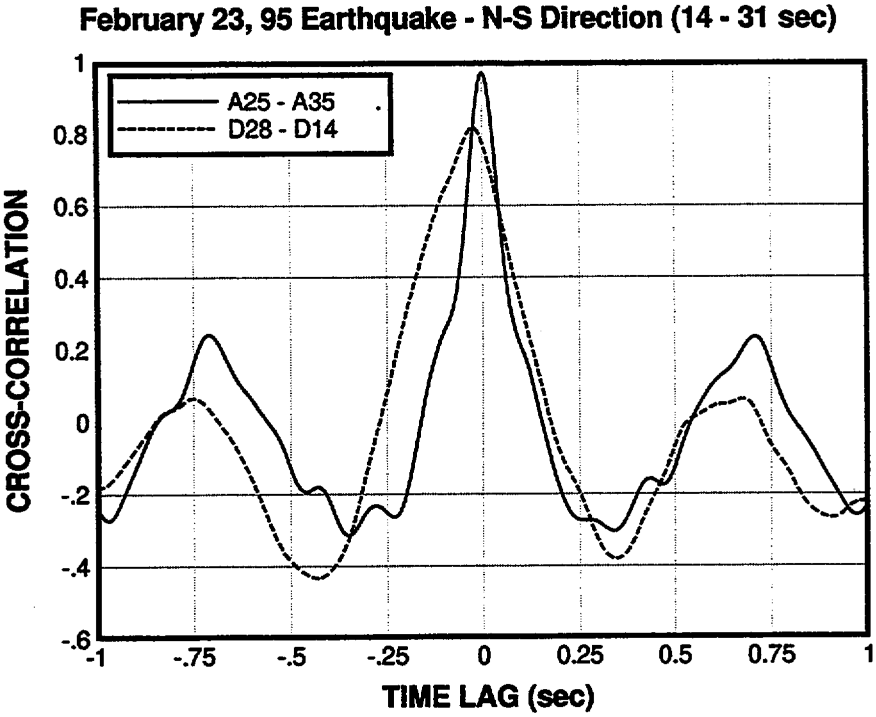

Figure 75 Cross-correlation function for NS accelerations at the same level (EQ6)

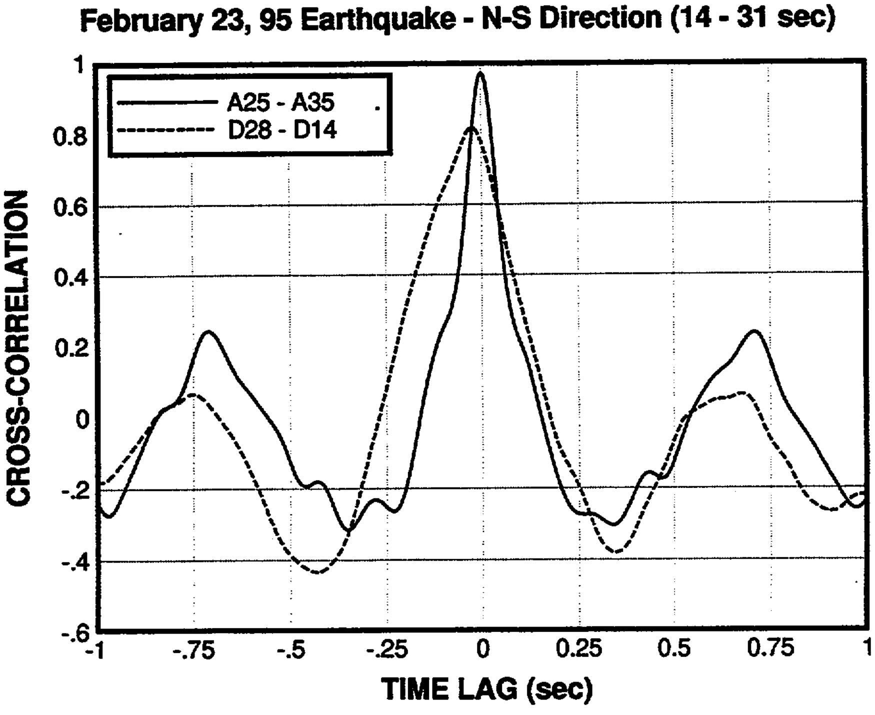

Figure 76 Cross-correlation function for EW accelerations at the same level (EQ6)

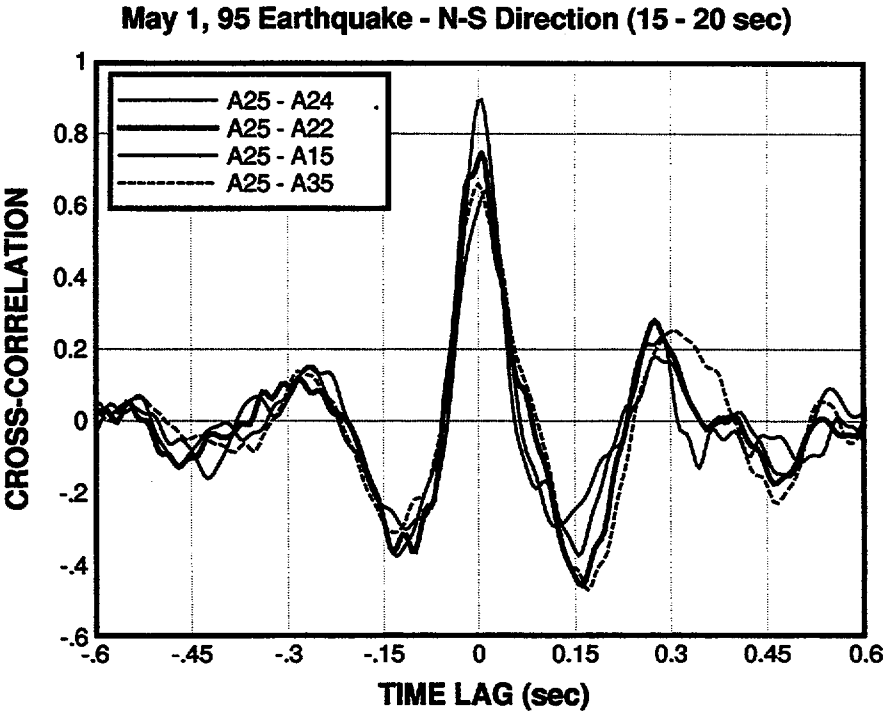

Figure 77 Cross-correlation function for surface NS accelerations (EQ7)

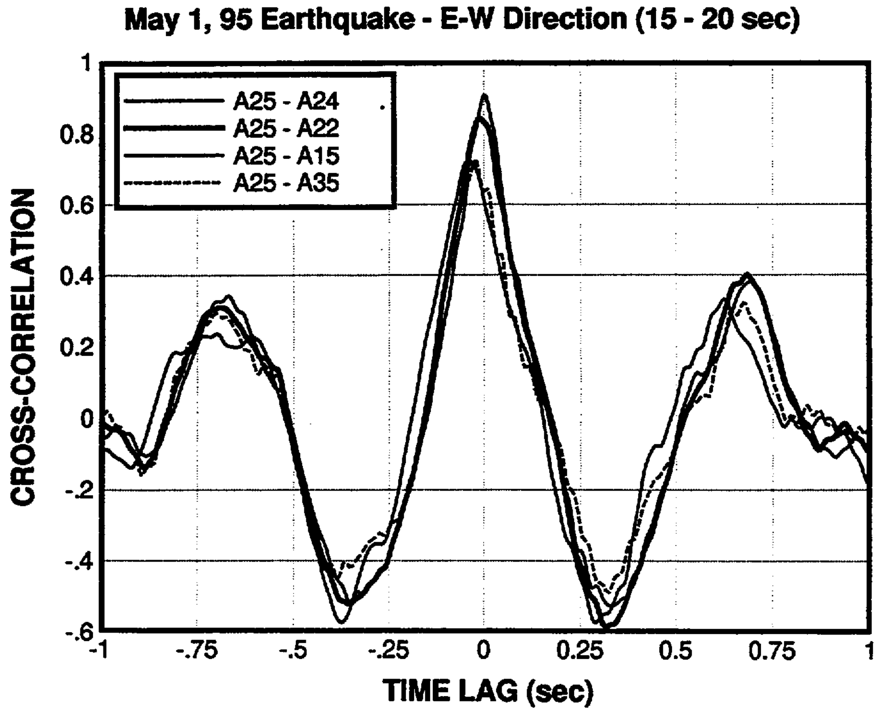

Figure 78 Cross-correlation function for surface EW accelerations (EQ7)

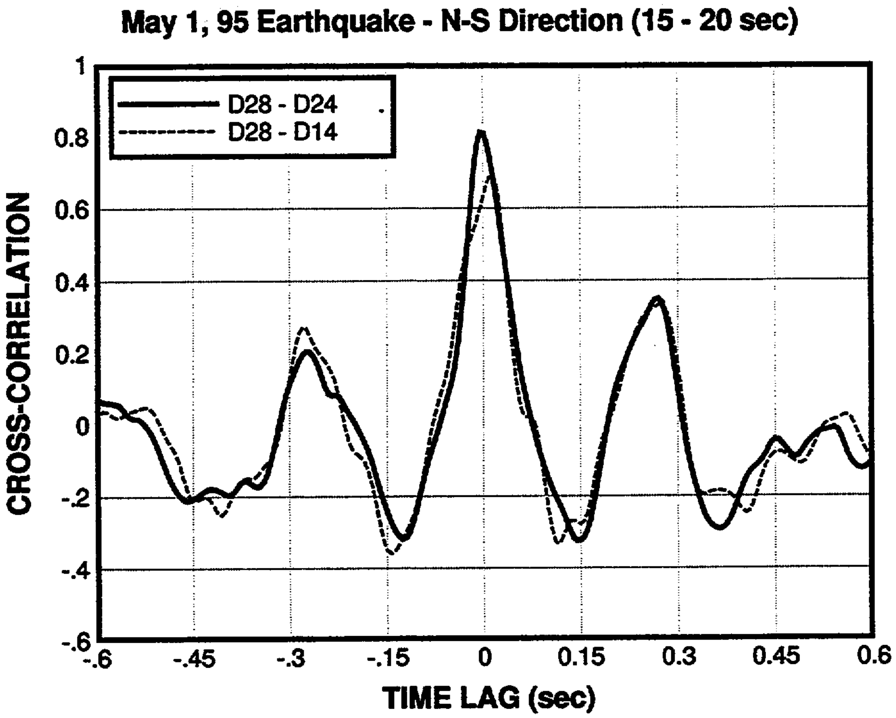

Figure 79 Cross-correlation functions for NS accelerations at -52.5 m (EQ7)

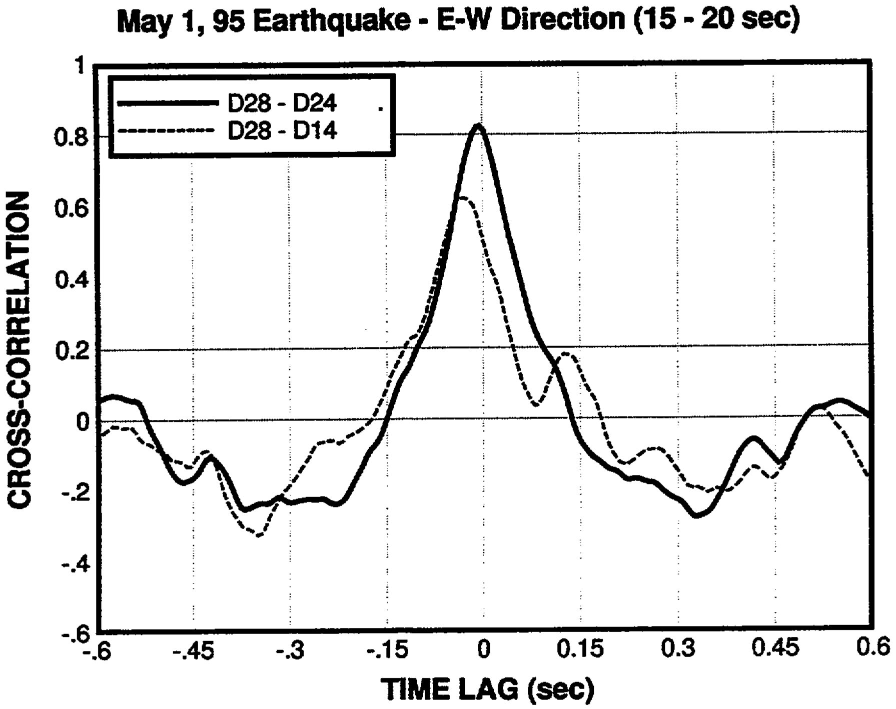

Figure 80 Cross-correlation functions for EW accelerations at -52.5m (EQ7)

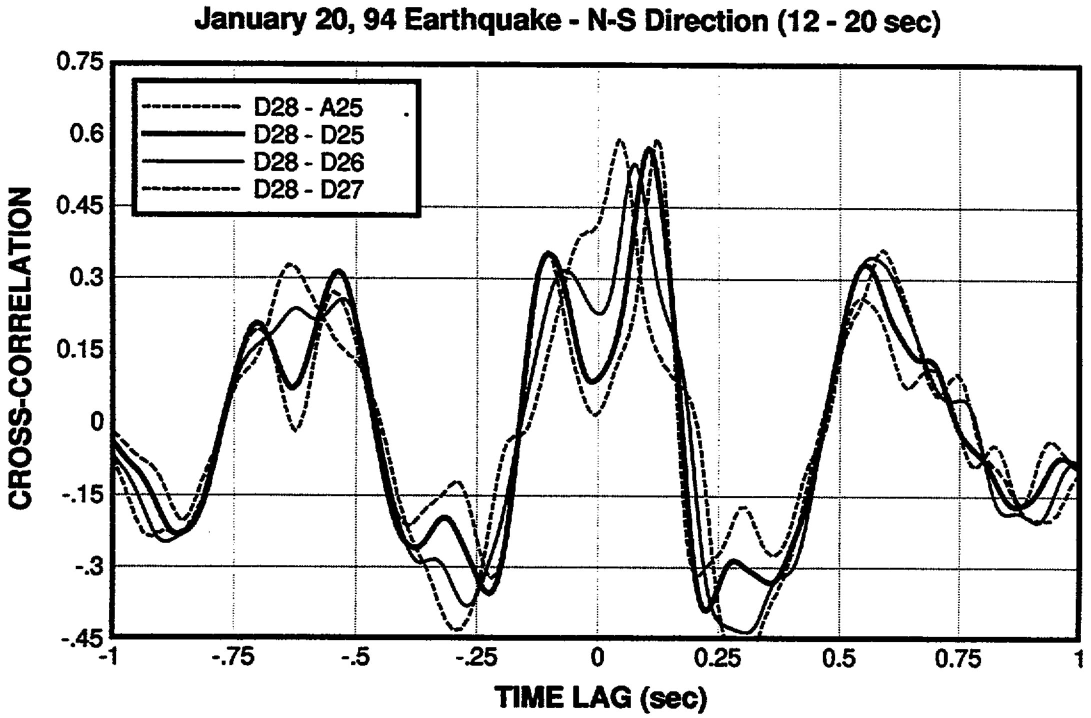
January 20, 94 Earthquake - N-S Direction (12 - 20 sec)

Figure 81 Cross-correlation functions for NS down-hole accelerations (EQ2)

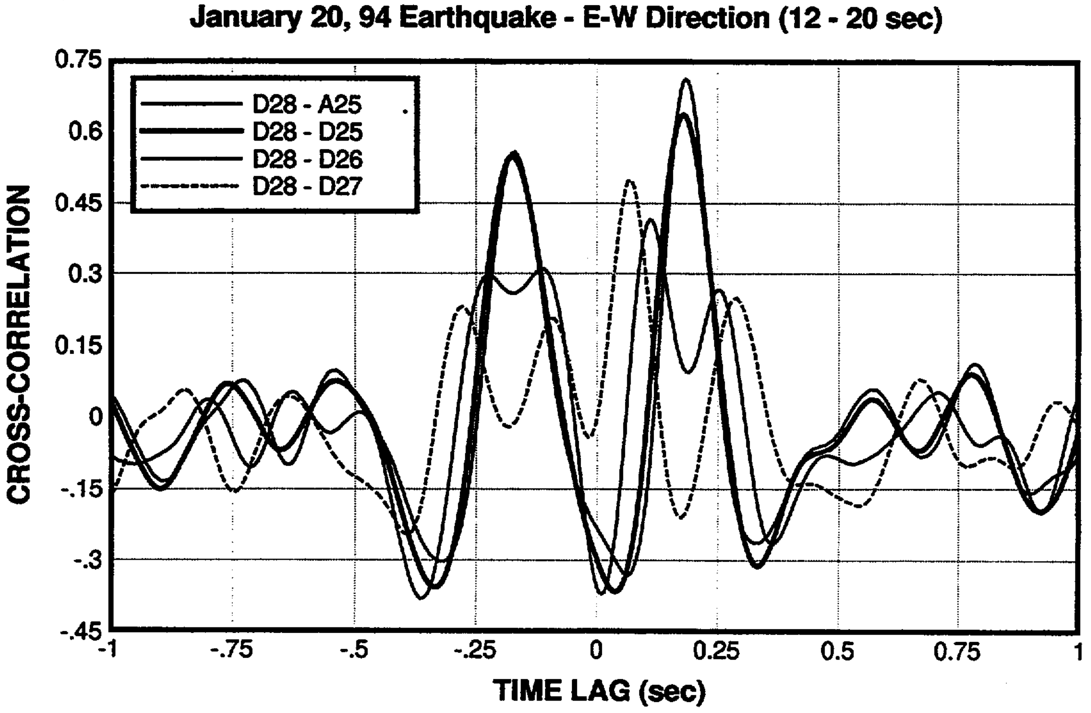
January 20, 94 Earthquake - E-W Direction (12 - 20 sec)

Figure 82 Cross-correlation functions for EW down-hole ground accelerations (EQ2)

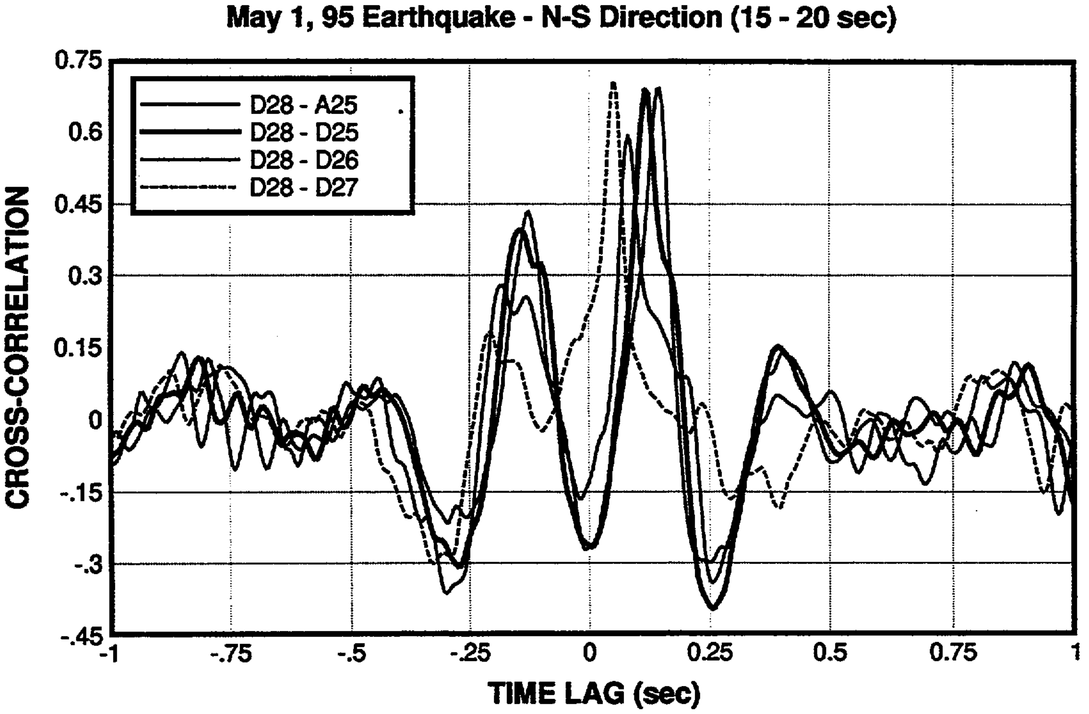

Figure 83 Cross-correlation function for NS down-hole accelerations (EQ7)

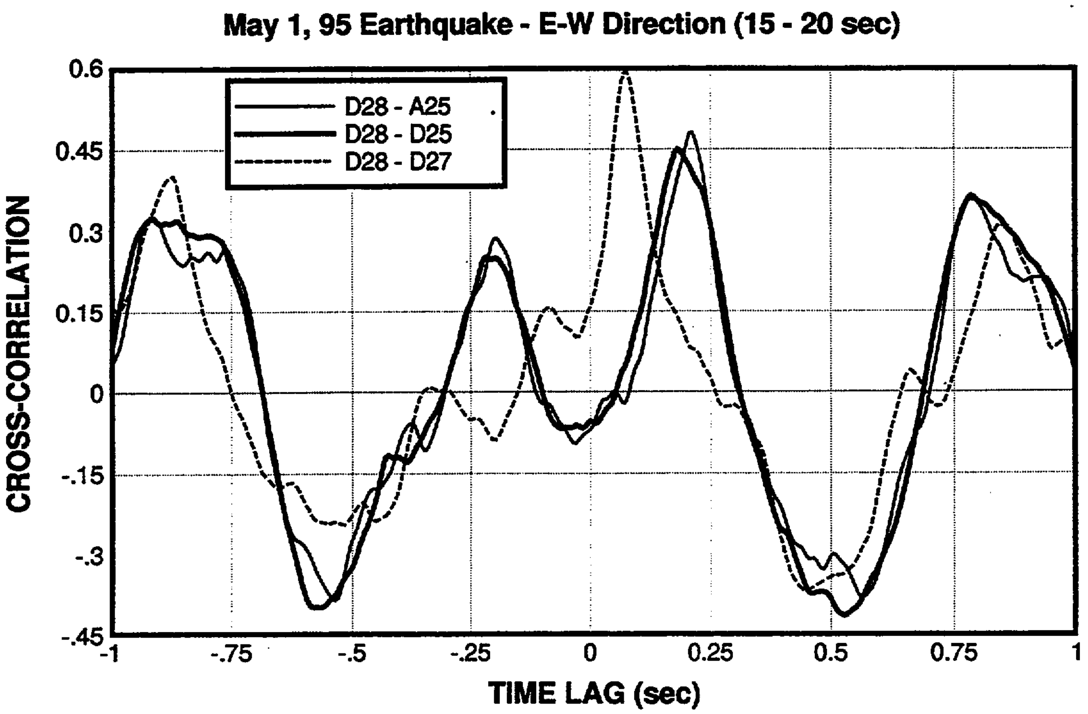

Figure 84 Cross-correlation functions for EW down-hole accelerations (EQ7)

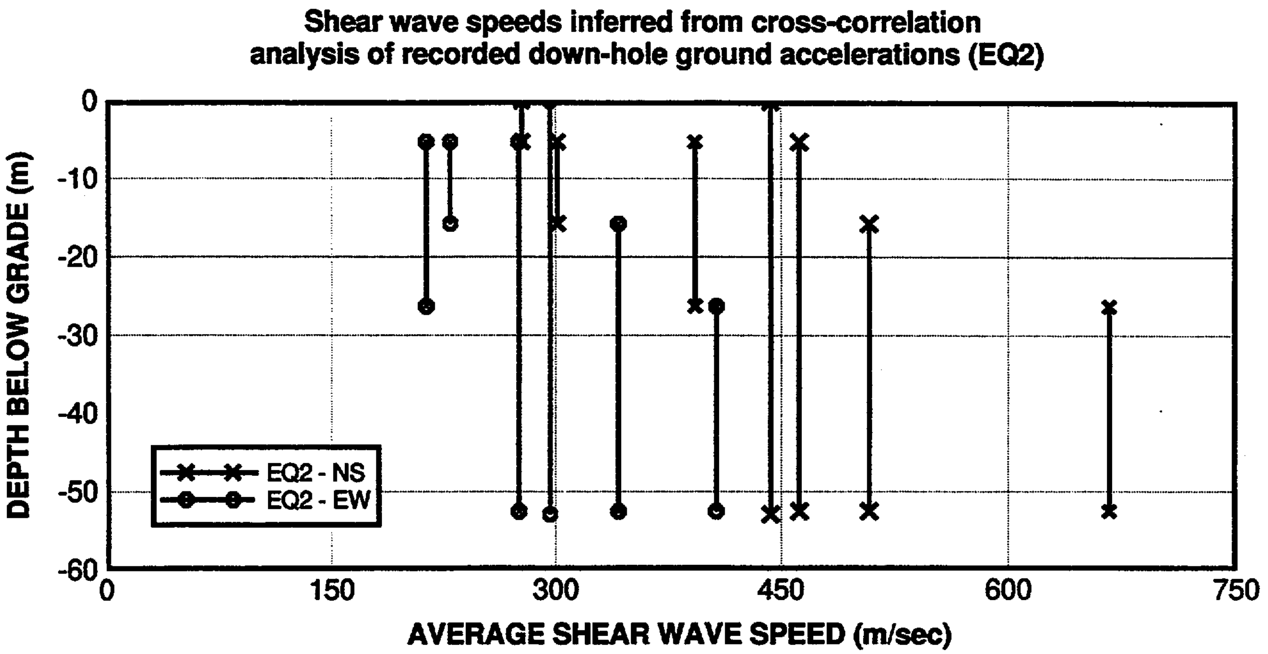

Figure 85 Average shear wave velocities inferred from cross-correlation analysis of down-hole ground accelerations (EQ2)

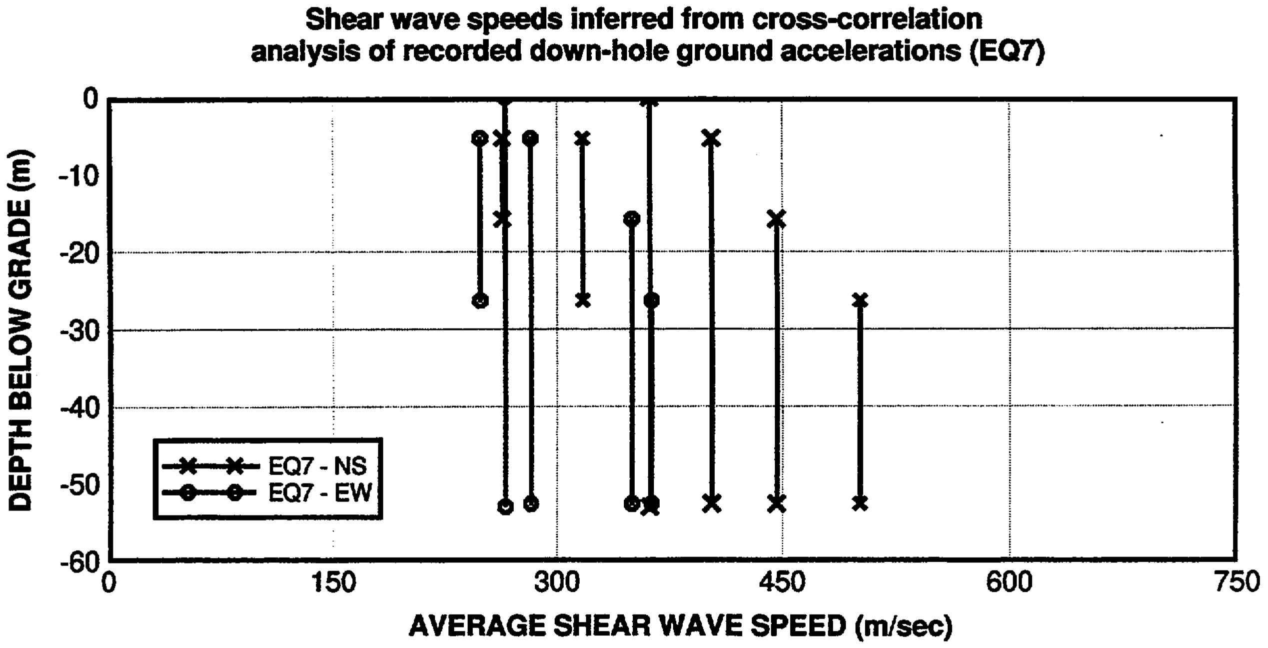

Figure 86 Average shear wave velocities inferred from cross-correlation analysis of down-hole ground accelerations (EQ6)

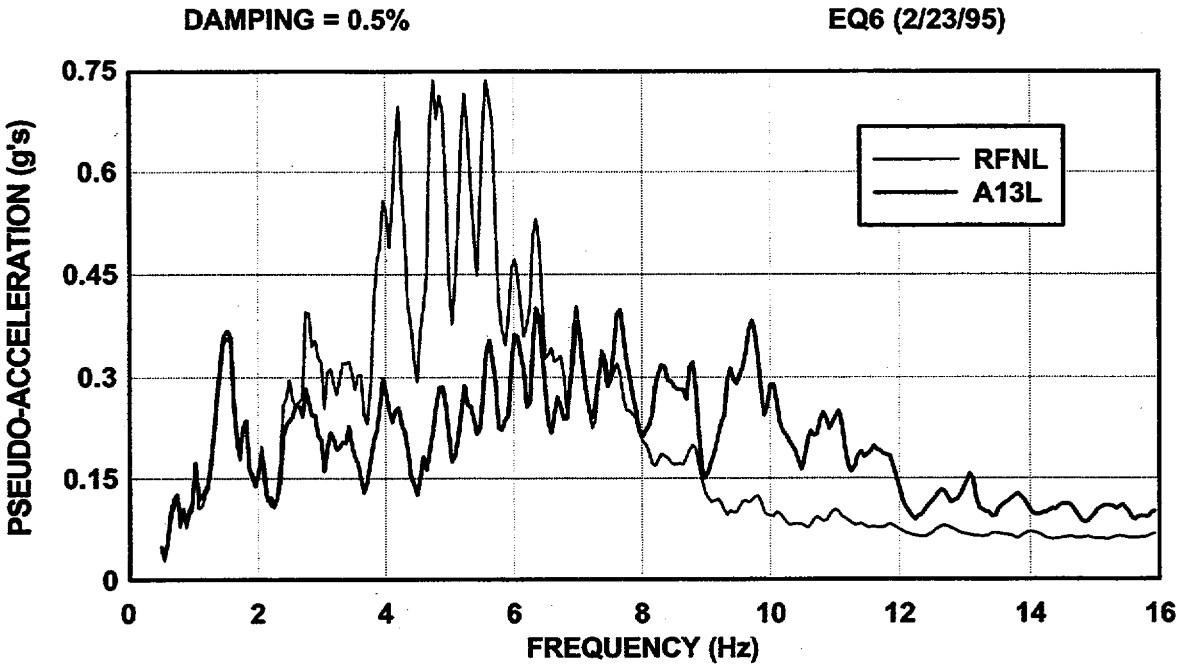

Figure 87 Response spectra for 0.5% damping: EQ6 L-direction

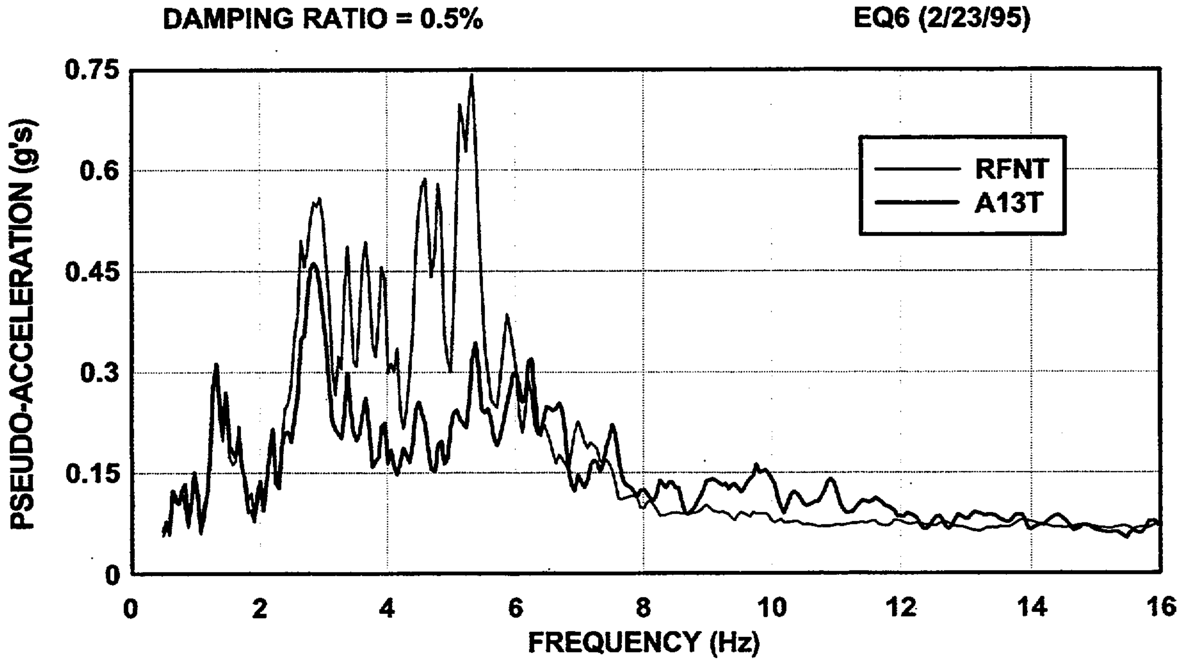

Figure 88 Response spectra for 0.5% damping: EQ6 T-direction

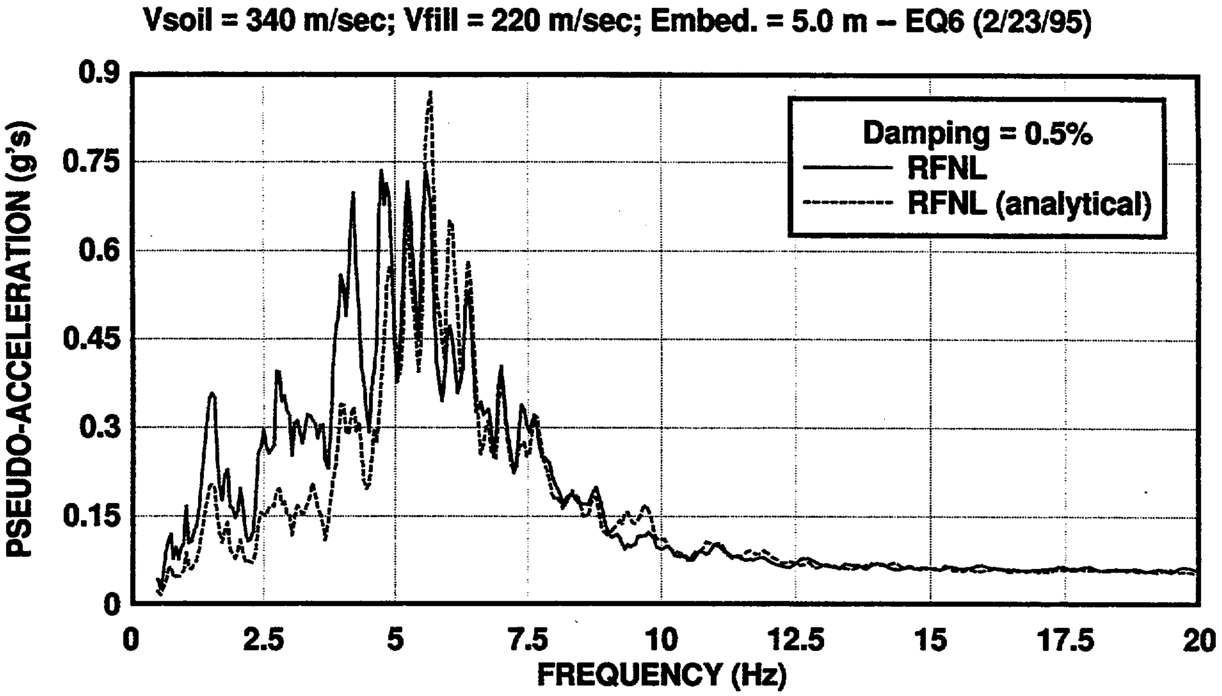

Figure 89 Observed and computed response spectra for 0.5% damping: EQ6 L-direction (embedment, *d* = 5.0 m)

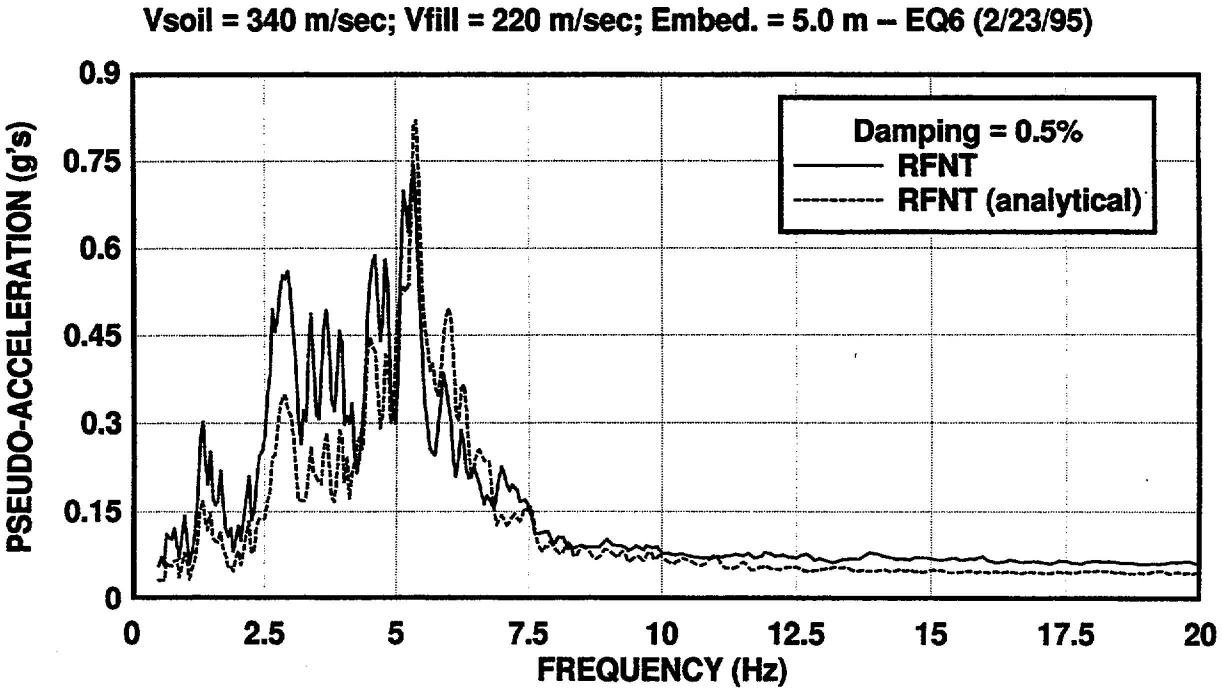

Figure 90 Observed and computed response spectra for 0.5% damping: EQ6 T-direction (embedment, *d* = 5.0 m)

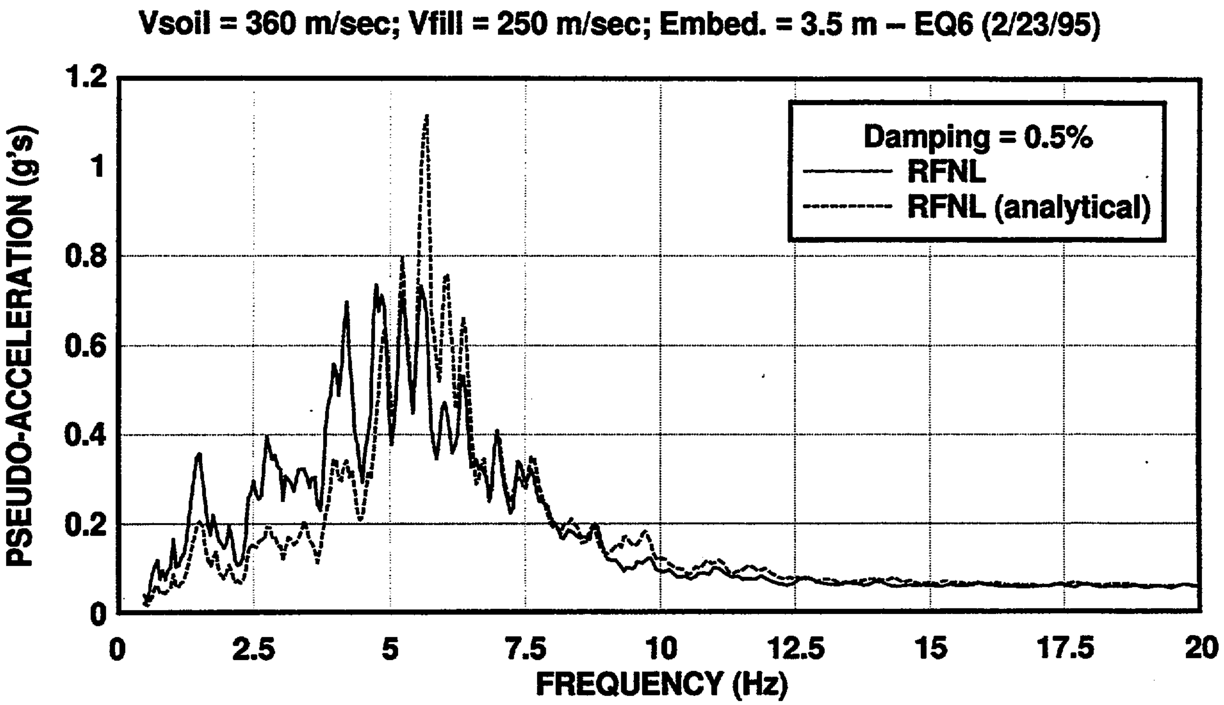

Figure 91 Observed and computed response spectra for 0.5% damping: EQ6 L-direction (embedment, *d* = 3.5 m)

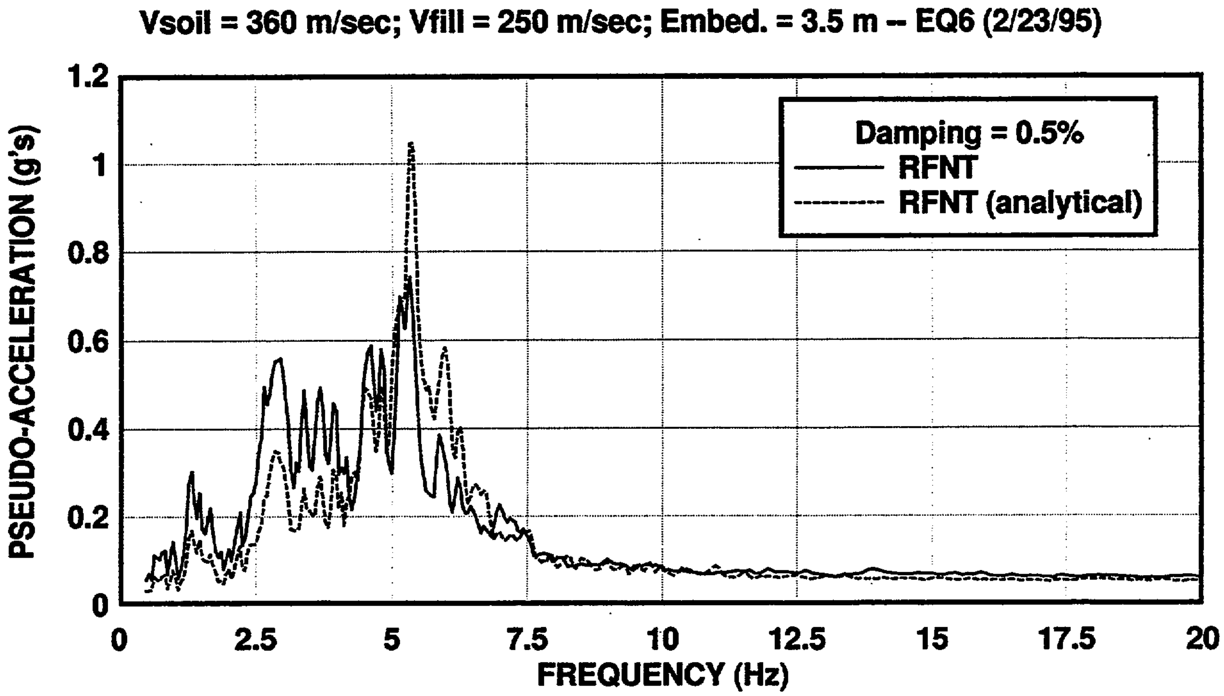

Figure 92 Observed and computed response spectra for 0.5% damping: EQ6 T-direction (embedment, *d* = 3.5 m)

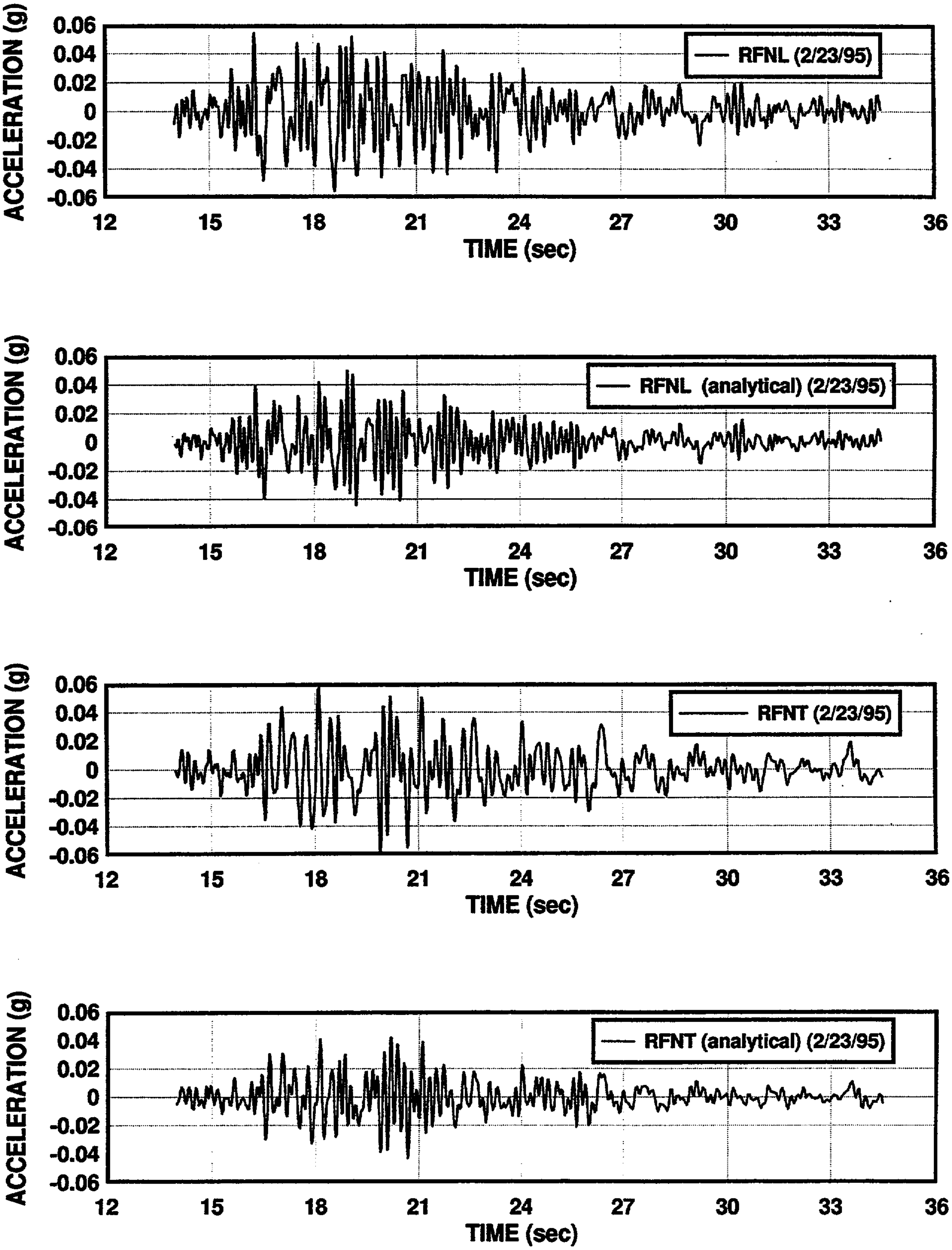

Figure 93 Observed and computed roof response time-histories: EQ6

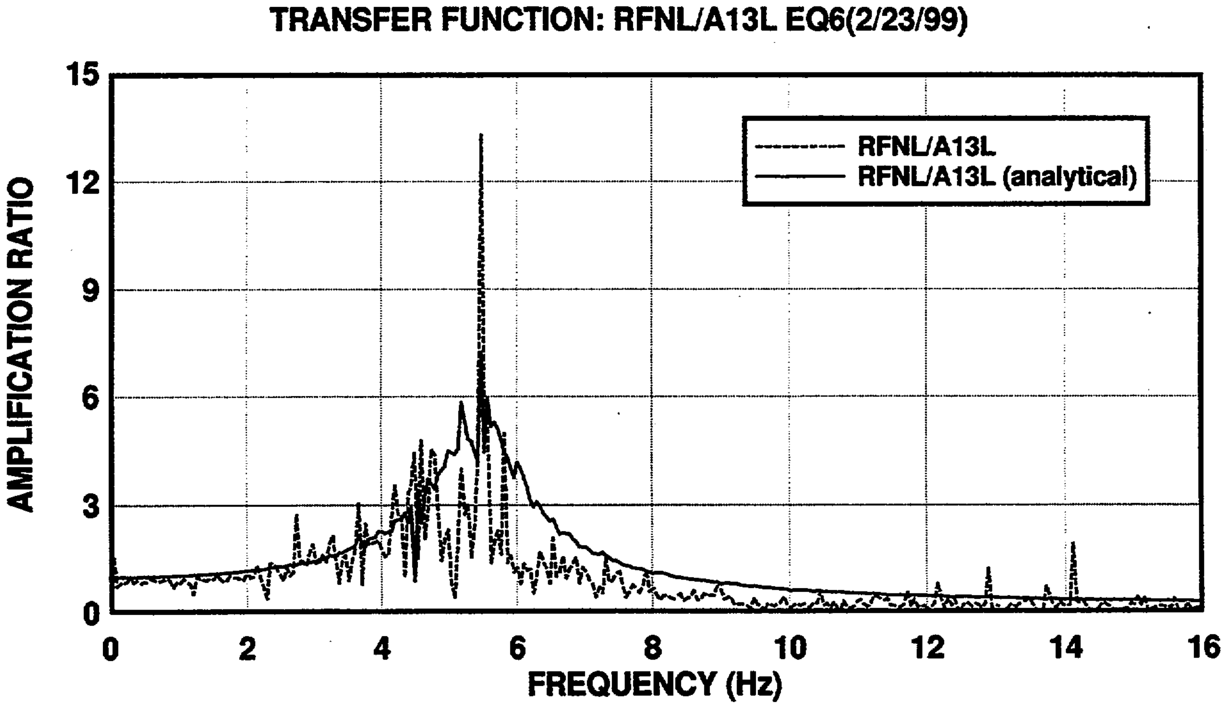

Figure 94 Transfer functions from free-field motion to roof response: EQ6 L-direction

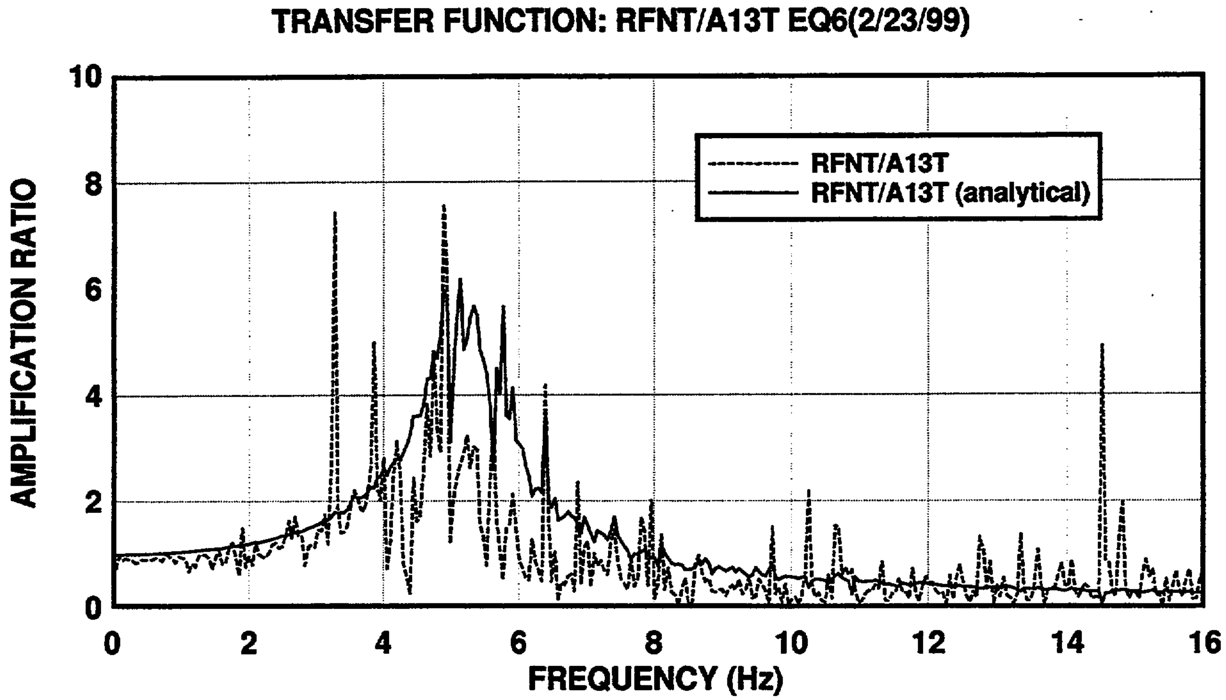

Figure 95 Transfer functions from free-field motion to roof response: EQ6 T-direction

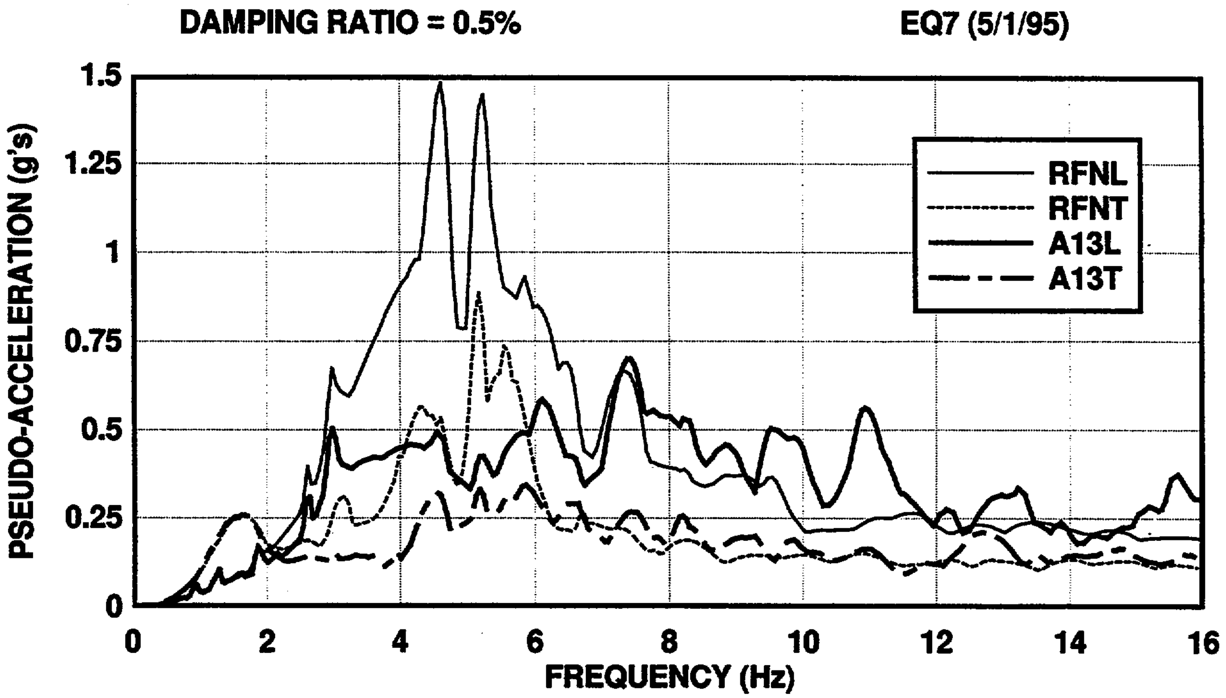

Figure 96 Pseudo-acceleration response spectra for 0.5% damping for EQ7

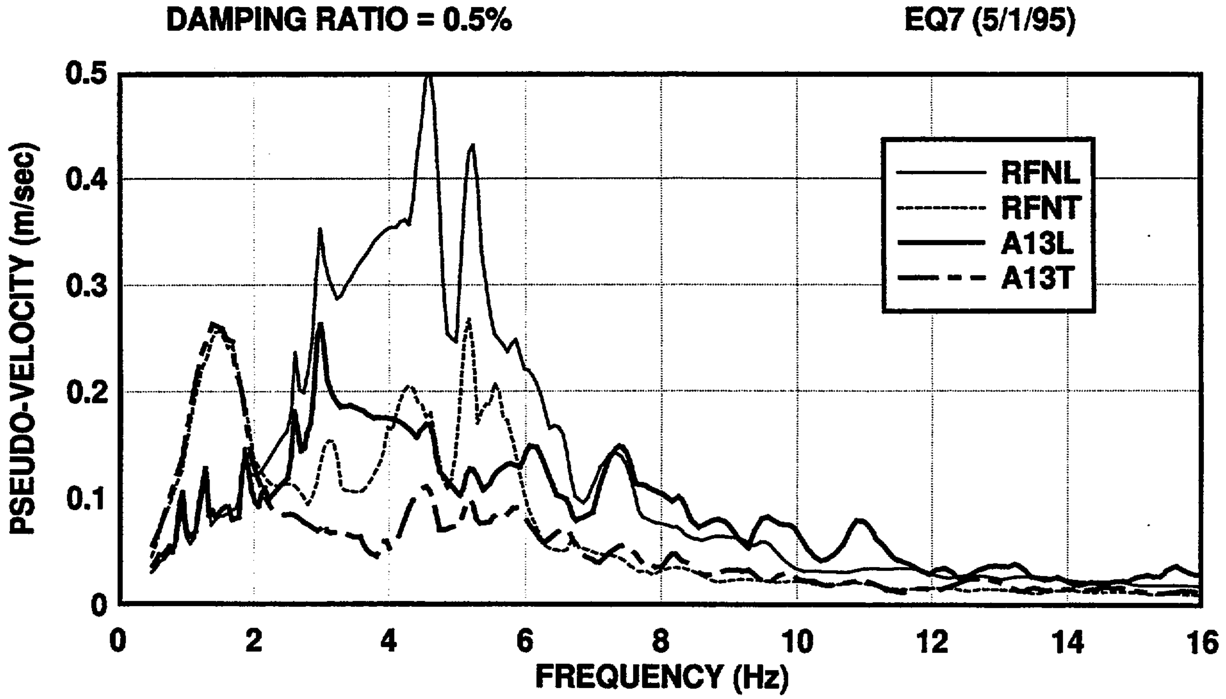

Figure 97 Pseudo-Velocity response spectra for 0.5% damping for EQ7

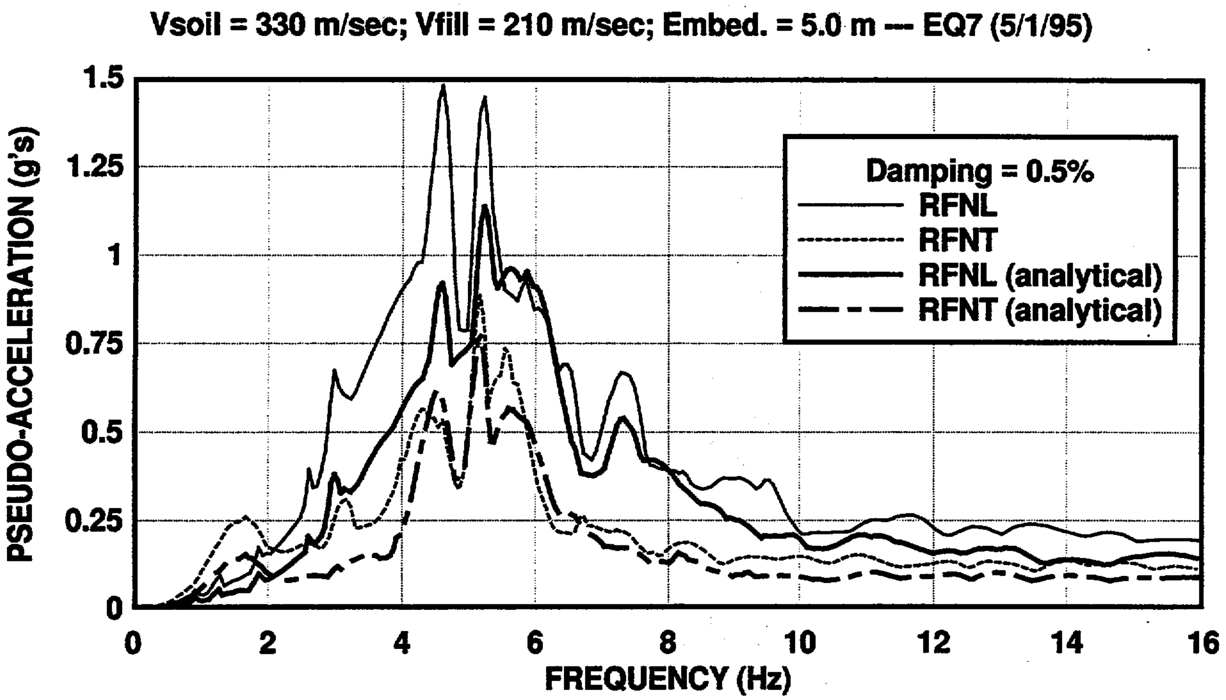

Figure 98 Observed and computed response spectra for 0.5% damping: EQ7 (*d* = 5.0 m)

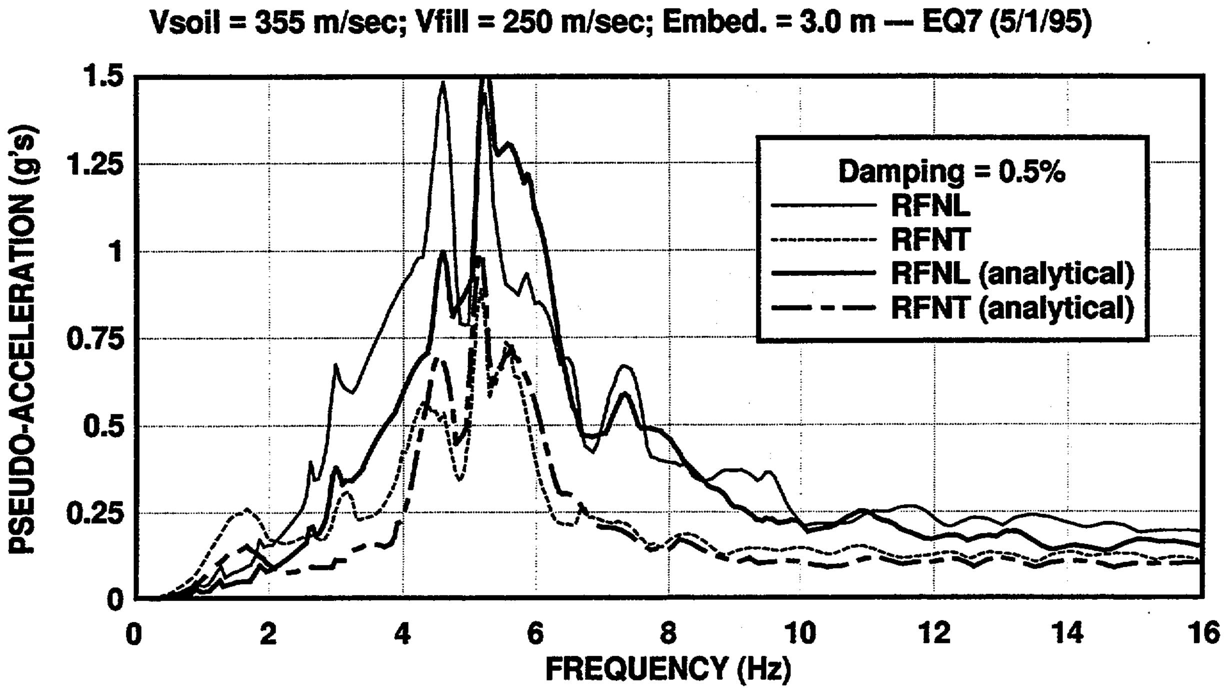

Figure 99 Observed and computed response spectra for 0.5% damping: EQ7 (*d* = 3.0 m)

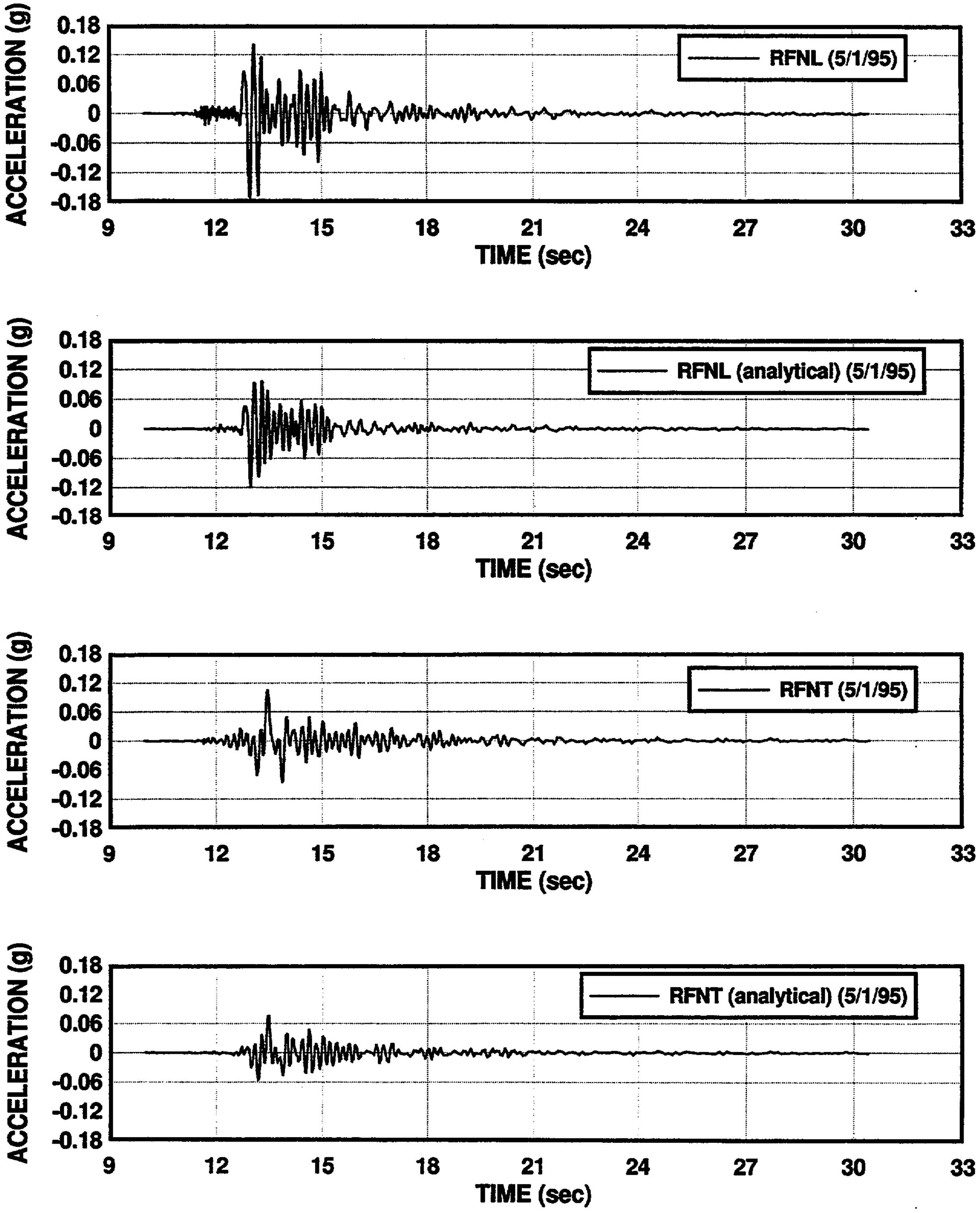

Figure 100 Observed and computed roof response time-histories: EQ7

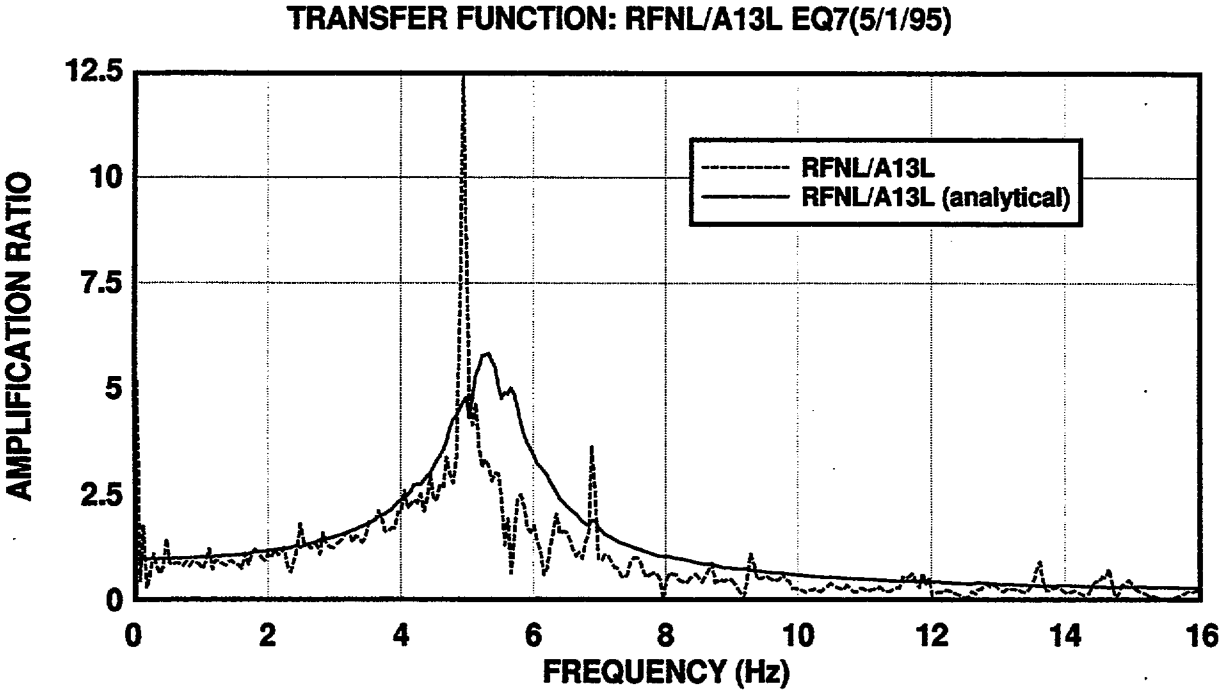

Figure 101 Transfer functions from free-field motion to roof response: EQ7 L-direction

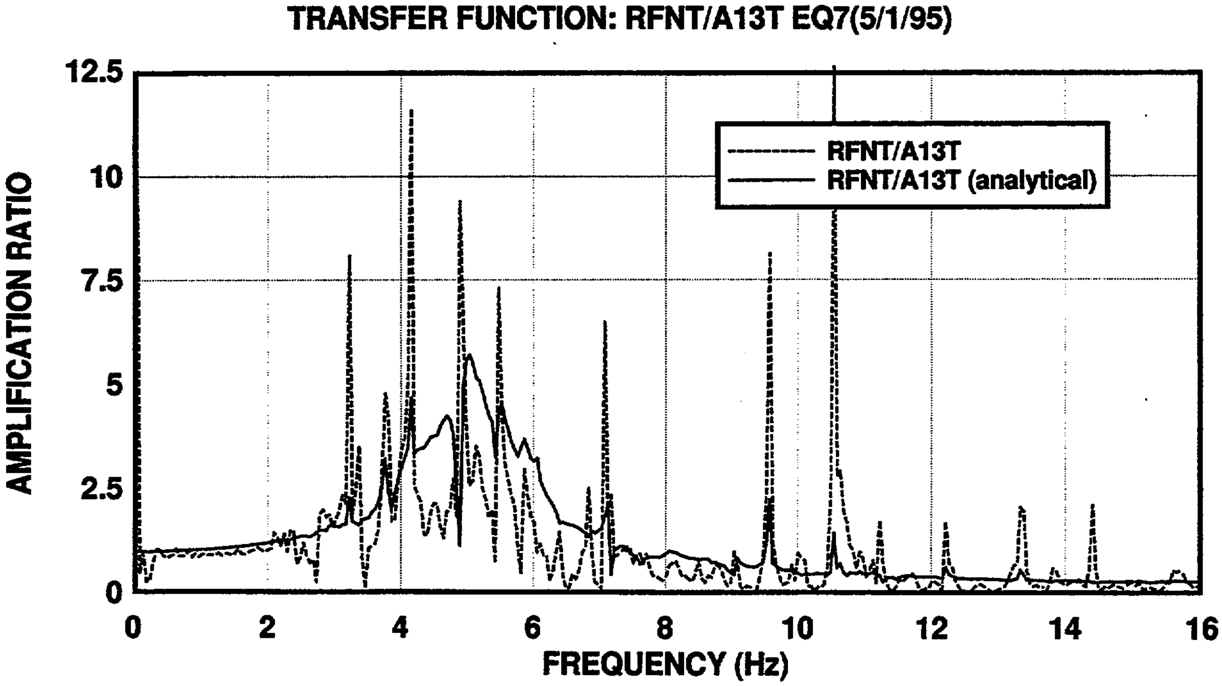

Figure 102 Transfer functions from free-field motion to roof response: EQ7 T-direction

8. SUMMARY AND CONCLUSIONS

A review of the site characterization program for the Hualien SSI Experiment has been presented. The review includes a detailed description of the methods used and of the results obtained, as well as an assessment of those results and of the recommended soil properties. It also includes further interpretation and assessment of the site conditions on the basis of the analysis of forced vibration test data and selected recorded earthquake loading data. An important feature of the site characterization was that it paid particular attention to the effect of the various construction operations on the in-situ shear wave speed and soil stiffness. This was shown by CRIEPI to be important for the cohesionless soils encountered whose stiffness and strength are controlled by the effective stress conditions at the site. The following observations and conclusions can be made on the basis of the review and analysis described in this report:

1. Analysis of the forced vibration test data indicated that the soil model proposed by CRIEPI could not reproduce well the observed results. Specifically, analysis of the forced vibration test data prior to the construction of the backfill (FVT-1) revealed anisotropic in-situ conditions for the gravel beneath the foundation, with different shear wave propagation speeds in different horizontal directions. The causes of the gravel anisotropy, however, still remain to be explained. Analysis of the forced vibration test data for the embedded case (FVT-2) permitted identification of average soil properties for the backfill and foundation soil.
2. On the basis of the FVT-2 data analysis a set of soil parameters denoted the best-estimated soil properties for FVT-2 are recommended for the soil-structure interaction analysis of the model under low-level lateral dynamic loading, including earthquake loading, *i.e.*, lateral loading such that the response remains in the linear, low-strains, range. The values recommended are spatial averages. Namely the value for the foundation soil is an average over the volume of the soil beneath the foundation to a depth of 12 m below ground level, and the value for the backfill soil is an average over the height of the backfill. The values recommended here differ somewhat from those proposed by CRIEPI, with the major difference being the identification of anisotropy in the foundation soil.
3. For strong lateral dynamic loading, including earthquake loading, such that non-linear soil behavior is anticipated, the best-estimated soil properties for FVT-2 should be used together with the values obtained by CRIEPI for the properties that describe the non-linear soil behavior. These properties include, at a minimum, the variation of the secant shear modulus and damping ratio with shear strain. For more sophisticated constitutive modeling, appropriate for nonlinear time-history analysis, additional soil properties such as shear strength parameters, soil response under cyclic hydrostatic loading, and the secant shear modulus for triaxial compression tests, were obtained by CRIEPI and are reported here. However, all properties needed for nonlinear soil modeling have been determined on the basis of laboratory testing and may not account for the in-situ soil anisotropy.
4. The site investigations conducted by CRIEPI focused primarily on the soils encountered to a depth of about 20 m below ground level. The site characterization for depths greater than about 20 m relies on scoping geophysical studies conducted by the IES either on the planning or preliminary stages of the Hualien SSI Experiment and large penetration test data at one

location. A more detailed characterization of the free-field soils at depths greater than 20 m below ground level may be desirable for site amplification and deconvolution analysis studies for correlation analysis with the ground motions recorded in the down-hole arrays, which extend to a depth of about 52.5 m below ground level.

5. A very comprehensive and rigorous site characterization program was conducted by CRIEPI between 1990 and 1994, which was at least as thorough as those commonly used for actual power plant sites. Nevertheless, considerable scatter can be observed on the data collected, particularly, for the in-situ shear wave speed measurements. Some of the scatter is the result of the soil anisotropy and some may be the result of random spatial variability of the shear wave speed. However, large uncertainties can still be observed even when the soil anisotropy is taken into consideration. Even greater scatter was encountered in the identification of the shear wave speed in the backfill.
6. Average values, averaged over a given soil volume, of the shear wave speeds were recommended by CRIEPI and in this study. Such spatial averages are useful for SSI analysis with the so-called spring method of analysis but may create difficulties with the more detailed and comprehensive finite element procedures whose results may be sensitive to local variations of the soil properties.
7. After the FVT-2 test, the shear wave speeds initially proposed for the as-built backfill (Phase IV-A) were found to be much too large and not representative of the backfill conditions near the containment walls. New in-situ tests were conducted (Phase IV-B) which lead to shear wave speeds in the backfill near the containment wall about 30 percent less that those initially estimated.
8. Cross-correlation analysis of earthquake ground accelerations recorded with the down-hole array indicates that the vertical shear wave propagation speed in the gravel differs significantly for particle motions in the NS and EW directions, with the larger wavespeeds in the NS direction. Those results were confirmed by cross-spectral density analysis of recorded down-hole ground accelerations conducted by others.
9. The fundamental soil-structure interaction frequencies under some of the recorded earthquake loads computed using the best-estimated soil properties for FVT-2 are 15 to 20 percent greater than those identified on the basis of the recorded responses. That observation implies that non-linear effects have strongly influenced the soil-structure interaction under the recorded loads. It is noteworthy that non-linear effects have significantly affected the response of the model under earthquake loads that are considered to be weak to moderate as compared to the seismic design loads for most nuclear power plant seismic category I structures.
10. A limited sensitivity analysis of the SSI response under two recorded earthquake loads was conducted. Equivalent linear parameters were found which provided a fair agreement between the observed and computed responses. Floor response spectra were predicted well with the equivalent linear system for frequencies greater than about 4.5 Hz, which includes the apparent fundamental SSI frequencies. However, the floor response spectra ordinates computed with the equivalent linear system were smaller than the observed ones for frequencies between about 1.5 and 4.5 Hz. The discrepancies may the result of non-linear behavior and of inaccurate input motions at the base of the SSI springs.

11. Transfer functions from the free-field motion to the roof response under recorded earthquake loading show evidence of site anisotropy beneath the foundation. This is, of course, evidence of a significant reduction on the contribution of the backfill to the stiffness and damping of the SSI system.

Uncertainties in the in-situ values of the soil properties, including random spatial variability, and modeling uncertainties were clearly illustrated with the results of the forced vibration tests, which revealed the unexpected effects of site anisotropy in the soil-structure interaction. Site anisotropy is not normally considered in most soil-structure interaction studies. This experiment indicates that it may be present and should be investigated for stiff soil sites.

Apart from the site anisotropy, the site characterization results show that considerable scatter in the in-situ values of the soil properties is still present even when thorough and sophisticated site characterization procedures are used. While spatial averages of the measured values may be adequate for SSI analysis with the simple spring method, the spatial variability of the soil properties creates difficulties for detailed finite element models whose results may be sensitive to localized variations in the soil properties.

Modeling uncertainties are, however, more evident in the analysis of the response under earthquake loads. The results of the experiment indicate that non-linear soil behavior is to be expected for a stiff soil site under weak earthquake loads. The behavior of the model under a more severe earthquake loading remains to be observed. In face of the already significant non-linear effects under weak earthquake loading and the unexpected effect of soil anisotropy, it appears worthwhile to extend for some time monitoring of the instrumentation already installed for the Hualien SSI experiment.

Furthermore, more detailed analysis of the recorded earthquake data at the site should also be continued. That analysis should address the following: (1) site amplification and deconvolution analysis studies, including the effect of soil anisotropy; (2) the adequacy of nonlinear time-history analysis procedures used in conjunction with simplified SSI methods such as the spring method, and of equivalent linearization procedures used with complex finite element methods, to represent the localized non-linear effects observed under earthquake loads; (3) the effects of kinematic interaction and wave scattering in the response; and (3) the sensitivity of the response under earthquake loading to modeling and parametric uncertainties, including nonlinear effects.

REFERENCES

1. Bendat, J.S. and A. G. Piersol, (1980), Engineering Application of Correlation and Spectral Analysis, John Wiley and Sons, Inc., New York, USA.
2. Bendat, J.S. and A.G. Piersol, (1986), Random Data Analysis and Measurement Procedures, 2nd Edition, John Wiley & Sons, Inc., New York, USA.
3. Beredugo, Y.O. and Novak, M., (1972), "Coupled horizontal and rocking vibration of embedded footings," *Canadian Geotechnical Journal,* Vol. 9, pp. 447-497.
4. Chen, C.-H., and Y.-J. Lee, (1996), "Response prediction for Hualien LSST model by using hybrid modeling," *Proceedings, 11th World Conf. Earthq. Engng,* Acapulco, Mexico, paper No. 472, Elsevier Science Ltd, Oxford, United Kingdom.
5. Chokshi, N., S. K. Shaukat and N. Anderson, (1988), "Regulatory analysis for USI A-40, "Seismic Design Criteria," draft report for comment," U.S. Nuclear Regulatory Commission, NUREG-1233.
6. Costantino, C.J. and C.A. Miller, (1993), "Consideration of uncertainties in soil-structure interaction computations," City College of New York of the City University of New York, NUREG/CR-5956. CRIEPI, (1991), "Interim Report on Geotechnical Investigation(Oct. to Dec., 1990) of Hualien Site," August 15.
7. CRIEPI, (1991), "Interim Report on the Geotechnical Investigation (Oct. to De. 1990) of Hualien Site," CRIEPI, August.
8. CRIEPI , (1992), "Interim Report on the Geotechnical Investigation Results of Hualien Site," *CRIEPI,* April.
9. CRIEPI, (1993a), "Status Report on Geotechnical Investigation at Hualien Site," *CRIEPI,* January.
10. CRIEPI, (1993b), "The Unified Model of the Ground for FVT-1 Analysis," *CRIEPI,* January 15, 1993. (addendum: fax to H. L. Graves, US NRC from Takeji Kokusho, CRIEPI, March 13.
11. CRIEPI, (1993c), "On the Unified Model for Analysis," *CRIEPI,* April.
12. CRIEPI, (1993d), "The Unified Model of the Ground for FVT-2 Analysis," *CRIEPI,* July 23.
13. CRIEPI, (1993e), "Main Results of March'93 CRIEPI Investigation," *CRIEPI,* November 1.
14. CRIEPI, (1993f), "Raw Data of Laboratory Test Results of Backfill Material," *CRIEPI,* November.
15. CRIEPI, (1994a), "Status Report on Geotechnical Investigation at Hualien Site," *CRIEPI,* January, 1993, rev. June 7-8, 1994.
16. CRIEPI, (1994b), "Digital Data of $G/G_0 \sim \gamma/\gamma_r$ and $h \sim G/G_0$ Relations of the Backfill Material for Numerical Analysis," *CRIEPI,* June 7~8.
17. CRIEPI, (1994c), "Additional Geophysical Survey on the Gravel Ground and the Backfill in 1994," *CRIEPI,* June.
18. CRIEPI, (1995a), "Non-Linearity of Ground Materials," *CRIEPI,* April, 18.
19. CRIEPI, (1995b), "Result of the Additional Geotechnical Site Soil Investigation: Focusing on the Survey of the Heterogeneity of Backfill and Foundation Gravel Zones Around the Part Just Underneath the Contact Plane Carried out Partly in April'94 and Mainly in October'94 by CRIEPI," *CRIEPI,* July.

20. Elgamal, A.-W., . Zeghal, H.T. Tang and J.C. Stepp, (1995), "Lotung downhole array. I: evaluation of site properties," ASCE, *J. Geotech. Engng.*, Vol. 121, No. 4, April, pp. 350-362.
21. Gazetas, G., (1982), "Analysis of machine foundation vibrations: state of the art," *Soil Dynamics and Earthquake Engineering*, Vol. 2, No. 1, pp. 2-42.
22. Gazetas, G., (1991), "Formulas and charts for impedances of surface and embedded foundations," ASCE, *J. Geotech. Engng.*, Vol. 117, No. 9, September, pp. 1363-1381.
23. Gazetas, G., (1991), "Foundation vibrations," Chapter 15 in *Foundation Engineering Handbook*, 2nd Edition, H. Y. Fang, Editor, Van Nostrand Reinhold, Inc, pp. 553-593.
24. Ganev, T., T. Katayama and T. Ueshima, (1996), "Analysis of soil-structure interaction of a model structure on stiff soil in Hualien, Taiwan," *Proceedings, 11th World Conf. Earthq. Engng*, Acapulco, Mexico, paper No. 951, Elsevier Science Ltd, Oxford, United Kingdom.
25. Hanazato, T., Y. Kishi, Y. Sakai and H. Tajimi, (1996), "Earthquake blind prediction analysis using ring exciting thin layer method in the international project of Hualien large scale seismic test," *Proceedings, 11th World Conf. Earthq. Engng*, Acapulco, Mexico, paper No. 1008, Elsevier Science Ltd, Oxford, United Kingdom.
26. Holtz, R.D. and W.D. Kovacs, (1981), An Introduction to Geotechnical Engineering, Prentice-Hall, Inc., Englewood Cliffs, Inc., New Jersey.
27. Hough, K.B., (1969), Basic Soils Engineering, *Ronald Press Co., John Wiley & Sons, Inc.*
28. Institute of Earth Sciences (IES), "Briefing on Hualien Stiff Site," (slides summarizing a preliminary study of the Hualien LSST).
29. Kausel, E., R.V. Whitman, J.P. Morray and F. Elsabee, (1978), "The spring method for embedded foundations," *Nuclear Engineering and Design*, Vol. 48, pp. 377-392.
30. Kobayashi, T., H. Yamaya, E. Kitamura, T. Sugiyama, (1996), "System identification of the Hualien LSST model structure," *Proceedings, 11th World Conf. Earthq. Engng*, Acapulco, Mexico, paper No. 67, Elsevier Science Ltd, Oxford, United Kingdom.
31. Kokusho, T., K. Nishi, T. Okamoto, T. Kataoka, Y. Tanaka, K. Kudo, H.T. Tang and Y.H. Cheng, (1993), "Geotechnical investigation in the Hualien large scale seismic test project," *Proceedings, 12th Int. Conf. Struct. Mech. Reactor Technology*, International Association for Structural Mechanics in Reactor Technology, August 15-20, Stuttgart, Germany, paper K03/4, Volume K1, pp. 85-90, Atomic Energy Society of Japan.
32. Lin, A.N., (1982), "Experimental observations of the effect of foundation embedment on structural response," *Thesis* in partial fulfillment of the requirements for the degree of Doctor of Philosophy, California Institute of Technology.
33. Morishita, H., H. Tanaka, N. Nakamura, T. Kobayashi, S. Kan, H. Yamaya and H. T. Tang, (1993), "Forced vibration test for the Hualien large scale SSI model," *Proceedings, 12th Int. Conf. Struct. Mech. Reactor Technology*, International Association for Structural Mechanics in Reactor Technology, August 15-20, Stuttgart, Germany, paper K02/1, Volume K1, pp. 37-42, Atomic Energy Society of Japan.
34. Richart, F.E., J.R. Hall, Jr., and R.D. Woods, (1970), "Vibrations of soils and foundations," Prentice-Hall, Englewood Cliffs, New Jersey.
35. Tajimi Engineering Services, Ltd., (1996), "Hualien LSST Project - Correlation SSI Analysis of Earthquake of 1/20/94," prepared by Tajimi Engineering Services, Ltd., for TEPCO group, October.

36. Tang, H.T., J.C. Stepp, Y.H. Cheng, Y.S. Yeh, K. Nishi, I. Tawate, T. Kokusho, H. Morishita, Y. Shirisaka, F. Gantenbeim, J.P. Touret, P. Sollogoub, H. Graves and J. Costello, (1991), "The Hualien large-scale seismic test for soil-structure interaction research," *Transactions, 11th Int. Conf. Struct. Mech. Reactor Technology*, International Association of Reactor Technology, August 18-23, Tokyo, Japan, Paper K04/4, Volume K1, pp. 69-74, North Holland, Elsevier Science Publishers, Amsterdam, The Netherlands.
37. TEPCO, (1993a), "Hualien LSST Project - Status Report of the Forced Vibration Test," prepared by Tokyo Electric Power Company, April.
38. TEPCO, (1993b), "Hualien LSST Project - Explanation of FVT-1 and FVT-2 Data Files," prepared by Tokyo Electric Power Company, November.
39. TEPCO and KTRI, (1993), "Hualien LSST Project - Correlation Analysis of FVT Before Backfill," prepared by Tokyo Electric Power Company (TEPCO) and Kajima Technical Research Institute (KTRI), November.
40. Ueshima, T. and H. Okano, (1996), "Further investigation on seismic response of soil and embedded structure in Hualien LSST program," *Proceedings, 11th World Conf. Earthq. Engng.*, Acapulco, Mexico, paper No. 1930, Elsevier Science Ltd., Oxford, United Kingdom.
41. United Geotech, Inc., *(1990)*, "Final Report of Geophysical Survey at Hualien Stiff Site for Lotung Large Scale Seismic Test Program," prepared for Taiwan Power Company, February.
42. U.S. Army Engineer Waterways Experiment Station, (1960), "The Unified Soil Classification System," *Technical Memorandum No. 3-357,* Appendix A, Characteristics of Soil Groups Pertaining to Embankments and Foundations, 1953; Appendix B, Characteristics of Soil Groups Pertaining to Roads and Airfields, 1957.
43. Wolf, J.P., (1985), Dynamic Soil-Structure Interaction, Prentice-Hall, Inc., Englewood Cliffs, New Jersey.
44. Wolf, J.P., (1988), Soil-Structure-Interaction Analysis in Time Domain, Prentice-Hall, Inc., Englewood-Cliffs, New Jersey.
45. Yang, Y-C., W-G. Huang, C-C. Lui, S-N. Cheng and T.Y. Yeong, (1995), "Strong-Motion Earthquake Records on the 2 May, 1995, in LSST Array, Hualien," Report IESER95-003, Institute of Earth Sciences, Academia Sinica, for Taiwan Power Company, June.
46. Yoshida, Y. and T. Kokusho, (1988), "A Proposal on Application of Penetration Tests on Gravelly Soils," CRIEPI report U87080 (in Japanese).

A APPENDIX A

Soil-Structure-Interaction Analysis.

Consider the 2-dimensional soil-structure interaction system with a rigid foundation shown in Figure A.1. The system's governing equations of motion, which can be obtained by imposing equilibrium of all horizontal forces and all moments about the base of foundation, are as follows:

$$\begin{bmatrix} m_s & m_s & m_s h \\ m_s & m_s + m & m_s h + m z_c \\ m_s h & m z_c + m_s h & m_s h^2 + m z_c^2 + I_0 + I_1 \end{bmatrix} \begin{Bmatrix} \ddot{y} \\ \ddot{u}_0 \\ \ddot{\psi} \end{Bmatrix} + \begin{bmatrix} k & 0 & 0 \\ 0 & k_{xx} & k_{x\psi} \\ 0 & k_{x\psi} & k_{\psi\psi} \end{bmatrix} \begin{Bmatrix} y \\ u_0 \\ \psi \end{Bmatrix} = \begin{Bmatrix} P \\ P \\ Pl \end{Bmatrix} \qquad (1)$$

where, u_o = displacement of the base (rigid body sliding), y = displacement of the SDOF structure with respect to its fixed base, ψ = rotation of the foundation about its center of gravity (rigid body rocking), m_s = lumped mass of the SDOF structure, m = mass of the foundation, I_o = mass moment of inertia of the foundation about its center of gravity, I_1 = mass moment of inertia of the roof plate with respect to an axis passing through its center of gravity and perpendicular to the plane of the figure, z_c = distance from center of gravity of the foundation mass to the base, h = height from the foundation plane to the center of gravity of the lumped mass of the SDOF structure, l = distance from the foundation plane to the point of application of the lateral load, P = dynamic lateral load, and

$$\left[K_f\right] = \begin{bmatrix} k_{xx} & k_{x\psi} \\ k_{x\psi} & k_{\psi\psi} \end{bmatrix} \qquad (2)$$

is the frequency-dependent foundation impedance matrix, such that

$$\begin{Bmatrix} R_u \\ M_r \end{Bmatrix} = \left[K_f\right] \begin{Bmatrix} u_0 \\ \psi \end{Bmatrix} \qquad (3)$$

are the horizontal force and moment reactions, respectively, at the base of the rigid foundation. A frequency-domain formulation is, of course, implied in the above formulation.

To extend this formulation to an anisotropic site condition, the following assumptions are made:

1. There are two orthogonal horizontal directions, denoted here as principal directions, such that loading in each one of these directions produces no cross-axis response;
2. For loading in a principal direction the soil-structure system can be analyzed using the classical stick model approach and their respective impedance functions developed for isotropic soil conditions on the basis of the S wave speed in this principal direction;
3. The impedance functions for isotropic soil conditions determined for each principal direction can be combined in the same manner as the stiffness of a beam with a non-symmetric cross-section under pure biaxial bending; and
4. The structural stiffness and the inertia of the structure and its foundation are considered isotropic.

Let $\mathbf{u}_1$ and $\mathbf{u}_2$ be the displacement vectors $[y,\ u_o,\ \psi]^T$ in each of the principal directions under lateral loading P_1 and P_2 acting in the principal direction 1 and 2, respectively. Then, the displacement vectors in two orthogonal directions E and N making an angle α with the directions 1 and 2, respectively, are given by

$$\begin{Bmatrix}\mathbf{u}_E\\ \mathbf{u}_N\end{Bmatrix}=\begin{bmatrix}\begin{bmatrix}1 & 0\\ 0 & \cos\alpha\,[\mathbf{I}]\end{bmatrix} & \begin{bmatrix}1 & 0\\ 0 & \sin\alpha\,[\mathbf{I}]\end{bmatrix}\\ \begin{bmatrix}1 & 0\\ 0 & -\sin\alpha\,[\mathbf{I}]\end{bmatrix} & \begin{bmatrix}1 & 0\\ 0 & \cos\alpha\,[\mathbf{I}]\end{bmatrix}\end{bmatrix}\begin{Bmatrix}\mathbf{u}_1\\ \mathbf{u}_2\end{Bmatrix}=[\mathrm{T}]\begin{Bmatrix}\mathbf{u}_1\\ \mathbf{u}_2\end{Bmatrix} \tag{4}$$

where **I** is a 2×2 stiffness matrix. When the mass of the structure is not considered, the displacements $\mathbf{u}_1$ and $\mathbf{u}_2$ are given by

$$\begin{Bmatrix}\mathbf{u}_1\\ \mathbf{u}_2\end{Bmatrix}=\begin{bmatrix}\begin{bmatrix}1/k & 0\\ 0 & [\mathrm{F}_1]\end{bmatrix} & \mathbf{0}\\ \mathbf{0} & \begin{bmatrix}1/k & 0\\ 0 & [\mathrm{F}_2]\end{bmatrix}\end{bmatrix}\begin{Bmatrix}\begin{Bmatrix}P_1\\ P_1\\ P_1 l\end{Bmatrix}\\ \begin{Bmatrix}P_2\\ P_2\\ P_2 l\end{Bmatrix}\end{Bmatrix}=[\mathrm{F}]\begin{Bmatrix}\mathbf{P}_1\\ \mathbf{P}_2\end{Bmatrix} \tag{5}$$

where, $\mathbf{F}_1$ and $\mathbf{F}_2$ are the compliance matrices of the foundation for the principal directions 1 and 2, which are the inverse of the impedance matrix $\mathbf{K}_f$ for each principal direction. The load vector for the principal directions can also be expressed in terms of the load vector for the E and N directions as follows:

$$\begin{Bmatrix}\mathbf{P}_1\\ \mathbf{P}_2\end{Bmatrix}=[\mathrm{T}]^T\begin{Bmatrix}\mathbf{P}_\mathrm{E}\\ \mathbf{P}_N\end{Bmatrix} \tag{6}$$

Replacing (5) and (6) into (4) it is

$$\begin{Bmatrix}\mathbf{u}_E\\ \mathbf{u}_N\end{Bmatrix}=[\mathrm{T}][\mathrm{F}][\mathrm{T}]^T\begin{Bmatrix}\mathbf{P}_E\\ \mathbf{P}_N\end{Bmatrix}=\left[\mathrm{F}^*\right]\begin{Bmatrix}\mathbf{P}_E\\ \mathbf{P}_N\end{Bmatrix} \tag{7}$$

Therefore, the stiffness matrix for the anisotropic soil-structure interaction system referred to the E and N axes is $[\mathrm{K}^*] = [\mathrm{F}^*]^{-1} = [\mathrm{T}]^{-T}[\mathrm{F}]^{-1}[\mathrm{T}]^{-1}$, where

$$[\mathrm{F}]^{-1}=\begin{bmatrix}\begin{bmatrix}k & 0\\ 0 & \mathrm{K}_1\end{bmatrix} & \mathbf{0}\\ \mathbf{0} & \begin{bmatrix}k & 0\\ 0 & [\mathrm{K}_2]\end{bmatrix}\end{bmatrix};\ [\mathrm{K}_1]=[\mathrm{F}_1]^{-1};\ [\mathrm{K}_2]=[\mathrm{F}_2]^{-1} \tag{8}$$

The equations of motion for the displacement in the E and N directions under lateral loads $\mathbf{P}_\mathrm{E}$ and $\mathbf{P}_\mathrm{N}$ can now be written as follows:

$$\begin{bmatrix}\mathbf{m} & \mathbf{0}\\ \mathbf{0} & \mathbf{m}\end{bmatrix}\begin{Bmatrix}\ddot{\mathbf{u}}_E\\ \ddot{\mathbf{u}}_N\end{Bmatrix}+\left[\mathrm{K}^*\right]\begin{Bmatrix}\mathbf{u}_E\\ \mathbf{u}_N\end{Bmatrix}=\begin{Bmatrix}\mathbf{P}_E\\ \mathbf{P}_N\end{Bmatrix} \tag{9}$$

where $\mathbf{m}$ is the 3×3 mass matrix in (1). The above equations of motion with 6 unknowns can be easily solved in the frequency domain. For an embedded foundation the impedance matrix for a given principal direction includes terms associated with the foundation soil and terms associated with the backfill. In this study, the backfill is considered to be isotropic for most of the analyses presented.

In the case of an earthquake loading, the loading vector is modified to account for the ground accelerations resulting from the kinematic interaction, which consist of a translation and a rotational component in each orthogonal direction. The right-hand-side of the equations of motion for this case becomes:

$$\begin{Bmatrix}\mathbf{P}_E\\ \mathbf{P}_N\end{Bmatrix}=-\left\{\begin{array}{c}\begin{Bmatrix}m_S\\ m_S+m\\ mz_c+m_Sh\end{Bmatrix}\ddot{a}_E\\ \begin{Bmatrix}m_S\\ m_S+m\\ mz_c+m_Sh\end{Bmatrix}\ddot{a}_N\end{array}\right\}-\left\{\begin{array}{c}\begin{Bmatrix}m_sh\\ m_sh+mz_c\\ mz_c^2+m_sh^2+I_0+I_1\end{Bmatrix}\ddot{\theta}_E\\ \begin{Bmatrix}m_sh\\ m_sh+mz_c\\ mz_c^2+m_sh^2+I_0+I_1\end{Bmatrix}\ddot{\theta}_N\end{array}\right\} \tag{10}$$

where $\ddot{a}$ and $\ddot{\theta}$ are the horizontal and rotational accelerations at the base of the soil springs with the symbols E and N denoting the loading directions. Those input accelerations are to be determined from the kinematic soil-structure interaction analysis. For the spring method, simplified procedures to determine the kinematic ground accelerations from the free-field ground accelerations have been proposed by Kausel *et al.* (1976) for isotropic site conditions and are utilized for this study.

Fixed-Base Single-Degree-of-Freedom Model of the Containment

The containment shell is modeled with a massless cantilever beam with a concentrated mass at the top equal to the mass of the roof plate, cross-section properties equal to those of the containment shell, and span from the top of the foundation plate to the center of gravity of the roof plate. The stiffness of the beam was computed accounting for both shear and flexural deformations. Using a Young's modulus of 28,200,000 kN/m^2 and a Poisson's ratio of 0.2, a natural frequency of 11.1 Hertz is computed for this single-degree-of-freedom system, which compares well with a frequency of 10.7 Hertz obtained with more complex structural models. With this model, the mass of the containment shell is not included in the fixed-base model. Instead, the mass of the shell is included in the mass of the rigid body foundation and is accounted for in the calculation of the total mass, center of gravity and mass-moment of inertia of the rigid foundation.

The stiffness and mass calculated for the fixed-base structural model as well as the elements of the mass matrix in (1) are shown in Table A.1.

Table A.1 Properties of fixed-base model and rigid foundation

Property	k (kN/m)	m_s (ton)	I_1 (ton-m^2)	m (ton)	I_0 (ton-m^2)	z_c (m)
Value	$0.0893E_c$	$207.8\rho_c$	$2{,}329\rho_c$	$387.9\rho_c$	$9{,}203\rho_c$	3.613

where E_c and ρ_c are the Young's modulus and density of the concrete, respectively.

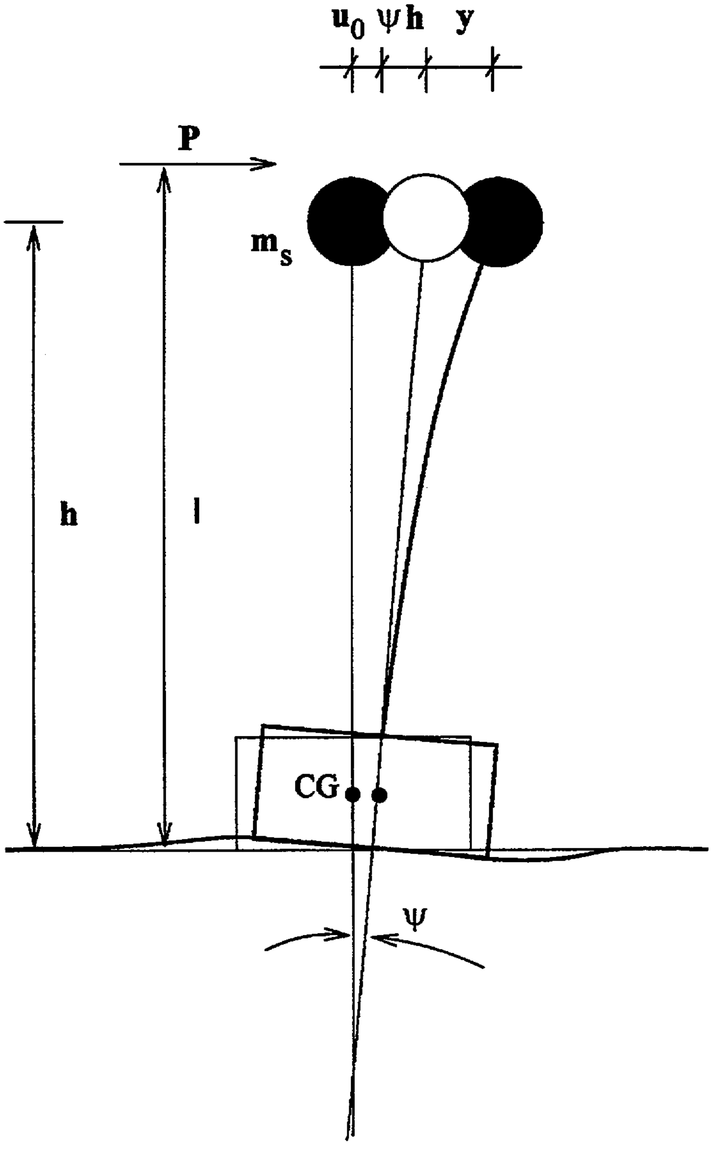

Figure A- 1. Two-dimensional SSI model

NRC FORM 335
(2-89)
NRCM 1102,
3201, 3202

U.S. NUCLEAR REGULATORY COMMISSION

BIBLIOGRAPHIC DATA SHEET

(See instructions on the reverse)

1. REPORT NUMBER
(Assigned by NRC, Add Vol., Supp., Rev., and Addendum Numbers, if any.)

NUREG/CR-6584

2. TITLE AND SUBTITLE

Evaluation of the Hualien Quarter Scale Model Seismic Experiment
Volume 2

3. DATE REPORT PUBLISHED

MONTH	YEAR
March	2001

4. FIN OR GRANT NUMBER
W6769

5. AUTHOR(S)

C. A. Miller, C. J. Costantino, CCNY
J. A. Pires, C. J. Higgins, ARA

6. TYPE OF REPORT
Final

7. PERIOD COVERED *(Inclusive Dates)*
3/92 to 10/99

8. PERFORMING ORGANIZATION - NAME AND ADDRESS *(If NRC, provide Division, Office or Region, U.S. Nuclear Regulatory Commission, and mailing address; if contractor, provide name and mailing address.)*

The City College of New York
Department of Civil Engineering
New York, NY 10031

Subcontractor:
Applied Research Associates, Inc.
Albuquerque, NM 87110

9. SPONSORING ORGANIZATION - NAME AND ADDRESS *(If NRC, type "Same as above"; if contractor, provide NRC Division, Office or Region, U.S. Nuclear Regulatory Commission, and mailing address.)*

Division of Engineering Technology
Office of Nuclear Regulatory Research
U. S. Nuclear Regulatory Commission
Washington, DC 20555-0001

10. SUPPLEMENTARY NOTES

Herman L. Graves, Project Manager

11. ABSTRACT *(200 words or less)*

A quarter scale model of a containment structure was constructed in Hualien, a seismically active region in Taiwan. Forced vibration tests were performed both before and after placement of the backfill. The structure and surrounding free field were then instrumented with accelerometers, pressure gages, and displacement gages. Recordings were taken when significant seismic events occurred at the site. This report describes analytical studies that were performed to correlate the measured response with predictions. Soil - structure interaction effects were represented with a lumped parameter model.

The work is summarized in Volume 1 of the 4 volume report. The site characteristics are described in Volume 2. This includes a discussion of the field program used to determine the characteristics. The predictions for the forced vibration tests are compared with the measured data in Volume 3. The correlation is found to be quite good except that the measured data indicated that the site is anisotropic. This is not found from the site exploration phase of the work. Comparisons between the predictions and measured data for the earthquake responses are made in Volume 4. The soil responses compare reasonably well but the in structure responses do not compare very well. This is attributed to the anisotropic site characteristics.

12. KEY WORDS/DESCRIPTORS *(List words or phrases that will assist researchers in locating the report.)*

Hualien, soil-structure interaction, shear wave velocity, forced vibration

13. AVAILABILITY STATEMENT
unlimited

14. SECURITY CLASSIFICATION
(This Page)
unclassified
(This Report)
unclassified

15. NUMBER OF PAGES

16. PRICE

UNITED STATES
NUCLEAR REGULATORY COMMISSION
WASHINGTON, DC 20555-0001

OFFICIAL BUSINESS
PENALTY FOR PRIVATE USE, $300